Effectiveness of Nano Silica Extracted from Rice Husk Ash (RHA) in Cementitious Media

By

Nadira Islam Nila [BSc Eng.]

Student ID: 22MCE009P

A thesis submitted in partial fulfillment of the requirements for the degree of

MASTER of SCIENCE in Civil Engineering

Department of Civil Engineering

CHITTAGONG UNIVERSITY OF ENGINEERING AND TECHNOLOGY

June 2025

Declaration

I hereby declare that the work contained in this Thesis has not been previously submitted to meet requirements for an award at this or any other higher education institution. To the best of my knowledge and belief, the Thesis contains no material previously published or written by another person except where due reference is cited. Furthermore, the Thesis complies with PLAGIARISM and ACADEMIC INTEGRITY regulations of CUET.

Nadira Islam Nila

22MCE009P

Department of Civil Engineering

Chittagong University of Engineering & Technology (CUET)

List of Publication

International Conference:

- Nila N I, Piyes M T I, Islam G M S and Islam M M (2024) Cementitious properties of rice husk ash (RHA) and extracted silica powder from RHA, *International Conference on Advances in Civil Engineering (ICACE2024)*, Chittagong University of Engineering & Technology, Bangladesh, 12-14 December 2024, (pp. 2495-2502).

Approval by the Supervisor

This is to certify that Nadira Islam Nila has carried out this research work under my supervision, and she has fulfilled the relevant Academic Ordinance of the Chittagong University of Engineering and Technology so that she is qualified to submit the following Thesis in the application for the degree of MASTER of SCIENCE in Civil Engineering. Furthermore, the Thesis complies with the PLAGIARISM and ACADEMIC INTEGRITY regulation of CUET.

Dr. G. M. Sadiqul Islam

Professor

Department of Civil Engineering

Chittagong University of Engineering & Technology

Acknowledgement

At first, I would like to express my gratitude to the divine entity, Allah, for bestowing upon me intelligence and the empowerment to successfully complete the thesis work in a state of well-being and security.

I would like to express my sincere appreciation and gratitude to my thesis supervisor, **Prof. Dr. G. M. Sadiqul Islam** of the Department of Civil Engineering at CUET, for his constant guidance, continuous supervision, constructive criticism, valuable recommendations, and enthusiastic support throughout the thesis work. Without his constant supervision and motivation, I might have faced considerable difficulties in successfully and punctually completing the thesis. I gratefully acknowledge the assistance provided by the Department of Civil Engineering at CUET, including laboratory facilities, technical support, and materials, which enabled me to complete the thesis work.

Also, I am sincerely thankful to **Sustainable Energy & Agro-Resource Ltd., Thakurgaon, Bangladesh**, for providing Rice Husk Ash (RHA), Silica Powder, and Nano Silica. The financial assistance received for this work through the research project (Grant ID: SD20222201) of BANBEIS, Ministry of Education, Bangladesh, is gratefully acknowledged.

Nadira Islam Nila

June 2025

ABSTRACT

The use of concrete is rapidly increasing worldwide, primarily harming the environment due to its primary component, cement, which accounts for roughly 8% of global CO_2 emissions. Hence, exploring sustainable alternatives is crucial. Extracted nano-silica (NS) from rice husk ash is gaining interest as a sustainable construction material. In this study, RHA and extracted SP and NS from RHA were characterized comprehensively at pH 3 and pH 10 to evaluate their suitability for application in cementitious media. By utilizing laser particle sizing, scanning electron microscopy (SEM), X-ray diffraction (XRD), and X-ray fluorescence (XRF) techniques, the chemical composition, physical characteristics, and microstructure of these binders were examined. The setting time, soundness, autoclave expansion, workability, microstructure, flexural strength, compressive strength, and durability of RHA/SP/NS blended mortar and concrete were assessed. Setting time increased with RHA and SP replacement but was significantly reduced with NS due to early hydration, resulting in early strength development. RHA, SP, and NS blended mortars showed better flexural and compressive strength than the control mix due to higher C-S-H formation. With 2.5% RHA, 10% SP, and 5% NS replacement, maximum strength and better durability were observed in the mortar. At a constant w/b ratio, the compressive strengths found were 59.2 MPa, 60.8 MPa, and 56.2 MPa after 90 days of curing. RHA increased drying shrinkage slightly. However, SP and NS reduced it and improved sulfate resistance at later stages of the curing process. RHA increased the water absorption rate in mortar, whereas adding SP and NS significantly decreased it. On the other hand, in concrete, 7.5% RHA/SP/NS achieved the maximum strength (31.7 MPa, 34.1 MPa, and 33.7 MPa, respectively) and exhibited better durability performance. By increasing the packing density of concrete and reducing porosity, the compressive strength of RHA/SP/NS blended concrete increased significantly, providing better chloride resistance than the control sample. The findings suggest that RHA, SP, and NS have potential as alternative construction materials.

বিমূর্ত

বিশ্বব্যাপী কংক্রিটের ব্যবহার দ্রুত বৃদ্ধি পাচ্ছে, যার প্রধান কারণ পরিবেশের ক্ষতি করছে এর প্রধান উপাদান সিমেন্ট, যা বিশ্বব্যাপী CO_2 নির্গমনের প্রায় ৮% নির্গমন করে। অতএব, টেকসই বিকল্প অনুসন্ধান অত্যন্ত গুরুত্বপূর্ণ। ধানের তুষের ছাই থেকে নিষ্কাশিত ন্যানো সিলিকা (NS) একটি টেকসই নির্মাণ বিকল্প হিসাবে আগ্রহ অর্জন করছে। এই গবেষণায়, RHA এবং pH 3 এবং pH 10 বজায় রেখে RHA থেকে নিষ্কাশিত SP এবং NS কে সিমেন্টিটিয়াস মিডিয়াতে প্রয়োগের জন্য তাদের উপযুক্ততা মূল্যায়ন করার জন্য ব্যাপকভাবে চিহ্নিত করা হয়েছিল। লেজার পার্টিকেল সাইজিং, স্ক্যানিং ইলেক্ট্রন মাইক্রোস্কোপি (SEM), এক্স-রে ডিফ্র্যাকশন (XRD), এবং এক্স-রে ফ্লুরোসেন্স (XRF) কৌশল ব্যবহার করে এই বাইন্ডারগুলির রাসায়নিক গঠন, ভৌত বৈশিষ্ট্য এবং মাইক্রোস্ট্রাকচার পরীক্ষা করা হয়েছিল। RHA/SP/NS মিশ্রিত মর্টার এবং কংক্রিটের সেটিং সময়, শব্দ, অটোক্লেভ সম্প্রসারণ, কার্যক্ষমতা, মাইক্রোস্ট্রাকচার, নমনীয় শক্তি, সংকোচন শক্তি এবং স্থায়িত্ব মূল্যায়ন করা হয়েছিল। RHA এবং SP প্রতিস্থাপনের সাথে সেটিং সময় বৃদ্ধি পেয়েছে কিন্তু প্রাথমিক হাইড্রেশনের কারণে NS এর সাথে উল্লেখযোগ্যভাবে হ্রাস পেয়েছে যার ফলে প্রাথমিক শক্তি বিকাশও পরিলক্ষিত হয়েছে। RHA, SP, এবং NS মিশ্রিত মর্টারগুলি উচ্চতর C-S-H গঠনের কারণে নিয়ন্ত্রণ মিশ্রণের তুলনায় ভাল নমনীয় এবং সংকোচনশীল শক্তি দেখিয়েছে। ২.৫% RHA/১০% SP/৫% NS প্রতিস্থাপনের সাথে সর্বাধিক শক্তি এবং মর্টারে আরও ভাল স্থায়িত্ব পরিলক্ষিত হয়েছে। স্থির w/b অনুপাতে 90 দিন নিরাময়ের পরে সংকোচনশীল শক্তি ছিল ৫৯.২ MPa, ৬০.৮ MPa এবং ৫৬.২ MPa। RHA শুকানোর সংকোচনকে কিছুটা বাড়িয়েছে, যদিও পরবর্তী নিরাময় পর্যায়ে এটি হ্রাস করতে এবং সালফেট প্রতিরোধের উন্নতি করতে SP এবং NS যুক্ত করা হয়েছিল। RHA মর্টারে জল শোষণের হার বাড়িয়েছে, যেখানে SP এবং NS যোগ করে তা নাটকীয়ভাবে হ্রাস করেছে। অন্যদিকে, ৭.৫% RHA/SP/NS কংক্রিটে সর্বাধিক শক্তি এবং আরও ভাল স্থায়িত্ব কর্মক্ষমতা দেখিয়েছে। RHA, SP এবং NS সহ কংক্রিটের নমুনার সংকোচনশীল শক্তি ছিল ৩১.৭ MPa, ৩৪.১ MPa এবং ৩৩.৭ MPa। কংক্রিটের প্যাকিং ঘনত্ব বৃদ্ধি এবং ছিদ্রতা হ্রাস করার মাধ্যমে, RHA/SP/NS মিশ্রিত কংক্রিটের সংকোচন শক্তি উল্লেখযোগ্যভাবে বৃদ্ধি পেয়েছে এবং নিয়ন্ত্রণ নমুনার তুলনায় ভাল ক্লোরাইড প্রতিরোধ ক্ষমতা দিয়েছে। অনুসন্ধানগুলি পরামর্শ দেয় যে বিকল্প নির্মাণ উপকরণ হিসাবে RHA, SP, এবং NS এর সম্ভাবনা রয়েছে।

Table of Contents

List of Figures

List of Tables

NOMENCLATURE

Acronyms and Abbreviations

Acronyms	Abbreviations
SCM	Supplementary Cementitious Materials
RHA	Rice Husk Ash
SP	Silica Powder
NS	Nano Silica
ASTM	American Society for Testing and Materials
BS	British Standard
PSD	Particle Size Distribution
XRD	X-Ray Diffraction
XRF	X-Ray Fluorescence
SEM	Scanning Electron Microscopy
EDX	Energy Dispersive X-ray
UPV	Ultrasonic Pulse Velocity
RCPT	Rapid Chloride Penetration Test

Chapter 1: INTRODUCTION

This chapter outlines the background and context of the research and its purposes. Next, section describes the significance and scope of this research and provides definitions of the terms used. Finally, this chapter includes an outline of the remaining chapters of the Thesis.

1.1 BACKGROUND

Concrete is the most produced material worldwide for construction and is an essential element of civil infrastructure since no other material can compare to its strength, durability, and broad availability. Due to population growth and the need for additional buildings and infrastructure, yearly concrete production in the world is expected to expand from 10 billion to 18 billion tons by 2050, as the population of the world is expected to increase significantly from 1.5 billion to 9 billion people (Aprianti et al., 2015; Meyer, 2009). Even though 20–40% of the concrete or mortar volume is made up of cement, it releases excessive CO_2 (around 0.95 tons per ton), significantly impacting the environment (Oh et al., 2014). Cement production also consumes considerable energy, which concerns sustainable development (Venkatanarayanan & Rangaraju, 2015). According to Shafigh (2014), it is the third most energy-intensive industry, which presents a significant environmental risk to the built environment. Conventional concrete manufacturing techniques must be improved to address these economic and environmental issues. In addition, risks associated with the production of cement and industrial and agricultural waste have significantly increased the problems related to pollution and waste. Anthropogenic waste, formerly worthless and posing a disposal risk due to its propensity to contaminate the environment, is now considered a source of supplementary cementitious materials (SCM). It is anticipated that waste needs to be turned into valuable material by being replaced with other raw materials for cement production, creating affordable cement.

There are only a few feasible and accessible substitutes for cement as SCM, such as fly ash, rice husk ash, bottom ash, sugar bagasse ash, etc, which are the by-products and waste disposal material. Their suitable use would prevent the degradation of the ecosystem with the continuation of cement production sources. This readily available garbage in large quantities has no commercial value and a low cost of transportation. Several studies have demonstrated that adding SCMs to concrete can enhance its qualities and reduce construction costs (Amrutha et al., 2011). Ashes from agricultural wastes, such as Rice Husk Ash (RHA), have pozzolanic properties. Research reported that waste products can be a partial replacement for other raw materials in cement manufacturing. Secondary, calcium-silicate-hydrate (C-S-H), is produced when a pozzolanic material is mixed with Portland cement and interacts with the $Ca(OH)_2$. As a result, the pozzolanic material helps to increase the amount of the C-S-H and decrease the quantities of the water soluble $Ca(OH)_2$. Therefore, blending an appropriate level of high-quality pozzolanic material with OPC improves the quality of the cementing process (Dwivedi et al., 2006). The pozzolanic properties of RHA have been documented by several investigators (Bui & Stroeven, 1999; Committee, 1989; Mehta, 1979; Vu et al., 1997), including the INSA, Rennes team (Cisse et al., 1999), who have looked into the cause of these effects.

One of the significant factors affecting the characteristics of RHA blended cement is its burning technique and production process. Researchers used rice husk ash from uncontrolled combustion in their studies until the early 1970s. Mehta (1978) looked at how pyro processing affected pozzolanic reactivity of RHA. Pitt (1976) created a fluidized bed furnace for the regulated burning of rice husk based on his research. It was found that pozzolanic RHA can be created by carefully controlling the burning temperature and the furnace residence duration. Figure 1.1 shows different techniques to produce RHA. Following heat treatment, RHA may be found in two different forms: crystalline and amorphous. Chopra (1981) observed that the silica was mainly amorphous at incineration temperatures up to 700°C and that the crystals in the ashes

grew beyond this temperature as the material incinerated. At 800°C, cristobalite was found, and at 1150°C, both cristobalite and tridymite were still present. The amorphous RHA is a highly reactive pozzolanic substance that may be substituted for Portland cement and used in lime-pozzolana mixtures (Hasparyk et al., 2000; Sakr, 2006; Sata et al., 2007; Smith & Kamwanja, 1986; Zhang & Malhotra, 1996).

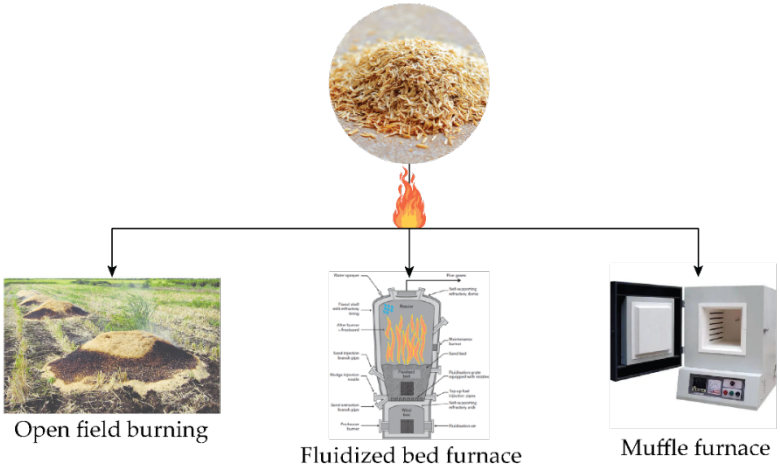

Figure 1.1: Different burning techniques of Rice Husk

Rice husk is considered an inexpensive natural silica source since it is utilized in several technical applications (Della et al., 2002). Precipitated silica from rice husk ash may be produced and used in various sectors, including the food, paint, tyre, and cosmetics industries. Some studies have reported silica produced using an extraction technique from RH combustion (Carmona et al., 2013; Rafiee et al., 2012; Suka et al., 2009). Della (2002) tried to extract silica from the RHA. They reported that 95% of the silica in the RHA sample, generated at 700°C, can be extracted. There are two primary categories of RHA silica extraction techniques: thermal and chemical. The sol-gel technique is an energy-efficient chemical process (Patel et al., 2017). It is based on synthesizing a gel-like silica network using chemical precursors. At pH<10, solubility of amorphous silica is relatively low, increasing dramatically at pH >10. Because of its distinct solubility behavior, silica may be recovered from RHA in its pure form by solubilizing in an alkaline environment and then precipitating at a lower pH (Iler,

1979; Kamath & Proctor, 1998). The production method influences the dynamics of market pricing by significantly adding to the expense of extracting silica from these natural sources. Because of the non-isothermal breakdown of rice husk ash in an air environment (Liou, 2004), nano silica (NS) particles derived from rice husk ash have a high specific surface area and are agglomerate-shaped, with dimensions ranging from 5 to 10 nm (Thuadaij & Nuntiya, 2008). It is crucial to understand that a wide range of parameters, such as soil type, climate, agricultural methods, and other relevant variables, may significantly influence the silica concentration of rice husk ash (RHA) (Bakar et al., 2016; Chen et al., 2018).

RHA is an efficient cementitious material substitute for cement in concrete and mortar (Antiohos et al., 2014; Asavapisit & Ruengrit, 2005; Kang et al., 2019; Rößler et al., 2013; Van Tuan et al., 2011; Zain et al., 2011; Zerbino et al., 2011). In an attempt to enhance the quality of concrete, several experiments have demonstrated notably favorable outcomes when low-dose nanosilica is added to concrete mixtures in place of cement (Colston et al., 2000; Du et al., 2014; Mussa et al., 2020; Xu et al., 2016; Zhang & Li, 2011). Nano silica can act as a catalyst in pozzolanic processes, facilitating the nucleation sites for calcium silicate hydrate (C-S-H) and the dissolution of tricalcium silicate (Jo et al., 2007; Rai & Tiwari, 2018).

1.2 AIMS AND OBJECTIVES

The primary goal of this study is to assess the properties of controlled-burned RHA and the silica powder and nano-silica extracted from it. Furthermore, their optimum application in cementitious systems will be evaluated. To accomplish the aim, the following specific objectives are set:

i. To evaluate the physical and chemical properties as well as microstructural and morphological phases of Rice Husk Ash (RHA), extracted Silica Powder (SP), and Nano silica (NS) from RHA.

ii. To investigate the hydration and microstructural development of cement paste with RHA, extracted SP, and NS from RHA.
iii. To evaluate fresh and hardened properties of mortar and concrete with RHA and extracted SP and NS.

1.3 SCOPE OF THIS STUDY

This study investigates the effectiveness of SP and NS extracted from RHA, as well as RHA itself, as a partial replacement for cement in various cementitious media. RHA, SP, and NS are characterized using standard techniques such as XRD, XRF, SEM, EDX, and Blaine surface area. Microstructural development with RHA/SP/NS is evaluated by SEM and EDX analysis. The fresh, hardened, and durability properties of mortar and concrete samples are evaluated, incorporating RHA, SP, and NS with CEM I at different volumetric ratios. To assess the fresh property flow value is measured in mortar samples, and workability, along with fresh density, is measured for concrete samples. Flexural strength, compressive strength, density, and volume of permeable pores are evaluated to evaluate the hardened properties of mortar samples. Additionally, for concrete samples, compressive strength, density, volume of permeable pores, and UPV tests are conducted to determine hardened properties. As a part of durability evaluation, water absorption, drying shrinkage, and sulfate resistance tests are performed for mortar samples and for concrete samples, RCPT, surface electrical resistivity, and sorptivity, along with water absorption tests are done. The replacement of CEM I with RHA, SP, and NS is done individually. Only laboratory-based experiments are included in the scope.

1.4 SIGNIFICANCE OF THIS STUDY

A key component of sustainable development is the conversion of waste into materials for construction. In developing nations, circular value chains that convert agricultural waste into building materials contribute to employment creation, reduced waste

dumping, economic growth, and environmentally sustainable building solutions. Rice husk is a byproduct of the agricultural industry. For the disposal of rice husk, open-air burning and landfilling were typically used. However, this traditional practice may lead to serious environmental issues. Rice husk silica can be extracted to provide this material with a more valuable application. Using Rice Husk Ash (RHA) as a feedstock for silica extraction could be more effective and cost-effective than directly extracting silica from rice husk. Silica can be extracted from RHA by an environmentally friendly process such as alkaline extraction. This method may also draw government incentives or subsidies for sustainable practice. The reason for selecting RHA for the extraction of nano-silica is that it is an inexpensive and readily available material. On the other hand, traditional methods for extracting silica from quartz, sand, and other sources are costly and time-consuming, as they require high temperatures and pressures. Additionally, they have a chance of hazardous effluent emissions.

Amorphous silica recovered from RHA can serve as a low-cost raw material for the manufacture of complex and technologically advanced silicon-based products. When used to manufacture concrete as a replacement for cement, extracted nano-silica from RHA offers several advantages due to its large surface area, increased reactivity, and capacity to enhance the microstructure of the cement matrix. Above all, by partially replacing cement with nano-silica, CO2 emissions can be reduced. Concrete gains strength earlier because nano silica accelerates the hydration process. This can be very helpful in projects where early load-bearing capacity is crucial.

1.5 THESIS OUTLINE

The evaluation of the performance of RHA/SP/NS as SCMs in cement paste, mortar, and concrete is organized as follows:

Chapter 1 presents the problem related to RHA and the opportunity to extract nano-silica from RHA for reducing dumping, promoting economic growth, and providing an environmentally sustainable solution.

Chapter 2 provides a comprehensive review of the literature on the nano-silica extraction process and the effect of various parameters on the silica extraction process. Besides, the physical, chemical, and pozzolanic behaviour of RHA and extracted SP/NS were reviewed.

In Chapter 3, materials and experimental design are provided with a detailed explanation. There are also details about sample preparation and testing.

In Chapter 4, results are presented along with a comprehensive discussion of the research findings. The effectiveness of the RHA/SP/NS blended cement is compared with CEM I. The relevance and significance of the findings are explored, and the data are evaluated in comparison with the literature.

In Chapter 5, the results of the experimental investigation are summarized. Additionally, the limitations and future scope of this study are discussed. The study concludes with references and an Appendix that illustrates extensive test data and calculations.

Chapter 2: LITERATURE REVIEW

This chapter outlines the rice husk preparation and, different extraction processes adopted by researchers. Physical, chemical properties, and hydration behaviour of these binders are described in this chapter. The effect of pH, NaOH, and surfactant during silica extraction is analysed.

2.1 GENERAL

This chapter reviews the fresh, hardened, and durable properties of mortar and concrete at various replacement ratios. It examines the fundamental properties of rice husk ash and nano-silica as supplemental cementitious materials.

2.2 CEMENT

Portland cement (CEM I) is the most widely used binder in a cementitious system. It offers the adhesive qualities required for adhering to masonry blocks and aggregates in concrete. Tricalcium silicate (C_3S), dicalcium silicate (C_2S), tricalcium aluminate (C_3A), and tetra calcium aluminoferrite (C_4AF) are the main components of Portland cement, which is a multi-component, multi-phase inorganic substance. Ordinary Portland Cement (OPC) is hydrated by the compounds C_3S, C_2S, C_3A, and C_4AF reacting with water to form calcium silicate hydrates (C-S-H) gel, which makes up roughly 70-75% of the cement paste in general. Secondary phases include calcium hydroxide [$Ca(OH)_2$], which makes up about 20-25%, and sulfoaluminate, which makes up 7% (Neville, 2011).

2.2.1 Hydration of cement

Different cement compositions react with water during the phase-by-phase hydration process to generate new solid products and release heat. Cement hydration results in a hard, porous material. Tazawa et al. (1995) claim that one chemical Equation cannot

adequately describe the chemical hydration reaction process in mortar or concrete. The following equations can be used to characterize the cement hydration process in mortar or concrete:

Tricalcium silicate (C_3S):

Calcium silicate hydrate (C-S-H), the main component that provides cement its strength, and calcium hydroxide (CH), which adds to alkalinity, are the products of the fast reaction between tricalcium silicate (C_3S) and water.

$$2(3CaO.2SiO_2) + 6H_2O \longrightarrow 3CaO.2SiO_2.3H_2O + 3Ca(OH)_2 \quad \text{(Eq. 2.1)}$$

Dicalcium silicate (C2S):

Although it reacts more slowly, dicalcium silicate (C_2S) may generate calcium silicate hydrate (C–S–H) and calcium hydroxide (CH) similarly.

$$2(CaO.SiO_2) + 4H_2O \longrightarrow 3CaO.2SiO_2.3H_2O + Ca(OH)_2 \quad \text{(Eq. 2.2)}$$

Tricalcium aluminate (C3A):

Early on, ettringite ($C_6A_6S_3H_{32}$), crystals that are like needles) is formed when tricalcium aluminate (C_3A) combines with water and gypsum, which is introduced during grinding. This assists in managing the cement setting time. Ettringite turns into monosulfat (C_4ASH_{12}) when the gypsum is depleted.

$$3CaO.Al_2O_3 + 3(CaSO_4.2H_2O) + 26H_2O \longrightarrow 3CaO.Al_2O_3.3CaSO_4.32H_2O \quad \text{(Eq. 2.3)}$$

$$3CaO.Al_2O_3.3CaSO_4.32H_2O + 2(3CaO.Al_2O_3) + 4H_2O \longrightarrow 3(3CaO.Al_2O_3.CaSO_4.12H_2O) \quad \text{(Eq. 2.4)}$$

Tetracalcium aluminoferrite (C4AF):

While it contributes less to the overall strength development, tetracalcium aluminoferrite (C_4AF) responds similarly to C_3A.

$$4CaO.Al_2O_3.Fe_2O_3 + 3(CaSO_4.2H_2O) + 27H_2O \longrightarrow C_3(Al_2O_3.Fe_2O_3)_3.CaSO_4.32H_2O + Ca(OH)_2 \quad \text{(Eq. 2.5)}$$

Figure 2.1 introduced the hydration of cement paste, which went through many phases of differentiation, showing the development of numbered peaks (Taylor, 1997).

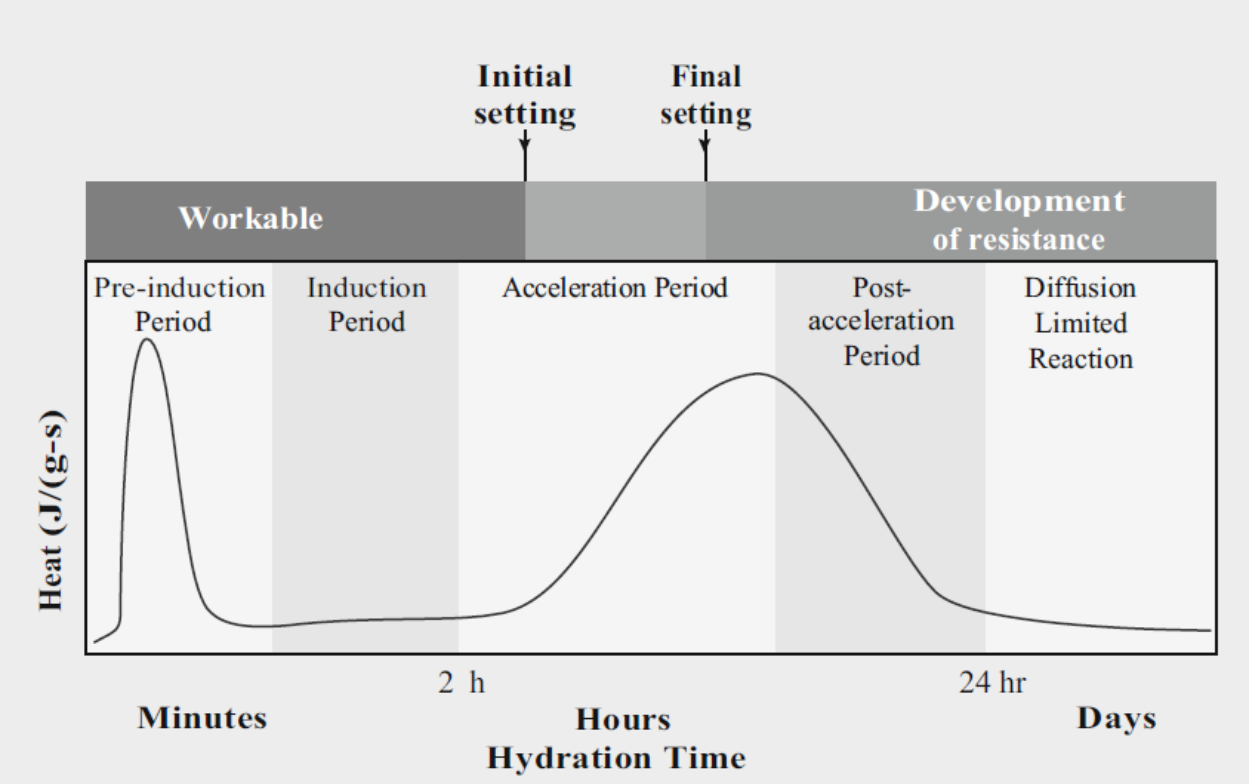

Figure 2.1: Heat rate growths during hydration of Portland cement (Taylor, 1997)

Pre-induction period:

The cement and water mixture causes a short period of rapid responses in the first few minutes. At that time, a layer of amorphous gel rich in alumina is formed around the cement particles due to the primary reactions between C_3A and C_4AF with water and gypsum.

Induction / dormant period:

In this stage, there is a short period of low activity after the quick initial reactions in the first minute. Small-scale chemical reactions generate very little heat.

Acceleration / post-induction period:

The rate of heat release and hydration responses reaccelerate, peaking generally less than 12 hours after the first mixing. The primary cause of this behaviour is the

hydration processes of tricalcium silicates (C_3S), which create a layer of C-S-H gel around the cement particles, referred to as "outer C-S-H."

Post-acceleration period:

During this time, the rate at which heat is released progressively decreases. As time passes, the percentage contribution of C_2S to the formation of the C-S-H phase rises.

Diffusion-limited reaction period:

The diffusional constraint of chemicals in the solid form causes reactions to dramatically slow down after 1-3 days of cement hydration.

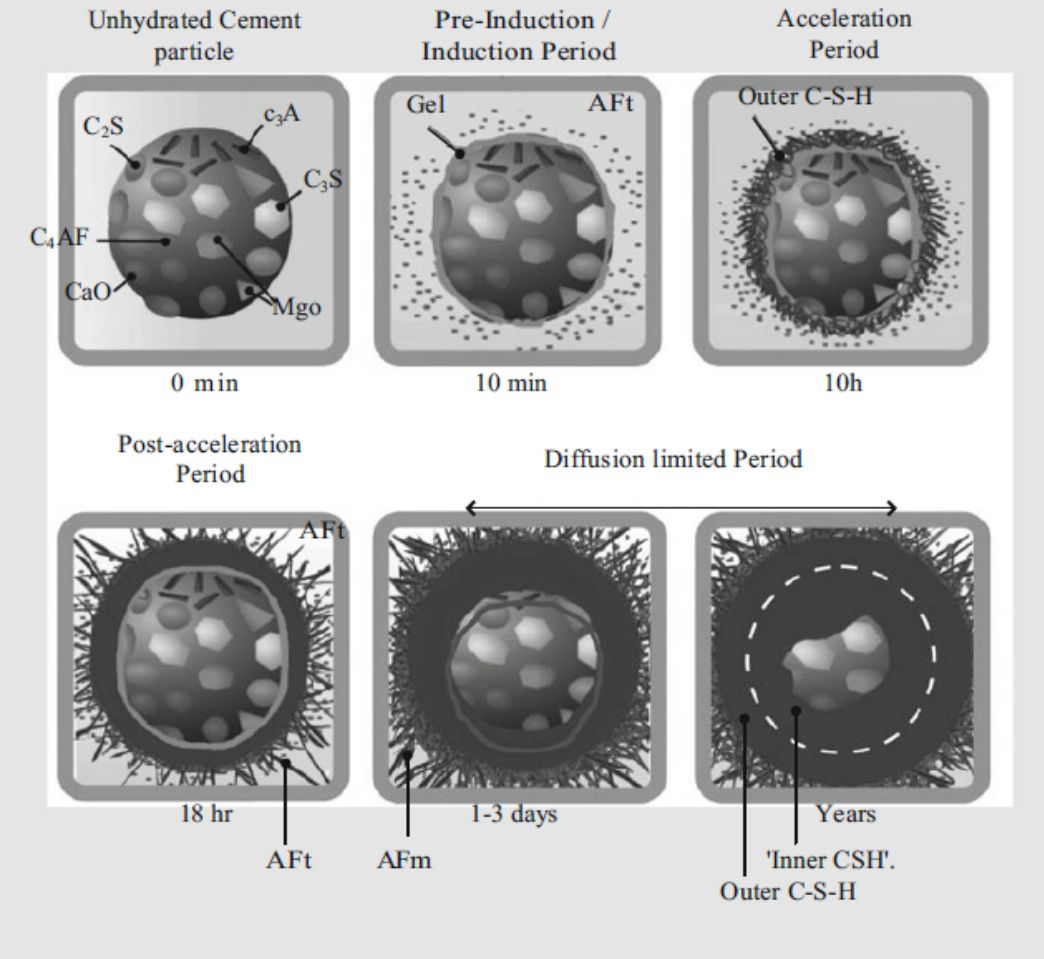

Figure 2.2: Diagram showing the phases in which a polymineral cement particle hydrates (Gonç alves & Fernanda, 2015)

2.3 SUPPLEMENTARY CEMENTITIOUS MATERIALS

In literature, "supplemental cementitious materials" refer to finely divided elements that, either by pozzolanic activity, hydraulic activity, or both, improve the characteristics of concrete. By creating secondary hydrated binder phases of calcium silicate hydrate (C-S-H) or calcium aluminosilicate hydrate (C-A-S-H), cementitious materials are compounds that take part in the hydration processes (Diamond et al., 2004; Taylor, 1997; Massazza, 1998; Moranville-Regourd, 2002; Richardson, 2008). Through their densification, these phases help cement matrices become more durable and have better mechanical properties. A portion of the costly cement used in mortar and concrete can be substituted with these SCMs. Classifications for cementitious materials include-

Pozzolanic materials:

Compounds that include siliceous or aluminosilicates react with water and calcium hydroxide (CH) to produce calcium aluminosilicates hydrate (C-A-S-H) or calcium silicates hydrate (C-S-H). The calcium silicates in the cement may have hydrolyzed, producing the CH employed in this process.

Latent hydraulic binders:

Calcium aluminosilicates gradually react with water to form a complex, spontaneous compound. Thus, the presence of an alkaline activator is necessary for the hardening process to become important. This molecule facilitates the development of C-A-S-H phases and the dissolution of ionic species by breaking the chemical bonds in the amorphous (or glassy) phase of binder.

2.3.1 HISTORY OF POZZOLANS

There are two different interpretations of the word "pozzolan." The initial one denotes the pyroclastic rocks, which are primarily glassy and occasionally zeolitized and may be found in Pozzuoli (the ancient Puteoli from Roman times) or the vicinity of Rome

(Stanley, 1982). The second definition encompasses any inorganic materials, natural or artificial, that, when combined with calcium hydroxide (lime) or compounds that can release calcium hydroxide, harden in water (Portland cement clinker). The Los Angeles aqueduct required the usage of more than 100,000 tons of pozzolana between 1910 and 1912. Pozzolanas have since been employed in marine structures and mass concrete construction in North America, Europe, and Japan. Since the most widely recognized categorization focuses on the pozzolanas' origin, the first separation is between natural and artificial pozzolans. Natural materials just need to be ground; artificial pozzolanas are made by altering the structure or composition of materials that were nonexistent or had very weak pozzolanic qualities.

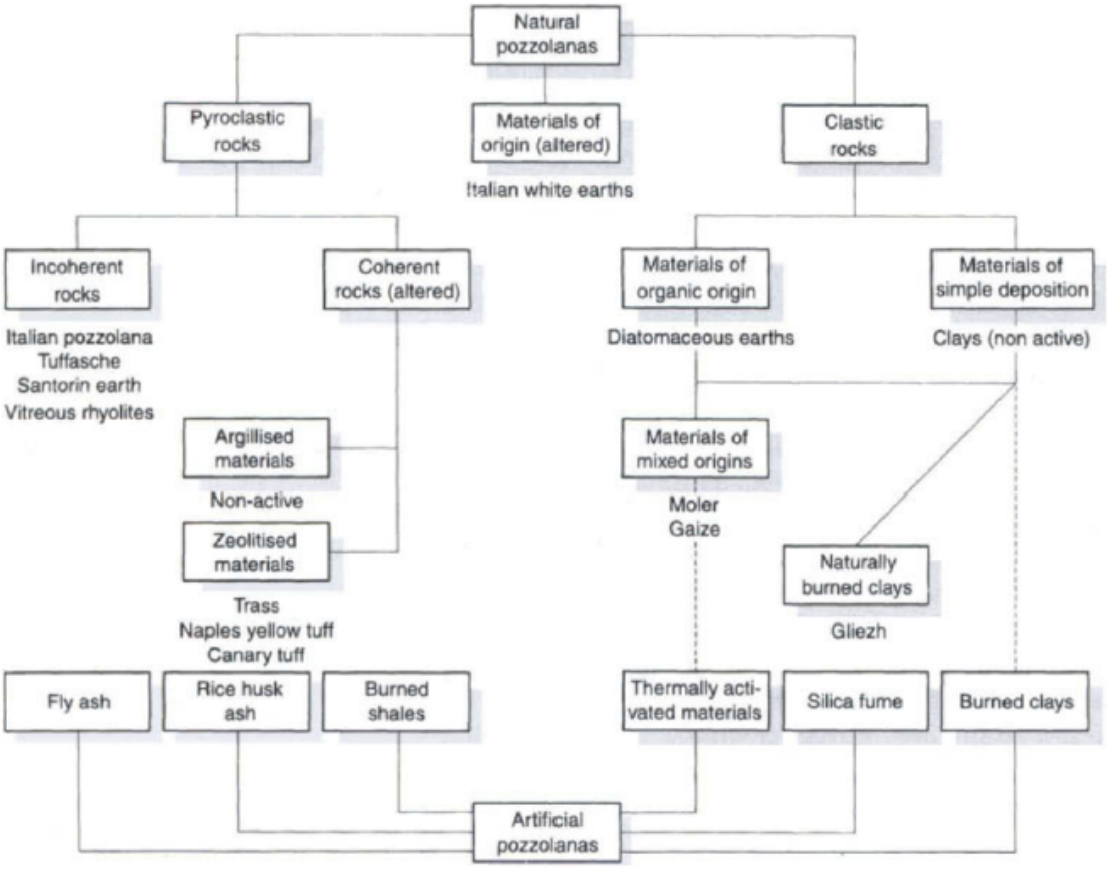

Figure 2.3: Classification of pozzolans (Fookes, 1985)

2.3.2 Mechanism of Pozzolanic Reaction

A siliceous or aluminous chemical combined with calcium hydroxide (C-H) in the presence of moisture often produces a pozzolanic reaction. According to (Villar-Cociña et al., 2003). The pozzolanic reaction will not begin until CH is released and a pozzolanic material is added to a mortar or concrete mix. The two primary ingredients of cement, C_3S and C_2S, hydrate to produce lime. The following is a representation of this response.

$$Ca(OH)_2 + SiO_2 + H_2O \longrightarrow C - S - H \qquad \text{(Eq. 2.6)}$$

The highest amount of lime that a pozzolana can combine with and the rate at which such a combination happens are the two criteria that constitute the phrase "pozzolanic activity." The quality and quantity of the active phases, or more specifically, the type of pozzolanas, determine both parameters. It is widely acknowledged that the following factors primarily determine the total amount of mixed lime: the specific surface area (BET) of the pozzolana, the water/solid mix ratio, temperature, the type of the active phases, their content in pozzolana, SiO_2 content, lime/pozzolana ratio in the mix and the duration of curing (Massazza, 1998).

Pozzolan-lime interactions happen slowly and usually begin one or more weeks later (Givi et al., 2010a). As a result of this delay, pozzolanic concrete will initially be more permeable but will eventually become denser than regular concrete. (Givi et al., 2010a) provides two explanations for this conduct. First, pozzolanic reactions are inhibited by the precipitation sites created by pozzolan particles for the early hydration of C-S-H and C-H. Second, the alkalinity of the pore water plays a crucial role in the breakdown of the glass phase since it can only reach a high pH after several days. The function of SCM in cement-based material hydration and their contribution to pozzolanic activity has been validated by earlier research. These results led to the classification of SCM reactivity processes into four main impacts: chemical, dilution,

nucleation, and filler effects. The ability of SCM particles to fill in spaces between cement grains, densifying the concrete microstructure and enhancing strength, is demonstrated by the filler effect (Ndahirwa et al., 2022). Additional nucleation sites offered by SCMs speed up the reaction process by facilitating the production of hydration products. SCMs may, however, have a diluting effect when added in large amounts, delaying pozzolanic reactivity and lowering the heat of hydration.

2.3.3 Advantages of using pozzolans

Pozzolanic materials can potentially replace some of the clinker or cement with the following benefits (Gonç alves & Fernanda, 2015):

Environmental:

Limit the fuel used and CO_2 emissions produced during the clinker production process. Because they are industrial byproducts, pozzolanic materials also help to reduce the number of natural resources extracted for their raw materials, as well as the dust, noise, and vibration that come with preparing raw materials for clinker production. Reusing byproducts also decreases the quantity of garbage dumped in landfills.

Economic:

Lower the cost of producing cement and enhance profits by adding value to waste when employing an industrial by-product.

Technological:

The densification of the cement/pozzolans blended paste matrix improves durability by reducing the rate and total amount of heat released because the hydration reaction of pozzolanic materials is less exothermic than that of cement, increasing mechanical properties due to the additional formation of C-S-H or C-A-S-H phases that contribute to the cement paste matrix densification; and reducing the likelihood of deleterious reactions occurring.

Due to their generally low alkali concentration, pozzolanic elements lower the overall alkali content in the concrete mix. This helps avoid several problems with durability, such as efflorescence (the build-up of salt deposits on the surface of concrete) and the alkali-silica interaction.

2.4 RICE HUSK ASH

One of the many agricultural by-products plentiful in many rice-producing nations worldwide is rice husk. About 200 kg of rice husk may be produced from one ton of paddy rice, and 40 kg of ash can be produced when the husk is burned (Bui, 2001). In the fiscal year 2020–21, Bangladesh produced 37.61 million metric tons of paddy, according to data from the Bangladesh Bureau of Statistics (BBS). 20% of them, or 7.52 million metric tons, are regarded as rice husks. In Bangladesh, the output of rice and rice husk is rising continuously. According to the map shown in Figure 2.4, the districts with the largest ash generation include Dinajpur, Mymensingh, Bogura, Naogaon, Rangpur, and Jashore.

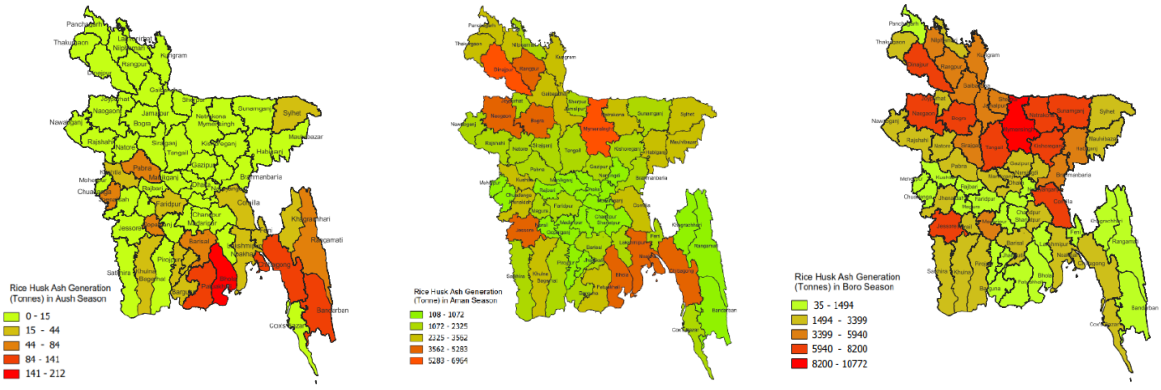

a) Aush season (April to July)

b) Aman season (July to November)

c) Boro season (November to April)

Figure 2.4: Rice husk ash generation in different seasons of the year 2020-21 (Hossain et al., 2024)

The rice plant takes silica from the soil and incorporates it into its structure as it grows (Smith & Kamwanja, 1986). The husk covers the grains and has a high silica

concentration, typically between 80 - 85 % (Siddique, 2004). When husks accumulate in large quantities to disrupt the surrounding environment, it is considered waste. Its poor nutritional content makes it unsuitable for use as animal feed, and it is typically indigestible for humans. When rice mills parboil rice, burning rice husk yields rice husk ash (RHA). Approximately 75% of the husk comprises organic volatile materials, with the remaining 25% being burned to produce ash (NPCS, 2013). These ashes are often disposed in open areas near the rice mills. The material includes a high level of silica (more than 90% of the total content) and very tiny particle sizes (59% of the particles had diameters smaller than 0.05 mm) (Farooque et al., 2009).

RHA is created by calcining rice husk, as was previously mentioned. As the cellulose-lignin composition of rice husk is burned, porous ash with a high silica content and a low concentration of alkali and other elements is left behind. Controlling the burning temperature is necessary to maintain the amorphous form of silica since it has a considerable impact on the chemical composition of RHA. Nonreactive silica minerals called cristobalite and tridymite are present in significant proportions in the ash that results from uncontrolled combustion, such as in open field burning or industrial furnaces operating at temperatures above 700°C to 800°C. The primary component of ash under controlled combustion, which involves burning at temperatures between 500 and 700°C for approximately an hour, is amorphous silica. The reactivity of this form of silica is attributed to its presence and to the large surface area that results from the microporous structure of ash particles. In general, controlled combustion produces a finer RHA than open heap incineration. Furthermore, RHA produced by open heap combustion has a lower reactive ash concentration and a higher residual carbon content.

Potassium makes up the bulk of the Alkali, a high percentage of non-silica elements found in rice husk ash, varying generally from 0.18% to 3.68% of the weight of ash (Mehta, 1994). As long as the sodium concentration is below 1.12% (Giaccio et al.,

2007). As per ASTM C618 (2023), the total weight of the pozzolanic material shall include at least 70% silicon oxide (SiO_2), iron oxide (Fe_2O_3), and aluminium oxide (Al_2O_3). Alkali oxides and residual carbon constitute the majority of the contaminants in RHA. It is challenging to get RHA with the same or nearly identical composition since the chemical characteristics of RHA differ depending on the source. Because of its low calcium oxide (CaO) content (less than 10%), RHA is categorized as a Class N pozzolan.

As a natural pozzolan, rice husk ash exhibits cementitious qualities when combined with lime (Cook, 1986; Mehta & Pitt, 1976). Much research has demonstrated that rice husk ash may be utilized as an additional cementitious material when mixed with cement to create concrete products because of its high amorphous silica concentration (Bakar et al., 2011; Barkakati et al., 1994; Ganesan et al., 2008). Rice husk utilization is influenced by a number of factors, including the reactivity of pozzolan in cement and concrete and chemical purity for the production of new materials (Chandrasekhar et al., 2006).

2.4.1 Preparation of Rice Husk Ash

The temperature and grinding method are the two elements that affect the production of rice husk ash. Between 500 and 800°C is generally considered to be the ideal burning temperature, according to research on optimal burning temperatures, rates of heating and cooling, and other factors (Bakar et al., 2016; Habeeb & Mahmud, 2010; Kang et al., 2019; Mboya et al., 2017; Olawale & Oyawale, 2012; Ramezanianpour et al., 2009). Organic matter can still be found in the ash below 500 °C. With a crystalline structure, a pozzolanic phase reaction of strength-forming hydrates, i.e., C-S-H formation, is impossible. Above 800°C, silica undergoes a structural change from amorphous to crystalline, reducing the pozzolanic reactivity between the RHA and the remaining portlandite (C-H) from the first hydration reaction. Yeoh (1979) stated that if the combustion duration was shorter than one hour, RHA silica may continue to exist in

its amorphous form even at temperatures as high as 900°C. When the temperature and time exceeded this range, the silica became crystalline. However, Nair (2008) found that if the combustion time is shorter than five minutes, temperatures as high as 1000 ºC may be reached. In most research, combustion periods under controlled settings are less than one hour (Hwang & Chandra, 1996). The volume of burnt ashes determines the duration of the combustion process. According to the findings of James & Rao (1986), the presence of minor elements in the RHA, such as Na, K, Mg, and Ca, is associated with the phenomena of changes in silica from amorphous to crystalline, which lowers the temperature at which the silica transforms. Researchers have generally concluded that further research is necessary on this topic since it is unclear at what temperature amorphous silica turns crystalline. The porosity of the RHA is affected by the heating rate; Chandrasekhar (2006) studied the increase in pore volume as the heating rate increased. Meanwhile, because of a larger inner specific surface area, reactivity rises with porosity. This has a good impact on ultimate strength (Chandrasekhar et al., 2006) but a detrimental impact on water adsorption and workability (Msinjili et al., 2017; Nair et al., 2008).

The fineness of RHA is decided by the grinding procedure. The mean particle diameter of RHA decreases as grinding energy and duration increase. The specific surface area of this material is often 10 to 100 times larger than that of cement and 5 to 10 times higher than that of silica fume, owing to its structure, which is frequently referred to as a honeycomb structure (Singh & Singh, 2015). The interior porosity of RHA reduces as fineness increases. By making the pozzolanic material more finely ground, reactivity may be elevated. However, according to Mehta (1979), RHA gets its pozzolanic activity mainly from the interior porosity of the particles; hence, it is best to avoid grinding it too small.

2.4.2 Combustion

The most popular technique for extracting silica from rice husks is direct burning, which yields 85–95% silica-containing rice husk ash (Fernandes et al., 2016; Lee et al., 2017; Zulfiqar et al., 2015). Both residential and commercial operations employ this technique, which may be carried out in open-fire stoves or various boiler types, including fluidized beds, stokers, and suspension-fired boilers (Witchakorn & Bundhit, 2004). Using heat exchangers, the heat generated during this burning process is either used to create steam or to be used again for drying processes. However, considerable amounts of particulate matter and greenhouse gases are released when the rice husks are directly burned (Junpen et al., 2018; Lasko & Vadrevu, 2018). Burning rice husk releases CO_2, CH_4, CO, NOx, SO_2, PM2.5, and PM10, all forms of black carbon. Therefore, it is crucial to constantly employ a dust collector and a gas absorber while using direct combustion. Remarkably, most organic chemicals included in the raw materials may be effectively eliminated by direct thermal burning of rice husks.

The phase transition of the silica material generated is significantly influenced by the temperature at which rice husk burns. The natural form of silica in rice husks is in a non-crystalline phase. Still, the methods used for combustion—whether with or without air—have a significant impact on the final silica compound composition. Tridymite and cristobalite phase transition begins at temperatures over 600°C during combustion (Nakata et al., 1989). However, depending on the chemical composition of rice husk ash, different temperatures were needed for crystallization (Beidaghy Dizaji et al., 2019). Variations in RHA composition are caused mainly by soil type, weather, agronomic practices, and other factors (Alvarez et al., 2014; Rößler et al., 2014). Fewer metal contaminants were found at a higher combustion temperature (900 °C). The creation of less stable and more volatile phases that are easily discharged into the gas phase might cause this phenomenon. Furthermore, high combustion

temperatures can cause sticky alkali silicate compounds to develop from alkali metal impurities in rice husk ash, including potassium, phosphorus, calcium, and magnesium. Due to the melting and agglomeration of the ash caused by these chemicals, meso and micropores decrease, and particle size increases (Soltani et al., 2015). By changing the combustion conditions, the shape, particle size, pore size, and uniformity cannot be adjusted. According to earlier research, various characteristics of silica, such as its specific surface area (11–39 m^2 g^{-1}), purity (29.7–96.7 wt%), and crystallinity (fully amorphous or partly crystalline), may all fluctuate within a specific range (Dizaji et al., 2019). Gomes et al. (2016) have carried out an extensive study of the production of rice husk ash (RHA) using bubbling fluidized-bed combustion (BFBC). They looked at several important factors, such as elutriation behavior, fluidization velocity, and combustion temperature, which directly affect the properties and purity of the resultant silica.

2.4.3 Pozzolanic Reaction of RHA

A siliceous and aluminous material that possesses little or no cementitious value can be classified as a pozzolan. However, when combined with calcium hydroxide at room temperature and in finely divided form, it will chemically react to form compounds possessing cementitious properties (Mehta & Pirtz, 1978). Through its pozzolanic reaction, RHA, a very fine material, may replace cement because of its microporous structure and predominantly amorphous silica (≥70%). Two parameters, namely the non-crystalline silica content and its specific surface, work together to determine the reactivity of RHA in lime (El-Dakroury & Gasser, 2008). When cement hydrates, RHA combines with lime to generate C-S-H, which is exactly what other common pozzolans do. More C-S-H is produced by the pozzolanic reaction when RHA is added because it reduces the C-H created when cement hydrates. The strength and durability of concrete are often enhanced by this (Azizi & Yousefpour, 2008; Givi et al., 2010a). Research has indicated that replacing cement with rice husk ash might

speed up the early hydration of C_3S. This can be verified by the large specific surface area of rice husk ash (Feng et al., 2004). This behavior is most noticeable when RHA particles are small. Pozzolan small particles create many nucleation sites for the precipitation of hydration products when they disperse in cement pastes, although they are less reactive than Portland cement (Mehta & Aïtcin, 1990). As a result of the pozzolanic interactions between the calcium hydroxide (CH) and the amorphous silica in the mineral admixture, this process produces a more uniform and denser paste in terms of the distribution of the finer pores (Isaia et al., 2003). Amorphous silica content, particle fineness, and specific surface area all affect RHA reactivity (Khan et al., 2015; Raman et al., 2011; Shukla et al., 2011; Zain et al., 2011).

2.4.4 Physical Properties of RHA

Rice husk combustion temperature is the primary determinant of the physical properties of RHA, such as fineness, color, particle size, and shape. For freshly produced concrete, characteristics like workability, bleeding, and segregation are more influenced by the physical characteristics of RHA. As previously indicated, the high internal surface area of RHA gives it pozzolanicity; hence, grinding this ash to a very fine texture will not be beneficial. While fine-grinding RHA might not increase its reactivity, it can change the pore structure and decrease water absorption.

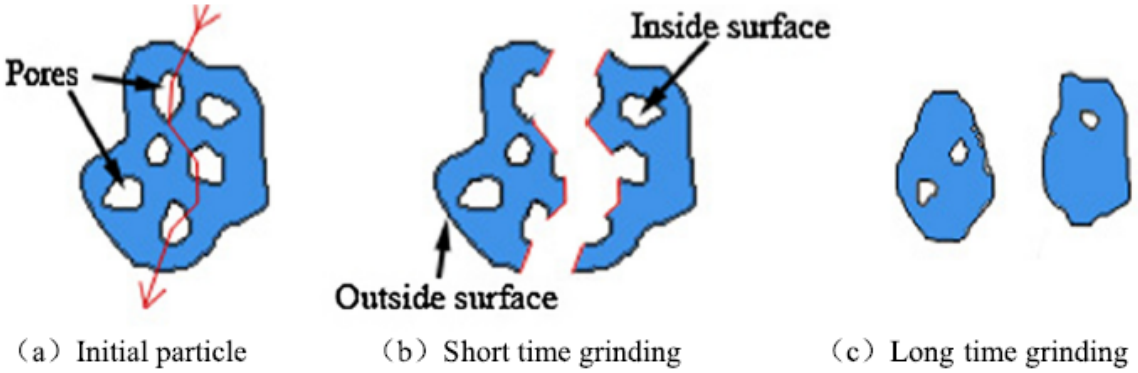

Figure 2.5: RHA particle state changes during grinding (Van Tuan et al., 2011)

The agglomeration process is caused by the collapse of the porous structure of RHA particles (shown in Figure 2.6) when the particle size reduces due to an increase in grinding particles. To improve RHA performance, it is thus essential to determine the proper fineness of RHA. According to Della (2002), the rate at which specific surface area decreases is directly related to the heating temperature and duration. Prolonged heating at high temperatures causes an accumulation effect that reduces porosity. Through refining and chaining the formation of unfavorable crystals during the hydration process, the RHA particle size influences the pore structure (Givi et al., 2010a). Lastly, the mineralogical phase and grinding duration significantly influence the size and form of the particles. RHA can be light grey, grey, or nearly black, depending on how the rice husks burn.

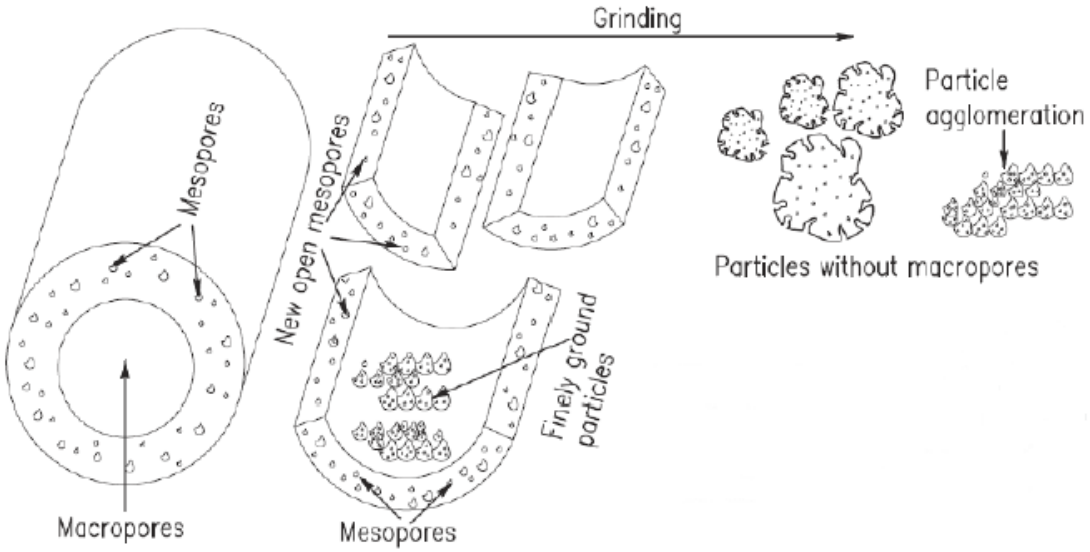

Figure 2.6: Various RHA particle phases and how they affect the pore volume throughout the grinding process.

2.4.5 Chemical Properties of RHA

The principal chemical component of RHA is SiO_2. These substances cause its pozzolanic action. In addition, it contains unburned carbon, Al_2O_3, Fe_2O_3, CaO, MgO,

TiO, P_2O_5, SO_3, and Na_2O. The performance of mortar or concrete may be impacted by these trace components, which can also affect the chemical and physical characteristics of RHA. The pozzolanic activity of RHA and efficacy as SCM in concrete and mortar applications are mostly determined by its chemical characteristics, which include its silica concentration, amorphous nature, alkalinity, carbon content, and trace element composition. Plant composition can vary from one to the next and even within a single plant on occasion. $SiO_2 + Al_2O_3 + Fe_2O_3 \geq 70\%$ and residual carbon content (loss on ignition) $\leq 12\%$ will be the two main ingredients that will generally vary.

2.4.6 Hydration of Cement Blended RHA

Once $Ca(OH)_2$ has been released from cement hydration, adding RHA to the mortar or concrete mix will initiate the pozzolanic process. OH^- and Ca^{2+} combine with SiO_2 or Al_2O_3-SiO_2 structure in the silica-lime reaction to create calcium silicate hydrate (C-S-H), calcium aluminate hydrate (C-A-H), and calcium aluminate ferrite hydrate (C-A-F-H) (Givi et al., 2010a; Ngun et al., 2010).

Calcium silicate hydrate:

$$2SiO_2 + 3Ca(OH)_2 \longrightarrow 3CaO.2SiO_2.3H_2O \quad \text{(Eq. 2.7)}$$

Calcium aluminate hydrate:

$$Al_2O_3 + Ca(OH)_2 + H_2O \longrightarrow CaO.Al_2O_3.Ca(OH)_2.H_2O \quad \text{(Eq. 2.8)}$$

Calcium aluminate ferrite hydrate:

$$Fe_2O_3 + Ca(OH)_2 + Al_2O_3 + H_2O \longrightarrow Ca(OH)_2.Al_2O_3.Fe_2O_3.H_2O \quad \text{(Eq. 2.9)}$$

As a result of the free lime being transformed into an insoluble C-S-H gel during the subsequent hydration reaction, the extra C-S-H creation helps to improve the durability and strength of concrete. As shown in Figure 2.7, Hwang & Chandra (1996) divided the interaction process into four sequential phases of time to describe the

hydration process response in cement paste with RHA. The water-binder ratio and RHA concentration are directly correlated with how RHA affects cement hydration (van Nguyen, 2011). The primary hydration exothermic peak is postponed with a fixed w/b ratio as the RHA concentration rises and the cement content in the pastes falls. At unchanged RHA concentration, the major hydration exothermic peak and acceleration period develop somewhat sooner with greater w/b.

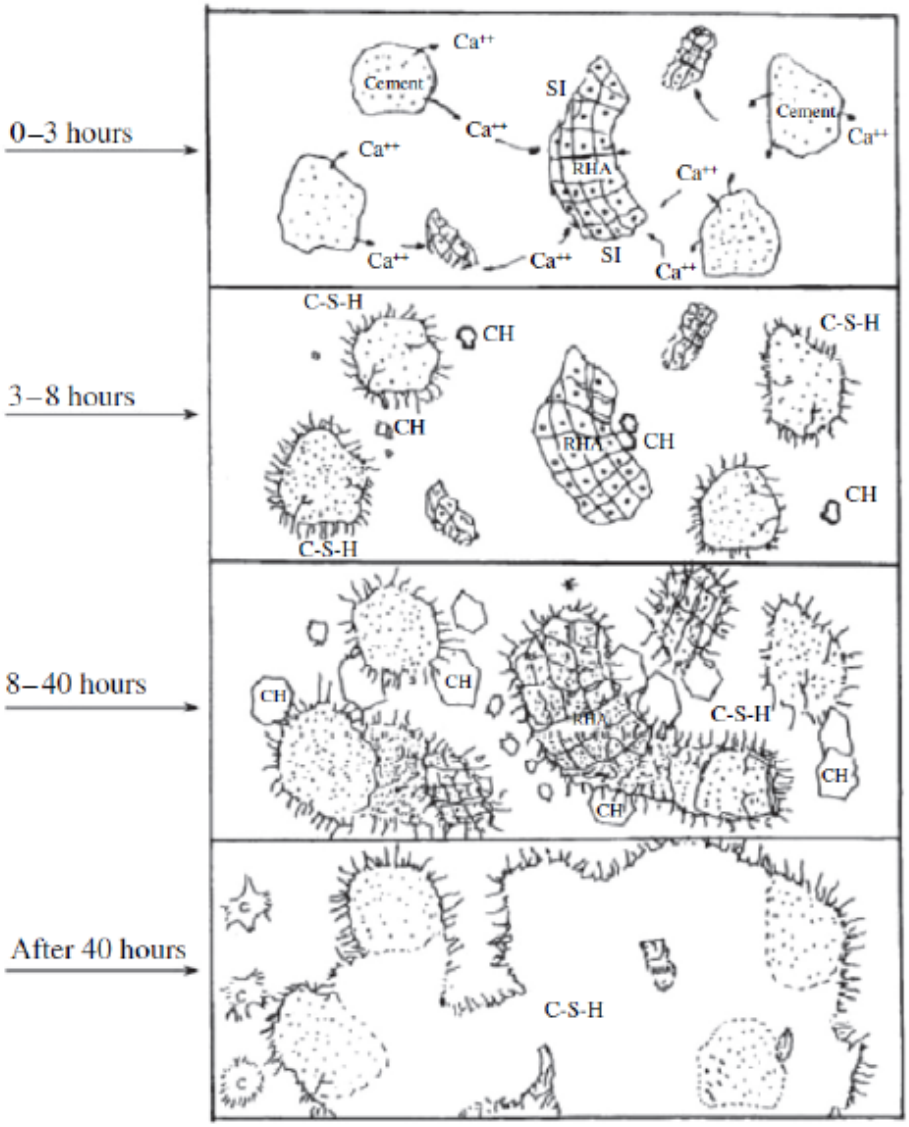

Figure 2.7: Diagrammatic representation of the hydration process of cement paste with RHA

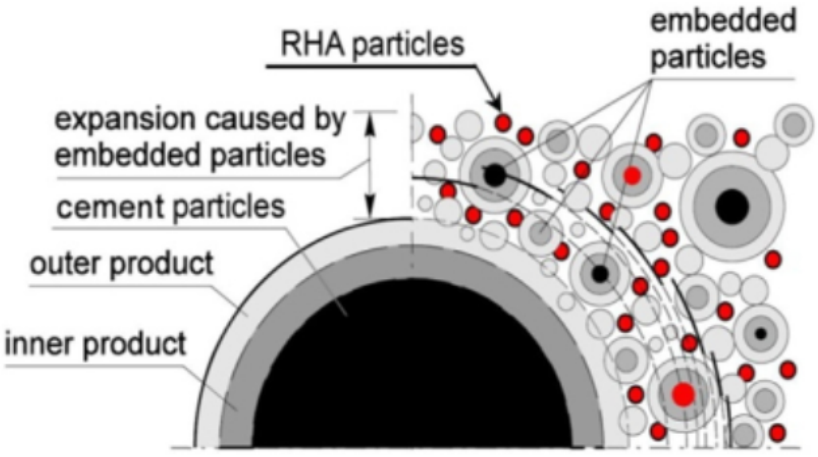

Figure 2.8: Cement and RHA particle hydration products in the shell layer (van Nguyen, 2011)

2.4.7 Silica in Rice Husk Ash

In the agricultural field, silica is regarded as a crucial micronutrient that is essential for the development and growth of plants. Additionally, it strengthens the leaves, shoots, and roots, increases their resistance to weather, and lessens the harmful effects of some poisonous soil components. During germination, silica can accelerate germination by sterilizing and destroying fungus.

The two main types of silica, a common substance in the crust of the Earth, are amorphous and crystalline. The main and adaptable silica polymorph identified in rice husk ash (RHA) extraction is amorphous silica (a-SiO_2). This silica is common in RHA and does not have the long-range atomic order seen in crystalline structures. The main methods used to extract amorphous silica from RHA are calcination or pyrolysis, often carried out between 550 and 750°C (Pedersen et al., 2010). These moderate temperatures are used to prevent crystallization, as is seen in cristobalite and quartz, and to preserve the amorphous properties. Amorphous rice husk silica finds application in several industries, including rubber, activated carbons, energy storage materials, drug delivery, carbon capture materials, glassmaking, steel, cement,

pharmaceuticals, paints, soap, cement pozzolan, and silicon integrated circuit insulators (Pode, 2016), as illustrated in Figure 2.9.

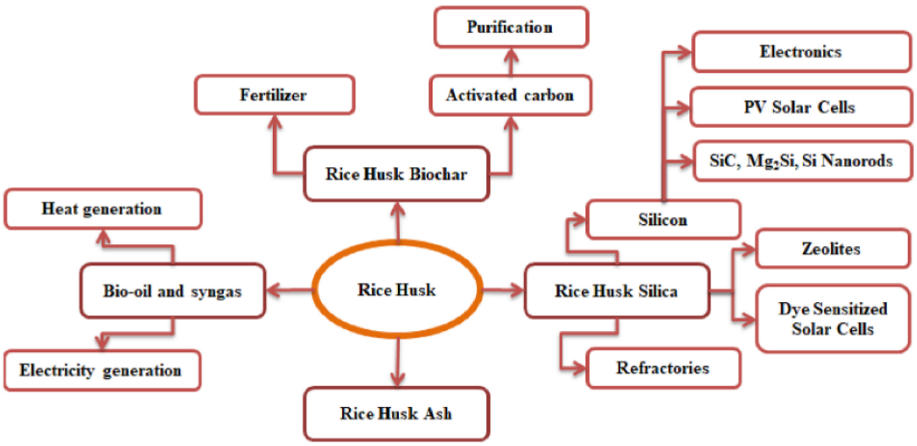

Figure 2.9: Diagram of application of rice husk (Hamidu et al., 2025)

2.5 EXTRACTION OF NANO SILICA FROM RICE HUSK ASH

Since silica has special qualities and can be found in large quantities in rice husks, its demand is increasing across many industries. Although the initial source is rice husk, several methods are employed to extract silica from different kinds of rice husk, such as ash. Impurities or undesirable elements must be eliminated from the raw materials to extract silica. Three techniques have been employed for extracting silica from rice husk: alkali extraction, acid leaching, and combustion (Chun & Lee, 2020).

2.5.1 Alkali Extraction

This method allows for the synthesis of silica from rice husk by dissolving it in an alkali medium such as KOH, Na_2CO_3, or NaOH and then precipitating it with an acidic media such as hydrochloric acid, sulfuric acid, citric acid, acetic acid, and oxalic acid. For pH values greater than ten, silica becomes much more soluble (Kalapathy et al., 2002). As a result, alkaline solvents are used to extract silica from rice husk ash (RHA). Before alkali extraction, the lignin is often removed by heat treatment to prevent silica and lignin from being extracted from rice husks. This might have an adverse influence

on the quality of the sodium silicate that is produced. Organosolv fractionation is another method, in addition to thermal treatment, that may be used to separate lignin using organic solvents like ethanol (Kim et al., 2019) and 1,4-butanediol (Zhang et al., 2015). The phenolic chemicals that are produced when the lignin is broken down by alkali extraction, such as coniferyl aldehyde, ferulic acid, and benzoic acid, cannot be used in other processes.

In earlier research, the starting materials for alkali extraction have been acid-treated rice husk or rice husk ash (Hossain et al., 2018; Jung et al., 2010; Pathak et al., 2020). Sodium silicate, which may be utilized as a precursor for Si-based products, is typically created by extracting silica from rice husk using sodium hydroxide (Chun et al., 2020; Jang et al., 2022; Kim et al., 2021).

$$SiO_2\ (s) + 2NaOH\ (l) \longrightarrow Na_2SiO_3\ (l) + H_2O\ (l) \qquad \text{(Eq. 2.10)}$$

Solvent concentration and the solvent-to-RHA ratio are two variables that impact the extraction process. The high concentration and usage of NaOH analytical grade solvent in the extraction process will impact the increased cost of producing silica. NaOH concentration will increase Na+ ion concentration and result in a greater Si reaction. An increase in NaOH concentration above 4N, according to Costa & Paranhos (2018), would not improve Si recovery. The solid SiO_2 and liquid NaOH reaction occurred at a 1:2 stoichiometric ratio, according to the reaction shown in Equation 2.11. In this instance, the SiO_2 conversion was not increased by the NaOH solution (Doran, 1995). Once filtered, the liquid was separated from the dispersion. When the latter was acidified with concentrated sulfuric acid, the dissolved silicate precipitated as a white, gelatinous solid (SiO_2).

$$Na_2SiO_3 + H_2SO_4 \longrightarrow SiO_2 + Na_2SO_4 + H_2O \qquad \text{(Eq. 2.11)}$$

Many researchers have used different concentrations of alkaline and acid to extract silica from acid-treated RHA or RHA, as summarized in Table 2.1. Using alkaline

solvents has several benefits, including ease of use, long-term storage stability, strong adsorption and ion exchange capabilities, and adjustable features upon combustion temperature (amorphous, quartz, cristobalite, and tridimite). The technique is easy, reasonable, reliable, and reproducible. Agglomerated silica could be produced by this method. The non-conductive nature of silica contributes to this since it accelerates the accumulation of charges on the surface of powder even after paladium sputtering. However, as concentration of NaOH increases, it is evident that the homogeneity of the agglomerated spherical shape of silica particles improves.

2.5.2 Acid Leaching

Acid leaching, the process of dissolving metallic impurities in a strong acid solution, produces high-purity silica in the solid phase. To get rid of organic compounds and metallic impurities, rice husks can be acid-treated either before or after the combustion process. Acid leaching is the general term for acid treatment performed before heating (Azat et al., 2019). More precisely, it is called acid extraction when the acid treatment is done after combustion to get silica from the ash (Nayak & Datta, 2021). Reports have shown that silica extraction from rice husks can be achieved more successfully with mineral acid leaching than with untreated rice husks.

The most efficient acid for removing metallic components is HCl (Vayghan et al., 2013), although HNO_3 (Liou & Yang, 2011), H_2SO_4, and other acids have also been tried in different doses. Acid solutions can dissolve organic and metallic pollutants from rice husk, depending on the concentration, reaction time, and temperature of the solution (Zulkifli et al., 2013). Many studies have shown that silica may become more amorphous as a result of acid leaching (Ahmad Alyosef et al., 2015; Chen et al., 2013; Lee et al., 2017). Researchers have also attempted to treat RHA using organic acids; nevertheless, pretreatment of Rice husk has been proven to be preferable to post-treatment (Skrifvars et al., 2005). Any organic acid previously applied to rice husk does not increase the amorphous nature of the RHA generated. Figure 2.11 shows a

flow chart outlining the stages involved in producing high-purity silica using the precipitation technique. Table 2.2 describes different acid pre-treatment, temperature, and calcination that have been done by many researchers.

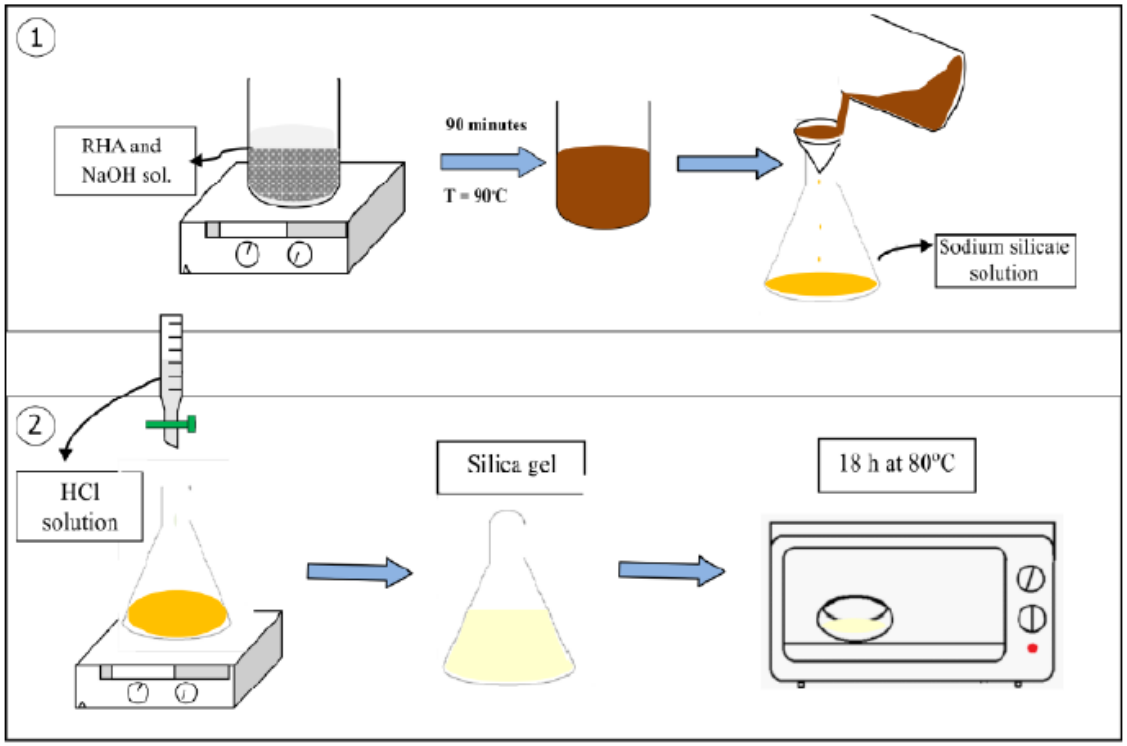

Figure 2.10: Schematic procedure for the preparation of nano silica powder (Liou & Yang, 2011)

Gu (2015) investigated the kinetics of several RH pretreatments prior to calcination. These techniques, which included grinding, soaking in water, and leaching acid, were shown to have a considerable influence on the breakdown of organic matter and the elimination of metallic contaminants, which in turn hindered the production of amorphous silica. One major aspect affecting the quality of amorphous silica is the SiO_2 bond strength. A trend toward the production of crystalline silica is indicated by a higher bond strength (Chindaprasirt & Kanchanda, et al., 2007).

Table 2.1: Different concentrations of alkali and acid in the alkali extraction process

References	Acid-treated RHA/ RHA	Concentration of alkali	Concentration of acid	Main results
(A'yuni et al., 2021)	No pretreatment	10%, 7.5%, 5% W/W NaOH solution	1 N HCl solution	Porous surfaces containing agglomerated nanoparticles are apparent in extracted silica
(Yuvakkumar et al., 2014)	Treated with 6 N HCl solution	0.5, 1, 1.5, 2, and 2.5 N NaOH solution	H_2SO_4 (concentration not mentioned)	2.5N NaOH treatment yielded approximately 99.9% pure silica
(Setyawan et al., 2021)		7%, 10%, and 13 % KOH solution	10% HCl solution	Maximum output of silica was produced at low concentrations of KOH.
(Andreola et al., 2020)	Treated with 5% H_2SO_4 solution	1 M, 1.5 M, 2 M, 3 M, 4 M NaOH solution	1 N HCl solution	For SiO_2/Na_2O ratios close to 2, the alkaline attack (NaOH solution) at 1.5 and 2 M yields the best results
(Daulay et al., 2021)	No pretreatment	10% NaOH solution	37% HCl solution	Quartz and calcite predominate in silica
(Amutha et al., 2010)		2.5 N NaOH solution	5 N H_2SO_4 solution	With an 80 mm diameter, the particles are in agglomeration form
(S. Kim et al., 2021)	No pretreatment	0.1 M, 0.15 M, 0.2 M, 0.5 M, and 1.0 M NaOH solution	CH_3COOH (concentration not mentioned)	The subsequently formed silica particles had a surface area of more than 200 $m^2 g^{-1}$ and were consistently spherical

(Kalapathy et al., 2002)	No pretreatment	1 M NaOH solution	6 M HCl, 3 M $C_6H_8O_7$, or 1.5 M $C_2H_2O_4$ solution	Depending on the pH and kind of acid employed to produce xerogels, different silica, sodium, carbon, and oxygen contents were present
Taguchi method (Nzereogu et al., 2023)	No pretreatment	1 M NaOH solution	1 M HCl solution	---

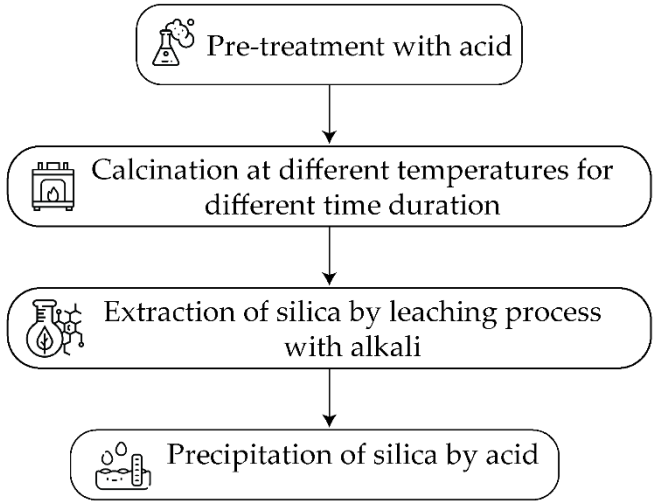

Figure 2.11: Flow chart for preparation of high-purity nano silica by acid leaching

Table 2.2: Different acid pre-treatment, temperature, and calcination for acid leaching

References	Pre-treatment of Rice husk	Calcination	Main result
(V. H. Le et al., 2013)	10% HCl and 30% wt H_2SO_4 solution	**Temperature:** 600°C **Duration:** 4 hrs	The resulting amorphous silica product showed uniformity at an average size of 3 nm
(Ajeel et al., 2020)	3 N HCl solution	**Temperature:** 700°C **Duration:** 4 hrs	From rice husk ash, high pure amorphous silica was found
(Costa & Paranhos, 2018)	3 $molL^{-1}$ HCl solution	**Temperature:** 500°C,600°C,700° C,800°C **Duration:** 1,2,4 hrs	Most of the RHAs' silica remained amorphous at every time and temperature examined. The ideal conditions for calcining the RHs were two hours at 700 °C.
(Sriwuryandari et al., 2020)	1 N HCl solution	**Temperature:** 500°C **Duration:** 6 hrs	The findings of this study included white silica with an 84.782% yield

2.5.3 Effect of Concentration of NaOH on Extracted Nano Silica

The amount of silica particles that may be produced from rice husk ash depends on the concentration of NaOH. The yield generated increases with increasing solvent concentration. The range of O-H groups is widened by the addition of NaOH concentration; the more O-H groups present in the silica, the greater the NaOH concentration. The quantity of silanol (Si-OH) groups in silica can be impacted by an

increase in O-H groups. It is simpler to react with other chemicals when the silanol (Si-OH) increases the number of silica particles (Rahman & Padavettan, 2012). Zuwanna (2021) reported that 3N NaOH was the ideal concentration for silica extraction from rice husk. Above 2.5N NaOH treatment, high purity of silica (~99.9%) was achieved by Yuvakkumar (2014).

2.5.4 Effect of pH on Extracted Nano Silica from Rice Husk Ash

The pH level is important to extract silica from rice husk ash (RHA) since it affects the purity of extracted silica and its yield. In highly alkaline (pH>10) conditions, silica is soluble, and when the pH of the silicate solution is dropped below 10, it forms a rigid three-dimensional gel network. Three types of silica gel are identified: Aerogel (solvent removed by supercritical extraction), Xero-gel (aqueous phase in the pores is removed by evaporation), and Aqua-gel (pores filled with water).

Sodium silicate added to an acidic solution might result in the production of silica gel. The first product is an aqua gel, which has a high water content and a hydrated, gel-like appearance. When this aqua gel is dried in a standard atmosphere, the water evaporates and leaves behind a solid, porous structure known as Xero gel. The silica turns into an aerogel, a lightweight, extremely porous substance with a very low density and exceptional insulating qualities if the drying process is carried out in a way that prevents collapsing the pore structure (such as by supercritical drying). To describe gels in which a gas replaces the liquid without causing the polymer network to break, Kistler established the term "aerogel" in 1931.

Lower pH values cause siloxane (Si-O-Si) to convert to silanol bonding (Si-O-H), which results in a smaller silica primary composition and slower gel formation (Liou & Yang, 2011). An element of water was produced in the silica gel result of acids contributing hydrogen ions to a sodium silicate solution, as per the Equation 2.12. The last hydrogen ions formed the Si-OH bonding when the moles of hydrogen grew, and

the amounts of oxygen and silicon remained constant. The main species in its aqueous solution is $Si(OH)_4$ with lower concentrations of silicate and pH values below 8. $Si(OH)_4$ groups in silanols spontaneously polymerize to form larger oligomers connected by a disiloxy bond at increasing concentrations. When one of the silanols deprotonates to a Si-O-group, the reaction is most favorably driven (Adam et al., 2008)When these oligomers develop into colloid-sized silica particles, smaller particles are displaced by bigger ones. Nevertheless, the significantly more concentrated silicate solution is stable at higher pH values (over 8). This is due to the nucleophilic assaults on disiloxy bonds by OH, which occur through a five-way coordination intermediate.

When silica solution (pH>10) was treated with acid, silica gel quickly began to develop at pH 10, and at pH 7.0, it solidified into a gel. Because of this, lowering the pH below 7.0 is challenging. Gel production was extremely slower at pH 4.0, and the resulting gels were noticeably softer (due to a lack of stiffness) than those formed at pH 7.0. This is to be anticipated since the gel structure at pH 7.0 was mostly caused by covalent Si–O–Si bonds, but at pH 4.0, the main contributing factors were H-bonds and the somewhat lower van der Waals attraction. (Kalapathy et al., 2000) produced silica gel at pH values of 9, 10, 10.5, and 11. They discovered that a higher pH produced condensed glassy solids and that a higher silica concentration produced very porous silica xerogel. Shwe et al. (2020) studied with pH levels of 5, 7, and 9. The SEM result showed the particle size of silica aerogel decreases at pH 7 and increases at pH 5 and pH 9. The pH 5 synthetic sample is detected as flakes and is not evenly distributed into particles for analysis. Even though the particles are aggregated at pH 7 and pH 9, each particle can be identified and connected to form a porous network. According to experimental findings, the best circumstances for silica production include gelation at pH 3, a concentration of 0.15 M of silicate, an ageing temperature of 50 °C, and a 12-hour ageing period (Liou & Yang, 2011).

2.5.5 Effect of Surfactant on Nano Silica

Surface energy is minimized because silica nanoparticles are prone to agglomeration, which is a population decline accompanied by an increase in size and no loss of mass (Keykhosravi & Simjoo, 2019). The colloidal stability of silica aqueous dispersions can be either improved or decreased by the addition of surfactants. The effects of surfactants on the synthesis of silica colloids in solution phases was studied (Esumi, 2001; Portet et al., 1998; Rubio & Kitchener, 1976; Szekeres et al., 1998; W. Wang et al., 2004). Few studies have looked at how surfactants at low concentrations may affect the processes of silica particle nucleation, particle growth, and interactions (O'Sullivan et al., 1994; Wang et al., 2005), even though surfactants at high concentrations (like liquid crystals and micellar solutions) have been widely used for controlled nanoparticle synthesis (John et al., 2002; Palmqvist, 2003).

Various surfactant types have been used as templates in numerous attempts to regulate the size and shape of silica nanoparticles. The pace at which particles formed and grew in the hydrolysis reaction was influenced by the type and concentration of surfactant additives. Silica extraction can be accomplished using a variety of surfactant types, such as cationic, anionic, and non-ionic surfactants, each of which has unique characteristics and uses.

Depending on the type of particle, either hydrophilic particles into the water domains of the surfactant phase or lipophilic particles into the carbon domains could be considered. In the presence of ionic surfactants that have opposing charges to the solid, the surfactant ions attach to the hydrophobic surface of the particle. When ionic surfactants have the same charge as solids, depletion forces cause the particles to be ejected from the surfactant phase. Figure 2.12 shows the paradigm for hydrophobic coagulation and peptization. A sol becomes coagulated upon the addition of an oppositely charged surfactant (a). Subsequently, the coagulated solution is peptized by adding either a nonionic surfactant (c), a surfactant charged opposite to the first

one (b), or the same surfactant as the first one (d). It has been discovered through experimental evidence in a number of adsorption systems that ionic surfactants adsorb significantly onto oppositely charged solids, causing the solids' zeta potential to change from positive to negative or vice versa.

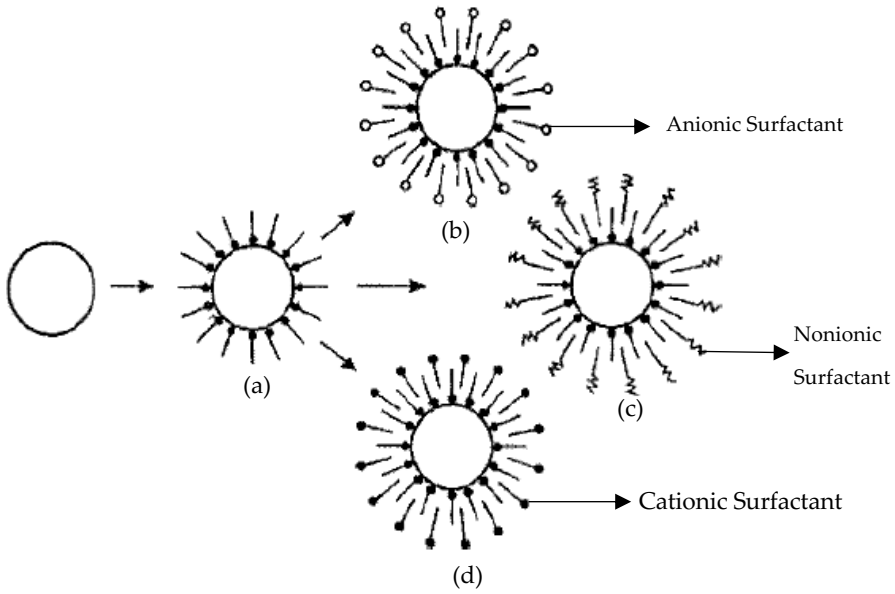

Figure 2.12: Model for surfactant-induced hydrophobic coagulation and peptization of negatively charged sol (Esumi, 2001)

A silica source and the head group of a cationic surfactant can be joined by electrostatic force or hydrogen bond contact in solution. This results in a complex self-organization process that includes surfactant/silicate self-assembly and silicate speciation processes. These procedures are sensitive to ageing duration, pH, temperature, surfactant type and concentration, and other factors. A minimum of three types of charged species are present in solution during synthesis processes: cationic surfactant (S+), its counter ion (X-), and silica species (I- or I+). The strong interaction (S+–I- or S-–I+) that favors a highly ordered mesostructure is formed under basic conditions by a charged silica precursor and a surfactant with opposite charges. Then, as the silica precursor is hydrolyzed and condensed, mesophases undergo transition. These procedures are sensitive to aging duration, pH, temperature, surfactant type and concentration, and other factors. A minimum of three types of charged species are

present in solution during synthesis processes: cationic surfactant (S+), its counter ion (X-), and silica species (I^- or I^+). The strong interaction ($S^+–I^-$ or $S^-–I^+$) that favors a highly ordered mesostructure is formed under basic conditions by a charged silica precursor and a surfactant with opposite charges. The potential effects of surfactants in the preparation media on nucleation, particle development, and particle interactions have mainly gone unnoticed up until now (O'Sullivan et al., 1994)

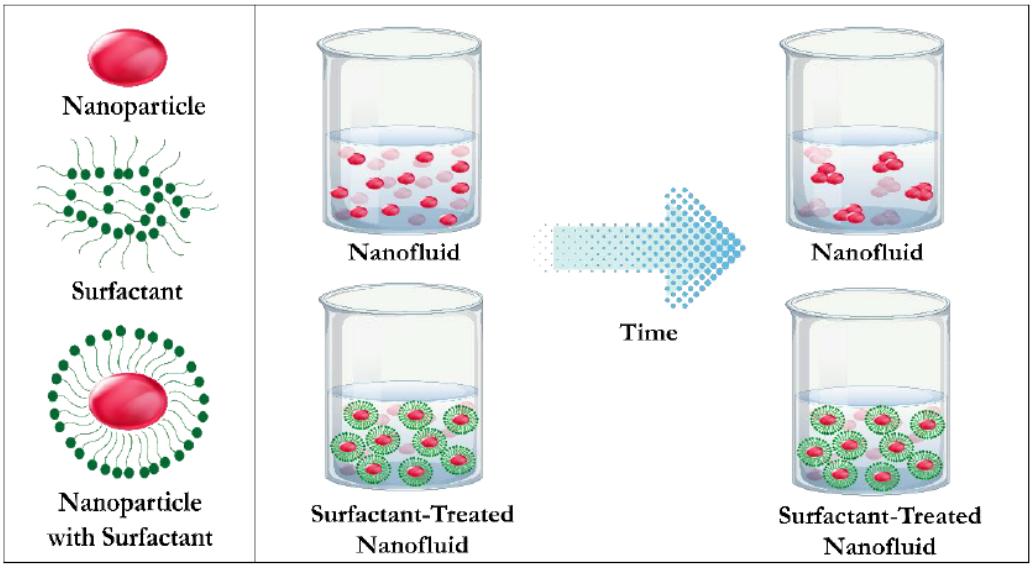

Figure 2.13: Nanofluid stability when surfactants are present (Bajpai et al., 2021)

Wang (2005) examined the effects of cationic, anionic (saturated and unsaturated), and nonionic surfactants on the shape, surface characteristics, and formation of silica nanoparticles produced by hydrolyzing tetraethoxysilane in alcoholic media with ammonium. According to Wang studies anionic and nonionic surfactants exhibited little effects on silica particle development at low concentrations, whereas cationic surfactants had a considerable impact. Using different concentrations of Cetyl Trimethyl Ammonium Bromide (CTAB) (1.5%, 1.75% and 2%) as a template, a sol-gel process was used to create mesoporous silica from RHA by Purwaningsih (2019).

The size of mesoporous silica particles was influenced by CTAB concentration; as CTAB concentration increased, the size of the particles decreased. Mesoporous surface

area of silica and total pore volume increased as the concentration of CTAB rose. In the meantime, the average size of pores dropped. Due to the combined or independent effects of surface charge neutralization and/or the hydrophobic effect of the long hydrocarbon tail, CTAB, which is made up of a cationic polar head and a hydrophobic tail, has the ability to aggregate negatively charged nanosilica (Bryleva et al., 2007). The way that silica nanoparticles and CTAB interact is as follows: small amounts of CTAB may initially form a monolayer that is regulated by the electrostatic interaction between the positively charged surfactant head groups and the siloxane groups (-SiO) on the surface of the nanosilica. Wang (2004) found that CTA+ molecules were firmly attached to the SiO2 surface by their trimethylammonium headgroups at minimal surface coverage (less than a monolayer).

2.5.6 Removal of Surfactant from the Solution

The extraction of the surfactant template is necessary to produce mesoporous silica nanoparticles (MSN), particularly in nanomedicine applications. This is particularly crucial in the case of CTAB, a surfactant that is utilized in the synthesis of MCM-41-type MSN and has a high toxicity even at residual concentrations (He et al., 2009; Hudson et al., 2008; Yildirim et al., 2016). Several techniques, including calcination, solvent extraction, and dialysis, have been conducted to extract the surfactant from MSN. Calcination is an easy and efficient thermal treatment technique that usually eliminates non-ionic surfactants around 300-350°C (Basso et al., 2020; Mahoney & Koodali, 2014). However, cationic surfactants such as CTAB in mesoporous silica nanoparticles (MSN) need to be thoroughly broken down at temperatures of about 450-600°C (Hudson et al., 2008; Mahoney & Koodali, 2014; Mukherjee et al., 2009). The process of solvent extraction weakens the bonds that hold surfactants to the silica surface by washing them with certain solutions at controlled temperatures. In the dialysis process, a dialysis membrane is employed to hold onto the nanoparticles and

make it easier for the solvent to be continually renewed, which shifts the equilibrium and forces the surfactant to be exchanged and removed.

2.6 POZZOLANIC BEHAVIOR OF NANO SILICA

RHA silica possesses a high level of amorphous silica with a large surface area, which enhances its reactivity and pozzolanic properties. When mixed with cement and water, RHA silica undergoes a pozzolanic reaction with calcium hydroxide, resulting in the formation of additional C-S-H gel ($Ca_{1.5}SiO_{3.5}.2H_2O$) (Yu et al., 1999). The chemical reaction is given in Equation 2.13.

$$2SiO_2 + 3Ca(OH)_2 + H_2O \longrightarrow Ca_{1.5}SiO_{3.5}2H_2O \quad \text{(Eq. 2.12)}$$

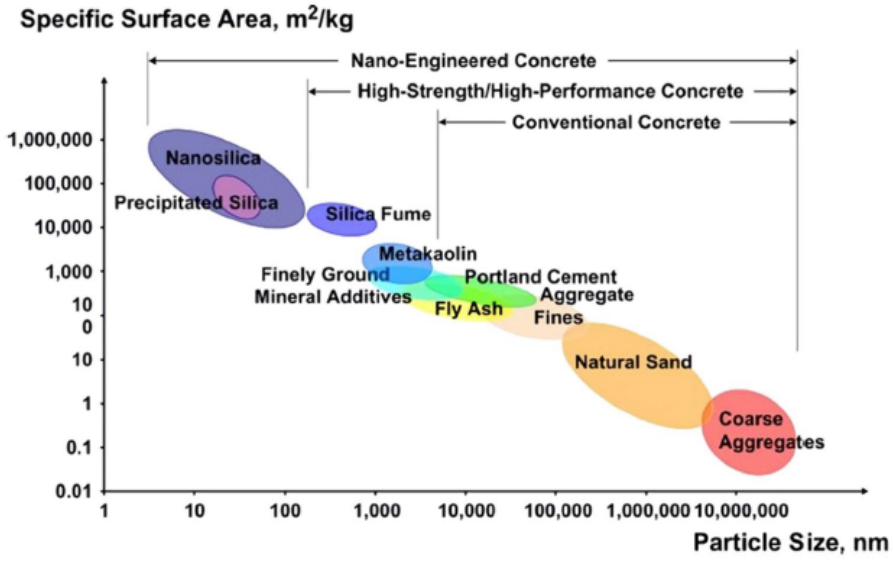

Figure 2.14: Concrete materials particle sizes and specific surface areas (Bekem Kara & Durmuş, 2019)

This reaction leads to the densification of the cementitious matrix, filling in pores and voids, and improving the overall performance of concrete and mortar mixes. The densification of the cementitious matrix through pozzolanic reaction improves the microstructure of concrete and mortar mixes. It helps to reduce permeability, mitigate alkali-silica reaction (ASR), and enhance resistance to chemical attacks and abrasion

(Khan et al., 2020). The densified structure minimizes the movement of water, aggressive chemicals, and harmful ions through the concrete or mortar, thereby improving its resistance to deterioration and increasing its service life.

2.6.1 Hydration of Cement Blended with Nano Silica

Several studies reported that the use of nano silica in cementitious systems may improve strength development, particularly in the early stages of hydration (Jo et al., 2007; Porro et al., 2005). Thomas (2009) demonstrated that adding nano silica or C–S–H-particles can speed up the hydration of tricalcium silicate (C_3S). The model describing these effects assumes that C-S-H particles act as seeds for the creation of the C-S-H phase and are dispersed in the water between the cement particles. As a result, unlike in pure C_3S, the C–S–H-phase is now formed in the pore space as well as on the grain surface. As a result of the many seeds and the avoidance of laborious nucleation procedures, C_3S hydration is accelerated. In addition, compared to pure C_3S, the hardened paste ought to exhibit reduced porosity. Adding nano silica causes a faster and higher temperature peak to develop and increasing the dose or fineness of nano silica has a stronger impact on hydration acceleration. Figure 2.15 shows the hydration of cement grains when silica (b) or C-S-H-particles (c) are introduced, as opposed to when they do not (a).

Since the high surface area of NS serves as a nucleation site for the precipitation of C-S-H gel, it is the primary mechanism underlying this working principle. However, according to Björnström (2004), it is still unclear if the hydration of cement increased in the presence of NS is because to its significant surface activity or its chemical reactivity upon dissolution (pozzolanic activity). Through the measurement of cement paste and mortar viscosity change (rheology), the accelerating effect of NS addition was also indirectly established (Senff et al., 2009, 2010).

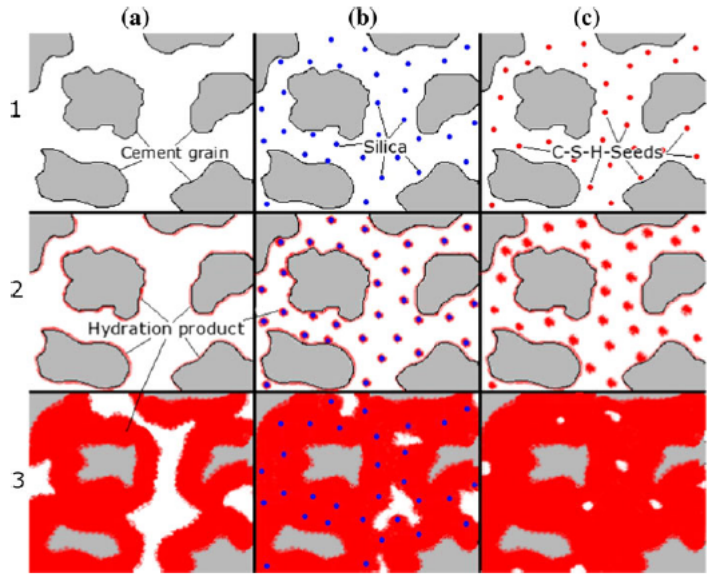

Figure 2.15: The process of hydrating pure cement (a) and adding nanosilica (b) and C-S-H seeds at various intervals (1–3) following mixing (Land & Stephan, 2012)

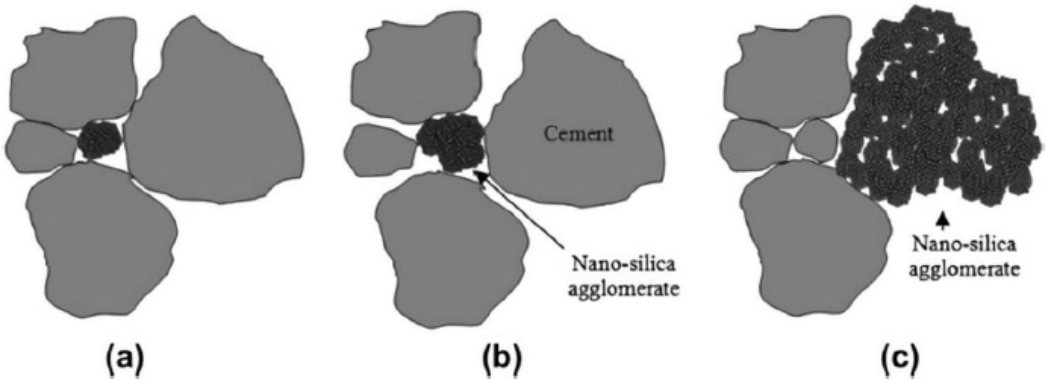

Figure 2.16: Effect of NS agglomeration on filling (Kong et al., 2013)

The viscosity test results indicate that cement paste and mortar with NS need additional water to maintain their workability. NS tends to adsorb ionic species in water, leading to agglomeration. Using a plasticizer or dispersion agent can mitigate this effect. The following is a summary of the role of NS: (i) NS serves as both fillers and activators to enhance the microstructure and promote pozzolanic reactions (Jo et al., 2007); (ii) they serve as a nucleation site for C-S-H seeds, which accelerates up cement hydration (Land & Stephan, 2012); (iii) NS accelerated the consumption of C_3S and the formation of portlandite (small CH) crystals and homogeneous clusters of C-

S-H composition (Land & Stephan, 2012); and (iv) NS enhances the microstructure of the interfacial transition zone between aggregates and cement pastes (Givi et al., 2010b).

2.6.2 Physical Properties of Nano Silica

The physical characteristics of silica derived from RHA are pivotal for its efficacy as a partial substitute for cement in construction. Silica usually comprises ultrafine particles with a high surface area-to-volume ratio. The fine particle size, often in the range of nanometers to micrometres, facilitates better dispersion within concrete and mortar mixes.

Silica exhibits a large specific surface area compared to cement, which allows for increased contact between the silica particles and cementitious phases. Surface area increased when silica samples were made using acid leaching (H_2SO_4, HCl, and $C_2H_2O_4$) and HCl leaching silica obtained the maximum surface area (Liou & Yang, 2011). This high surface area enhances the reactivity of RHA silica, promoting faster and more complete pozzolanic reactions with calcium hydroxide produced during cement hydration. The density of silica is typically lower than that of cement, but its incorporation into concrete and mortar mixes can contribute to increased bulk density and reduced porosity of the cementitious matrix. This densification leads to improved mechanical properties, such as compressive strength and enhanced durability of the construction materials. Silica is characterized by its fine PSD and high fineness modulus. The fine particles contribute to better workability and improve the rheological properties of concrete and mortar mixes, allowing for easier placement and compaction during construction.

Another research demonstrated that silica extracted from RHA is amorphous and white, whereas burning untreated husks yields gray powder containing silica and impurities (Carmona et al., 2013). Overall, the physical properties of silica from RHA,

including particle size, specific surface area, density, fineness, and color, influence its behavior and performance as an SCM in construction works.

2.6.3 Chemical Properties of Nano Silica

The chemical properties of silica from RHA, including its high silica content, amorphous nature, and presence of reactive alkaline compounds, contribute to its effectiveness as a partial replacement for cement in construction works. Silica from RHA is predominantly composed of silica (SiO_2), which is typically present in high concentrations ranging from 80% to 95% by weight (An et al., 2010; Tharani & Ananthasubramanian, 2024). The silica present in RHA is largely in amorphous form with a small crystalline structure. Amorphous silica exhibits higher reactivity compared to crystalline silica, making it highly suitable for pozzolanic reactions in concrete and mortar mixes. The high silica content contributes to the pozzolanic reactivity and large surface area, enabling it to react with calcium hydroxide.

Silica may contain reactive alkaline compounds, such as potassium oxide (K_2O) and sodium oxide (Na_2O), derived from the combustion of rice husks. These alkaline compounds can promote the dissolution of silica and enhance the overall reactivity of RHA silica, facilitating faster and more complete pozzolanic reactions with calcium hydroxide. In addition to silica, it contains other chemicals such as Al_2O_3, CaO, MgO, Fe_2O_3, and SO_3 (Jamil et al., 2016). Depending on the source and processing methods of RHA, these trace elements can influence chemical composition and reactivity of silica but typically do not significantly affect its pozzolanic behavior or performance in constructional works. Overall, the chemical properties of silica from RHA in partial substitution of cement play a significant role in its effectiveness as an SCM in constructional work.

2.7 MORTAR

Mortar, an essential component in engineering, is primarily made up of cementitious material, water, and fine aggregate. It has been widely utilized in building engineering and has many benefits, including excellent workability, high strength, convenient construction, and strong bonding performance with blocks (Wang et al., 2020). The primary feature of mortar is its tensile bond strength or its ability to bind individual units together (Mamlouk & Zaniewski, 2014). The coarse aggregates, such as crushed stone or gravel, are bonded by significant adhesive properties in mortar. This guarantees structural integrity and strength by keeping the concrete mass homogenous.

Along with its workability and water retention, performance of mortar is also influenced by its strength in compression. Because of this, many cement mortar types are created according to factors like strength or water resistance. Unfortunately, scientific information is scarce on the ideal mixture percentage needed to produce structural grade mortar with the necessary strength requirements and workability to be properly placed into constructing formwork.

2.7.1 Composition of the Mortar

Mortar is a flexible construction material that gives structural support for various construction purposes, fills joints and binds masonry blocks together. Its adaptability makes it essential for both traditional and modern construction techniques, allowing for customization to meet specific performance requirements.

2.7.2 Sand

The characteristics of the sand influence the workability of the mortar but have minimal effect on its strength (Haach et al., 2011). An important factor affecting the pore structure of cement mortar is the amount of sand present.

2.7.3 Water

The chemical interaction between cement and water, known as hydration, is the mechanism that gives mortar its strength and hardness. Water is necessary for this process to happen. In cement hydration, too much water reduces mortar strength, while too little water hinders workability.

Numerous investigations into the various characteristics of concrete have been conducted since Feret (1896) study, which initially identified the significance of the water/cement ratio on the strength of concrete. About twenty years later, ABrAMS (1919) developed his law on the impact of the ratio of cement to water on the strength of concrete. The following is the statement of water-cement ratio guidelines by Abram.

$$f_c = \frac{k_1}{k_2^{\frac{w}{c}}} \qquad \text{(Eq. 2.13)}$$

Where,

f_c is the compressive strength of concrete at a designed age,

while, $\frac{w}{c}$ is the water-to-cement ratio in the concrete mix, and

k_1 and k_2 are the empirical constants. Later, a typical curve was constructed for a different design, which shows this relationship in Figure 2.16.

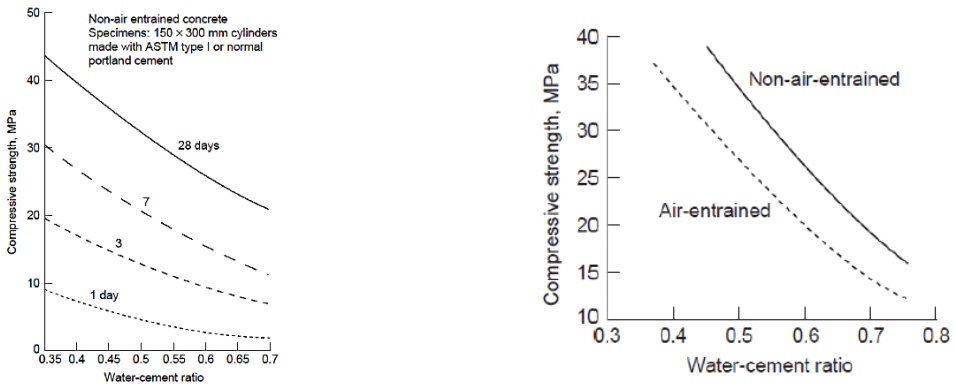

Figure 2.17: Concrete strength with the w/b ratio and moist curing age (Mehta & Monteiro, 2001)

2.8 MECHANISM OF SULFATE ATTACK

One of the adverse chemical reactions that causes cementitious mixes in structures exposed to it to crack, spall, and pop out is called sulfate attack, a major durability issue (Nassar et al., 2021). Therefore, high sulfate resistance is subsequently crucial for the durability of structures constructed with it. Santhanam (2002, 2003) revealed the mechanism of sodium sulfate-induced sulfate attack. When mortars are exposed to sodium sulfate solution, calcium hydroxide from the hydration reaction of cement combines with sodium sulfate and turns into gypsum, changing the outer skin of the specimen because of the expansion. The aluminum compounds then react with gypsum to form ettringite, becomes more unstable and has a larger volume. Further cracking of the mortar interior is caused by this expansion of the cement matrix. Equation 2.14 and 2.15 show the chemical reactions.

$$Ca(OH)_2 + Na_2SO_4 + 2H_2O \longrightarrow CaSO_4.2H_2O + 2NaOH \quad \text{(Eq. 2.14)}$$

$$CaSO_4.2H_2O + \text{Aluminum compounds} \longrightarrow \text{Ettringite} \quad \text{(Eq. 2.15)}$$

2.9 ELECTRICAL RESISTIVITY

The electrical resistivity of cementitious mix indicates their permeability to the movement of harmful chemicals, which is one of their key durability parameters. The metallic embedment corrosion rates inside a cementitious media are indirectly correlated with electrical resistance. Since the Surface Resistivity (SR) test is quicker, simpler, requires no sample preparation, and offers findings with less variability than the Rapid Chloride Permeability Test (RCPT), it has been deemed a possible substitute (Tanesi & Ardani, 2012).

2.10 CHAPTER SUMMARY

Based on the existing literature, the preparation of RHA is influenced by various parameters, including temperature, burning time, and grinding process, which affect its fineness, colour, and silica content. RHA is itself a pozzolanic material. When cement is replaced with RHA, due to its pozzolanic reaction, it creates a secondary C-S-H gel. As RHA contains amorphous silica, an inexpensive material for silica extraction, various techniques have been applied by researchers to extract nano-silica from it. The alkaline method is one of these, where an alkaline solution (NaOH/KOH) is used to form Na_2SiO_3, and then silica acid (HCl/H2SO4, etc.) is used to precipitate it. Precipitated silica tends to agglomerate. To reduce this agglomeration, researchers used surfactant. Generally, extracted silica is mesoporous, but when surfactant is used, a highly ordered mesostructure is formed under basic conditions by a charged silica precursor and a surfactant with opposite charges. If surfactant is used during silica extraction, it should be removed from the particles also using a different technique, such as calcination, solvent exchange, or dialysis. According to the existing literature, the calcination process is straightforward, but the calcination temperature should be above 500 °C. This extracted silica has more pozzolanic reactivity than RHA because of its smaller particle sizes and larger surface areas. The particle size of extracted silica depends on the pH levels during acid addition.

Chapter 3: MATERIALS AND METHODOLOGY

This chapter of the thesis describes the research materials and methods. This comprises the experimental program flowchart and the various analysis programs. The experimental programs were designed for tests at three levels. The methodology includes test procedures for binder characterization, for fresh and hardened properties of mortar and concrete.

3.1 MATERIALS

Materials utilized for this study are i) Rice Husk Ash (RHA), ii) Extracted Silica Powder (SP), iii) Extracted Nano Silica (NS), iv) Portland Cement (CEM I), v) EN Standard Sand, vi) Ottawa Sand, vii) Sylhet sand, viii) Coarse aggregate, and ix) Potable Water.

CEM I | RHA | SP | NS

EN Sand | ASTM Standard Sand | Sylhet Sand | Coarse aggregate

Figure 3.1: Materials used in this study to cast samples

3.1.1 Rice Husk Ash

This study uses RHA as a SCM in the paste, mortar, and concrete mix. RHA, a byproduct of rice milling, possesses pozzolanic properties. The incineration process

influences the properties of RHA. Rice husk is composed of around 50% cellulose, 25%–30% lignin, and 15%–20% silica. Silica ash remains after cellulose and lignin are burned away. The two ways to burn rice husk are controlled and open firing methods. Due to environmental concerns and the low quality of the produced RHA, open burning is discouraged.

The RHA used in this study was collected from Sustainable Energy and Agro-Resource Ltd. (SEAL), located in the Thakurgaon district of Bangladesh. The industry collected Rice Husk (RH) from the northern region of Bangladesh. They follow the control burning procedure shown in the flow diagram of Figure 3.2.

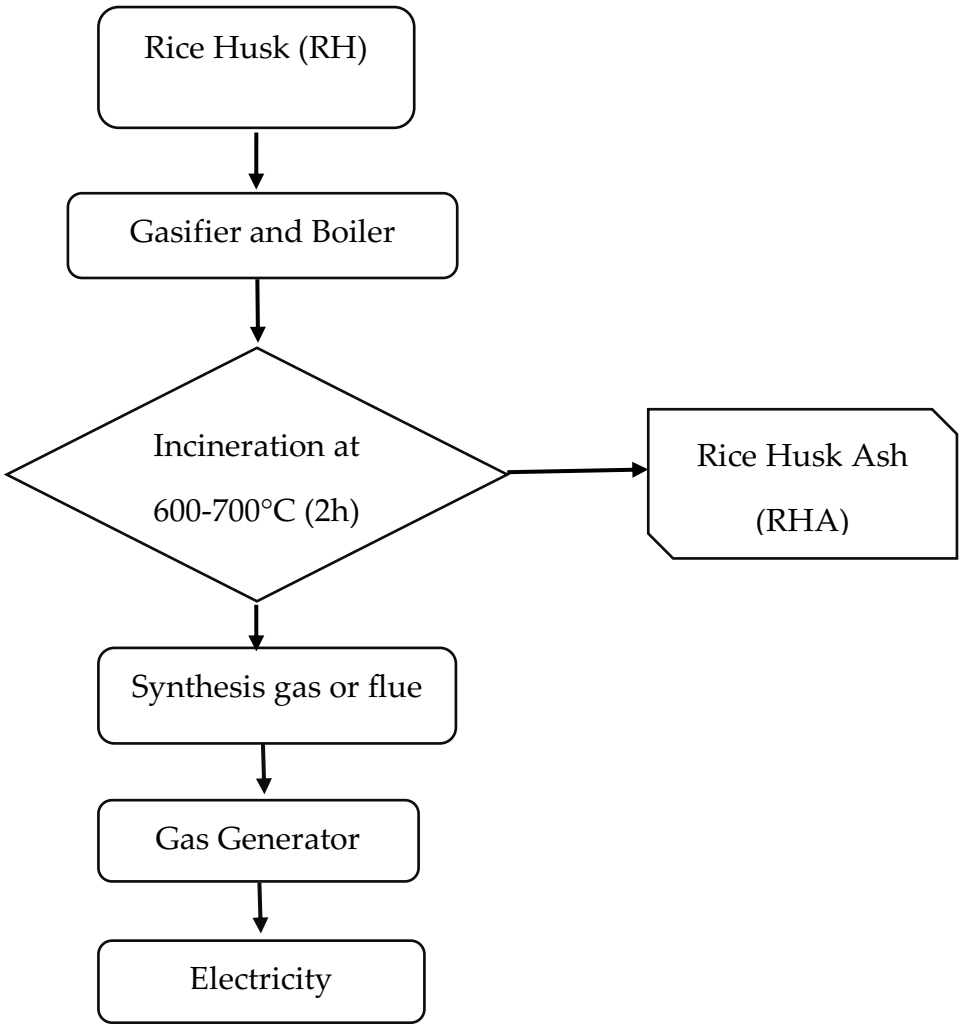

Figure 3.2: Flow chart of RHA processing

3.1.2 Extracted Silica Powder (SP) & Extracted Nano Silica

This work used silica powder and nano-silica as a partial replacement for cement in paste, mortar, and concrete mix, which is extracted from RHA. Silica from RHA is a valuable resource with several uses, notably in the construction sector. RHA has a high proportion of silica, making it a rich supply of this essential mineral. The silica possesses distinctive physical and chemical properties that make it a valuable material for various applications.

Physically, RHA-derived silica is typically present as a fine powder with a high surface area and fine particle size. This morphology enhances its reactivity and ensures efficient incorporation into cementitious systems. Chemically, RHA silica is composed of amorphous silica (SiO_2), with purity levels ranging from 80% to 95% by weight. Additionally, this tends to have low levels of impurities, such as alkalis and organic matter, which enhances its suitability for use in construction materials. The primary component responsible for the pozzolanic qualities of these materials, silica, was subsequently extracted from RHA using several techniques. The extraction process involves the purification of RHA to isolate the silica component, which is then processed into various forms, such as silica nanoparticles or colloidal silica. This study collected RHA-extracted silica from Sustainable Energy and Agro-Resource Ltd. (SEAL). The whole silica extraction procedure is shown by a flow diagram in Figure 3.3.

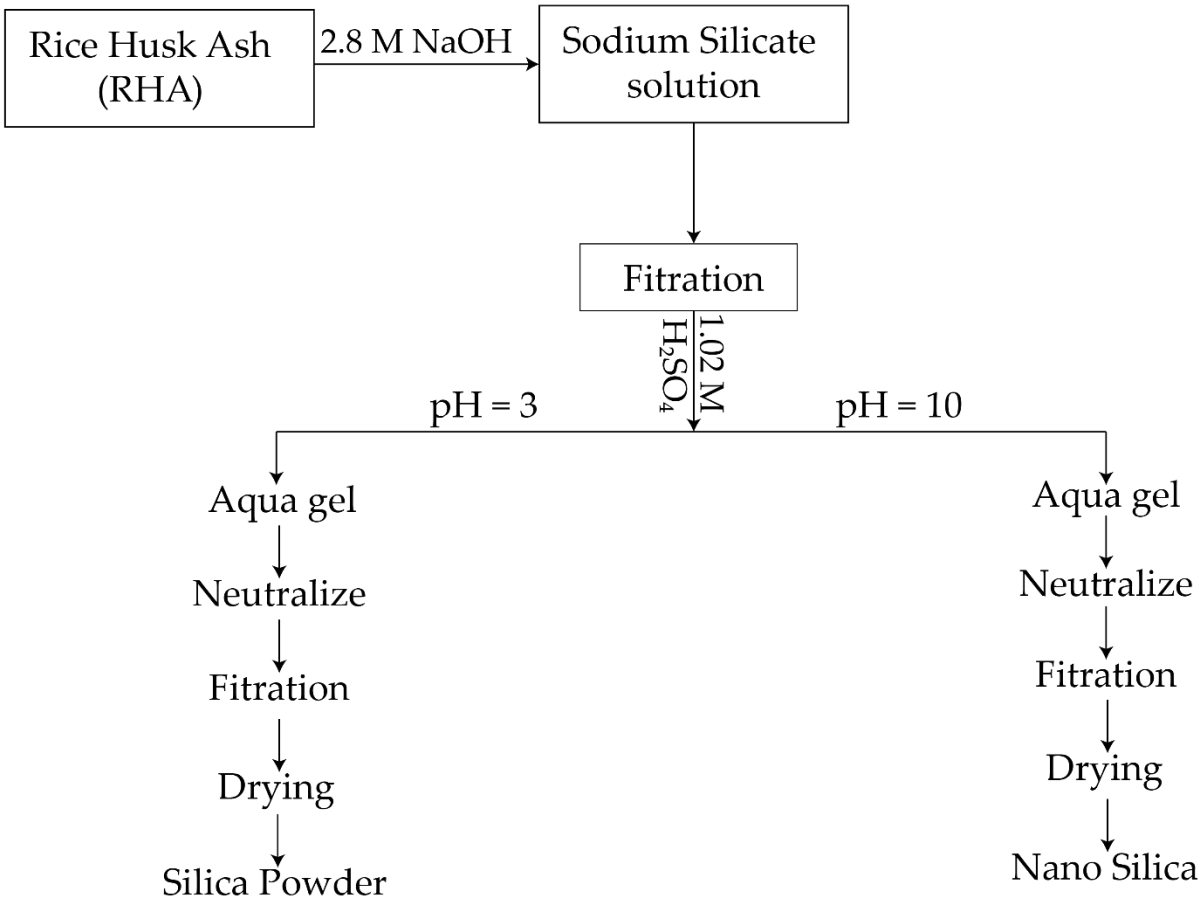

Figure 3.3: Flow chart of the Silica synthesis process from RHA

3.1.3 Portland Cement (CEM I)

As the composition is known, Portland Cement (CEM I) is used as a reference material. The physical properties were tested in the lab and chemical properties of the cement were obtained from the manufacturer.

Table 3.1: Physical properties of CEM I

Serial No.	Physical Properties	Test Result
01.	Normal consistency	27%
02.	Initial Setting (Minutes)	85
03.	Final Setting (Minutes)	180
04.	Soundness by Le Chatelier's Test (mm)	2
05.	Blaine Specific surface (cm^2/gm)	3766
06.	Specific gravity	3.11

Table 3.2: Chemical composition of CEM I

Oxides	%
Calcium Oxide (CaO)	63.53
Silicon Dioxide (SiO_2)	20.37
Aluminum Oxide (Al_2O_3)	5.64
Ferric Oxide (Fe_2O_3)	3.42
Magnesium Oxide (MgO)	1.12
Sulfur Trioxide (SO_3)	2.36

3.1.4 EN (CEN) Standard Sand

CEN standard sand, which is naturally siliceous, especially in its finest fractions, is known as standard sand (ISO standard sand). The particles are rounded, often isometric, and clean. This sand complies with EN 196-1 certification. The grading of this sand is shown in Table 3.3.

Table 3.3: Particle size distribution of EN Standard sand

Square mesh size (mm)	2.00	1.60	1.00	0.50	0.16	0.08
Cumulative sieve residue (%)	0	7±5	33±5	67±5	87±5	99±1

3.1.5 ASTM Standard Sand

Graded sand according to ASTM C778 (2021) was used as fine aggregate. The sand is a high-purity silica used in laboratory experiments, research studies, and industrial applications. Its uniformity and purity ensure reliable and reproducible results in scientific investigations. As shown in Table 3.4, the fineness modulus of ASTM Standard Sand is = 143/100 =1.43.

Table 3.4: Sieve analysis of ASTM Standard sand

Sieve No.	Sieve Opening (mm)	Materials Retained (gm)	% Materials Retained	Cumulative % Materials Retained	% Finer
#4	4.75	0	0	0	100
#8	2.36	0	0	0	100
#16	1.18	0	0	0	100
#30	0.6	2.0	0.4	0.4	99.6
#50	0.3	218.8	43.9	44.3	57.3
#100	0.15	269.3	54.0	98.3	1.7
#200	0.075	8.6	1.7	100	0
pan	-	-	-	-	-
Total		498.7	-	-	

3.1.6 Fine Aggregate (Coarse Sand)

Coarse sand was used for concrete experiments. The size distribution of sand was assessed following ASTM C136-06. According to ASTM C33/C33M (2023) guidelines, the fineness modulus (FM) of fine aggregate should be between 2.3 and 3.1. Table 3.5 shows the results of the sieve analysis. Specific gravity and water absorption were found 2.66 and 2% respectively.

Table 3.5: Sieve analysis of fine aggregates

Sieve No. (ASTM)	Sieve Opening	Weight Retained	Cumulative Weight Retained		% Finer	F.M. Value
	(mm)	(gm)	(gm)	(%)		
#4	4.75	0	0	0	100	
#8	2.36	42	42	8.4	91.6	2.67
#16	1.18	101	143	28.6	71.4	

#30	0.60	128	271	54.2	45.8
#50	0.30	118	389	77.8	22.2
#100	0.15	101	119	98	2
#200	0.075	7	N/A	N/A	N/A
Pan	--	1	N/A	N/A	N/A

3.1.7 Coarse Aggregate

The concrete batches contained crushed coarse aggregate with $\frac{3}{4}$" nominal size, following ASTM C33/C33M (2023). Table 3.6 shows the sieve analysis. Bulk density of coarse aggregate was 1660 kg/m^3. Specific gravity and absorption were found 2.91 and 0.6% respectively.

Table 3.6: Sieve analysis of coarse aggregate

Sieve No. (ASTM)	Sieve Opening	Weight Retained	Cumulative Weight Retained		% Finer
	(mm)	(gm)	(gm)	(%)	
1 inch	25	0	0	0	100
¾ inch	19	0	0	0	100
½ inch	12.5	2730	2730	54.6	45.4
3/8 inch	9.5	1360	4090	81.8	18.2
#4	4.75	910	5000	100	0

3.1.8 Admixture

Admixtures are substances that are added to a batch either before or during mixing and are used as an ingredient to change the properties of a cementitious mixture. These include materials other than water, aggregates, cementitious materials, and fiber reinforcement. In this study, high-range water reducing admixture (HRWRA)

was used for making workable concrete. HRWR is defined by ASTM C494/C494M (2024) as an additive that can lower the amount of mixing water needed to build concrete by more than 12% while preserving a specific degree of slump value consistency. Key properties of HRWRA are given below:

Improves workability: In the production of concrete, high-range water-reducing admixtures (HRWRA) are frequently used. Their capacity to increase workability has drawn particular attention. When a water-reducing admixture is added to cement paste, its hydrophobic group will adhere to the cement particles surface, causing their surface to absorb the same charges. This can cause electrical repulsion, which can distract cement particles (Figure 3.4 (b)). Free water is then released from the floe, increasing mobility without the need for additional water. Furthermore, a solvent water film can be formed by a water-reducing admixture (Figure 3.4(c)), which serves as an effective lubricant between cement particles.

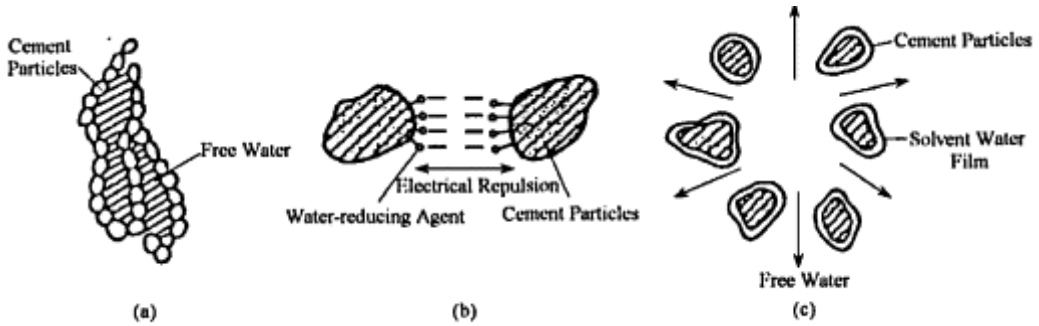

Figure 3.4: The interaction of a water-reducing agent with the flocculated structure of cement particles (Zhang, 2011)

Reduces cement content and bleeding: For a specific free water/cement ratio at the required consistency class, HRWRA is recommended to prevent excessive cement content. It also minimizes the free water content, which lessens the tendency for excessive bleeding.

Improves strength: HRWRA improves the resistance of concrete to extreme environments by permitting a lower water-to-cement ratio, which results in increased compressive strength and decreased permeability.

3.2 METHODOLOGY

Firstly, a comprehensive literature review is needed to collect relevant information about environment-friendly cementing materials. The materials are then chosen as necessary for the study. After material selection, the physical, chemical, and morphological properties of the pozzolanic materials were assessed using suitable experimental methods, and a partial replacement was designed to optimize performance. Several replacement levels of RHA, SP, and NS were used, gradually increasing the replacement ratio and decreasing the cement in total cementitious materials.

3.3 WORKFLOW DIAGRAM

The workflow diagram is a visual representation of the systematic process followed during this study. Subsequently, the diagram illustrates the methodology employed, providing procedures for sample selection, data processing, and data gathering. Figure 3.5 illustrates the flow diagram. Figure 3.6 provides an overview of the experimental methods and programs used at various stages of this research.

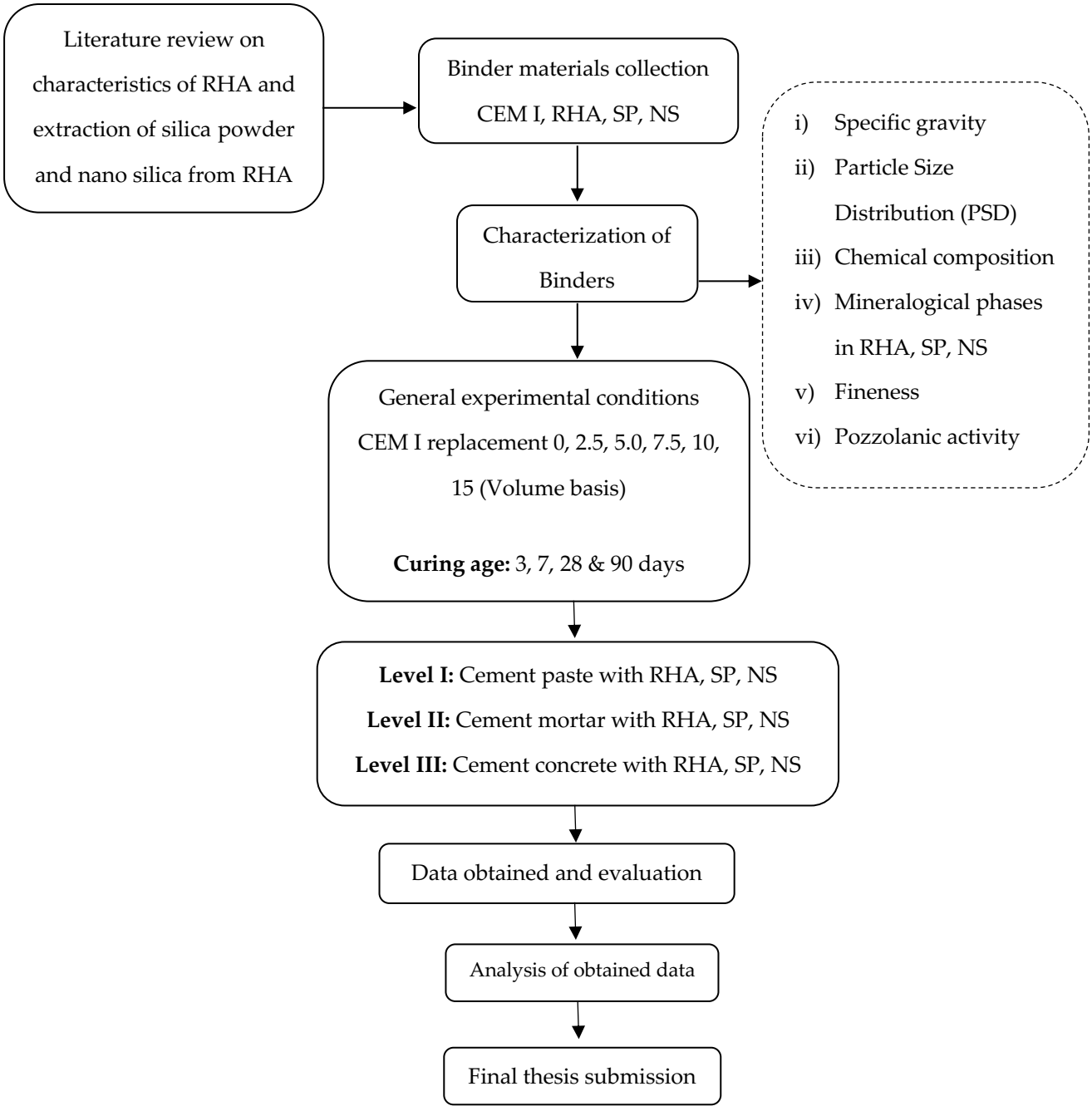

Figure 3.5: General outline of the methodology

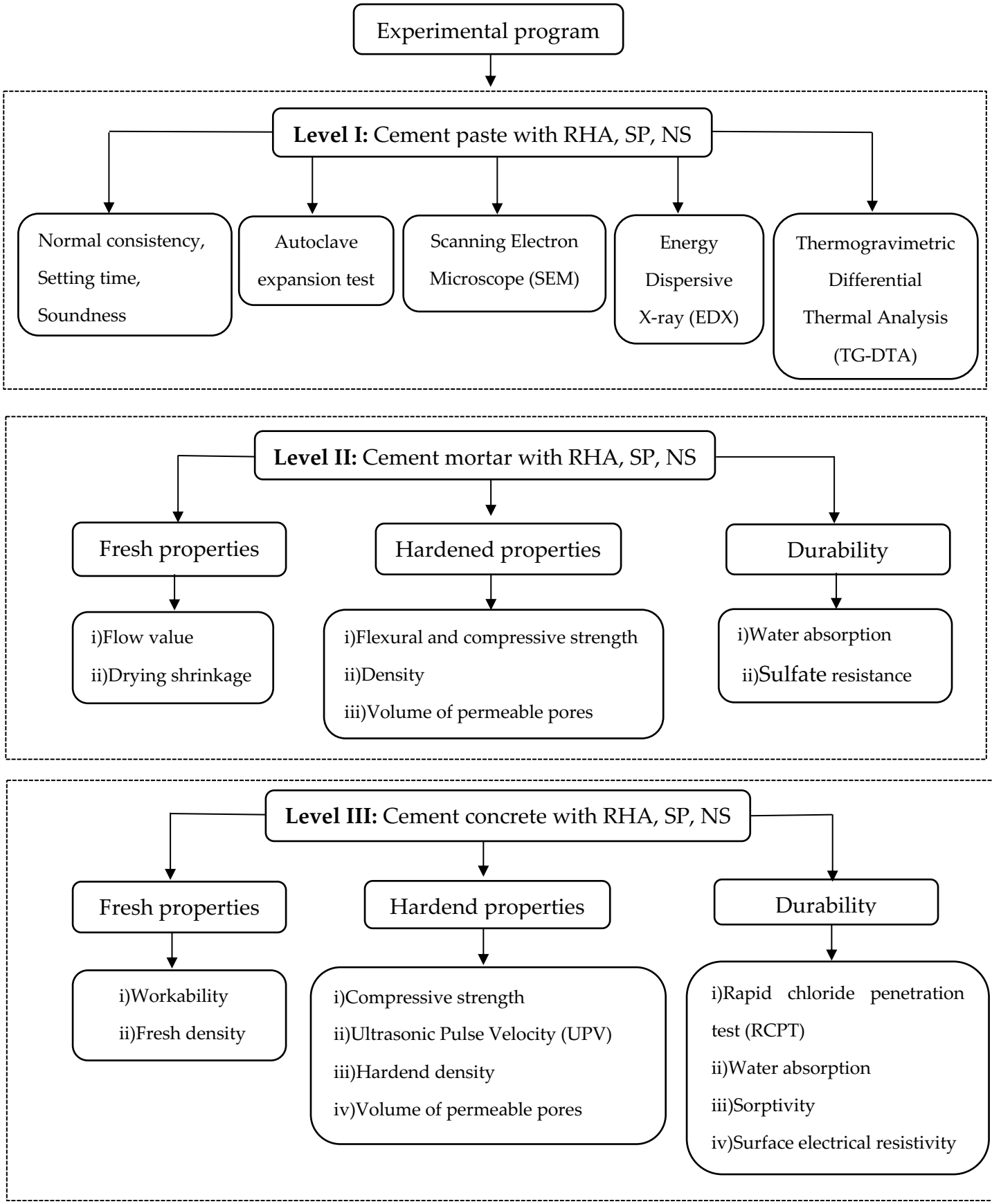

Figure 3.6: Experimental program at different levels

3.4 MIX DESIGN

The mix design for this research incorporates SP, NS (both extracted from RHA), and RHA as partial substitutions for cement in mortar and concrete production. The study adopts a systematic approach by replacing 2.5%, 5%, 7.5%, 10%, and 15% cement with RHA, SP, and NS. To ensure consistency and accuracy in the mix proportions, the absolute volume equivalency method outlined in the standard practice for selecting proportions for normal, heavyweight, and mass concrete ACI PRC-211.1 (2022) was followed. This method calculated the volume of each component in the mortar and concrete mix, considering the specific gravity and absolute volume of the materials used. The equations for converting a target water-cement ratio w/c to a weight ratio of water to cement plus pozzolanic materials w/(c + p) by volume equivalency are as follows:

$$\frac{\mathrm{W}}{\mathrm{C}+\mathrm{P}} = \frac{\mathrm{G_C}\frac{\mathrm{W}}{\mathrm{C}}}{\mathrm{G_C}(1-\mathrm{F_V})+\mathrm{G_P}(\mathrm{F_V})} \quad \text{(Eq. 3.1)}$$

$$F_W = \frac{1}{1+(\frac{G_C}{G_P})(\frac{1}{F_V}-1)} \quad \text{(Eq.3.2)}$$

$$\mathrm{F_W} = \frac{\mathrm{P}}{\mathrm{C}+\mathrm{P}} \quad \text{(Eq. 3.3)}$$

Where,

W = weight of water

P = weight of pozzolanic materials.

C = weight of cement.

W/C = target water-cement ratio

F_w = pozzolanic materials percentage by weight.

F_v = pozzolanic materials percentage by absolute volume of the total absolute volume of cement plus pozzolanic materials.

G_P = specific gravity of pozzolanic materials

G_c = specific gravity of Portland cement= 3.11

ρ_w = Density of water = 1 gm/cm^3

3.4.1 Mix Design for Mortar

A constant water/binder ratio of 0.5 and a consistent binder/sand ratio of 1:3 conforming to BS EN 196-1 (2016) was used for the mortar samples. Table 3.7 shows an overview of the mix designs for the five distinct partial replacements of each RHA, SP, and NS utilized in the research, indicated by their corresponding replacement level. Different amounts of cement, or RHA/SP/NS were used in each mix design.

Table 3.7: Mortar mix proportions

Sample Name	Cement (gm)	Pozzolanic materials (g)	EN Sand (g)	Water (g)
Control	450.0	--	1350	225
2.5% RHA	438.75	7.535		
5% RHA	427.50	15.070		
7.5% RHA	416.25	22.605		
10% RHA	405.0	30.140		
15% RHA	382.50	45.210		
2.5% SP	438.75	7.419		
5% SP	427.50	14.838		
7.5% SP	416.25	22.258		
10% SP	405.0	29.677		
15% SP	382.50	44.515		
2.5% NS	438.75	7.303		
5% NS	427.50	14.607		
7.5% NS	416.25	21.910		
10% NS	405.0	29.214		
15% NS	382.50	43.821		

3.4.2 Mix Design for Concrete

At 56 days, the average concrete strength mixture target was 4000 psi for the control mixed with cement. 360 kg/m^3 of binder, 920 kg/m^3 of fine aggregate, and 1060 kg/m^3 of coarse aggregate were used. The water-to-binder ratio (w/b) remained constant at 0.45. A water reduction of 25% was considered for the mix design by using 0.7% (of cement) high water-reducing admixture.

Table 3.8: Mix proportion for 1m^3 fresh concrete

Sample Name	Cement (kg/m^3)	Pozzolanic materials (kg/m^3)	Fine aggregate (kg/m^3)	Coarse aggregate (kg/m^3)	Water (kg/m^3)	Admixture (kg/m^3)
Control	360.0	--	920	1060	162	2.52
2.5% RHA	351.0	6.028				
5% RHA	342.0	12.056				
7.5% RHA	333.0	18.084				
10% RHA	324.0	24.112				
15% RHA	306.0	36.168				
2.5% SP	351.0	5.935				
5% SP	342.0	11.871				
7.5% SP	333.0	17.806				
10% SP	324.0	23.741				
15% SP	306.0	35.612				
2.5% NS	351.0	5.843				
5% NS	342.0	11.686				
7.5% NS	333.0	17.528				
10% NS	324.0	23.371				
15% NS	306.0	35.057				

3.5 LABORATORY TESTS

This section covers all the studies performed with partial substitution of cement using RHA, SP, and NS. It also covers the methods used to carry out these tests and the steps that follow to obtain test results. After getting the physical, chemical, and morphological properties of the pozzolanic materials, different tests were carried out for paste, mortar, and concrete specimens.

3.5.1 Tests on Binders

Characterization tests of binders included specific gravity, particle size distribution (PSD), X-ray Fluorescence Spectroscopy (XRF), X-Ray Diffraction (XRD), loss on ignition, pozzolanic activity, and water demand tests.

3.5.1.1 Specific Gravity

ASTM C188 (2023) was used to determine the specific gravities of the cement, RHA, SP, and NS. Specific gravity is an essential property as it helps assess the quality and consistency of cement and other materials. It can be stated that the ratio of a sample density to that of water at a specific temperature. The test is typically conducted using a Le Chatelier flask, a unique flask designed to measure hydraulic specific gravity of cement. Distilled water was utilized as a solvent to determine the specific gravity of RHA, SP, and NS. Kerosene was used as a liquid medium for cement.

3.5.1.2 Specific Surface Area (Blaine Fineness)

One attribute of solids is their specific surface area (SSA), which is the total surface area of a material per unit of mass (m^2/g). Surface area and fineness are directly correlated. Fineness is a key parameter that determines the average grain size of a material and regulates the rate and completeness of hydration. According to ASTM C 204 (2012), the Blaine specific area of the RHA, SP, and NS was measured. The resistance to airflow through a compressed powder bed under pressure is measured

by Blaine air permeability. In general, the reactivity of binders is enhanced with their fineness. However, high amorphous silica content and the porous nature are responsible for better reactivity of RHA.

3.5.1.3 Particle Size Distribution (PSD) analysis

Particle size distribution (PSD) using laser diffraction (LD) analysis was performed using a Mastersizer 3000 (Malvern Instruments, UK) with a Hydro MV maximum volume of 120 ml. The Hydro MV functions as a medium-volume unit that allows a controlled and automated aqueous dispersion of materials for particle size characterization. Mastersizer 3000 measures PSD from 0.01 µm to 1500+ µm using the laser diffraction technique. It is chemically suitable for a large variety of inorganic and organic dispersants. Water was used as a dispersion. The sample does not react with the dispersant, as it is also insoluble in water. Sonication power and frequencies of 40w max and 40 kHz (nominal) were utilized to de-agglomerate the particles, which increased dispersion efficiency. A refractive index of 1.640 was used for water.

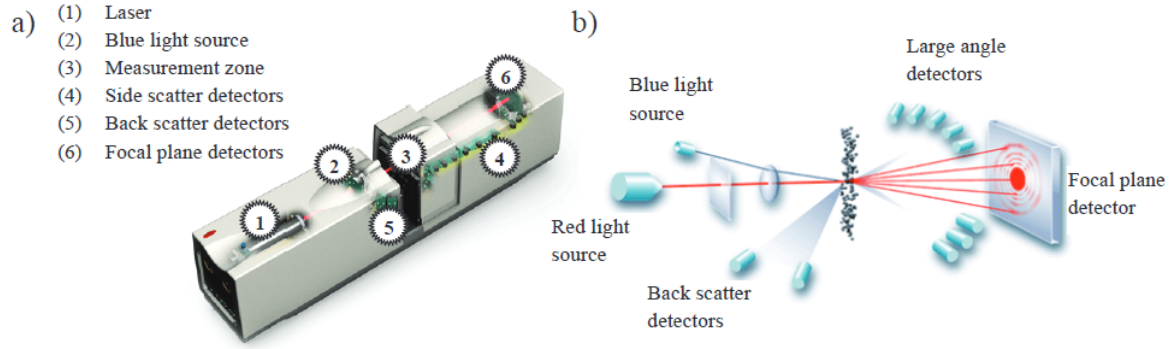

Figure 3.7: a) Key modules of typical systems (Mastersizer® 2000) b) Diagram displaying a diffraction pattern of particles

3.5.1.4 X-ray Fluorescence Spectroscopy (XRF) analysis

An X-ray fluorescence (XRF) investigation provides information on the chemical constituents of materials. Cement, RHA, SP, and NS chemical compositions were

identified via wavelength dispersive (WD) XRF spectroscopy. The results in percentage of mass, computed for the oxide amount, and standardized to 100% using carbon values. The specimens were ground and tested against an auxiliary RHA and silica standard.

3.5.1.5 X-Ray Diffraction (XRD) Analysis

X-ray diffraction (XRD) analysis is a powerful analytical technique used to identify the crystal structure, phase composition, and other structural properties of materials. XRD was used to examine the mineralogical composition of materials using a 1D Kβ filter for copper emission (Cu). The parameters used for the experiment were 40 kV, 50 mA, and a 2θ scanning rate of 30°/min, with a range of 10° to 80°. The HyPix-400 (horizontal) detector was used to collect two-dimensional diffraction images.

3.5.1.6 Moisture Content

The amount of water in a material is referred to as its moisture content, and it is often expressed as a percentage of its dry weight or wet weight. In this study, the moisture content of binders was evaluated according to ASTM D2216 (2019). To calculate it, the test sample with the container is weighed both before and after being exposed to 110±5°c for 24 hrs. Equation 3.4 was used for the calculation.

$$w = \left[\frac{M_{cws} - M_{cs}}{M_{cs} - M_c}\right] \times 100 = \frac{M_w}{M_s} \times 100 \qquad \text{(Eq. 3.4)}$$

Where,

w= Water content (%)

M_{cws}= Mass of container and wet specimen (g)

M_{cs}= Mass of container and oven dry specimen (g)

M_c= Mass of container (g)

M_w= Mass of water ($M_w = M_{cws} - M_{cs}$) (g)

M_s= Mass of solid particles ($M_s = M_{cs} - M_c$) (g)

3.5.1.7 Loss on Ignition (LOI)

The amount of organic matter in waste, sludge, cement, and soil is measured by loss on ignition. Concrete and mortar water requirements are influenced by the residual carbon content, which is the most significant component of loss on ignition. Combined water (hydrates, for example) and CO_2 from carbonates are the usual volatile components lost during analysis. It is computed by weighing a sample both before and after it is exposed to high temperatures during ignition. In this study, the loss on ignition of cement, RHA, SP, and NS was evaluated according to EN 196-2 (2005). Because RHA, SP, and NS have a high porosity and a large specific surface area due to their carbon content, they absorb water and organic admixtures, such as water-reducing agents. The following formula was used to determine the ignition loss.

$$L = \frac{m_1 - m_2}{m_1} \times 100 \qquad \text{(Eq. 3.5)}$$

Where,

m_1 = Mass of the test sample before combustion (gm)

m_2 = Mass of the test sample after combustion (gm)

3.5.1.8 Pozzolanic Activity

Pozzolanic activity assesses the degree of chemical interaction between water, calcium hydroxide, and the active ingredients of pozzolana. This property is essential because it shows how well it can contribute to the reaction that provides strength in concrete. Several pozzolanic reactivity test techniques, both direct and indirect, were found in the literature. Direct techniques evaluate the quantity of calcium hydroxide used, whereas indirect techniques evaluate changes in the physical characteristics of

specimen caused by pozzolanic actions. The strength development by the products of the pozzolanic reaction is schematically illustrated in Figure 3.8.

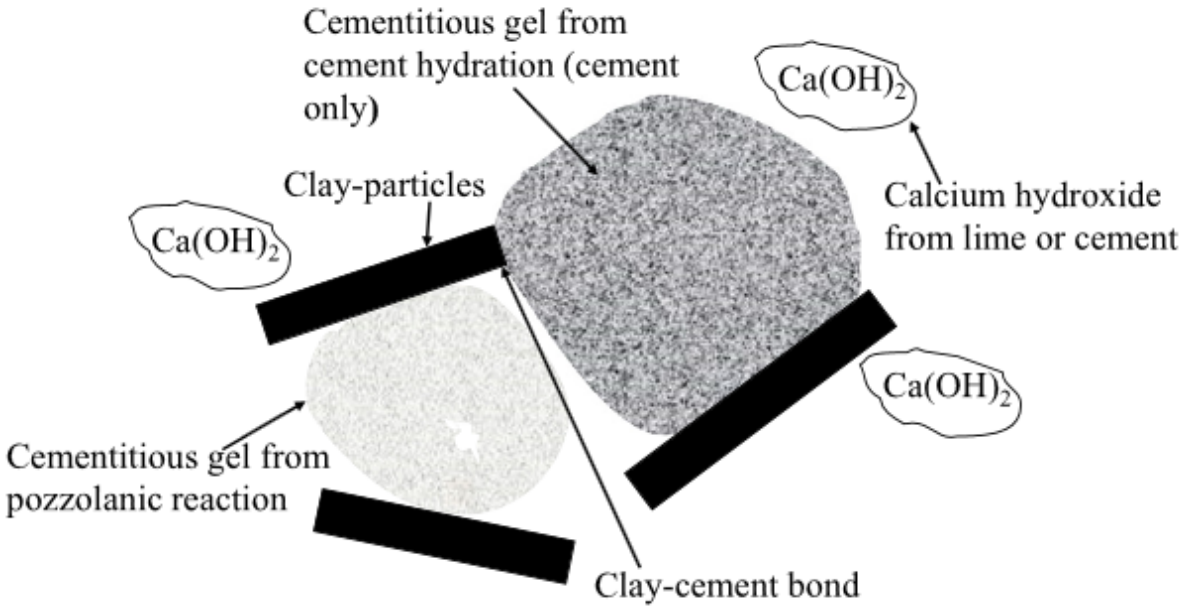

Figure 3.8: Strength development caused by products of the pozzolanic reaction (Barman & Dash, 2022)

The Strength Activity Index (SAI), as specified in BS 8615-1 (2019), was used to examine the pozzolanic performance of RHA, SP, and NS. The cementitious matrix densification and packing effect, which increase compressive strength, are evaluated by this method for the pozzolanic reaction (Black, 2016; Jang et al., 2018). The ratio of the f'_c of the mortar prism containing RHA/SP/NS to the f'_c of the control mortar prism (100% cement) at 28 and 90 days is used to compute the SAI of RHA, SP, and NS according to BS 8615-1 (2019). SAI was calculated using the following Equation 3.6.

$$\text{SAI} = \frac{\text{A}}{\text{B}} \times 100 \qquad \text{(Eq. 3.6)}$$

Where,

A = Strength of the test mortar prism containing RHA/SP/NS

B = Strength of the control mortar prism with CEM I binder only

3.5.1.9 Water Demand Test

A flow table test was used to determine the water content following BS 3892-1 (1997). The amount of water needed to create a flow value $\pm$ 5 units of the control mortar (165 mm for the control flow), was added to each mortar. The water requirement of RHA, SP, and NS was calculated by using the following Equation 3.7.

$$\text{Water demand} = \frac{X}{225} \times 100 \qquad \text{(Eq. 3.7)}$$

Where,

X = Mass of water used in the RHA/SP/NS blended mortar

3.5.2 Paste Samples Test

Tests on paste samples were denoted as Level I. In this level, normal consistency, setting time, soundness, autoclave expansion, scanning electron microscope (SEM), and energy dispersive x-ray (EDX) tests were conducted.

3.5.2.1 Normal Consistency

Normal consistency indicates the ideal water content necessary to create a standard level of wetness in a cement paste. It is the point where the paste exhibits a particular degree of stiffness. Assessing normal consistency is essential because it affects the workability, flow, and setting time of concrete and mortar. Furthermore, it is crucial in determining hardened characteristics and hydration behavior. In this investigation, the influence of RHA, SP, and NS blends (2.5%, 5%, 7.5%, 10%, and 15%) on the water requirement was explored by determining the normal consistency for the pastes using the VICAT apparatus according to ASTM C187 (2016).

3.5.2.2 Setting Time

The setting is evaluated during two time periods, viz., initial setting time and final setting time. The term "initial setting time" describes the time after water is added to a cementitious mixture before the material starts to harden and decrease its plasticity. The final setting period is needed for the cementitious mixture to reach a suitable degree of stiffness and withstand indentation at a specific pressure. In the present study, setting time tests help evaluate how the supplementary materials influence the setting characteristics of the cementitious mixture. RHA, SP, and NS blended cement pastes of standard consistency were utilized to establish the initial and final setting times in line with ASTM C191 (2021).

Figure 3.9: Setting time test apparatus

3.5.2.3 Soundness Test

Soundness is a cement quality assurance aimed at investigating expansion caused by free lime in the cement. It is crucial to confirm that the cement will not expand

significantly after setting. A small split cylinder of spring brass to another non-corrodible metal with a thickness of 0.5 mm was used in the Le-Chateliers apparatus (Figure 3.10) to create a mold that was 30 mm high and 30 mm in internal diameter. Two indicators are appropriately brazed on either side of the split, with pointed ends made of brass wire with a diameter of 2 mm. The ends are placed 165 mm from the center of the cylinder. The split cylinder was kept between two glass plates and immersed in water for 24 hrs. After 24 hrs of water immersion, the split cylinder was removed and the distance between indicators was measured with a Vernier caliper. Then the split cylinder was kept in water for boiling at 100°c for 3 hrs. After that, the expansion was measured again with a Vernier caliper.

Figure 3.10: Le-Chatelier apparatus

3.5.2.4 Autoclave Expansion Test

An autoclave expansion test was developed to quickly detect the influence of thermally cured free lime (CaO) as well as free magnesia (MgO) in Portland cement

(CEM I). Autoclave expansion experiments are durability indications used in this study to investigate the probability of late expansion in paste containing the RHA, SP, and NS. According to Lun (2008), autoclave conditions almost entirely achieve the hydration of free CaO and free MgO. To find out how hardened CEM I and blended pastes of RHA, SP, and NS expanded in the autoclave, experiments were carried out using the standard test procedure given in ASTM C151 (2018). After 24 hours of curing in the moist closet, the hardened paste samples were removed from the molds and examined in an autoclave at a high temperature of 216±2°C and a high pressure of 2 ± 0.07 MPa for 3 hours. Variations in length were measured using a length comparator and a standard reference bar.

Figure 3.11: Autoclave expansion test apparatus

3.5.2.5 Scanning Electron Microscope (SEM)

SEM analysis is one of the most widely utilized high-resolution surface imaging methods today because it is quick, disruptive-free, and incredibly accurate. A concentrated electron beam is used in SEM analysis to scan the material under examination and create a high-resolution picture of its surface. This study used SEM analysis in cementitious materials (RHA, SP, NS) and pastes with RHA, SP, and NS. After stopping hydration with 99.9% pure ethanol at a particular curing age, the cement paste specimens were broken into small pieces for SEM evaluation.

Figure 3.12: SEM image acquisition

3.5.2.6 Energy Dispersive X-Ray (EDX)

The types and quantities of elements at the surface of the material or close to it are analyzed using energy-dispersive X-ray analysis (EDX), which is used along with scanning electron microscopy (SEM) to create a specimen map. EDX is not a fully reliable method for surface characterization since X-rays are generated in a 2-μm deep region only. EDS may be used for qualitative and quantitative analysis, identifying the chemical elements in a sample, and estimating their relative abundance.

3.5.3 Mortar Samples Test

Tests on mortar samples were denoted as Level II. In this level flow table, flexural and compressive strength, water absorption, density, volume of permeable pore, drying shrinkage, and sulfate resistance were determined.

3.5.3.1 Flow Table Test

A mortar flow test was performed using a flow table in compliance with EN 1015-3 (2004). This test aimed to evaluate mortar flowability at various replacement ratios of RHA, SP, and NS. A mini frustum of a cone was used to take these measurements.

The cone is 100 mm in diameter at the bottom, 70 mm at the top, and 60 mm in height. It is set on a center-of-flow table and then filled with fresh mortar molded into two layers, each tamped 10 times with a tamper. The mortar should be compacted evenly by tamping pressure. Once the top surface of the mold was cleaned and aligned, it immediately elevated vertically, and the flow table was dropped 15 times in 15 seconds. The diameter of the mortar in two directions at right angles to one another was measured using slide calipers, and the mean value of these two measurements is the flow value.

Figure 3.13: Flow table test

3.5.3.2 Flexural Strength Test of Mortar

Tensile strength in bending is measured by flexural strength, sometimes called the modulus of rupture. Three 40x40x160 mm mortar prism specimens of each combination were subjected to flexural strength tests at ages 3, 7, 28, and 90 days. The samples were subjected to three-point loading. Flexural strength was calculated using Equation 3.8, as per EN 196-1 (2006).

Figure 3.14: Flexural strength setup

$$R_f = \frac{1.5 \times F_f \times l}{b^3} \quad \text{(Eq. 3.8)}$$

Where,

R_f is the flexural strength (MPa)

B is the side of the square section of the prism (mm)

F_f is the load applied to the middle of the prism at fracture (N)

l is the distance between the supports (mm)

3.5.3.3 Compressive Strength

The primary attribute of cementitious materials that characterizes the mechanical properties of mortar is its compressive strength. The pozzolanic reaction contributes to the compressive strength of mortar physically and chemically from RHA, SP, and NS. In this study, compressive strength was determined using the six sections that were left over from the flexural test according to BS EN 196-1 (2016). The mortar specimens were examined for compressive strength at 3, 7, 28, and 90 days of age. Compressive strength was calculated using the following formula:

$$R_c = \frac{F_c}{1600} \quad \text{(Eq. 3.9)}$$

Where,

R_c is the compressive strength (MPa)

F_c is the maximum load at fracture (N)

1600 is the area of platens or auxiliary plates (40 mm x 40 mm)

Figure 3.15: Compression Test Setup

3.5.3.4 Water Absorption Test

The quantity of water that a material can absorb is known as water absorption. Additionally, it is the amount of pore space in the specimen matrix that allows liquid elements to pass through. In this study, water absorption was tested at 90 days of age. The water absorption of mortar is measured using ASTM C642 (2022). This test involves drying mortar specimens for 24 hours at 100°C, submerging them in water for 48 hours, and boiling them for 5 hours for each replacement with RHA, SP, and NS. Following this, the amount of water absorbed by the specimen is measured. According to ASTM C642, water absorption is the ratio of water absorbed to the test dry weight of the specimen. Equations 3.10 and 3.11 provide the formula for calculating water absorption.

$$\text{Absorption after immersion (\%)} = \frac{B-A}{A} \times 100 \qquad \text{(Eq. 3.10)}$$

$$\text{Absorption after immersion and boiling (\%)} = \frac{C-A}{A} \times 100 \qquad \text{(Eq. 3.11)}$$

Where,

A is the oven-dry mass

B is the saturated mass after immersion

C is the saturated mass after boiling

3.5.3.5 Density

Densities were calculated using Equations 3.12 and 3.13 after the oven-dried mass (A), saturated mass after boiling (C), and immersed apparent mass (D) were recorded according to ASTM C642 (2022).

$$\text{Bulk density, dry} = \left[\frac{A}{(C-D)}\right].\rho = g_1 \quad \text{(Eq. 3.12)}$$

$$\text{Apparent density} = \left[\frac{A}{(A-D)}\right].\rho = g_2 \quad \text{(Eq. 3.13)}$$

Where,

ρ = Density of water = 1 g/cm^3 = 1 Mg/m^3

3.5.3.6 Volume of Permeable Pore

The volume of permeable pores of the mortar prisms was tested at 90 days for mortar specimens. Voids were calculated according to ASTM C642 (2022). Equation 3.14 gives the calculation process.

$$\text{Volume of permeable pore space (voids), \%} = \frac{(g_2-g_1)}{g_2} \times 100 \quad \text{(Eq. 3.14)}$$

Where,

g_1= Bulk density, dry

g_2= Apparent density

3.5.3.7 Drying Shrinkage Test

Drying shrinkage is defined as the reduction in test specimen length caused by conditions other than forces applied externally to the specified temperature, relative humidity, and evaporation rate conditions in the environment. This term also encompasses the overall effect of various phenomena that tend to cause both increases and decreases in length when the test specimens are being stored in the environment, where multiple processes, such as cement hydration, are occurring at varying rates. With an effective gage length of 250 mm, this study makes use of mortar prisms of 25x25x285 mm according to ASTM C596 (2023).

Figure 3.16: Drying shrinkage test setup

A batch of mortar was made with 750 g of cement, 1500 g of ASTM Standard sand, and enough mixing water to provide a 105% to 115% flow. The samples are preserved in molds for 24 h±30 min. The specimens are then taken out and allowed to cure in lime water for 48 h±30 min. When the specimens reached 72 h±30 min of age, they were taken out of the lime water, and length comparator reading of each specimen was taken right away according to ASTM C490 (2018). After 4, 11, 18, and 25 days of air storage, comparator measurements were obtained. Length change was calculated using Equation 3.15.

$$\Delta L = \frac{L_x - L_i}{L_g} \times 100 \qquad \text{(Eq. 3.15)}$$

Where,

ΔL = Percentage change in length at measuring age

L_X = Reading of specimen at measuring age

L_i = Initial reading of specimen

L_g = Gauge Length

3.5.3.8 Sulfate Resistance

Sulfate attacks are frequent and detrimental to mortar and concrete. Sulfate attack is caused by sulfate-containing salts, such as calcium, magnesium, sodium, and potassium sulfate compounds, which can react chemically with concrete components. Using 25 x 25 x 285 mm bars, the length change caused by sulfate attacks was carried out in compliance with ASTM C1012 (2022). The ratio of sand to binder components and water to cement ratio was 2.75 and 0.485 by mass. Water-cement ratios that provide a flow within $\pm$ 5 of Portland-cement mortar at a water-cement ratio of 0.485 were utilized for blends of Portland cement with RHA/SP/NS. 2 bars and up to 21 cubes were cast as part of a series of specimens to test one type of cement. Following demolding, every bar and cube—aside from the three that needed to be broken—was kept in a curing tank filled with saturated limewater. To determine whether 20 MPa was reached, two cubes in compression were broken. Comparator measurements were taken, and all the bars were submerged in the sulfate solution (50 g/L of Na_2SO_4) when the mean strength of the two cubes was found 20 MPa or higher. Using the length comparator, the bars were examined for length change at 1, 2, 3, 4, 8, 13, and 15 weeks following their immersion in the sulfate solution, in compliance with Specification ASTM C490 (2018).

3.5.4 Concrete Samples Test

Tests on concrete samples were denoted Level III. Fresh density, workability, compressive strength, water absorption, density, volume of permeable pore, ultrasonic pulse velocity (UPV), rapid chloride penetration (RCPT), sorptivity, and surface electrical resistivity tests were conducted at this level.

3.5.4.1 Fresh Density

Density greatly influences the mechanical properties of concrete. Generally, denser concrete often has fewer voids and porosity, which increases its strength, durability, and resistance to permeability. The fresh density of concrete was calculated following ASTM C138 (2017). Density was calculated using Equations 3.16 and 3.17.

a) Mass of measure

b) Mass of the measure filled with

Figure 3.17: Measurement of the mass of concrete

$$D = \frac{M_c - M_m}{V_m} \quad \text{(Eq. 3.16)}$$

$$T = \frac{M}{V} \quad \text{(Eq. 3.17)}$$

Where,

D = Density of concrete (kg/m^3)

M_c = Mass of the measure filled with concrete (kg)

M_m = Mass of the measure (kg)

T = Theoretical density of the concrete computed on an air-free basis (kg/m^3)

M = Total mass of all materials batched (kg)

V = Total absolute volume of the component ingredients in the batch (m^3)

3.5.4.2 Workability

According to the American Concrete Institute (ACI), workability is a property of newly mixed concrete or mortar that indicates how easily it can be mixed, placed, completed, and finished in a uniform state (Zulu, 2017). The slump test was used in this study to assess the workability of concrete following ASTM C143 (2008). Three layers of concrete, each about one-third the volume of the mold, were instantly poured into the mold from the fresh concrete sample. Using the rounded end of the temping rod, each layer was evenly rodded 25 times throughout the cross-section. Then the mold was uplifted, and the subsidence from the original height is measured and reported as the slump value of concrete. Figure 3.18 shows a concrete slump test.

Figure 3.18: Workability of concrete (Slump test)

3.5.4.3 Compressive Strength

Compressive strength is one of the prime properties of hardened concrete. A strength of material is its capacity to withstand stress without failing (Neville, 2010). The compressive strength test was done on an average of three 100 x 200 mm concrete cylinders. Specimens were cast with OPC (control), and then OPC was substituted with RHA/SP/NS at 2.5%, 5%, 7.5%, 10%, and 15% replacement levels. The specimens were taken out of the mold after 24 hours and allowed to cure in water for 14, 28, and 56 days.

Figure 3.19: Compressive strength test of a Cylindrical sample

3.5.4.4 Water Absorption, Density, and Volume of Permeable Pore

To determine the water absorption, density, and volume of permeable pores ASTM C642 (2022) code was followed. As with the mortar samples, the same procedure was used for concrete samples.

3.5.4.5 Ultrasonic Pulse Velocity (UPV)

Using the propagation velocity of a vibrational energy pulse that has traveled through a concrete material, this test determines if voids and cracks are present and how well crack repairs are working. To assess the density and internal cracks of concrete, the UPV test was also performed. Before the compression test, this test was conducted on

100 x 200 mm cylinder specimens after 56 days of curing in compliance with ASTM C597 (2003). Pulse velocity was calculated using Equation 3.18.

$$V = \frac{L}{T} \qquad \text{(Eq. 3.18)}$$

Where,

V = Pulse velocity (m/s)

L = Distance between centers of transducer faces (m)

T = Transit time (s)

Higher velocity is a sign of better density, homogeneity, and uniformity in the concrete. The pulse velocity value may be used to categorize concrete quality ratings following BS 1881 (2021), as Table 3.9 illustrates.

Figure 3.20: Ultrasonic pulse velocity test

Table 3.9: Classification of concrete quality based on UPV test as per BS 1881 (2021)

Pulse velocity (km/s)	Concrete quality (ratings)
≥ 4.5	Excellent (E)
3.5 – 4.5	Good (G)
3.0 – 3.5	Medium (M)
2.0 – 3.0	Doubtful (D)
≤ 2.0	Very weak (VW)

3.5.4.6 Rapid Chloride Penetration Test (RCPT)

The most frequent damage in reinforced concrete (RC) structures that caused by corrosion from exposure to seawater or de-icing salt is chloride ion penetration (Jones, 1997). Standard cylindrical cube samples measuring 100 mm in diameter and 50 mm in height were used to measure the chloride resistivity of hardened concrete using the RCPT following ASTM C1202 (2012). An external electrical voltage is provided to drive the chloride ion into the sample. The ions move from the 3% NaCl solution via the concrete specimen and toward the 0.3N NaOH solution because of the potential difference between the electrodes (Anolyte) and chloride (Catholyte) for 6 hours. The total charge passed from the concrete sample was calculated from Equation 3.19. Chloride ion penetrability chances can be predicted using Table 3.10.

$$Q = 900(I_0 + 2I_{30} + \cdots + 2I_{330} + I_{360}) \qquad \text{(Eq. 3.19)}$$

Where,

Q = Charge passed (coulombs)

I_0 = Current (amperes) immediately after voltage is applied

I_t = Current (amperes) at t min after voltage is applied

a) Vacuum saturation setup

b) Specimen setup for test

Figure 3.21: Rapid chloride penetration test setup

Table 3.10: Chloride Ion Penetrability Based on Charge Passed

Charge passed (coulombs)	Chloride ion penetrability
>4000	High
2000 – 4000	Moderate
1000 – 2000	Low
100 – 1000	Very Low
<100	Negligible

3.5.4.7 Sorptivity

The purpose of this test is to evaluate susceptibility to water penetration of an unsaturated concretes. It uses capillary suction to assess the rate at which water and other liquids are absorbed into unsaturated concrete. The cylinder specimens were cured for 28 days. A 50-mm slice was taken out from the cylinder and kept in an evaporation chamber for three days at 50±2 °C and 80±3 % relative humidity. After that, it was sealed in a container for a minimum of 15 days.

Before the slice was submerged in water, its exterior side was covered with a non-absorbent substance, and the side that was not exposed to water was loosely sealed with a plastic sheet. The water level was 3 mm above the sample base when the specimens were submerged. The surface water was removed using a moistened cloth, and the amount of water absorbed within the allotted time was quantified to the closest 0.01g using a balance and following ASTM C1585 (2013). Table 3.11 shows the acceptance criteria for durability indices.

Table 3.11: Suggested range for durability classifications using index values (Alexander et al., 1999)

Durability class	Sorptivity (mm/√h)
Excellent	<6
Good	6-10
Poor	10-15
Very poor	>15

a) Samples in humidity chamber

b) Samples in sealed container

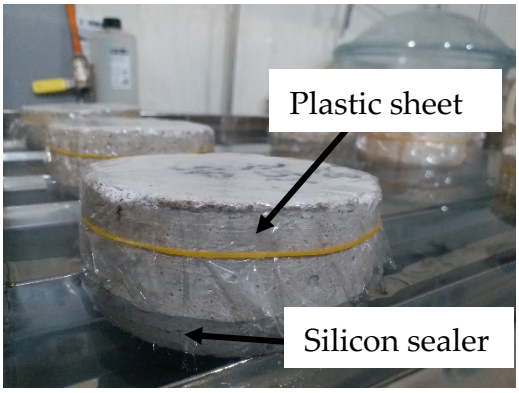

c) Prepared sample before testing

d) Submerged samples in water

Figure 3.22: Sorptivity test setup

$$I = \frac{\Delta W}{Ad} \qquad \text{(Eq. 3.20)}$$

$$S = \frac{I}{\sqrt{t}} \qquad \text{(Eq. 3.21)}$$

Where,

I = Water absorption (mm)

ΔW = Change in mass (g)

A = Cross sectional area of specimen (mm^2)

d = Density of water (g/mm^3)

S = Sorptivity (mm)

t = time (s)

3.5.4.8 Surface Electrical Resistivity

One crucial physical characteristic of Portland cement concrete that is directly related to the corrosion process caused by chloride is electrical resistance. A commercially available 4-point Wenner probe surface resistivity (SR) meter made by Proceq was used to measure the surface resistivity. Using this method, the surface electrical resistivity of concrete is measured using four linear electrodes that are evenly spaced.

Table 3.12: Relationship between permeability class and surface resistivity (AASHTO T358, 2015)

Chloride ion permeability classification	**Surface resistivity (kΩ − cm)**
High	<12
Moderate	12-21
Low	21-37
Very low	37-254
Negligible	>254

Figure 3.23: Surface electrical resistivity test setup

While the inside probes monitor the electrical potential, the two external electrodes provide an AC current to the concrete surface. It should be mentioned that DC current is undesirable as the polarization effect might lead to inaccurate readings. A 100 x 200 mm cylindrical specimen was examined for surface resistivity at 56 days. As recommended by AASHTO T358 (2015) specification, Table 3.12 shows how the chloride ion permeability requirements of various concrete mixes are categorized based on surface electrical resistivity. Figure 3.23 shows the surface electrical resistivity test setup using a 4-point Wenner probe.

3.6 TEST MATRIX

Table 3.13 presents a summary of the characterization tests conducted on binders during the preliminary study. Tables 3.14, 3.15, and 3.16 provide summaries of the tests performed on different cementitious media at three distinct levels.

Table 3.13: Preliminary analysis for binder characterization with standards

SL No.	Name of the tests	Standards / Methods
1	Specific gravity	ASTM C188
2	Specific surface area (Blaine)	ASTM C204
3	Particle size distribution (PSD)	Laser diffraction
4	Mineralogical analysis	X-ray diffraction (XRD)
5	Chemical analysis	X-ray fluorescence (XRF)
6	Loss on ignition (LOI)	EN 196-2
7	Pozzolanic activity (SAI)	BS 8615-1
8	Water demand test	ASTM C311

In Level I tests were conducted on paste samples. Table 3.14 shows the conducted tests with standards for paste samples. Mortar samples were used in Level II testing. The tests that were performed using standards for mortar samples are presented in Table

3.15. Tests were conducted on concrete samples at Level III. The tests that were performed on concrete samples using standards are presented in Table 3.16.

Table 3.14: Conducted tests on paste samples with standards

SL No.	Name of the tests	Standards / Methods
1	Normal consistency, setting time, and Soundness	BS EN 196-3
2	Autoclave expansion test	ASTM C151
3	Scanning electron microscopy (SEM) and Energy Dispersive X-ray (EDX)	–

Table 3.15: Conducted tests on mortar samples with standards

SL No.	Name of the tests	Standards / Methods
1	Flow table test	BS EN 1015-3
2	Flexural and compressive strength	BS EN 196-1
3	Water absorption, Density, and VPP	ASTM C642
4	Drying shrinkage	ASTM C596
5	Sulfate resistance	ASTM C1012

Table 3.16: Conducted tests on concrete samples with standards

SL No.	Name of the tests	Standards / Methods
1	Fresh density of concrete	ASTM C138/138M
2	Workability (Slump)	ASTM C143
3	Compressive strength	ASTM C39
4	Water absorption, Density, and VPV	ASTM C642
5	Ultrasonic pulse velocity	ASTM C597
6	Rapid chloride penetration test	ASTM C1202
7	Sorptivity	ASTM C1585
8	Surface electrical resistivity	ASTM C1760

3.7 CHAPTER SUMMARY

For the experimental program, CEM I, RHA, SP, and NS were used as binders. Firstly, for binder characterization, specific gravity, particle size distribution, moisture content, loss on ignition, pozzolanic activity, and water demand tests were programmed. To evaluate the binder performance, an experimental program was divided into three different levels (paste, mortar, and concrete). Partial replacement (0%, 2.5%, 5%, 7.5%, 10%, and 15%) of CEM I by these binders was done by volume. EN sand was used in those mortar samples (40 x 40 x 160 mm) that were used to test flexural, compressive, water absorption, density, and volume of permeable pores. A total of 240 mortar samples were cast using EN sand. Flexural and compressive strength data were taken after 3, 7, 28, and 90 days of curing. ASTM standard sand was used to make 25 x 25 x 285 mm size samples that were used to evaluate drying shrinkage and expansion under sulfate attack.

For concrete samples, a mix design was done to achieve a 27MPa strength. A total of 208 cylinders (100 x 200 mm) were cast, and the tests were done after 14, 28, and 56 days of curing. Fresh density, workability, compressive strength, water absorption, density, volume of permeable pores, UPV, RCPT, sorptivity, and surface electrical resistivity tests were done in concrete samples.

Chapter 4: RESULTS AND DISCUSSIONS

This section combines all the results of tests that were performed in a sequence and the individual analysis of each test. Combining all the results and analysis has concluded the effectiveness of rice husk ash, silica powder, and nano silica as a partial replacement of cement.

4.1 TEST RESULTS OF BINDER SAMPLES

In this section, preliminary analysis results of binders are presented. Specific gravity, surface area, particle size, mineralogical and chemical analysis, SEM and EDX, and loss on ignition results are included in this section.

4.1.1 Specific Gravity and Particle Size Distribution

The RHA, SP, and NS used in this investigation had specific gravities of 2.083, 2.051, and 2.02, respectively. These binders have a lower density compared to cement. The reduced specific gravity of RHA is primarily due to its porous structure. Similarly, both SP and NS extracted from RHA also show lower specific gravity as a result of their porous and amorphous characteristics. The extraction process does not eliminate porosity for SP and NS. The specific gravity values for RHA, SP, and NS were measured to be 33.0%, 34.1%, and 35.1% lower than that of cement, respectively. The PSD of RHA, SP, and NS was determined using laser diffraction analysis. The analysis provides information on the particle size of the materials, which is essential for understanding their suitability for various applications. The PSD of RHA, SP, and NS is illustrated in Figure 4.1 and Figure 4.2. The percentile value and specific gravity are present in Table 4.1.

As shown in Figure 4.2, the particle size of RHA ranges from 1.6 μm to 1100 μm, with an average particle size (d_{50}) of 87.3 μm. The 10^{th} percentile (d_{10}) and 90^{th} percentile (d_{90}) values show that 10% and 90% of the particles are smaller than 21.1 μm and 375.3 μm, respectively. Similarly, the particle size range of the SP, which was extracted from

RHA by maintaining a pH level of 3, is mainly between 0.67 μm and 90 μm, with an average particle size (d_{50}) of 14.2 μm. The 10th percentile (d_{10}) and 90th percentile (d_{90}) values were 4.0 μm and 40.5 μm, respectively.

Table 4.1: Specific gravity and PSD percentile value of RHA, SP, and NS

Sample	Sp. Gravity	Percentile (μm)								
		Dv_{10}	Dv_{20}	Dv_{50}	Dv_{70}	Dv_{90}	Dv_{95}	Dv_{97}	Dv_{99}	Dv_{100}
RHA	2.083	21.1	36.5	87.3	156.7	375.3	527.5	633.6	831.4	1251.6
SP	2.051	4.0	6.0	14.2	23.4	40.5	49.4	55.2	65.0	85.4
NS	2.019	5.1	7.3	15.5	24.0	39.0	46.5	51.2	59.1	75.7

The size of NS extracted from RHA by maintaining pH 10 is mainly between 0.75 μm and 90 μm, with an average particle size (Dv_{50}) of 15.5 μm. The 10th percentile (Dv_{10}) and 90th percentile (Dv_{90}) values were 5.1 μm and 39.0 μm, respectively. So, SP and NS particle sizes are very close, as shown in Figure 4.1. The average particle size (d_{50}) of SP and NS was 83.7% and 82.2% smaller than the average particle size (d_{50}) of RHA. The PSD analysis shows that SP and NS have a finer particle size with a larger surface area, with most particles within the 0.67 - 100 μm range. In the case of RHA, the particles are within 1.67 - 1100 μm, indicating a relatively coarser particle size.

This suggests that, compared to RHA, SP, and NS have finer particle sizes. When compared to rice husk ash, precipitated silica or nano-silica has the smallest particle sizes, which is consistent with research by Land & Stephan (2012), Wan (2016), and Gosalvitr (2015). The unimodal density patterns of RHA, SP, and NS in Figure 4.2 demonstrate the homogeneity of these samples. PSD data for RHA and SP were collected from the research conducted by Nila (2024).

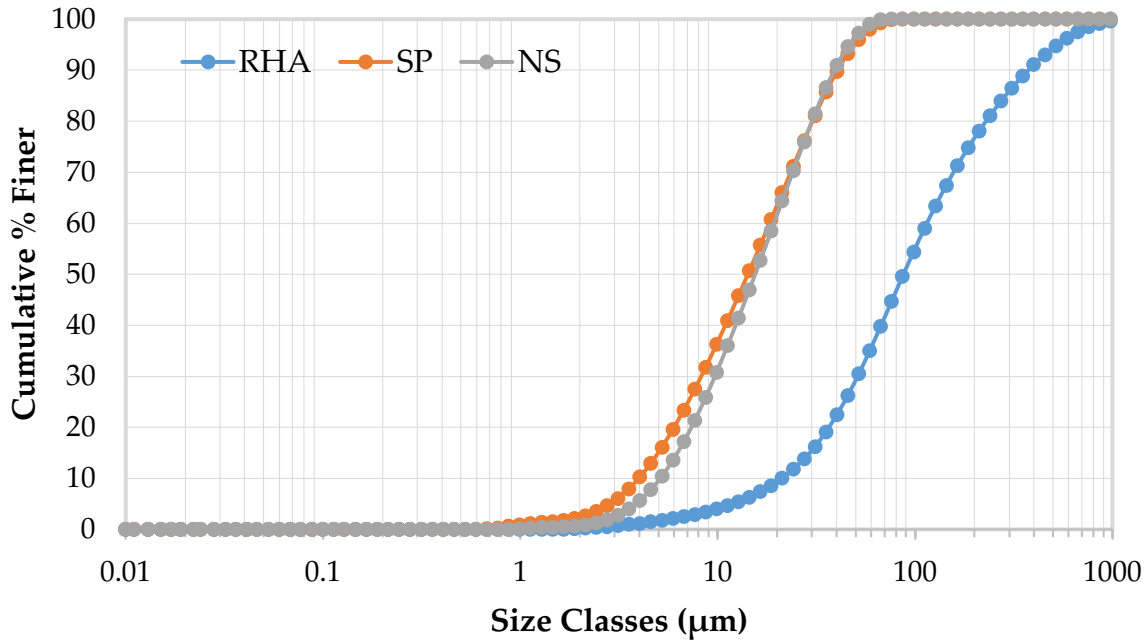

Figure 4.1: PSD curve of RHA, SP, and NS

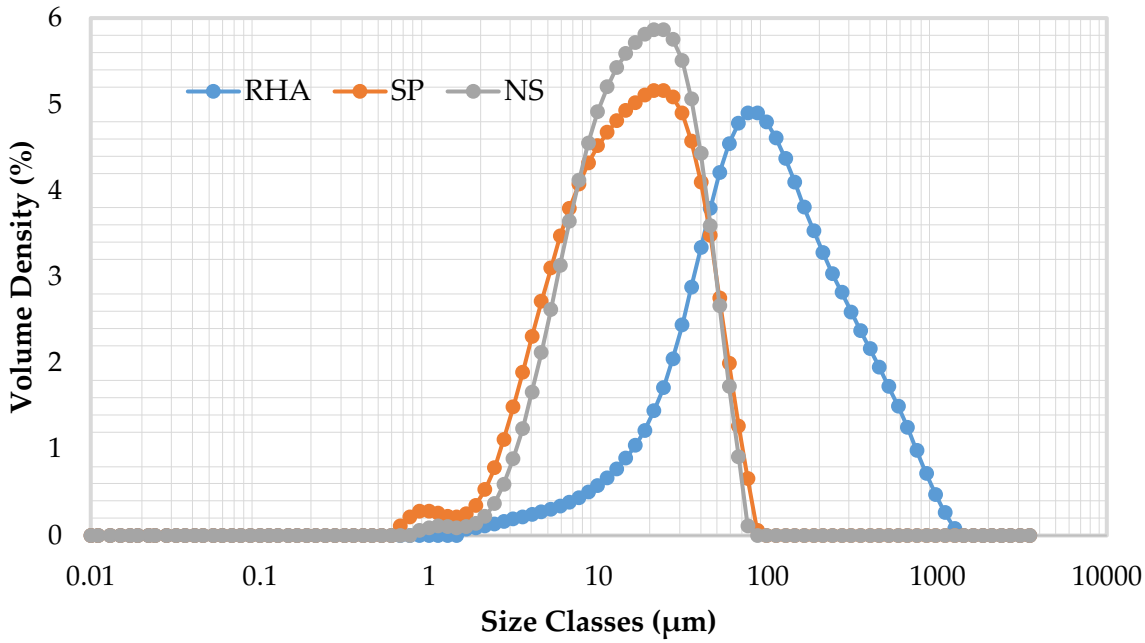

Figure 4.2: Particle size (µm) vs volume density (%) of RHA, SP, and NS.

4.1.2 Specific Surface Area (Blaine Fineness) & 45µ Residue

Blaine fineness of RHA, SP, and NS is shown in Table 4.2. The fineness was found 4044 cm^2/g, 4838 cm^2/g, and 4573 cm^2/g for RHA, SP, and NS, respectively. A pozzolanic substance must not retain more than 40% and 34% of particles on a 45 micron screen,

according to physical requirements BS 8615-1 (2019) and ASTM C618-22 (2023), respectively. Only SP satisfied this limit with 19% residue on 45μ sieve. Because of the larger particle size, RHA did not satisfy this limit, and agglomeration of particles could be the reason for NS.

Table 4.2: Blaine surface area and 45μ sieve residue of RHA, SP, and NS

Sample name	Blaine Fineness (cm^2/g)	Residue on 45μ (%)
RHA	4044	73.4
Silica powder (SP)	4838	19
Nano silica (NS)	4573	63

4.1.3 X-Ray Fluorescence Spectroscopy (XRF) Analysis

The chemical composition of research materials is shown in Table 4.3. The silica contents of RHA 79.4% and SP 79.3% were found to be similar. However, with more purification, the silica content in NS is higher than in RHA and SP, which was 92.6%. A pozzolan is categorized as F type by ASTM C618 (2023) if its sum of SiO_2, Al_2O_3, and Fe_2O_3 content is greater than 70%. As a result, these oxides (SiO_2 + Al_2O_3 + Fe_2O_3) can be categorized as N pozzolans in this instance because their overall amount in RHA is 81.3%, SP is 79.8%, and NS is 92.9%. Furthermore, RHA, SP, and NS contain less than 4% sulfur trioxide (SO_3), the maximum permitted level per ASTM C618. Chemical composition of RHA and SP was taken from the research done by Nila (2024).

It is also observed that RHA presents K_2O, primarily owing to the application of chemical fertilizers to improve rice fields. As such, RHA, SP, and NS can be categorized as class N pozzolan. These chemical characteristics are consistent with published researches (Antiohos et al., 2014; Karim et al., 2014; Zain et al., 2011). According to Ugheoke & Mamat (2012), metallic impurities, particularly potassium and sodium oxides, make it more difficult to produce silica with a purity of over 97%

from rice husk by direct incineration. These compounds influence silica particles' surfaces, increasing their reactivity and surface area while also speeding up the crystallization of silica.

Table 4.3: Chemical composition of RHA, SP, and NS

Oxides	Mass (%)		
	RHA	SP	NS
SiO_2	79.4	79.3	92.6
Na_2O	0.106	8.06	3.58
K_2O	6.53	0.938	0.444
CaO	3.65	1.03	0.34
MgO	1.48	0.081	0.06
Al_2O_3	0.385	0.167	0.2
Fe_2O_3	1.48	0.343	0.105
P_2O_5	4.47	0.151	ND
SO_3	1.27	0.576	0.23
MnO	0.866	ND	0.03
ZnO	ND	0.02	0.04
Cl	0.18	9.34	2.33

*ND: Not Detected

4.1.4 X-Ray Diffraction (XRD) Analysis

To find variations in the development of amorphous or crystalline silica, an XRD examination was carried out for RHA, SP, and NS. Baseline correction of all XRD data was done using Origin Pro software, and peak value was detected using Expert High Score Plus software. Figure 4.3 presents the XRD patterns of RHA. Without any treatment, the XRD of RHA displays a hump form, signifying the presence of amorphous content. The crystalline silica concentration peaks may also be seen at the Bragg 2-theta angle limit of 25–27 (Chandrasekhar et al., 2003; Cordeiro et al., 2009; Khan et al., 2012). There was an amorphous halo in the XRD pattern of RHA found between 15º to 31°, with a maximum intensity at $2\theta = 26.6°$, shown in Figure 4.3(a).

Figure 4.4 shows XRD patterns of SP and NS. For SP shown in Figure 4.4(a), the prominent peaks or reflections of crystalline quartz are found at Bragg 2θ angles of 45.47° and 31.74°. No other distinct peaks in Figure 4.4(a) correspond to these Bragg 2θ angles. The observed peak spans 2θ and is relatively broad, typical of amorphous formations. Figure 4.4(b) shows the XRD pattern for NS. As is observed, these X-ray patterns show a large hump shape between 10° and 30° (2θ). By this pattern, NS shows a pure amorphous nature without any distinct peaks. Balakrishnan (2013) stated that because of the amorphous nature of silica nanoparticles, prominent scattering peaks were found between 2θ angles of 10° to 30°.

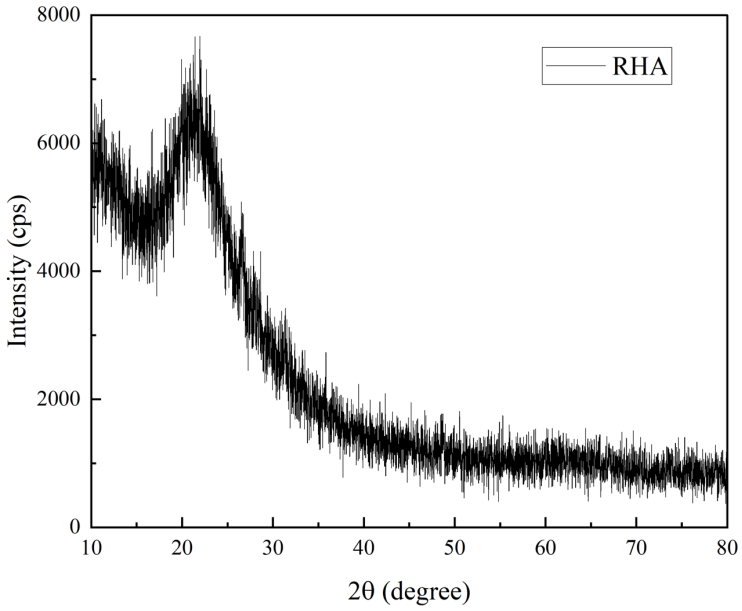

a) Without baseline correction

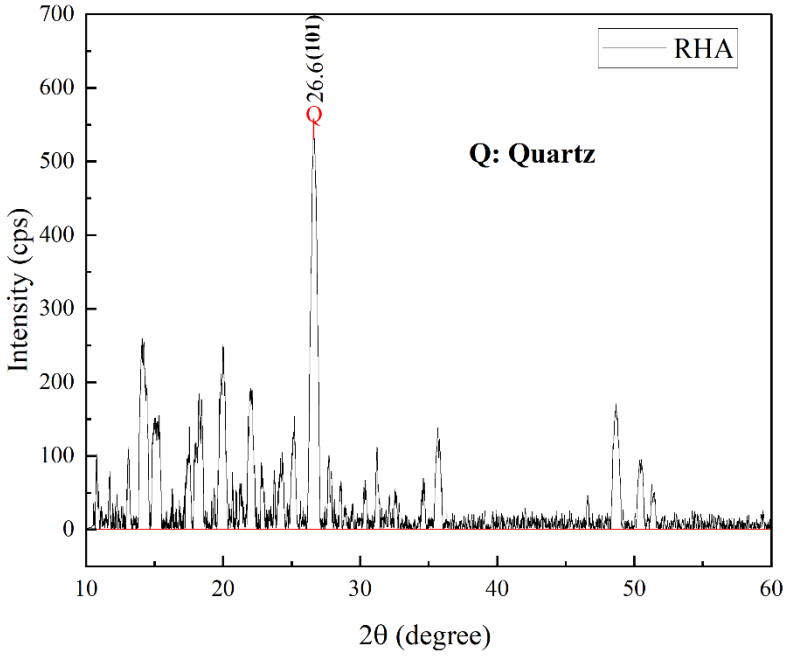

b. With baseline correction by Origin pro software

Figure 4.3: XRD pattern of RHA

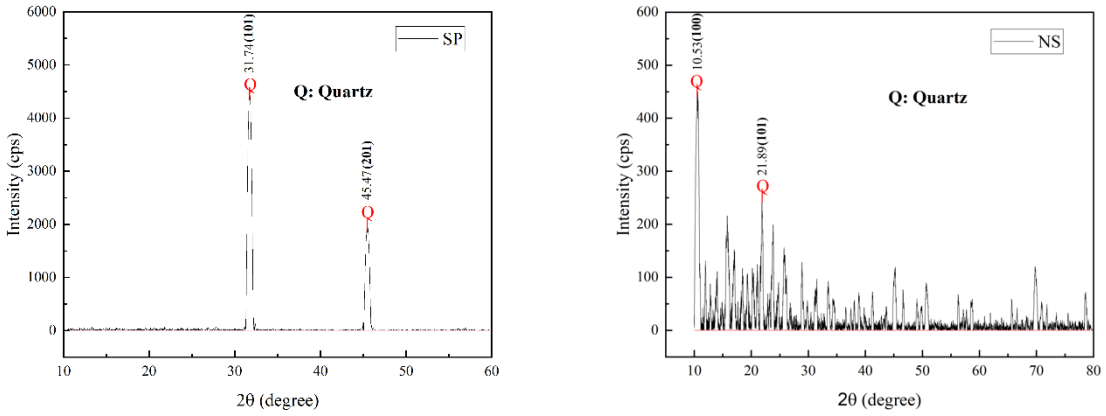

a) XRD pattern of SP

b) XRD pattern of NS

Figure 4.4: XRD pattern of SP and NS from RHA

4.1.5 Moisture Content

Figure 4.5 shows the moisture content of cement, RHA, SP, and NS. Moisture content in cement was very less (0.3%) compared to RHA, SP, and NS. Extracted SP and NS had more moisture content than RHA. It may be related to the extraction process. Because the alkaline extraction process involves an aqueous solution named as aqua gel, which could retain water even after filtration and drying.

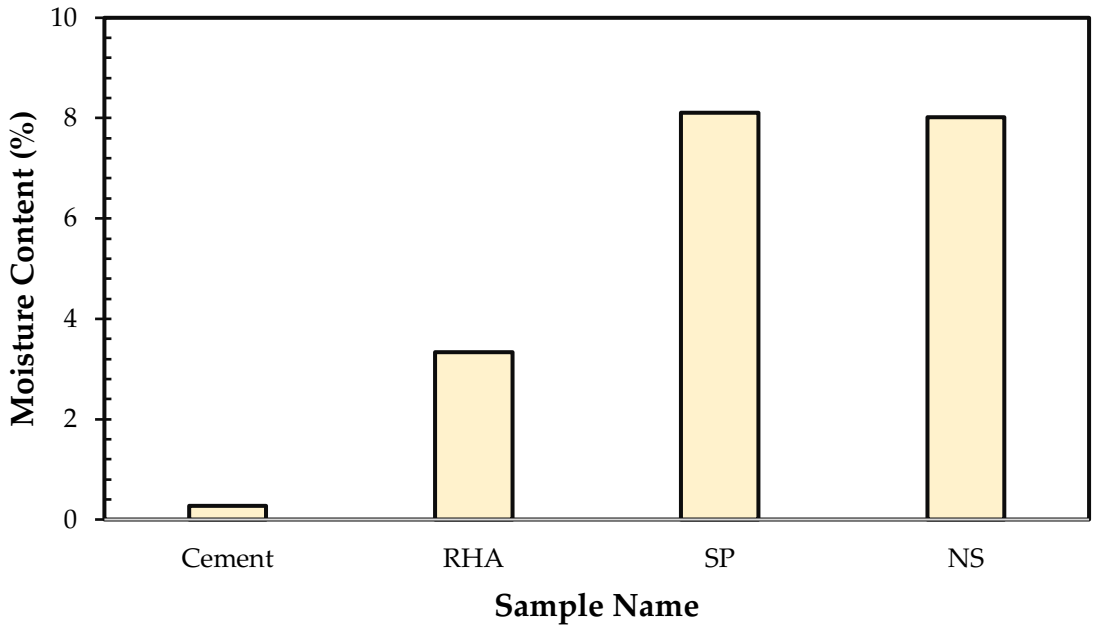

Figure 4.5: Moisture content of test samples

4.1.6 Loss on Ignition (LOI)

Figure 4.6 shows the residual organic content (loss on ignition) of cement, RHA, SP, and NS samples. The LOI for RHA was found to be 3.8, and it was within ASTM C618 (2023) limitations. Different researchers found the LOI of RHA ranges from 1 to 12% (Kumar Das et al., 2022). The presence of unburned residues and unstable mineral phases at high temperatures is often the cause of high loss of ignition (LOI) in rice husk ash (RHA). The varying amounts of unburned residues and moisture may cause variations in LOI (Santasnachok et al., 2015). LOI has increased in extracted SP and

NS. Residual acid or alkali byproducts may be left in the silica structure after extraction with NaOH or H_2SO_4. During testing at high temperatures, these byproducts may break down, adding to the mass loss and raising the LOI. Mohammed (2018) found the LOI of nano silica to be 6%.

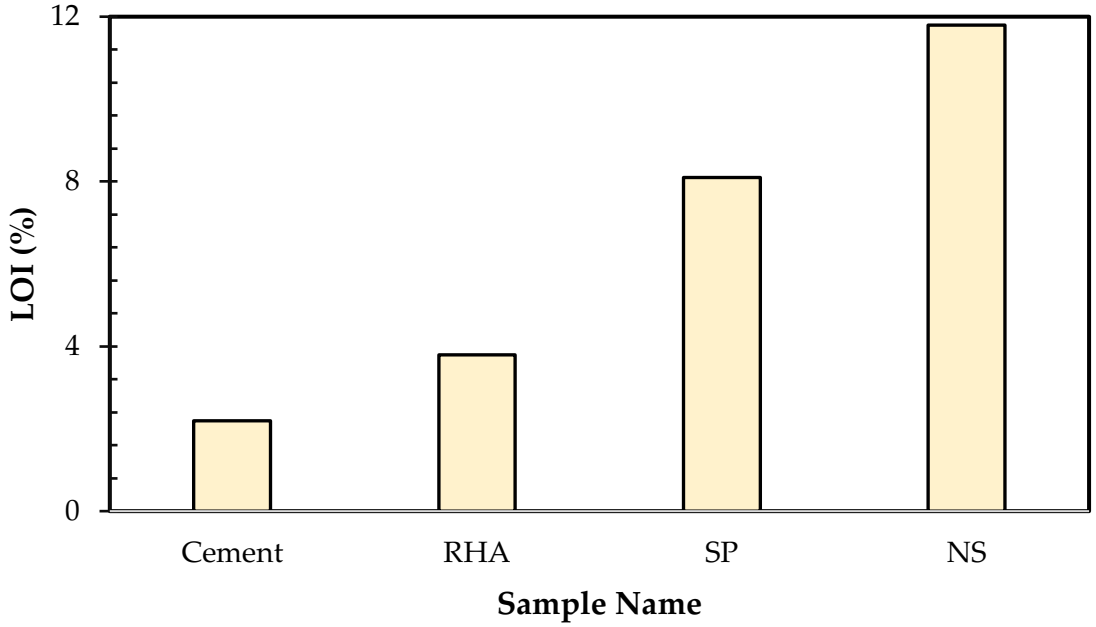

Figure 4.6: Loss on ignition (LOI) of test samples

4.1.7 Scanning Electron Microscope (SEM)

The size, shape, and morphological properties of the RHA, SP, and NS particles are crucial for understanding and explaining flow, strength, and shrinkage in cementitious media. The microstructure of the RHA, SP, and NS samples was examined using scanning electron microscopy. After burning the outer layer of the rice husk, was found as a corrugated structure was found to be well-organized, as seen in Figure 4.7(a). The inner epidermis has loose layers and a highly porous structure (Figure 4.7(b)). The ash particle has a hull-like form. But because of their fragility, some of these particles tend to disintegrate when handled, losing their hull-like form. The grinding time has a significant impact on the microstructure of RHA

(Chindaprasirt et al., 2008). RHA particles are coarse, porous, and have an uneven distribution, as seen in the images. Additionally, they vary in size and shape.

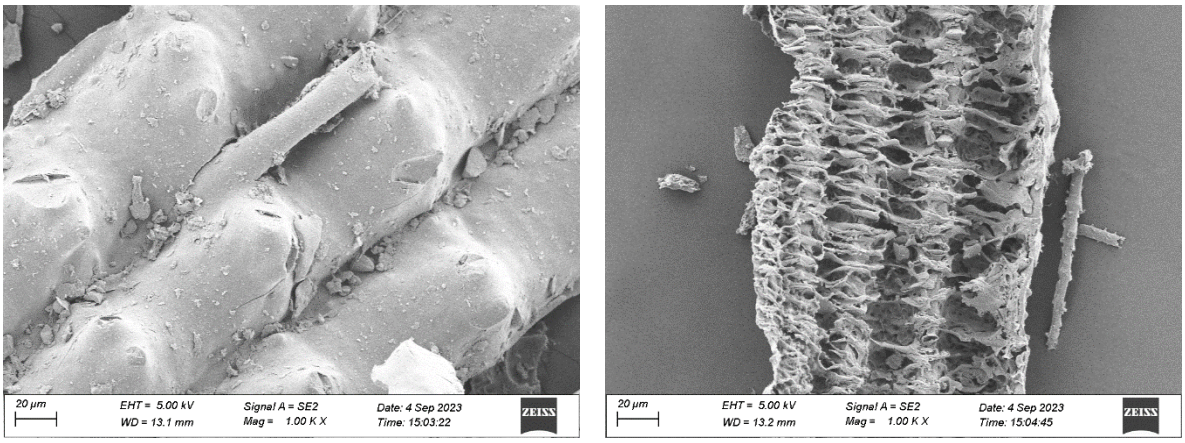

a) Outer surface b) Inner surface

Figure 4.7: SEM images of control burned RHA

Rice husks have distinct morphologies on their inner and exterior surfaces. The silica is mainly found in the strong interlayer, or epidermis, of rice husk, filling up the gaps between the cells (Deshmukh et al., 2012; Sharma et al., 1984). The study by Krishnarao & Godkhindi (1992) found that the exterior epidermal cells contained most of the silica, with the dome-shaped protrusions having the highest concentration. The rice husk has a very porous structure because it has broken apart during the thermal breakdown of organic materials. As seen in Figure 4.8, the grain of the rice husk ash-derived silica has an uneven form, and particle size varies from 50-70 nm for SP and 40-60 nm for NS. With a greater SEM magnification, it is evident that the synthesized silica has heterogeneous mesopores because of the different sizes of the grains. Pore holes are shown by dark-hued surfaces, while amorphous silica is indicated by brilliantly colored surfaces. On the other hand, the structure of synthesized silica indicates a propensity to agglomerate. Younesi & Ghasemi (2011) produced nano-silica with a small particle range from 50 to 120 nm. Owing to their amorphous and aggregated state, silica powder and nano-silica particles lack distinct boundaries.

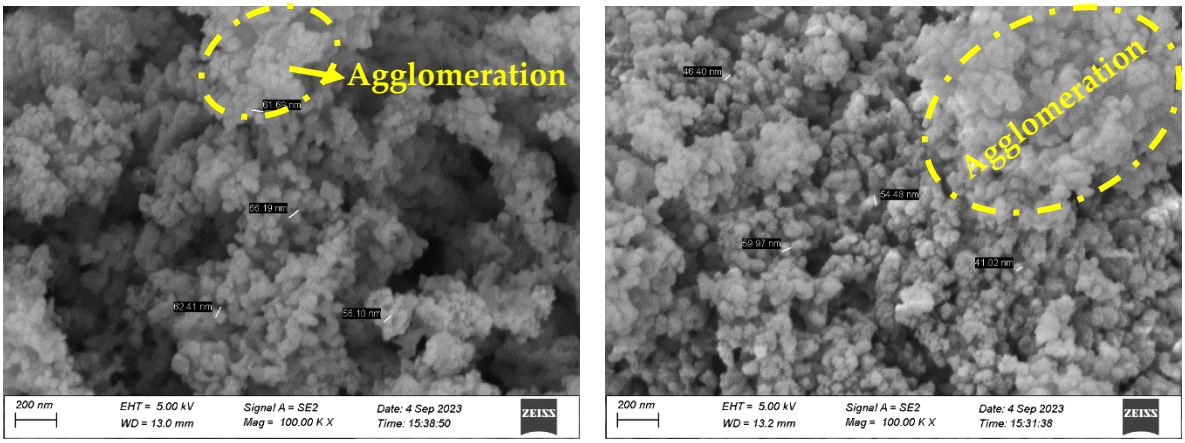

a) SEM image of SP b) SEM images of NS

Figure 4.8: SEM images of extracted SP, and NS from RHA

4.1.8 Energy Dispersive X-Ray (EDX)

The proportion of silica in the samples was ascertained by EDX analysis of the RHA, SP, and NS. Si and O, which accumulate as SiO_2, were the most prevalent components in RHA, SP, and NS. The existence of silica is confirmed by the Si and O peaks (Figure 4.9). Both components exhibit the primary distinctions. The weight percentage of silicon in RHA, SP, and NS was 42.44%, 34.14%, and 27.42%, respectively, according to the EDX. RHA was mostly composed of oxygen and silicon at weight concentrations (Bakdash et al., 2020; Nduka et al., 2022). These findings aligned with the quantitative analysis of XRF. Nano silica with a composition of 65% was reported by Ma (2012). Ghorbani (2015) produced silica nanoparticles in a purer form with a composition of 95.5%.

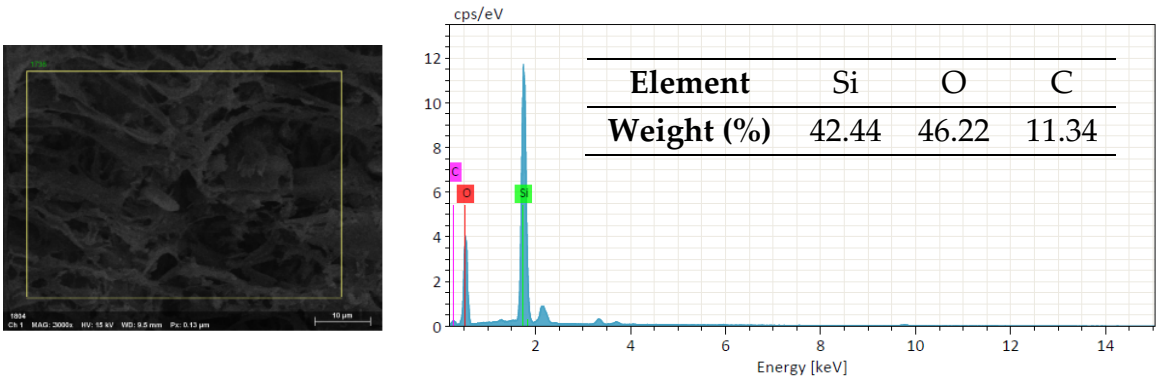

a) Rice Husk Ash (RHA)

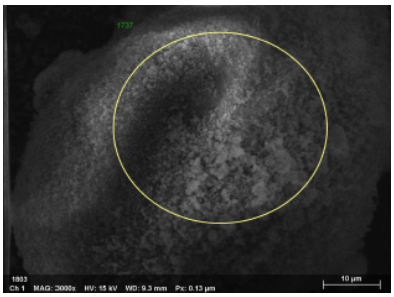

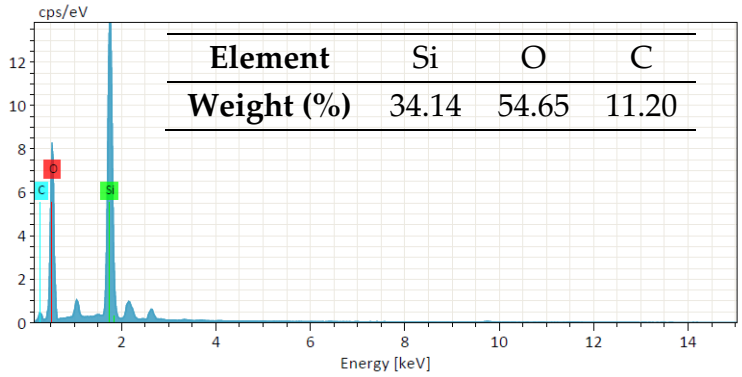

b) Silica Powder (SP)

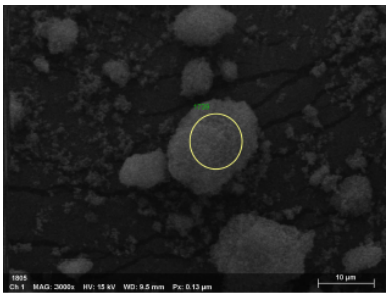

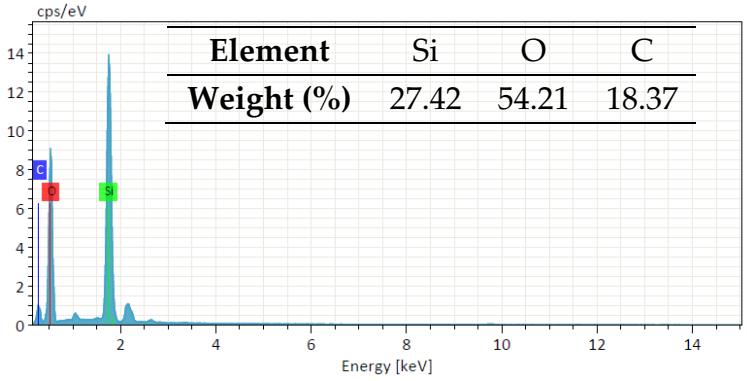

c) Nano Silica (NS)

Figure 4.9: EDX spot analysis results of RHA, SP, and NS powder samples

4.2 TEST RESULTS OF PASTE SAMPLES

In this section test results of the paste samples are discussed. Normal consistency, setting time, soundness, autoclave expansion, SEM, and EDX results are included.

4.2.1 Normal Consistency

Figure 4.10 shows the influence of RHA, SP, and NS on the normal consistency of the cement paste. As the amount of RHA, SP, and NS in the paste increased, it was noticed that the water demand increased gradually. The low specific gravity and larger specific surface area of RHA, SP, and NS in comparison to cement are the primary causes of the increased water demand in paste samples. Therefore, the porous nature and extremely small RHA, SP, and NS particles require more water than regular cement particles to maintain the proper flow. Figure 4.10 shows that the water

requirement of cement paste containing 2.5% to 15% RHA, SP, and NS was raised to 11.1% to 51.9% for RHA, 11.1% to 55.6% for SP, and 3.7% to 33.3% for NS as compared to the control sample. Normal consistency value with RHA and SP was collected from the research done by Nila (2024).

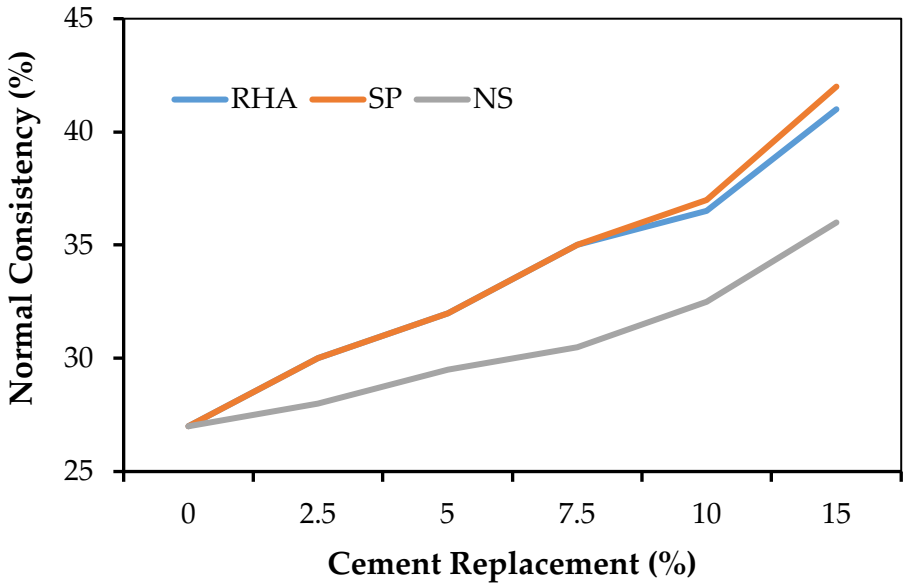

Figure 4.10: Normal Consistency of RHA, SP, and NS blended cement paste

Consistency also gradually increased as the amount of NS in the sample increased. In contrast to specimens with RHA and SP, these cement paste specimens had a lower consistency. The findings align with previous research findings from other investigators. According to Rao (2003), the cement pastes containing 20% to 30% SP demanded water needs up to 40% higher than the control sample. Qing (2007) studied the influence of nano silica and found very high consistency values compared to the control samples with 100% cement. Calica (2008) and Marthong (2012) also studied, pastes incorporating RHA needed more water to attain normal consistency than samples without RHA. Due to improved water-binder particle interaction, the water consumption of binder particles rises, resulting in higher consistency (Ltifi et al., 2011).

4.2.2 Initial and Final Setting Time

Initial and final setting times of the blended cement paste with different levels of RHA, SP, NS, and the control samples are illustrated in Figures 4.11 and 4.12. Figures 4.11 and 4.12 show that the initial and final setting times increase when the percentage of RHA and SP increases (from 0% to 15%). On the other hand, the initial time rises gradually up to 5% with NS replacement, after that it decreases, and the final setting time gradually decreases with NS in comparison to the control. Various factors influence setting times, including cement type, water-cement ratio, admixtures, and the chemical process known as hydration. Compared to the control cement paste, the initial setting time increased by 30.6% and 38.8% for 2.5% and 5% RHA, 24.7% and 35.3% for 2.5% and 5% SP, and 37.7% and 35.3% for 2.5% and 5% NS.

Furthermore, the final setting time was increased by 12.2% and 16.7% for 2.5% and 5% RHA, respectively. Compared to the control cement paste, the 2.5% and 5% SP showed a 13.3% and 19.4% increase in the final setting time, respectively. On the other hand, the final setting time decreased with the NS replacement by 2.9% to 11.1% for a 2.5% to 15% replacement level. When cement-based materials contain nano silica particles, the initial and final setting times of the mixture are decreased (Babu et al., 2019; Hou et al., 2013; Kumar et al., 2021; Mukharjee & Barai, 2014; L. P. Singh et al., 2012; M.-H. Zhang et al., 2012). The hydration process is further slowed, and the setting time increases as the amount of RHA/ SP containing smaller microparticles (Qing et al., 2007). In contrast to cement, RHA, and SP particles, nano-silica particles are finer. Because NS particles have a greater specific surface than RHA, SP, and cement particles, an increasing NS content causes the paste to become even thicker (Kontoleontos et al., 2012). Consequently, early hydration is facilitated, which decreases the setting time. The setting time with RHA and SP was collected from the research done by Nila (2024).

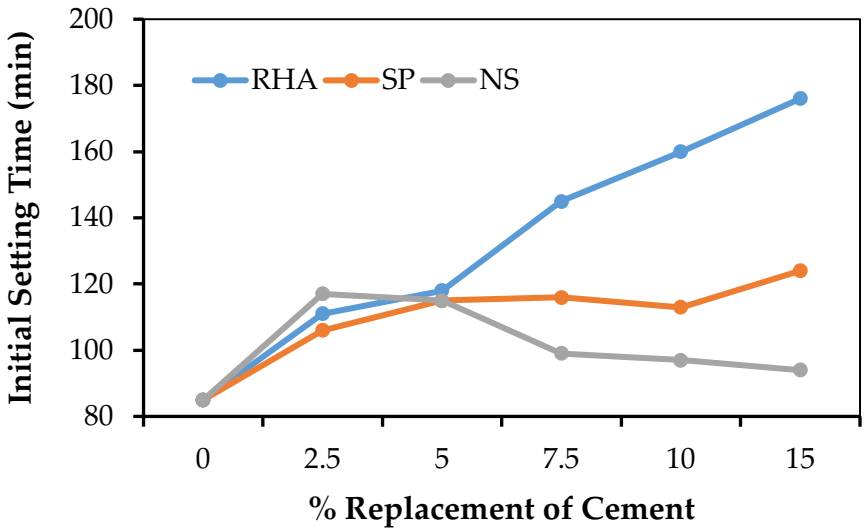

Figure 4.11: Initial setting time with RHA, SP, and NS replacement

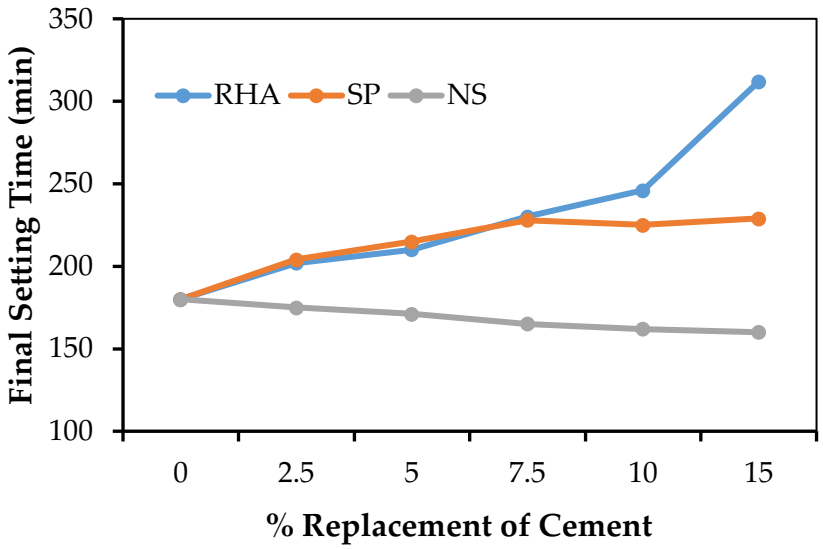

Figure 4.12: Final setting time with RHA, SP, and NS replacement

4.2.3 Soundness Test

The result of the soundness test with Le- Chateliers apparatus is shown in Figure 4.13. It demonstrates that the soundness was < 10 mm for every paste combination. Thus, it is concluded that adding RHA/SP/NS to CEM I paste does not significantly alter volume after setting.

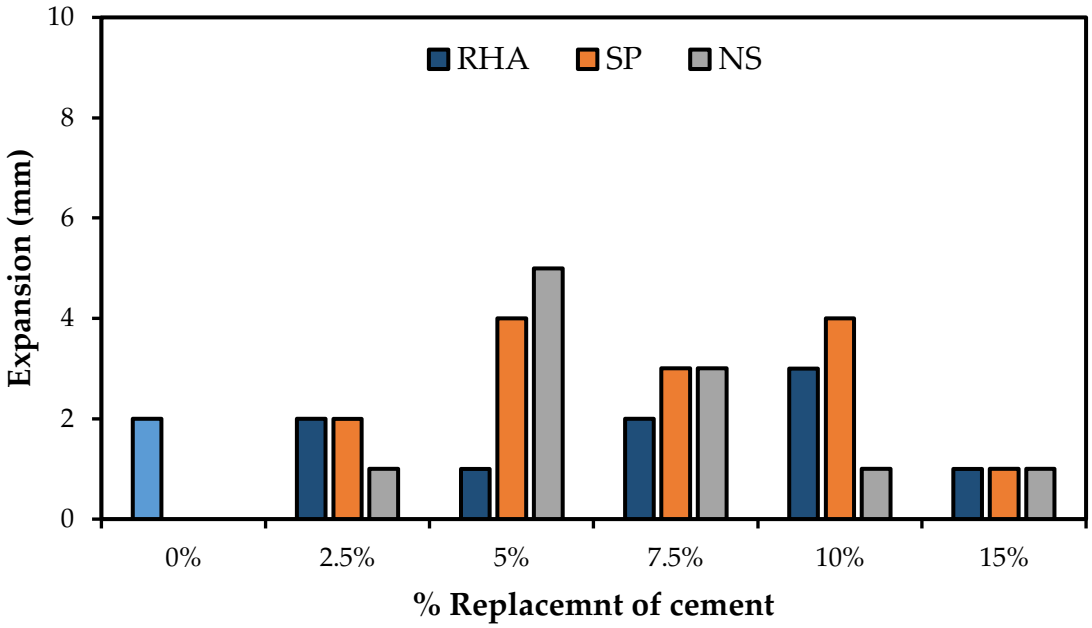

Figure 4.13: Soundness test of RHA, SP, NS blended paste

4.2.4 Autoclave Expansion Test

Figure 4.14 shows the autoclave expansion results for RHA, SP, and NS mixtures. The effect of cement replacement with RHA, SP, and NS was minor, although the growth pattern was nonlinear. The soundness result showed that the blended cement paste grater sometimes expanded on higher replacement than lower replacement, and sometimes the opposite result. Autoclave expansion demonstrated promising results. Converse findings were also observed in a prior investigation (Abbas et al., 2017). In general, the autoclave expansion test revealed that every mixture satisfied the 0.8% allowable limit given by ASTM C596 (2023) and ASTM C1157 (2008). Autoclave expansion value for RHA and SP blended cement was taken from the research done by Nila (2024).

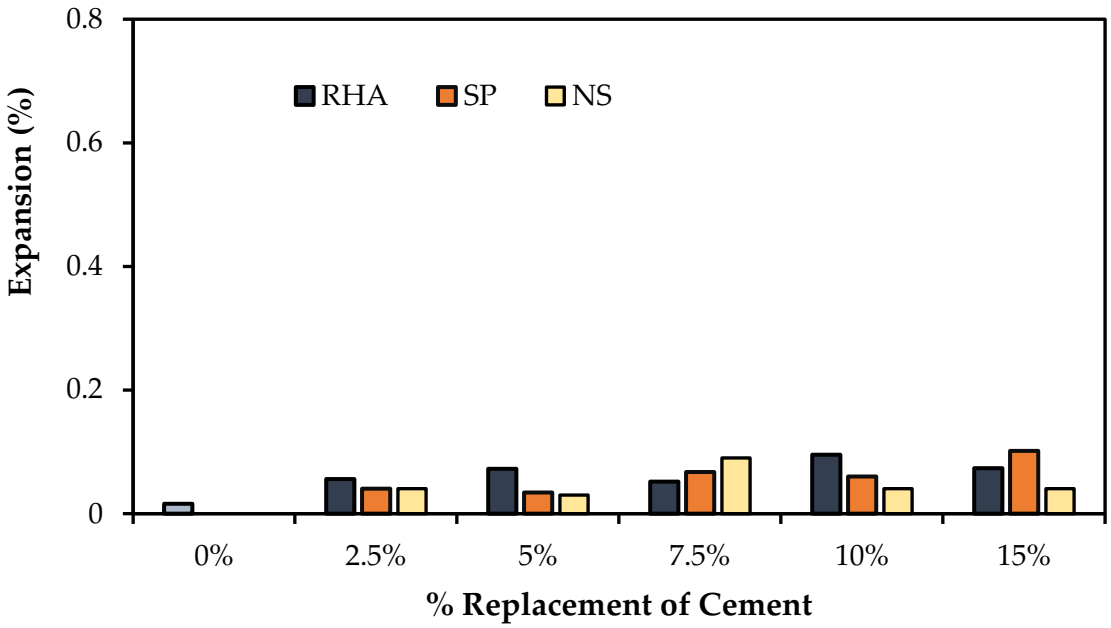

Figure 4.14: Expansion of Cement, RHA, SP, and NS blended pastes

4.2.5 Scanning Electron Microscopy (SEM) of Paste

SEM analysis was used to determine the microstructure of hardened cement pastes with or without RHA, SP, and NS with a w/b ratio of 0.27 and an age of 3, 7, and 28 days; the results are shown in Figures 4.15, 4.16, 4.17, and 4.18, respectively. Figure 4.15 shows that the calcium hydroxide (C-H) content of the regular Portland cement specimen is comparatively higher than that of the calcium-silicate-hydrate (C-S-H) gel, though with increasing curing days C-S-H gel increased. On the other hand, specimens containing RHA/SP/NS particles have a clear, strong gel structure with less C-H. The pozzolanic reaction of RHA/SP/NS particles may cause this. Therefore, RHA/SP/NS acts as a pozzolanic activator and a filler.

Figure 4.16 shows SEM micrographs with 5%, 7.5%, and 10% RHA at various ages (3, 7, and 28 days). The hydration products C–S–H and calcium hydroxide are detected in the composite at 3, 7, and 28 days. At 7 days of curing, the micrograph shows the foil honey-comb structure of calcium silicate hydrate (C-S-H) and the hexagonal-shaped C-H crystals ($Ca(OH)_2$) with big crystalline particles. The strength of the

cement is mainly determined by the C-S-H, which comprises more than 70 -75% of the hydrated cement paste.

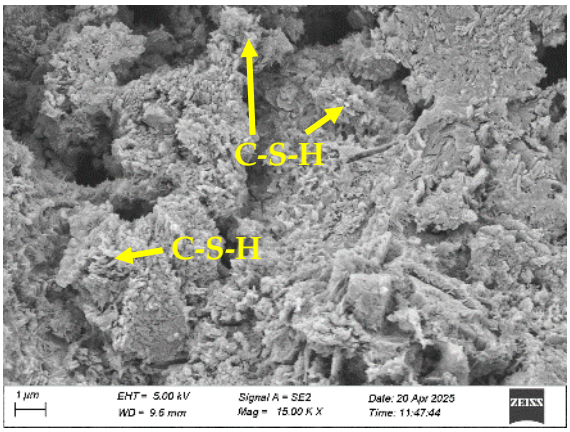

a) 3 days curing

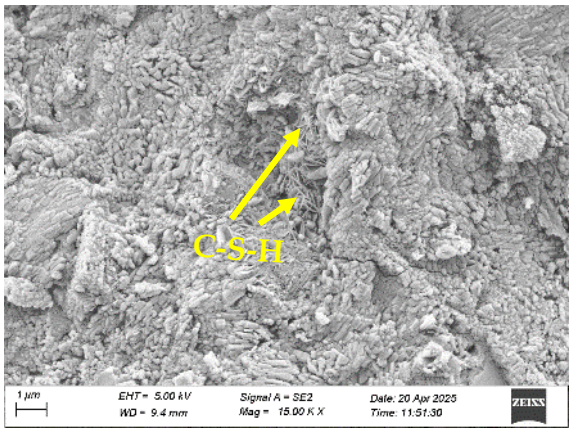

b) 7 days curing

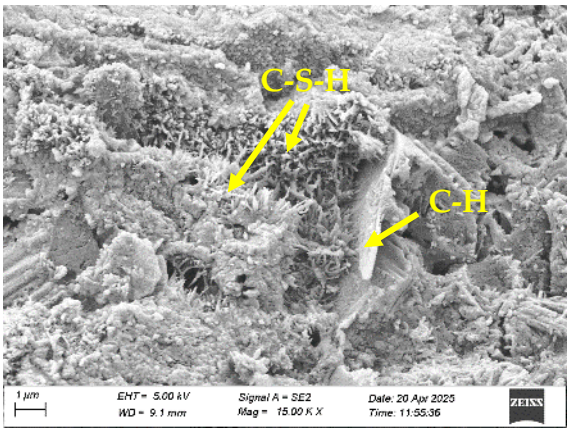

c) 28 days curing

Figure 4.15: SEM images of Cement paste at different curing ages

The Ca/Si ratio of C-S-H decreased when RHAs with a high amorphous silica content were used in place of cement Khan (1985); Uchikawa (1986); Yu (1999). Richardson (1999) claims that the morphology of C-S-H changes as the Ca/Si ratio decreases, becoming "foil-like" for lower ratios and fibrillar for higher ratios. By reducing the linked capillary pores and improving the pore structure of system, the "foil-like" morphology of C-S-H is more effective for filling the voids.

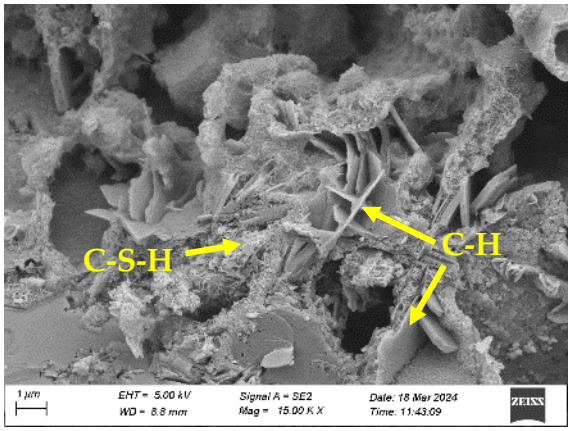

a) 3 days curing

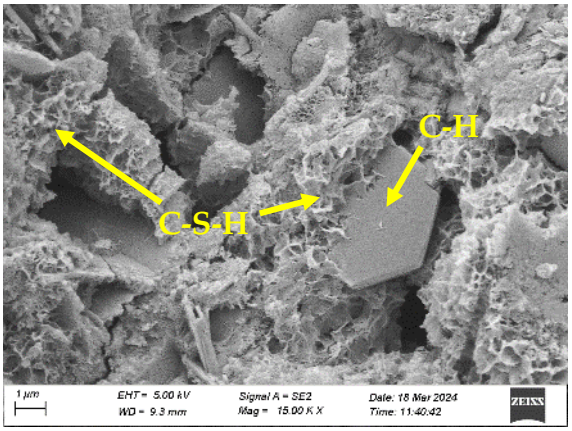

b) 7 days curing

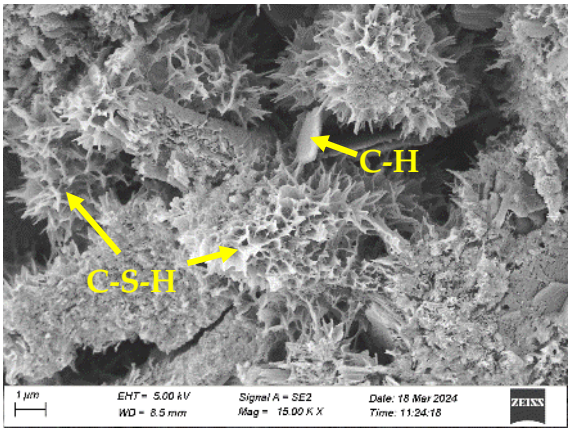

c) 28 days curing

i) 5% RHA in cement paste

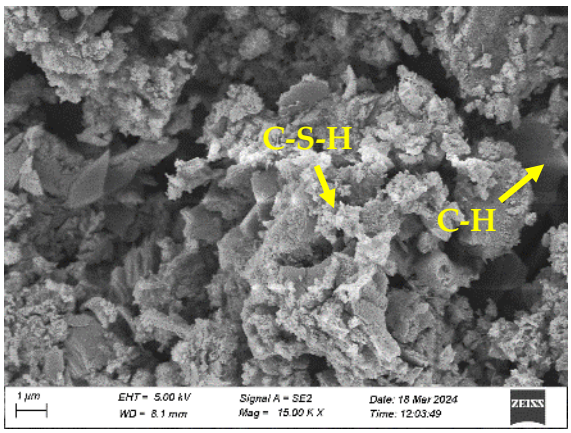

a) 3 days curing

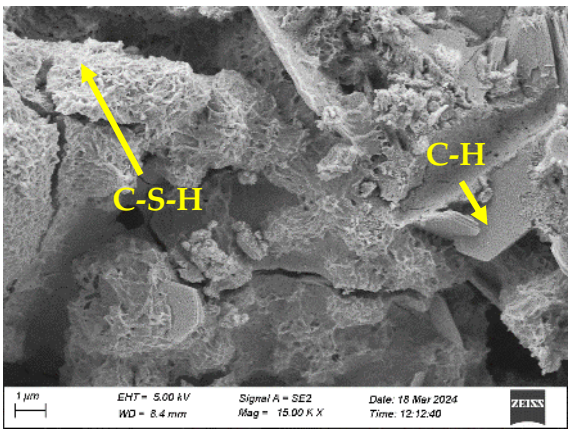

b) 7 days curing

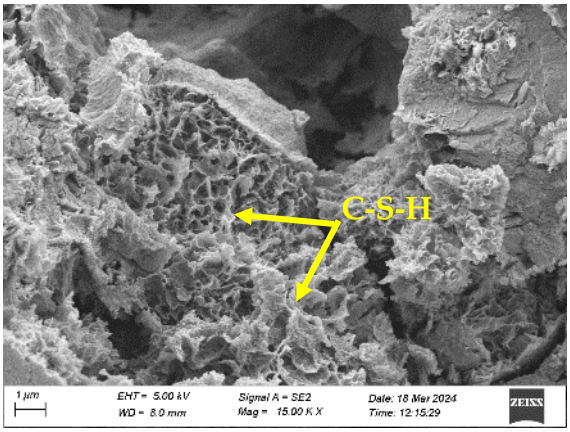

c) 28 days curing

ii) 7.5% RHA in cement paste

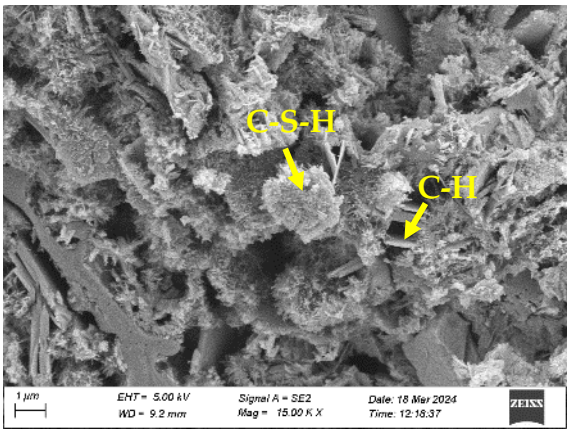

a) 3 days curing

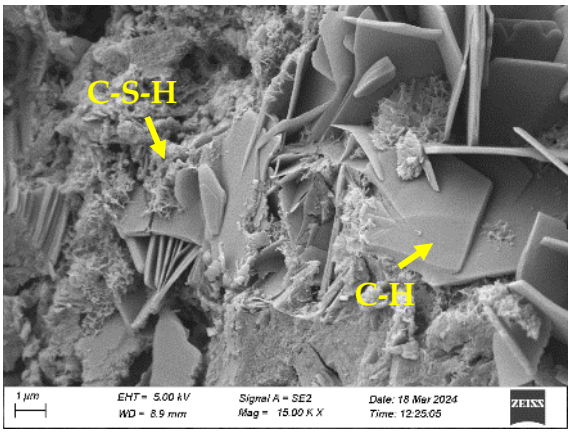

b) 7 days curing

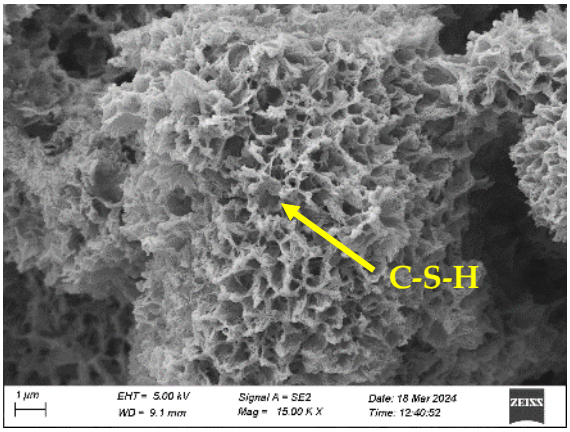

c) 28 days curing

iii) 10% RHA in cement paste

Figure 4.16: SEM images with different % replacement of RHA in Cement paste at different curing ages

As shown in Figure 4.16, the amount of unhydrated cement (C_3S, C_2S, C_3A, and C_4AF) decreased as the curing period and RHA concentration increased. The calcium hydroxide created by the hydration of Portland cement interacts with the amorphous RHA silica when introduced to cement paste. This process produces secondary C-S-H. Although primary C-S-H is generated during cement hydration, and the secondary C-S-H created by the pozzolanic reaction is chemically identical, the latter helps to increase strength and reduce porosity in the cementitious system. By consuming unused calcium hydroxide and enabling unhydrated cement particles to continue hydrating, RHA also accelerates early hydration through nucleation effects and encourages long-term hydration.

As SP has approximately the same amount of silica as RHA, it has shown similar behavior under the replacement, as shown in Figure 4.17. A few silica agglomerations were also seen. With higher replacement, this agglomeration increases. This agglomeration of SP may introduce a weak interfacial transition zone. C-S-H gel made by SP agglomerates has been observed to have inferior binding performance (Kong et al., 2013). The locations of agglomerated particles are indicated on the SEM images to detect the presence of unreacted particles.

Oversaturation and inadequate mixing are the causes of these agglomerated particles, which are predictably unreacted cement and silica particles. As a result, compressive strength decreased as the replacement of SP increased. Agglomeration of fine silica particles reduces cement hydration through localized dehydration, which creates voids with little to no strength-bearing structures. This, in turn, is the cause of decreased mechanical resistance and durability performance, according to Nazari & Riahi (2011) and Said (2012). It has been discovered that nano-silica particles affect the hydration behavior of hardened cement-based materials and cause variations in their microstructure (Hou et al., 2013; Jo et al., 2007). Additionally, a few nano-silica agglomerates have also been seen in SEM analysis, as shown in Figure 4.18.

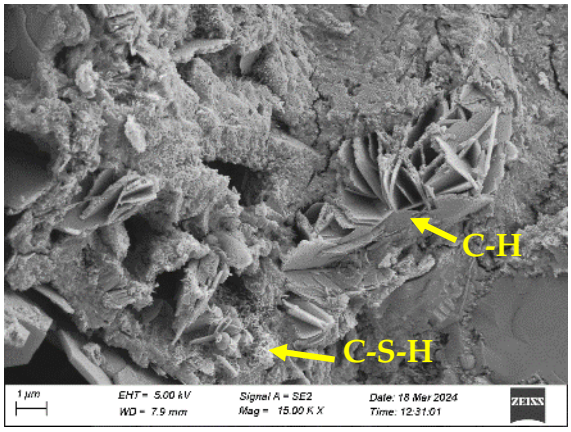

a) 3 days curing

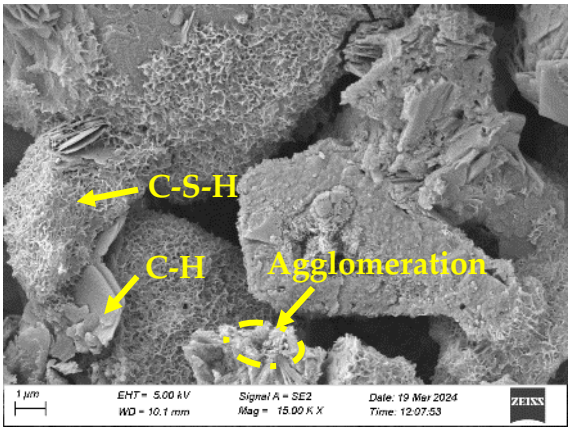

b) 7 days curing

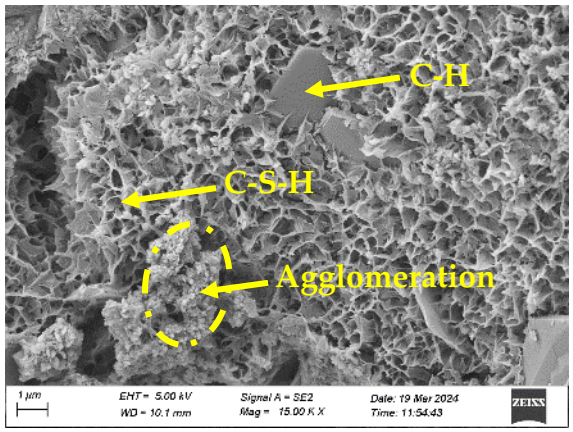

c) 28 days curing

i) 5% SP in cement paste

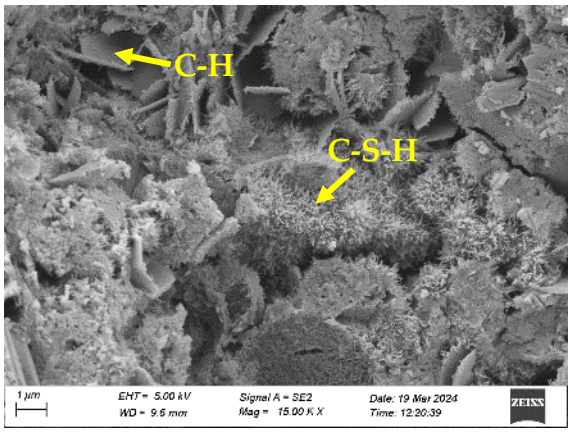

a) 3 days curing

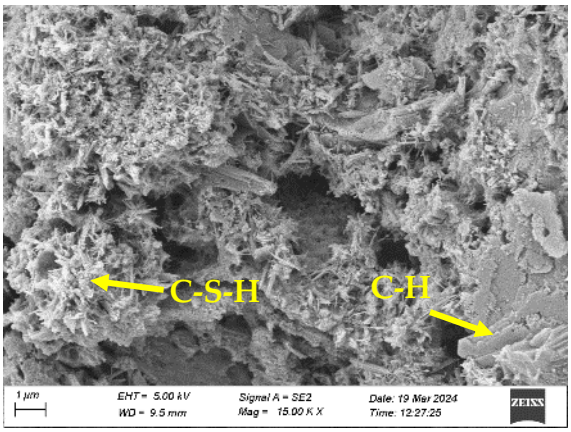

b) 7 days curing

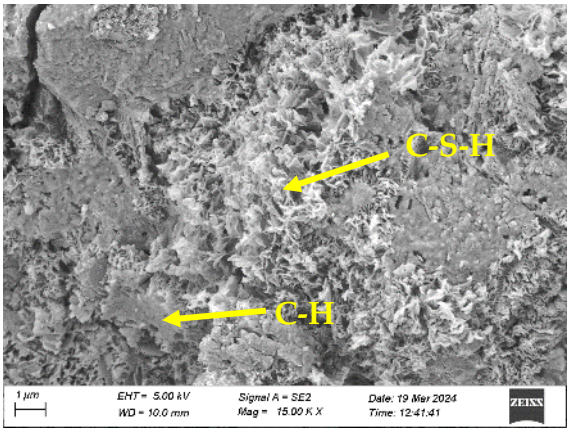

c) 28 days curing

ii) 7.5% SP in cement paste

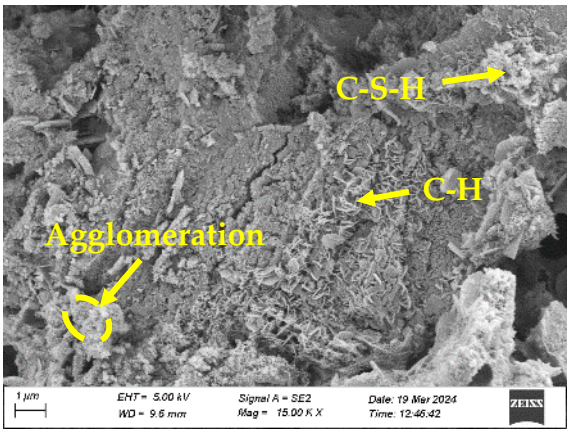

a) 3 days curing

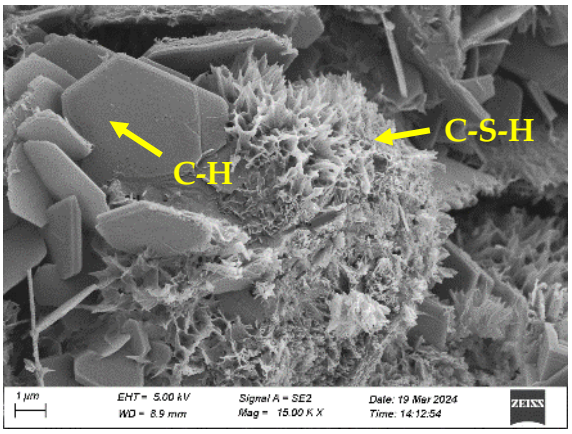

b) 7 days curing

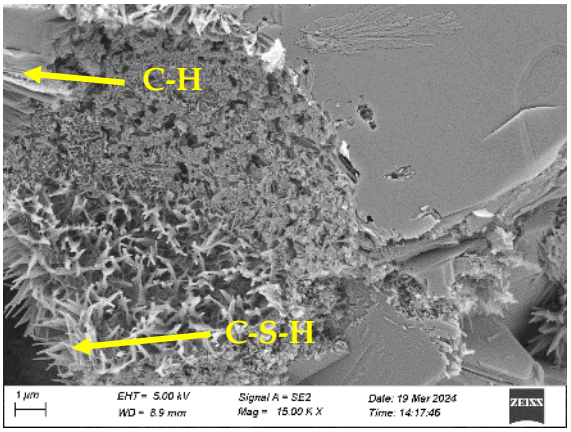

c) 28 days curing

iii) 10% SP in cement paste

Figure 4.17: SEM images with different % replacement of SP in Cement paste at different curing ages

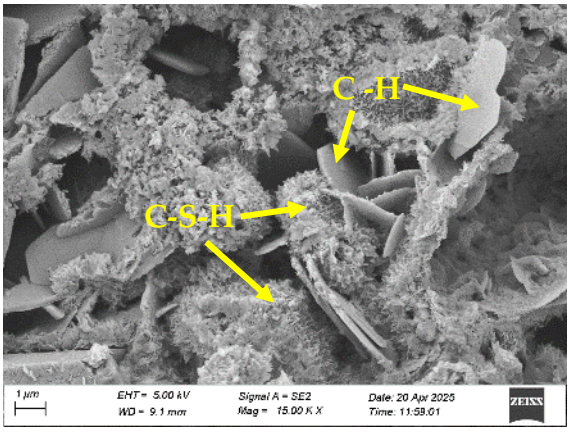

a) 3 days curing

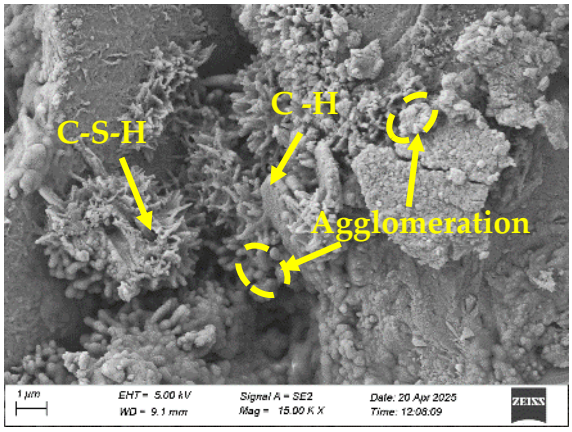

b) 7 days curing

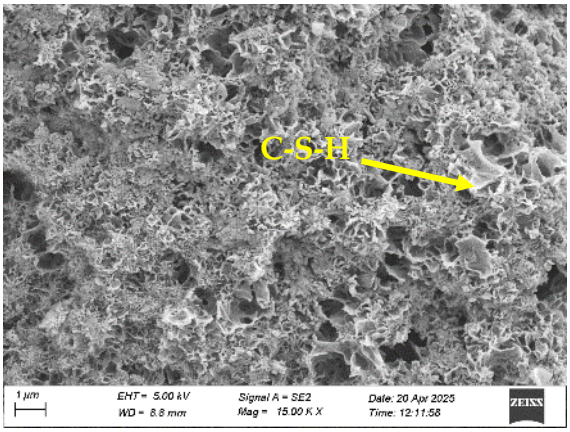

c) 28 days curing

i) 5% NS in cement paste

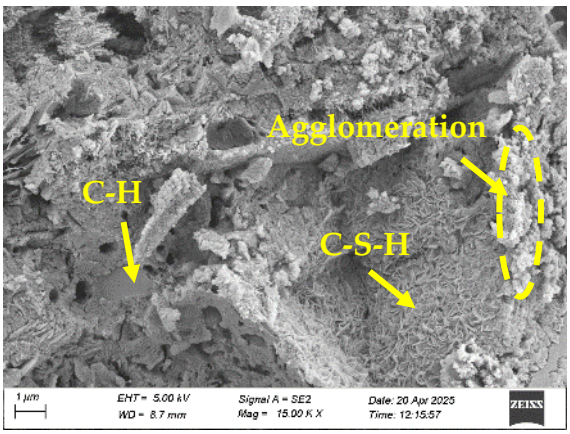

a) 3 days curing

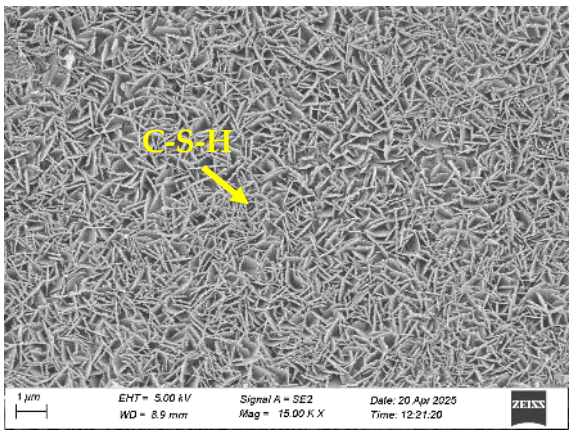

b) 7 days curing

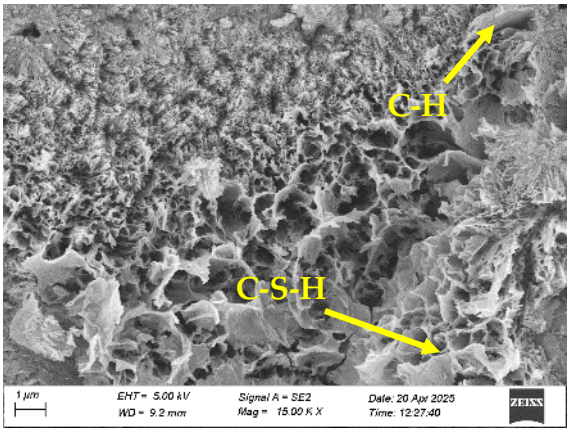

c) 28 days curing

ii) 7.5% NS in cement paste

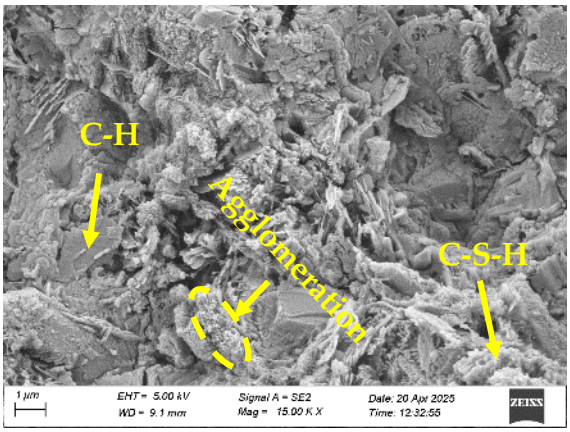

a) 3 days curing

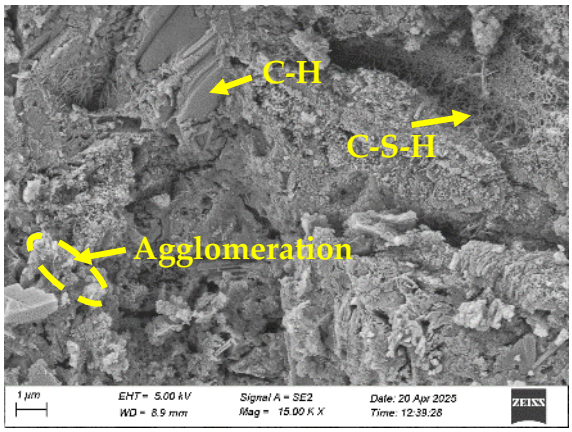

b) 7 days curing

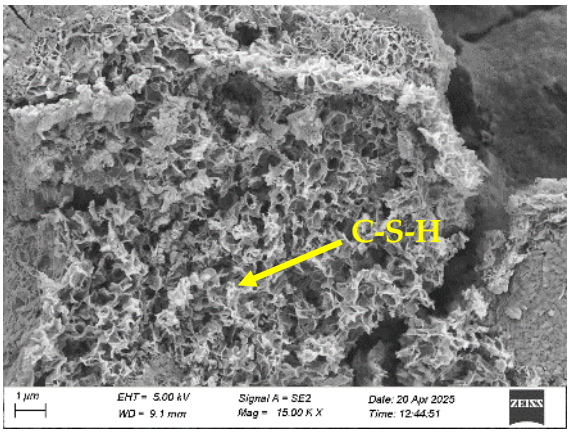

c) 28 days curing

iii) 10% NS in cement paste

Figure 4.18: SEM images with different replacement of NS in cement paste at different curing ages

In cement-based products, NS agglomerates due to the high pH and ionic strength of the cement hydration system as well as its high surface energy, which affects the materials' efficiency (Amiri et al., 2009; Kirby & Lewis, 2004; Kong et al., 2015; Reches et al., 2018). Researchers found that the primary cause of the decreased compressive strength with a high level of NS was the agglomeration of particles (Bolhassani & Samani, 2015; Mendes & Repette, 2021).

4.2.6 Energy Dispersive X-Ray (EDX)

The atomic ratio of Ca and Si, as measured by EDX analysis, is the stoichiometric Ca/Si ratio, which measures the crystals in different parts of the sample. Pure Portland cement undergoes hydration to produce a C–S–H phase with a Ca/Si ratio of around 1.7 (Richardson, 1999). As SCM substitution increases, this ratio drops. When this ratio decreases, it signifies the formation of the C-S-H phase as the C-H content decreases, and when it increases, it indicates the excess of C-H as the pozzolanic reaction decreases (Karunarathne et al., 2019). Figure 4.19(a) shows that by 28 days, the Ca/Si ratio of C-S-H in the control is extremely high (5.13). As RHA content increased from 5% to 7.5%, the Ca/Si ratio value steadily dropped to assist the pozzolanic process as shown in Figure 4.19 (b) and (c). At 5% RHA Ca/Si ratio was 3.93, which was decreased to 2.04 with 7.5% RHA. The low Ca/Si ratio with 7.5% RHA should show better compressive strength, but with 5% RHA, this study found higher compressive strength in mortar at 28 days curing.

Although a significant number of studies have been done on C-S-H phases in hydrated Portland cements, the relationship between the chemical composition of the phase and the compressive strength of the hardened material is not well understood (Papatzani et al., 2015). Micromechanical and elastic properties of the material study have shown that C-S-H phases with low Ca/Si ratios have appropriate properties (Kim et al., 2013; Pelisser et al., 2012). However, the results cannot be directly translated into macroscopic mechanical properties because compressive strength depends on a

variety of factors, including the materials and mix design (Cordon & Gillespie, 1963; Rao, 2001; Weaver et al., 1974), the chemical composition, the specimen geometry (Bažant, 1996; Carpinteri, 1994; Karihaloo et al., 2003), and test conditions like loading rate (Sukontasukkul et al., 2004; Zhang et al., 2012).

Figure 4.19 (d) and (e) illustrate how the Ca/Si ratio value gradually decreased to support the pozzolanic process as the SP concentration increased from 5% to 7.5%. The Ca/Si ratio was 4.75 for 5% SP and dropped to 3.33 with 7.5% SP. The increased compressive strength in mortar specimens at 28 days was validated by the low Ca/Si ratio in specimens with 7.5% SP. As the NS concentration increased from 5% to 7.5%, Figure 4.19 (f) and (g) indicated that the Ca/Si ratio value progressively dropped to assist the pozzolanic process.

At 5% NS, the Ca/Si ratio was 4.35 while with 7.5% NS, it reduced to 3.77. Though 7.5% NS had a lower Ca/Si ratio, the compressive strength of mortar with 7.5% NS decreased in comparison to 5% NS it might be because of the agglomeration, which was confirmed by SEM analysis. It appears that the 5% NS has the best dispersion in the sample, with less agglomeration than larger replacements. As a result, pozzolanic reactivity of NS, nucleation effect, and filling effect all improved in mortar with 5% NS.

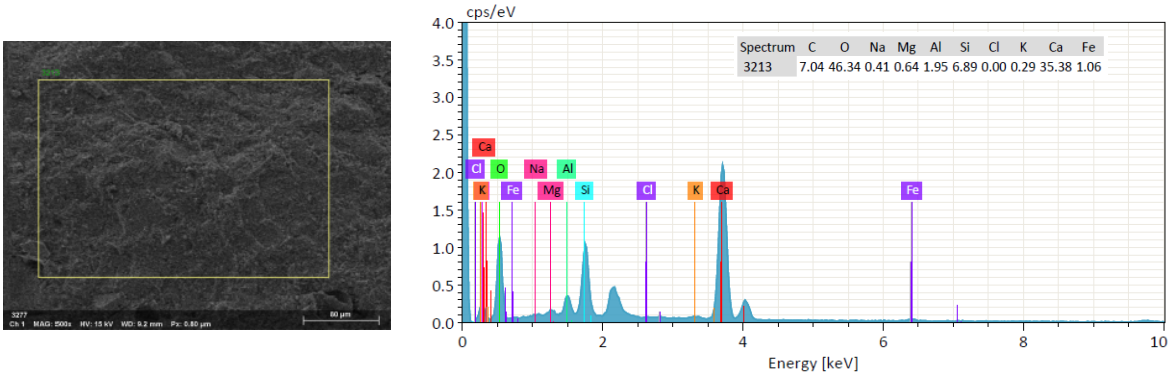

a) Control – 28 days curing

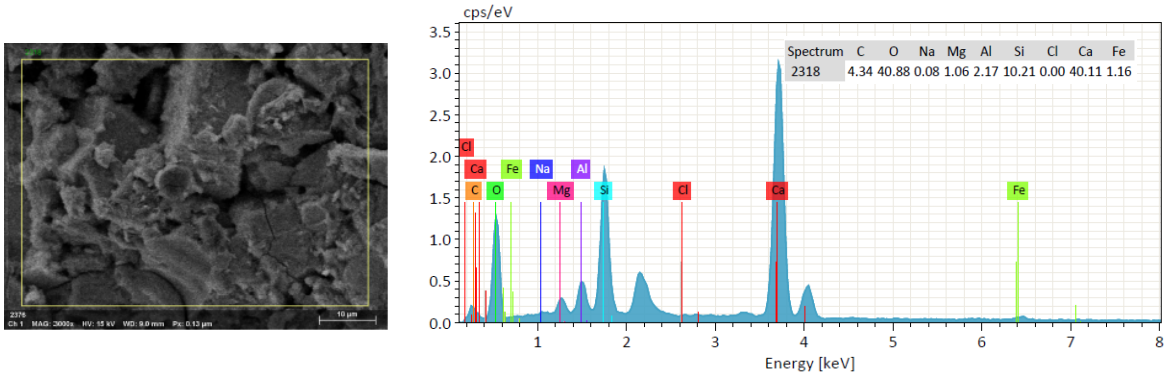

b) 5% RHA – 28 days curing

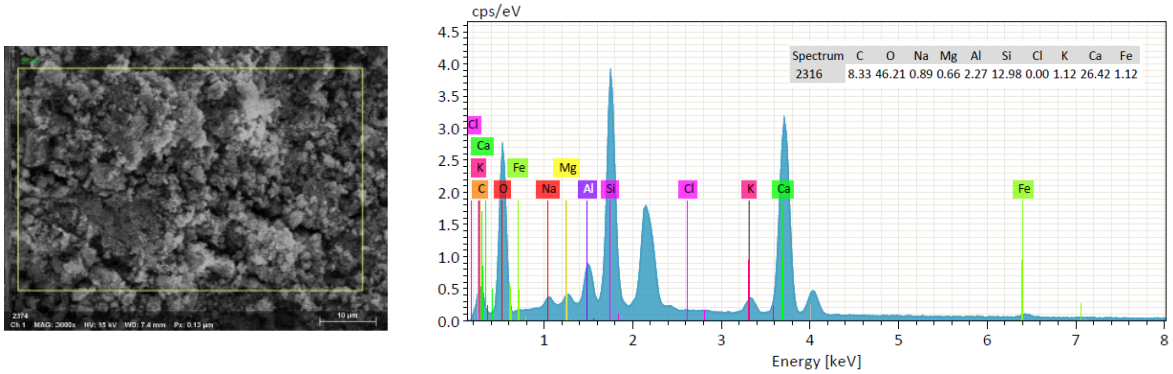

c) 7.5% RHA – 28 days curing

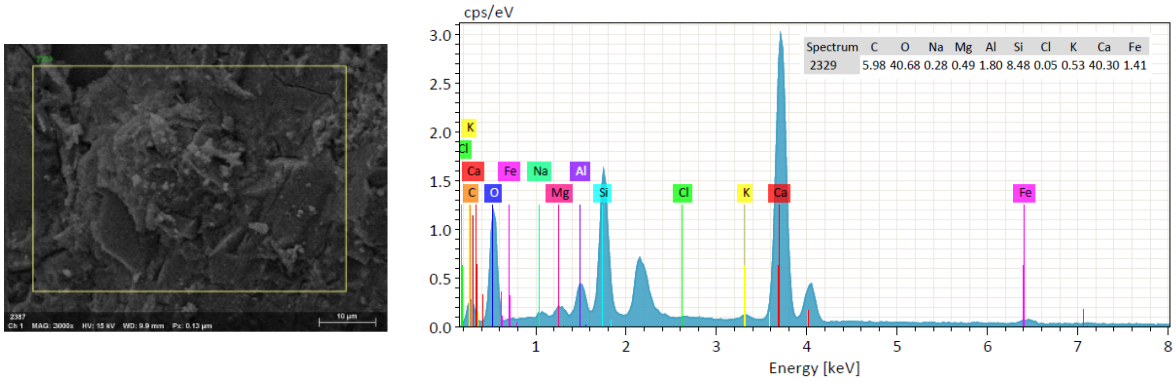

d) 5% SP – 28 days curing

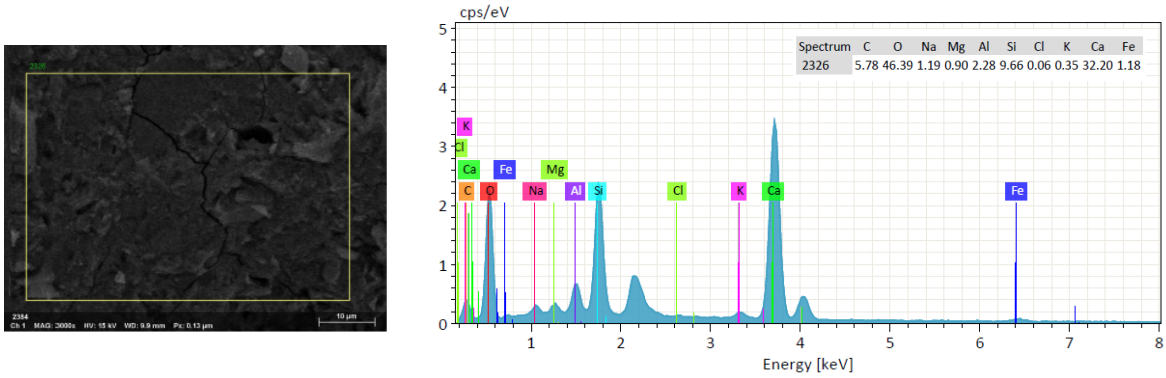

e) 7.5% SP – 28 days curing

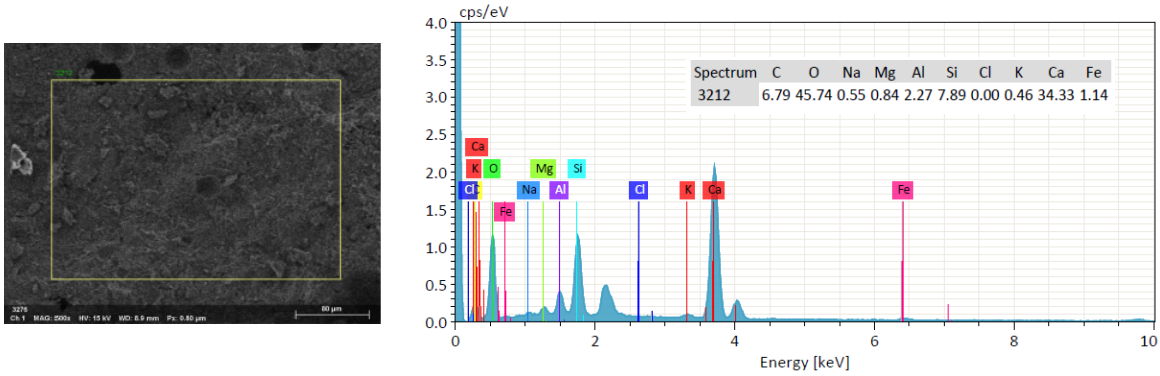

f) 5% NS – 28 days curing

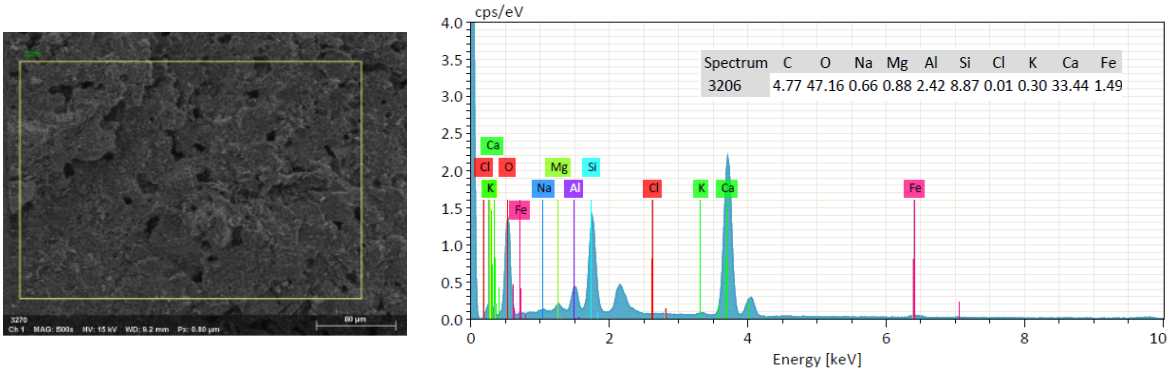

g) 7.5% NS – 28 days curing

Figure 4.19: EDX result of RHA, SP, and NS blended paste samples

4.3 TEST RESULTS OF MORTAR SAMPLES

In this section test results of mortar samples are discussed. Flow table, water demand, flexural and compressive strength, pozzolanic activity, water absorption, density, volume of permeable pores, drying shrinkage, and sulfate resistance test results are included in this section.

4.3.1 Flow Table Test

Figure 4.20 illustrates the flow of RHA, SP, and NS-induced mortar samples. A flow table conforming to EN 1015-3 (2004) was used. The addition of RHA reduced flowability from 163 mm (control) to 125 mm compared to the reference control sample. Its large specific surface area is the cause of this reduction in flowability. As the replacement ratio increases, RHA absorbs more mixing water on its surface and pores, reducing free water and flowability. The addition of SP and NS reduced flowability from 163 mm (control) to 117 mm and 114 mm, respectively, compared to the reference sample. In general, the higher specific surface area of RHA, SP, and NS reduces the flowability of the fresh mixture.

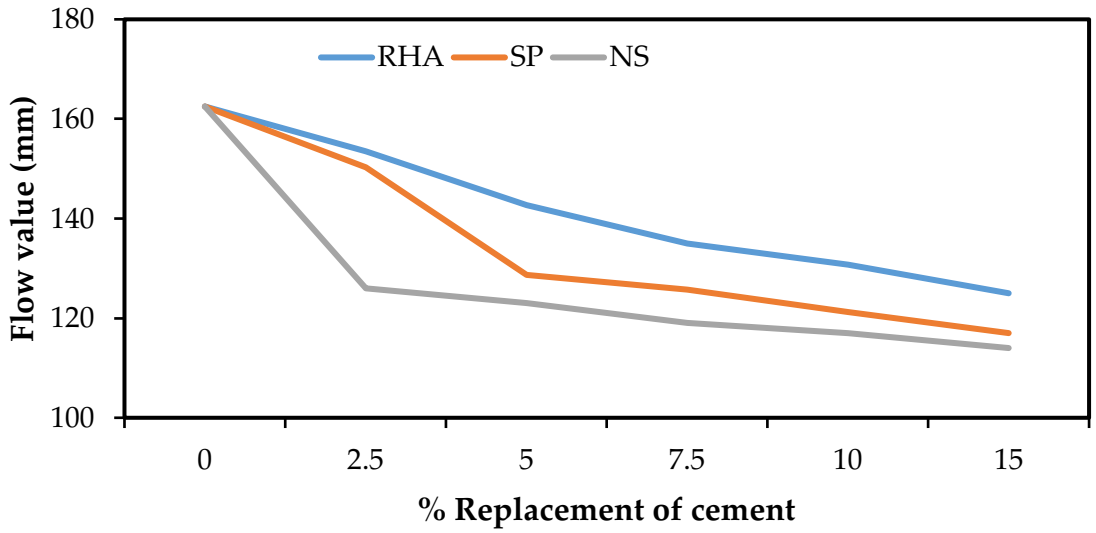

Figure 4.20: Flow of RHA, SP, and NS mortars

4.3.2 Water Demand Test

Figure 4.21 shows the water demand of RHA, SP, and NS. The BS 8615-1 (2019) threshold value is shown by a dotted reference line. According to the standard, the water demand should not exceed 115% of that required for cement cement-only test. According to the findings, the paste required more water to give a similar flow to the control as the RHA, SP, and NS levels increased. As a result, the use of RHA, SP, and NS replacing cement increases the water/binder ratio and water demand of cement mortars. In light of this, the water/cement ratios were adjusted from 0.5 to 0.62, 0.5 to 0.67, and 0.5 to 0.60 for RHA, SP, and NS replacement quantities, respectively. When cement was substituted by 15% RHA, SP, and NS of cement, the water requirement increased by 118%, 117%, and 114%, respectively. This indicates that with large surface area mineral particles, adding to cement mixes requires more water or chemical admixtures to maintain the workability of the mixture.

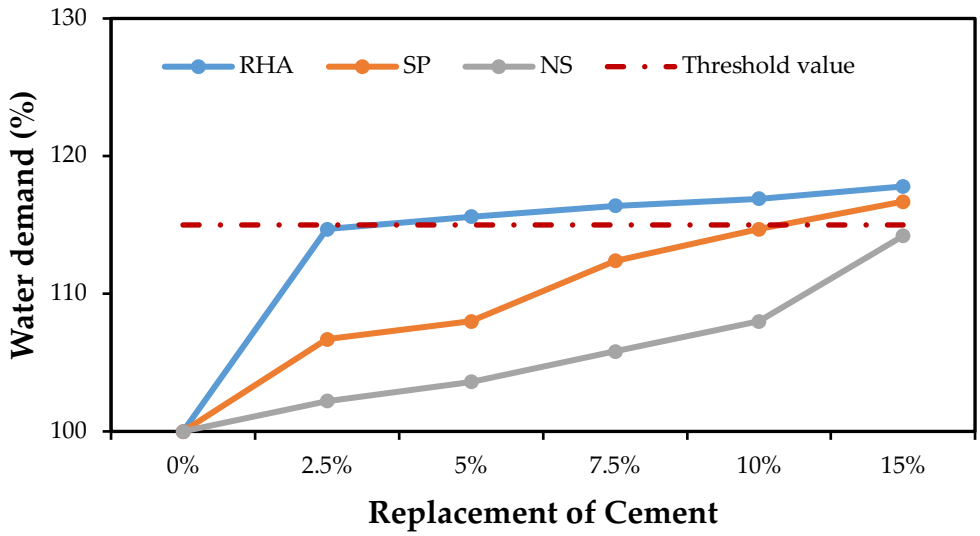

Figure 4.21: Water demand of RHA, SP, and NS

The obtained results showed that the water demand of NS remains lower than the optimum value specified by BS 8615-1 up to 15% replacement because of agglomeration that was also observed in SEM analysis. Besides, for SP up to 10% replacement, the water demand remains lower than the threshold value.

Agglomeration was also observed in SP, but lower rate than in NS because of slightly higher particle sizes. The rheological behavior of cementitious mixes reported in the literature indicated that adding nano-silica significantly increases the water demand of cementitious mixes compared to the control (Aggarwal et al., 2015). On the other hand, the water demand of RHA exceeded the limit from 5% replacement. According to other research, RHA increases the water requirements for Portland cement mortars and concrete due to additional unburnt carbon (Ganesan et al., 2008; Mehta, 1994; Rukzon et al., 2009; Rukzon & Chindaprasirt, 2006).

4.3.3 Flexural Strength Test

The flexural strength of mortar samples with constant and varying w/b ratios was examined. With the constant w/b ratio, no water adjustment was made, which affected the flow as discussed earlier and might affect the compaction due to that change in workability.

a) Constant w/b ratio

The flexural strength of RHA, SP, and NS mortars was examined at 3, 7, 28, and 90 days of curing with cement replacement rates of 2.5%, 5%, 7.5%, 10%, and 15%. The findings indicated that the flexural strengths of every batch increased with the curing period increased. The development of the flexural strength of RHA, SP, and NS mortars at different curing ages in comparison to the control sample is shown in Figure 4.22 (a), (b), and (c) with a constant w/b ratio (0.5).

Figure 4.22(a) shows that mortar with RHA for all replacements has 0.3–7.9% greater flexural strength than the control at 90 days of curing. The slow pozzolanic reaction is widely acknowledged to cause the prolonged strength development of pozzolanic pastes and composites. According to the findings of this study, pozzolanic and filler effects cause RHA mortars to develop a notable increase in flexural strength over time. After 28 and 90 days of curing, the maximum flexural strengths, 6.45 and 6.83 MPa,

were obtained with 7.5% volume replacement of cement by RHA. With a 15-20% cement replacement at 28 days of age, Jamil (2016) and Venkatanarayanan & Rangaraju (2015) found a slight increase in the flexural strength of RHA-mortar.

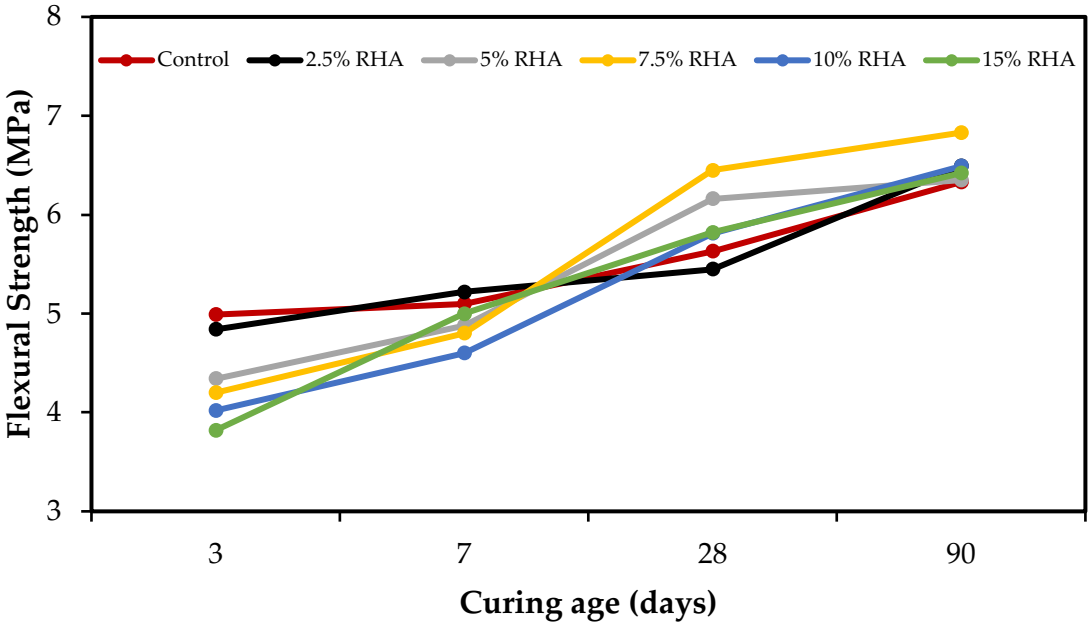

a) Cement replacement with RHA

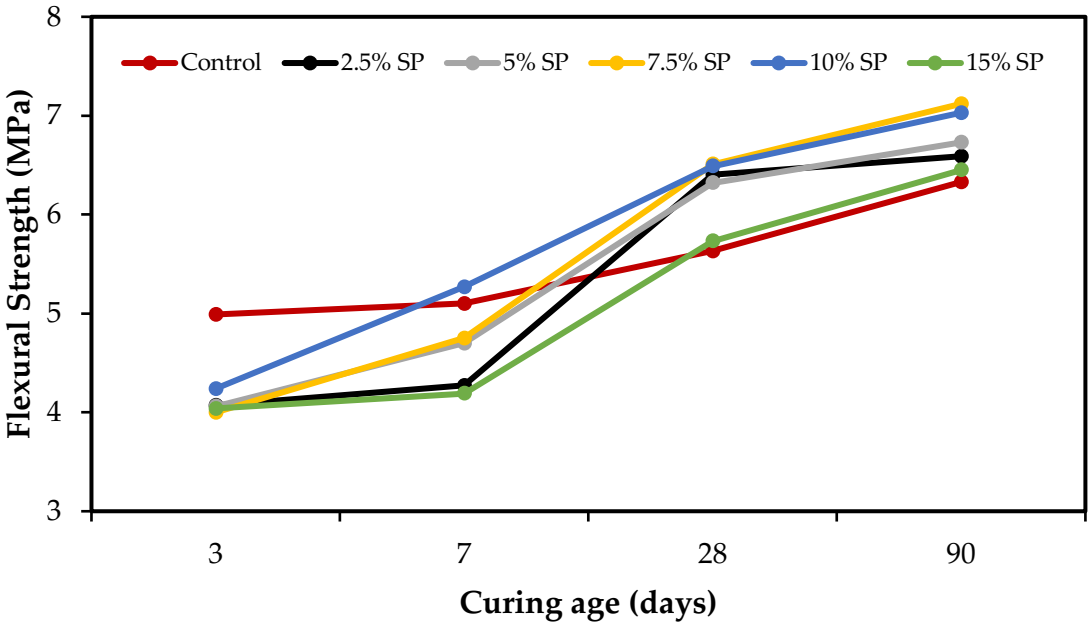

b) Cement replacement with SP

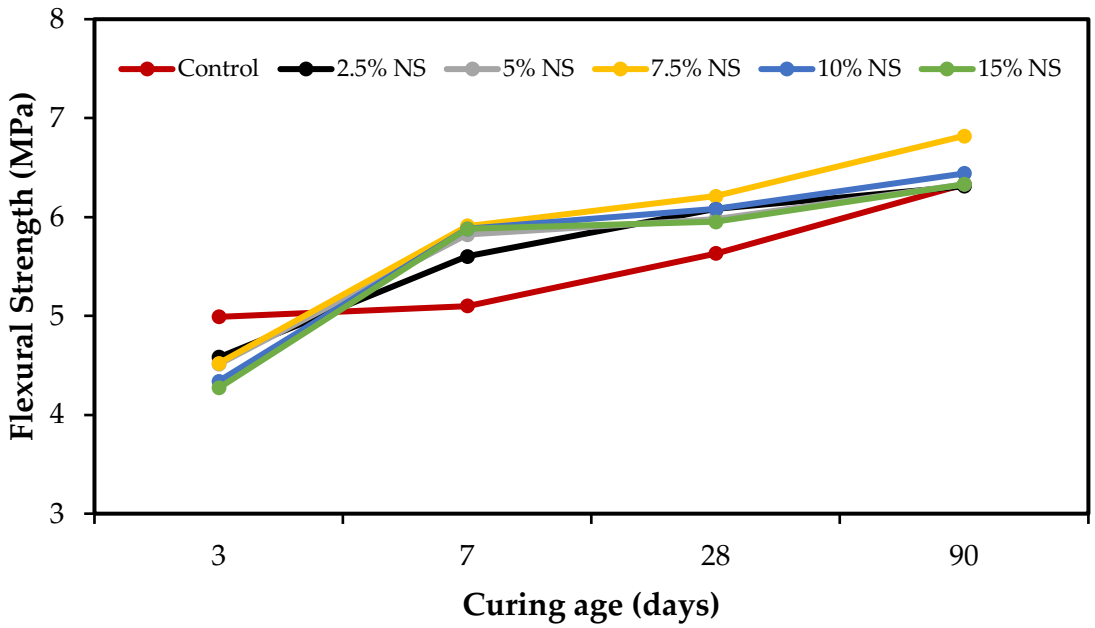

c) Cement replacement with NS

Figure 4.22: Comparison of flexural strength among control, RHA, SP, and NS blended mortar with constant w/b ratio

In Figure 4.22(b), mortar with SP up to 10% replacement gave 4.1–12.5% greater flexural strength than the control at 90 days of curing. This result is due to the increased binding strength of the cement paste-fine aggregate interfacial zone. After 28 and 90 days of curing, the maximum flexural strengths, 6.51 and 7.12 MPa, respectively, were obtained with 7.5% volume replacement of cement by SP.

On the other hand, the flexural strength of mortar can be improved in the early days of curing when NS is used to replace the cement content. Figure 4.22(c) shows that mortar with NS for all replacements has 5.7–10.3% greater flexural strength than the control at 28 days of curing. At 90 days of curing, 7.5% NS replacement showed a 7.7% increase in strength compared to the control, where other replacement strengths were close to the control. After 28 and 90 days of curing, the maximum flexural strengths of 6.21 and 6.82 MPa were obtained with 7.5% volume replacement of cement by NS. Flexural strength with NS slightly decreased compared to RHA and SP. Because of

their large surface area, these particles cannot be spread equally, which may cause this reduction.

b) Varying w/b ratios

Figure 4.23 shows the flexural strength of RHA, SP, and NS mortars developed with various curing ages relative to the control sample while maintaining flow by adjusting water demand for different replacements. Figure 4.23(a) and (c) show that mortar with RHA, NS, and varying w/b ratios for all replacements has reduced the flexural strength than the control up to 90 days of curing. In Figure 4.23(b), mortar with SP for 2.5% and 5% replacement gave 2.8-6.2% higher flexural strength than the control at 90 days of curing. At this age, the maximum flexural strength, 6.72 MPa, was obtained with 2.5% volume replacement of cement by SP.

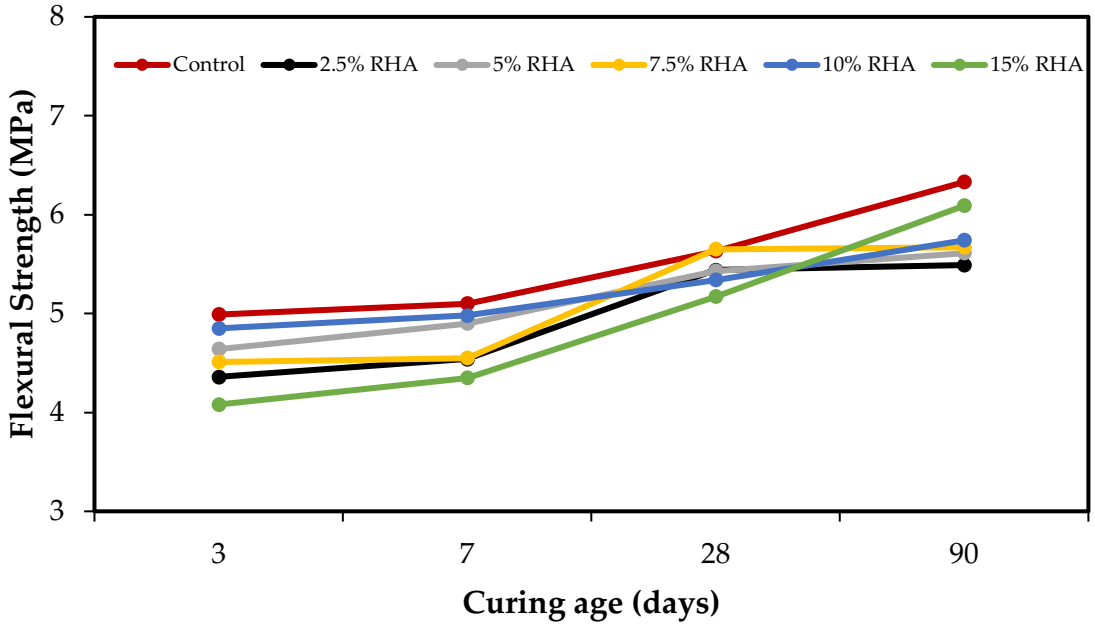

a) Cement replacement with RHA

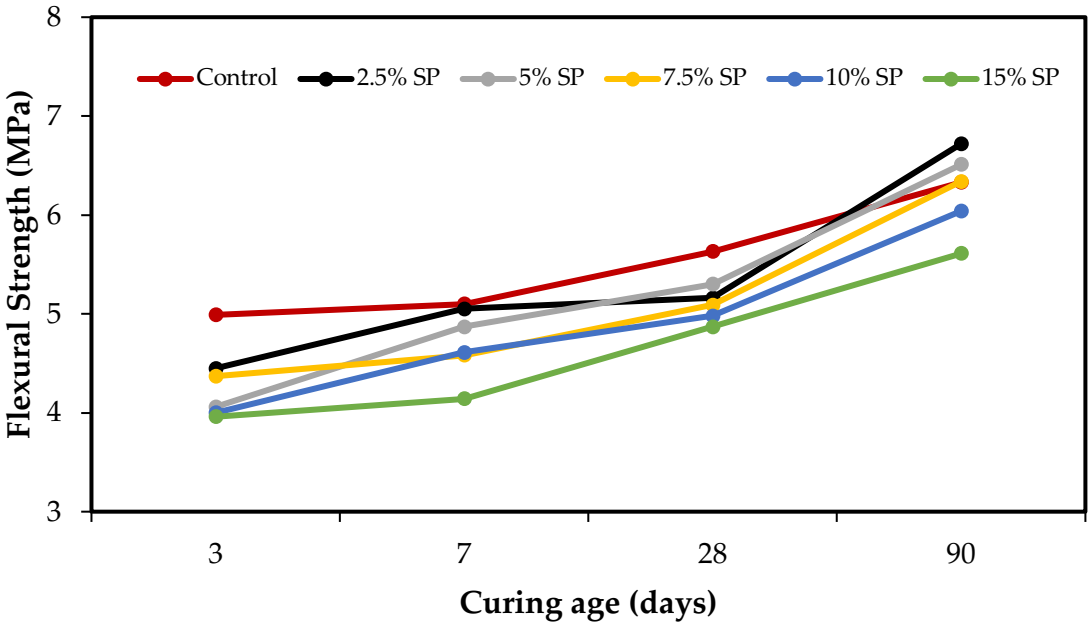

b) Cement replacement with SP

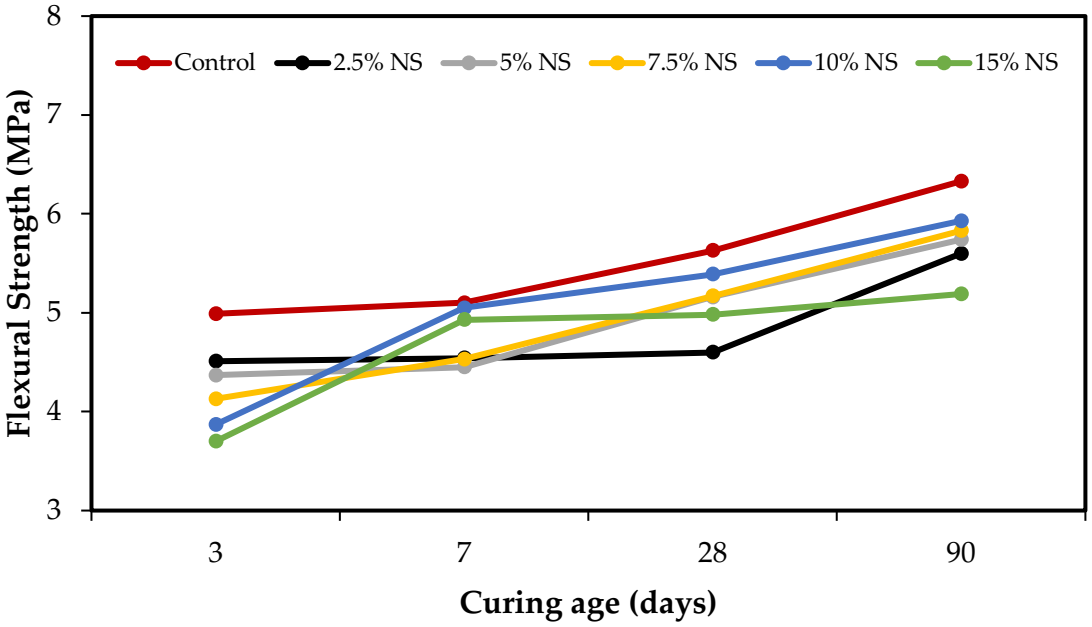

c) Cement replacement with NS

Figure 4.23: Comparison of flexural strength among control, RHA, SP, and NS blended mortar with varying w/b ratios

According to ABrAMS (1919) law, as long as the mix is workable, the water/binder ratio is the only factor affecting concrete strength. Flexural strength of concrete is

determined by $0.7\sqrt{f_{ck}}$ according to IS 456 (2000). Therefore, there is a direct correlation between flexural and compressive strengths. Thus, generally, when the water-to-binder ratio rises, the flexural strength reduces.

4.3.4 Compressive Strength Test

The compressive strength of mortar samples was measured with constant and varying w/b ratios. With varying w/b ratios, the compaction effect was expected to be the same as the flow was maintained the same, and only the pozzolanic reaction effect may be found.

a) Constant w/b ratio

Figure 4.24 shows the compressive strength of mortar with a constant w/b ratio (0.5). As shown in Figure 4.24(a), the control mortar gave a higher compressive strength than the RHA replaced mortar at the age of 3 days. However, samples with 2.5% and 5% RHA outperform compared to the control mortar at a later age (90 days). The 2.5% and 5% RHA replacement increased compressive strength by 6.9% and 1.2%, respectively. The proper ratio of SiO_2 (from RHA and cement) and $Ca(OH)_2$ (a by-product of the cement hydration reaction) results in a C-S-H reaction known as pozzolanic, which enhances the microstructure and improves compressive strength of mortar (McCarthy et al., 2013). Studies have reported that the pozzolanic reaction and reactive silica in RHA may be partially responsible for the increase in strength (Al-Khalaf & Yousif, 1984; Ganesan et al., 2008; Islam & Akter, 2012). Researches suggested that pozzolanic activity of RHA begins later than usual and becomes significant when a considerable amount of $Ca(OH)_2$ is generated as a cement hydration product. Following 90 days of curing and a 2.5% cement replacement level, the highest compressive strength of mortar resulting from the pozzolanic reaction of RHA is 59.2 MPa.

At that age and 5% cement replacement level, the maximum compressive strength of mortar was found by the RHA pozzolanic reaction to be 56.1 MPa. According to Zhang & Malhotra (1996), 10% RHA replacement showed greater strength at all ages than the control. With SP, compressive strengths at 3, 7, 28, and 90 days are given in Figure 4.24(b), indicating that adding 2.5%, 5%, 7.5%, 10%, and 15% dosages of SP increased the compressive strength. Maximum compressive strength was found with a 10% cement replacement with SP. It increased compressive strengths by 8.9%, 41.4%, 19%, and 9.7% from the control at 3, 7, 28, and 90 days, respectively. These enhancements resulted from the increased surface area of the particles, which increases the rate of pozzolanic reaction. Additionally, SiO_2 serves as an activator and packing material to further accelerate the pozzolanic process.

On the other hand, NS blended mortar achieved maximum compressive strength at 28 days of curing. This study found that NS showed a 0.4 – 1.7% strength increment up to 7.5% replacement at 28 days of curing. Maximum compressive strength was found with 5% replacement at 90 days curing age (56.2 MPa), shown in Figure 4.24(c).

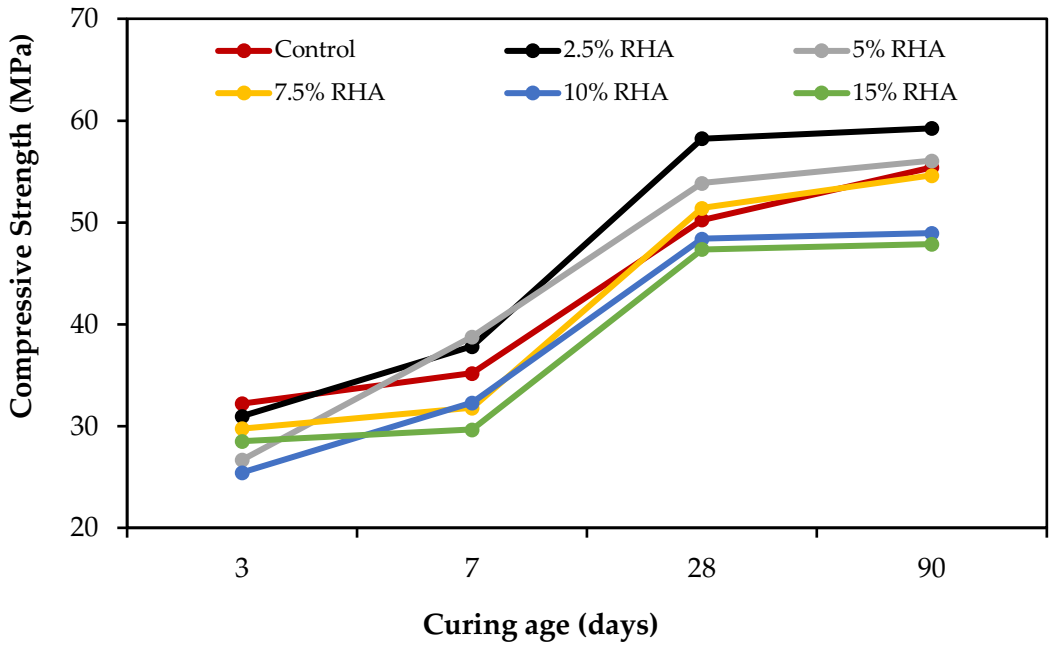

a) Cement replacement with RHA

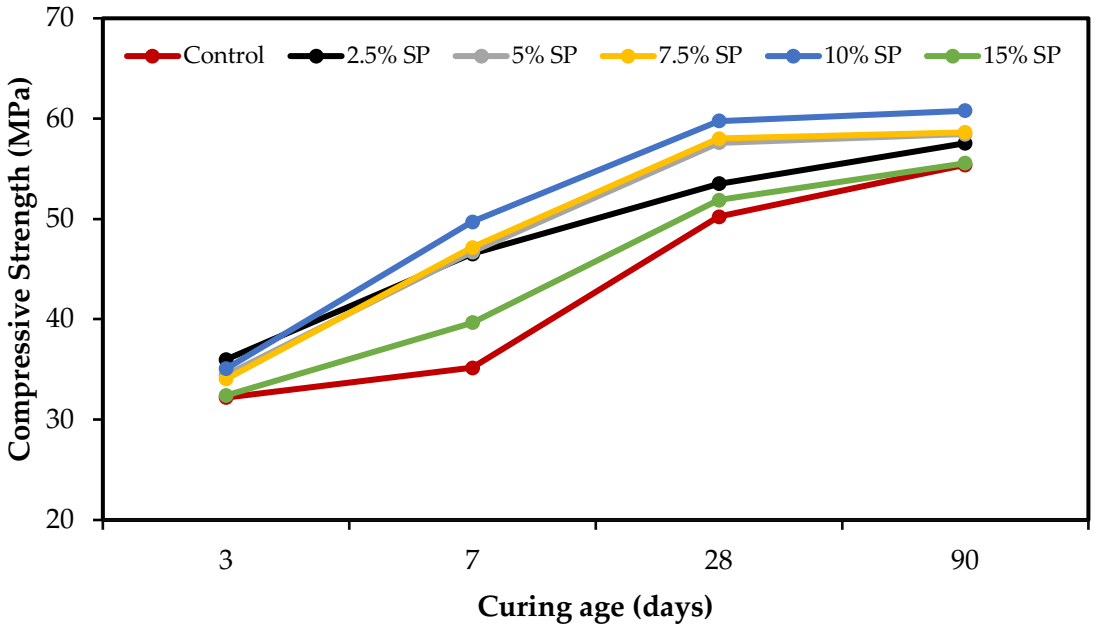

b) Cement replacement with SP

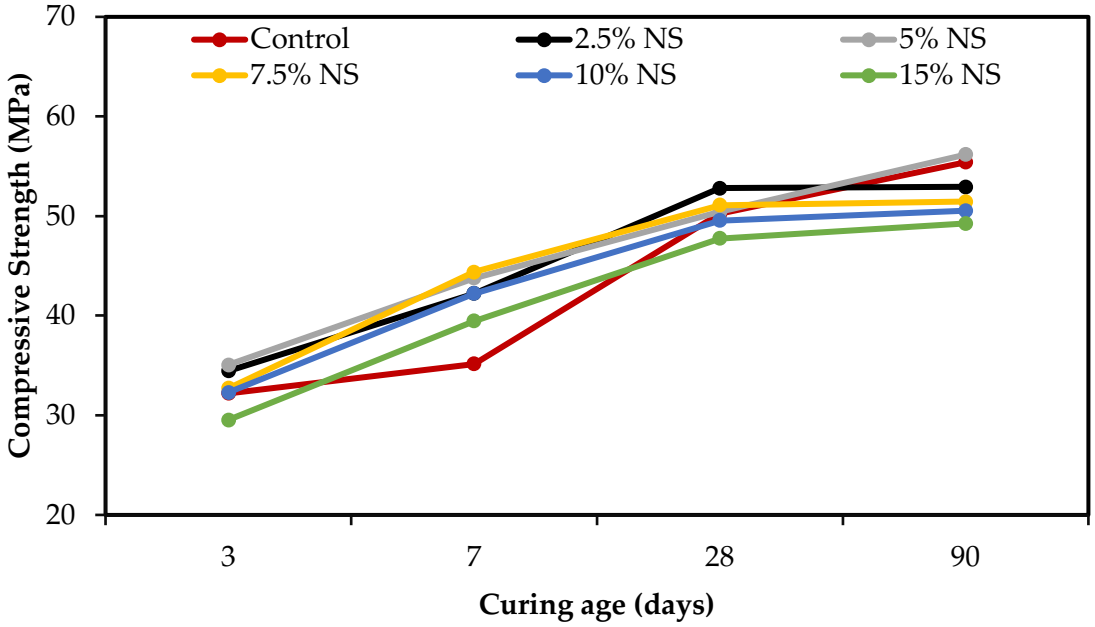

c) Cement replacement with NS

Figure 4.24: Compressive strength of RHA, SP, and NS mortars with constant w/b ratio

Because of the large surface area, the reactivity of the nano-silica, which accelerated the creation of C-S-H gel, the compressive strength of mixes, including NS, has steadily increased when compared to the control mix. However, with increasing replacement after 5% NS, the compressive strength begins to reduce. The results of this study align with Kuli (2016).

b) Varying w/b ratios

The compressive strengths of mortar with varying w/b ratios are shown in Figure 4.25. Samples with 5%, 7.5%, and 10% RHA marginally enhanced compressive strength compared with the control mortar at a later age of 90 days, even though raising the w/b ratio reduces compressive strength. Compressive strength increased 1.9%, 1.9%, and 1.7%, respectively, with 5%, 7.5%, and 10% RHA replacement. The pozzolanic reaction of RHA produces mortar with a maximum compressive strength of 56.5 MPa after 90 days of curing with a 7.5% cement replacement level. Figure 4.25(b) shows compressive strengths with SP at 3, 7, 28, and 90 days. The compressive strength improved with the replacement of cement by SP up to 10%. At 90 days of age and 7.5% cement replacement level, the maximum compressive strength 63.4 MPa of mortar. The increase was 14.4% more than the control at 90 days.

The NS mixed mortar increased compressive strength compared to the control sample with every replacement. According to this study, after 90 days of curing, NS showed a 2.8 – 15.8% strength increase up to 15% replacement. As seen in Figure 4.25(c), the maximum compressive strength with 2.5% replacement after 90 days of curing age is 64.2 MPa, which increased the strength by 15.8% compared to the control sample. More agglomeration was seen in SEM analysis when the w/b ratio was constant, while the amount of SP or NS was increased. This is because there may not be enough water available to adequately disperse the increased amount of SP or NS. More water is available to spread the silica particles when the w/b ratio is raised. Because the

additional water may serve as a medium for improved dispersion of the silica, this may assist in lessening agglomeration.

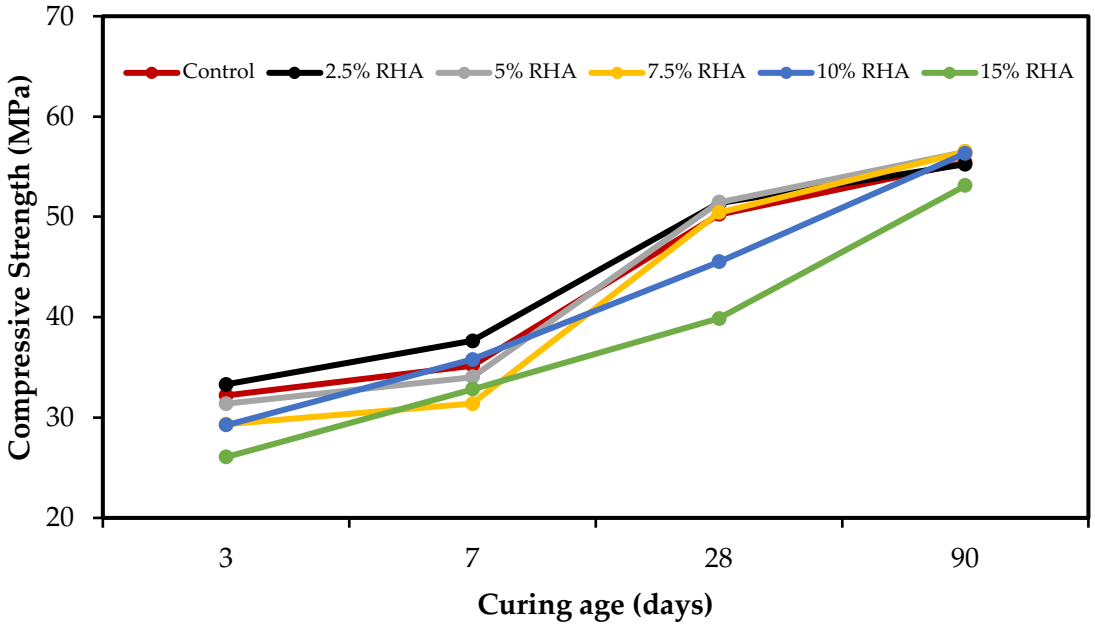

a) Cement replacement with RHA

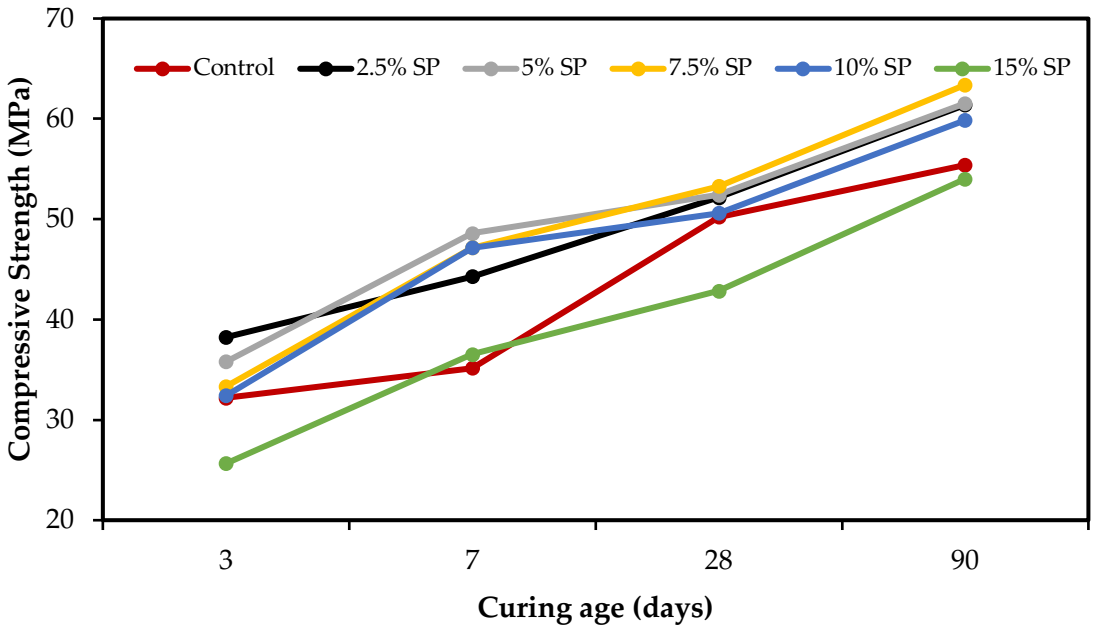

b) Cement replacement with SP

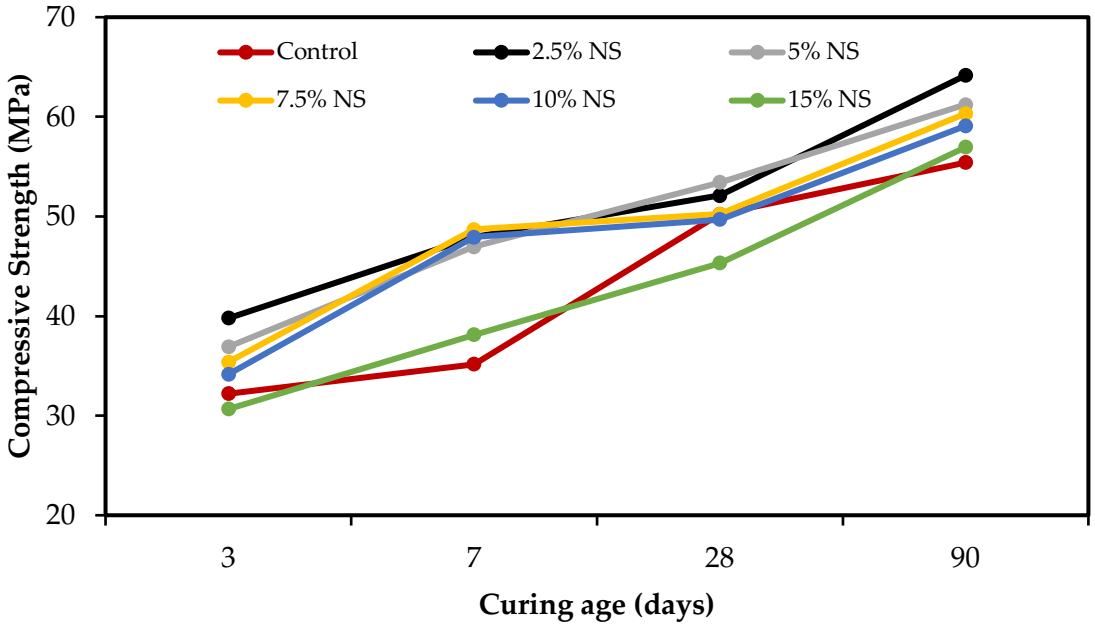

c) Cement replacement with NS

Figure 4.25: Compressive strengths of RHA, SP, and NS mortars with varying w/b ratios

SP or NS may fill small voids in the cement paste and react with calcium hydroxide to create additional C-S-H gel, increasing the strength, if it is sufficiently dispersed. Therefore, higher compressive strength was achieved even with increased w/b ratio because of the improved microstructure, pozzolanic reaction, and decreased porosity by SP and NS replacement.

4.3.5 Pozzolanic Activity

Pozzolanic activity of RHA, SP, and NS with constant and varying w/b ratios was analyzed by the Strength Activity Index (SAI) method. The BS 8615-1 (2019) standard was followed for this.

a) Constant w/b ratio

To evaluate the pozzolanic reactivity of RHA, SP, and NS in mortar, SAI was conducted. The threshold SAI as per BS 8615-1 (2019) is shown by a reference line.

According to the standard, the activity index at 28 days and 90 days shall not be less than 75% and 85% of the strength of the control mortar, respectively. At 28 and 90 days, the compressive strength of the control mortar was found to be 50.2 MPa and 55.4 MPa by a constant w/b ratio (0.5).

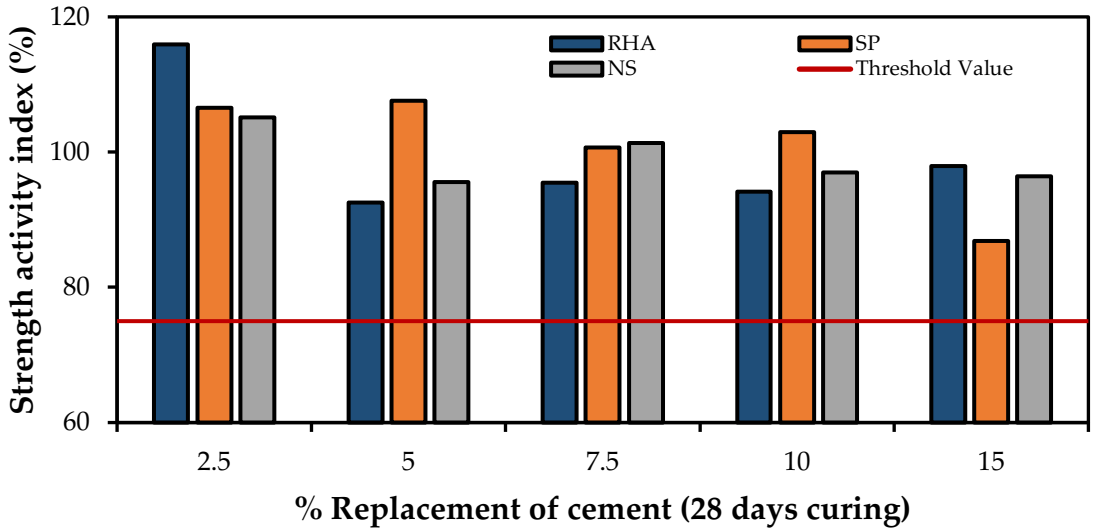

a) Strength activity indices of RHA, SP, and NS at 28 days

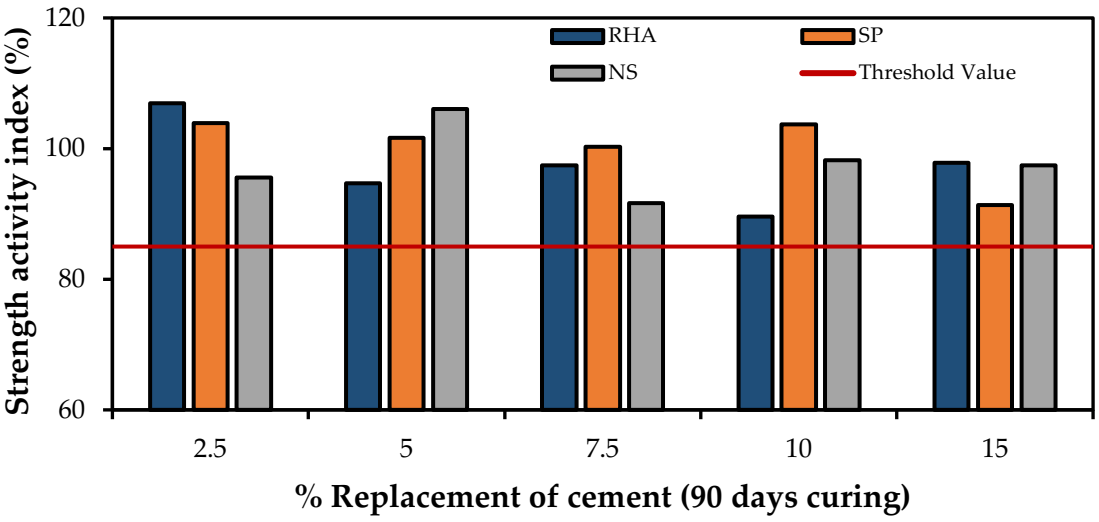

b) Strength activity indices of RHA, SP, and NS at 90 days

Figure 4.26: Pozzolanic reactivity comparison among RHA, SP, and NS at a constant w/b ratio

Figure 4.26 (a) and (b) show the strength activity indices of RHA, SP, and NS. At 28 days of curing age, the compressive strength of mortar containing 2.5%, 5%, 7.5%, 10%, and 15% RHA was determined to be 58.2, 53.9, 51.4, 48.9, and 47.4 MPa, respectively. At 90 days of curing age, the same values were 59.2, 56.1, 54.6, 49.0, and 47.9 MPa, respectively. The SAI for RHA, SP, and NS exceed the minimum criteria for both 28 and 90 days, as stated in BS 8615-1 (2019). SP gave more than 100% of SAI up to 10% replacement level, whereas only 2.5% RHA and 5% NS gave at 106.9% and 106.1%, respectively, of SAI at 90 days curing. The increased water requirement resulting from the high specific surface of RHA, SP, and NS could be the reason for this trend in the strength activity index. One significant drawback of the SAI test is that, in certain situations, it would not be able to distinguish between an active pozzolan and an inert filler (Borges et al., 2021; Kasaniya et al., 2021).

b) Varying w/b ratios

Figure 4.27 (a) and (b) shows the strength activity index of RHA, SP, and NS with varying w/b ratios. At 28 days, the compressive strength of mortar containing 2.5%, 5%, 7.5%, 10%, and 15% RHA was determined to be 51.4, 51.5, 50.4, 45.5, and 39.9MPa, respectively. At 90 days of curing age, the same values were 55.3, 56.5, 56.5, 56.3, and 53.1 MPa, respectively.

The SAI of RHA, SP, and NS exceed the minimum criteria for both 28 and 90 days, as stated in BS 8615-1 (2019). SP demonstrated more than 100% of SAI up to 7.5% replacement, whereas 5% and 7.5% RHA gave at 102.2% and 100%, respectively, SAI at 90 days of curing. Conversely, 2.5% of NS showed more than 100% SAI, which was 115.8% SAI at 90 days curing. Despite having a greater w/b ratio, the extra C-S-H gel created by silica powder or nano-silica increases strength and reduces the usual strength-lowering effect that a higher w/b ratio would have.

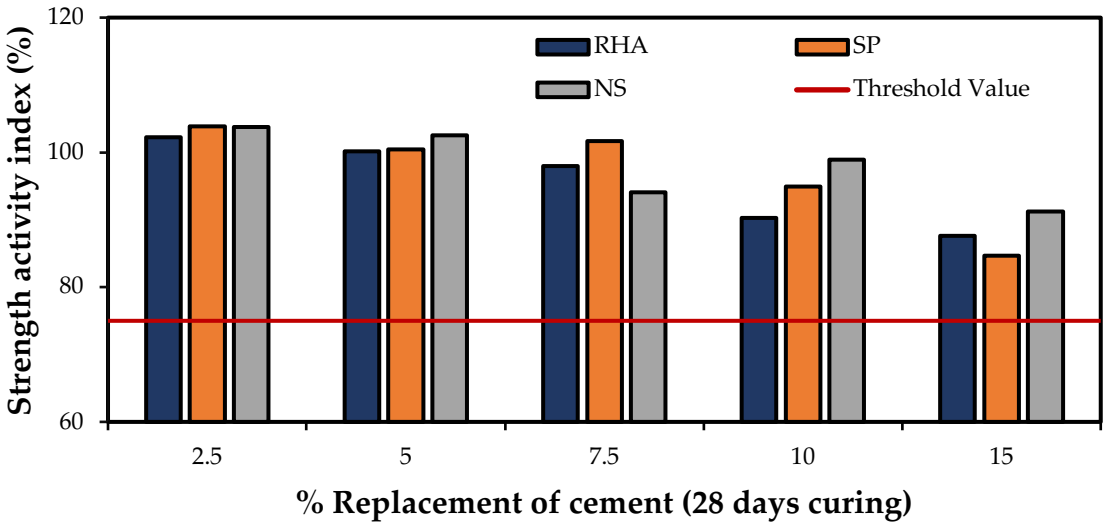

a) Strength activity indices of RHA, SP, and NS at 28 days

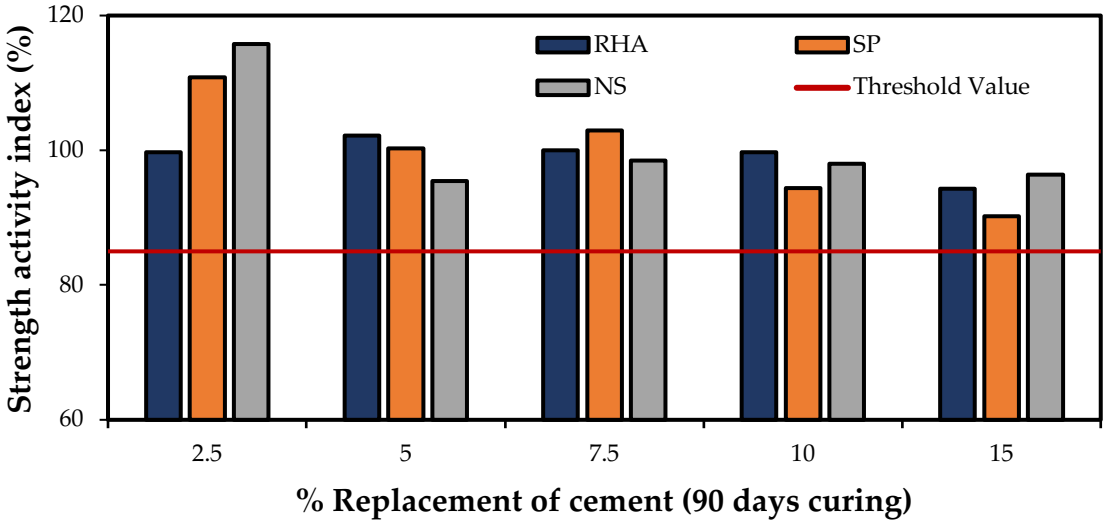

b) Strength activity indices of RHA, SP, and NS at 90 days

Figure 4.27: Pozzolanic activity comparison among RHA, SP, and NS at varying w/b ratios

4.3.6 Water Absorption Test

Water absorption test of mortar samples with constant and varying w/b ratios were conducted. This should reflect the effect of water content on the compaction and thereby voids inside the matrix.

a) Constant w/b ratio

The strength and durability of cement composites are increased with a decrease in water absorption. Figure 4.28 shows the water absorption of RHA, SP, and NS blended mortar at a constant w/b ratio. The RHA substitution for cement gave higher absorption values than the control mix at 90 days of curing. The first reason for this might be the larger size of the RHA particles, and the second is that the hydration of the cement is primarily responsible for the water absorption of RHA mortar. Still, the pozzolanic reaction of RHA particles is less relevant because of the presence of larger RHA particles. In this regard, a decrease in cement may lead to an increase in the water absorption of RHA mortar, which is correlated with an increase in RHA content. According to Antiohos (2013), the coarse texture of RHA does not enhance water resistance through pore filling or pozzolanic effects. In contrast to finer or smaller RHA particles, coarser or larger RHA particles have a lower propensity to evenly disperse over vast regions in the wet mixture evenly, according to Venkatanarayanan & Rangaraju (2015).

Because of this higher water absorption, RHA blended mortar showed lower compressive strength. Figure 4.28 demonstrates that just 2.5% and 5% RHA have water absorption of 7.6%, which is quite like the control mix water absorption (7.5%) and indicates an improvement in compressive strength. Up to 5% replacement of cement with RHA water absorption increased slightly (1.2%) in compare to control. The final products have more voids and are more permeable to liquid when RHA is added to the combinations in higher percentages. The RHA mortars absorb more water when the replacement level of RHA rises due to the increase in permeability. This result is supported by the result found by Potty (2014). The primary cause of porosity was the decreased workability of RHA blended mortar at a constant w/b ratio during casting.

On the other hand, when SP or NS was added, the water absorption of specimens decreased at 90 days of curing. The increase in C-S-H in the mortar and the performance of the silica filler are the leading causes of the reduced water absorption in SP or NS blended specimens (Abhilash et al., 2021).

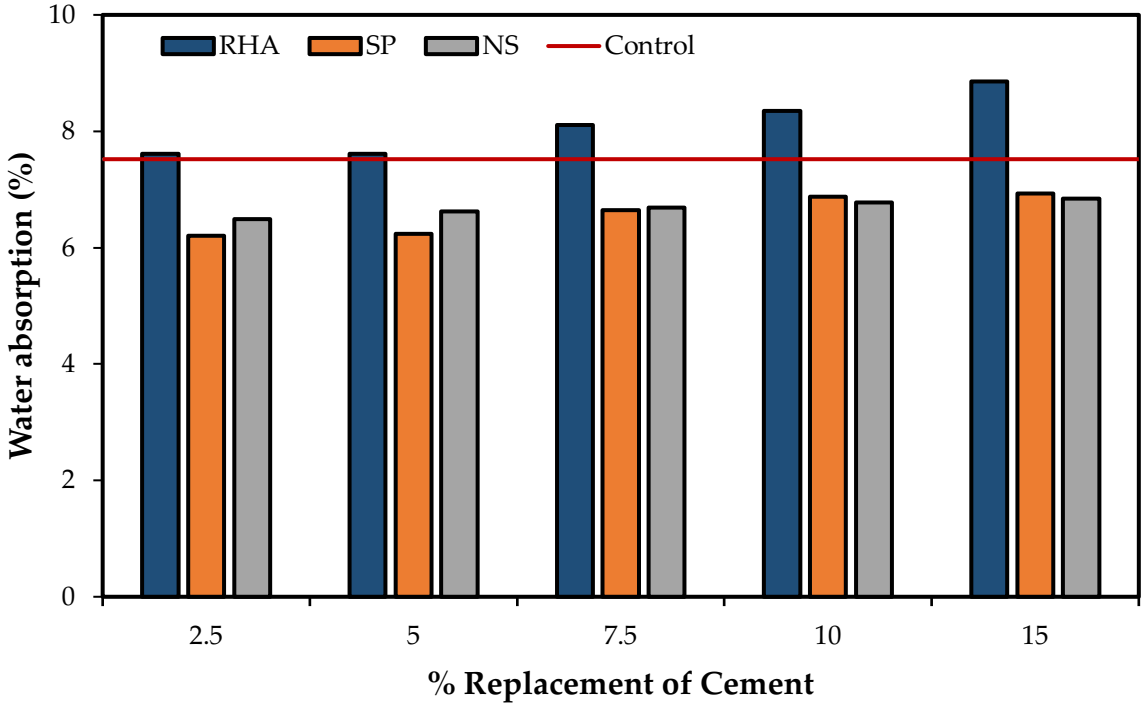

Figure 4.28: Water absorption of RHA, SP, and NS blended mortar at constant w/b ratio

Though SP or NS decreases water absorption in comparison to the control mix, the water absorption increases with the increased replacement of SP or NS. This may be due to poor dispersion of the SP or NS in the mortar, which might cause the particles to agglomerate, and agglomeration was seen in SEM analysis with higher replacement. Inadequately distributed silica did not react well and might cause internal gaps or cracks in the structure, which increased water absorption.

b) Varying w/b ratios

Figure 4.29 shows the water absorption of RHA, SP, and NS blended mortar at varying w/b ratios. The result indicates that cement replacement with RHA reduced water

absorption compared to the control mix at varying w/b ratios. Water absorption decreased when the w/b ratio increased, maybe because more water was available. However, the total hydration process remained insufficient, leading to a decrease in compressive strength compared to a constant w/b ratio.

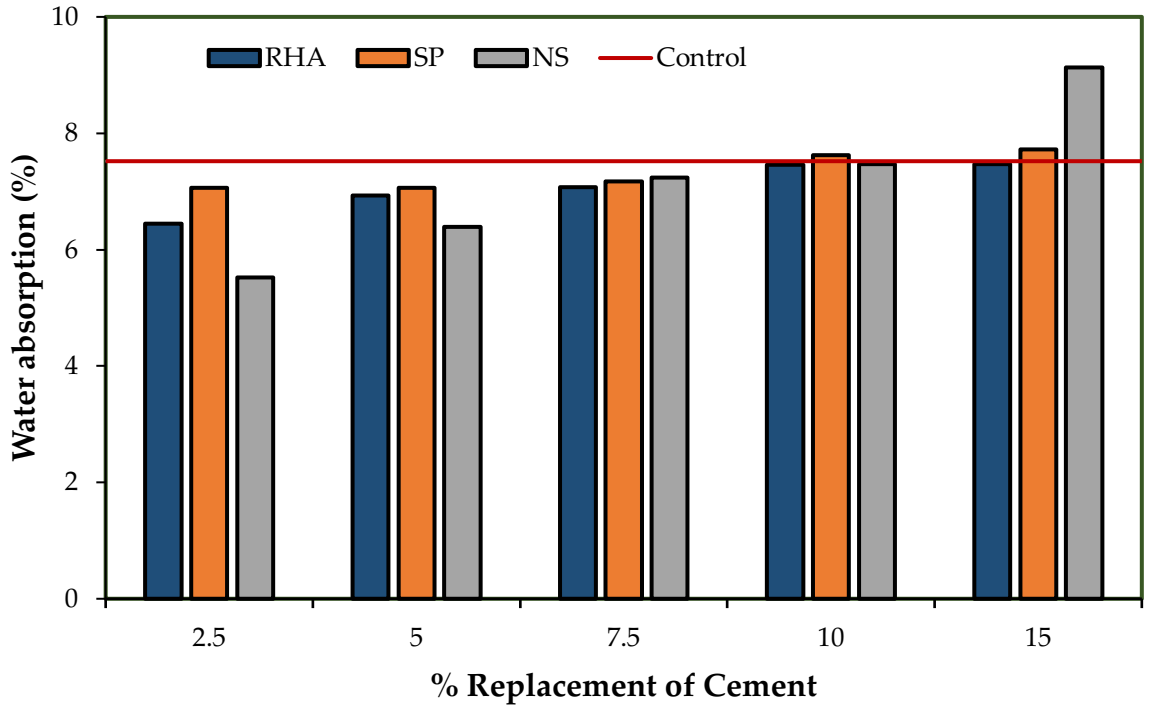

Figure 4.29: Water absorption of RHA, SP, and NS blended mortar at varying w/b ratios

For SP and NS blended mortar, the water absorption decreased up to 7.5% and 10% cement replacement with varying w/b ratios, respectively, but increased in comparison to a constant w/b ratio at 90 days curing. 7.5% SP reduced water absorption by 11.7% and 4.6% with a constant and varying w/b ratio, respectively. Besides, 10% NS reduced water absorption by 9.8% and 0.7% with a constant and varying w/b ratio, respectively. The greater the w/b ratio, the more free water there is, and it will not be bound in the hydration products, which leads to a more porous matrix. Although silica powder or nano-silica assists in better packing and hydration, too much water in the system might cause bigger capillary pores to develop, raising the overall porosity of the specimens.

4.3.7 Density

The density of mortar samples with constant and varying w/b ratios was measured. The effect of varying w/b ratios in compaction was visible in this section. Properly compacted specimens should be denser.

a) Constant w/b ratio

Figure 4.30 shows the dry bulk density values of hardened mortars at a constant w/b ratio. The density of the control mix (0% replacement) is shown by a horizontal line in this figure. For the control mix, the bulk density achieved 2285 kg/m^3. RHA blended mortar increased bulk density up to 5% replacement. It increases density by 2.2-6.8% from the control mix. RHA blended mortar with 5% replacement showed the maximum density of 2440 kg/m^3. Though 5% replacement showed maximum density, maximum compressive strength was found with 2.5% replacement. It may be beyond 2.5% replacement of cement with RHA gives more filler effect rather than a pozzolanic reaction.

For SP blended mortar, 5%, 7.5%, and 10% replacement showed higher density. Maximum density achieved at 7.5% replacement of cement by SP, which was 2390 kg/m^3. Mortar with NS increased density by 7.1-9.8% to the control mix. A 2.5% replacement of cement by NS showed the maximum density of 2505 kg/m^3. However, with 10% SP or 5% NS, maximum compressive strength was found to be greater than that of the control. It may be a higher pozzolanic reaction and nucleation effect of SP/NS. The development of more C-S-H and the micro filler effect of the increased RHA/SP/NS might be the cause of this. As seen in Figure 4.24, this increase in compressive strength was a direct result of the hardened density improvement. As the amount of RHA/SP/NS content increased, the density of the RHA/SP/NS blended mortar dropped because RHA/SP/NS has a lower density than other materials. As the amount of rice husk increased, the density reduced because of the porosity caused by

the presence of rice husk, according to the results of another study (Ahmad et al., 2015; Yuzer et al., 2013). However, the change in overall density for using pozzolanic material was minor (2% to 9%).

The apparent density is shown in Figure 4.31. The apparent density was calculated considering internal pores as a component of the volume of the specimen. In addition to internal pores, the volume corresponding to bulk density also contains open pores of particles and voids created by several particles packing together as a single unit (referred to as stacking pores).

The apparent density of the control sample increased by 21.4% of its bulk density. Figure 4.31 shows that the replacement of cement by RHA increased apparent density by 22.2 – 25% of its bulk density, which was greater than that of the control sample. That means that the replacement of cement by RHA slightly increased internal porosity, which was confirmed by the water absorption result shown in Figure 4.28. On the other hand, the apparent density of SP and NS blended mortar increases by 13.1 – 20.9% and 17.3 – 20.1% respectively, compared to its bulk density, which was less than that of the control sample. The internal porosity seemed to decrease with the replacement of cement by SP and NS.

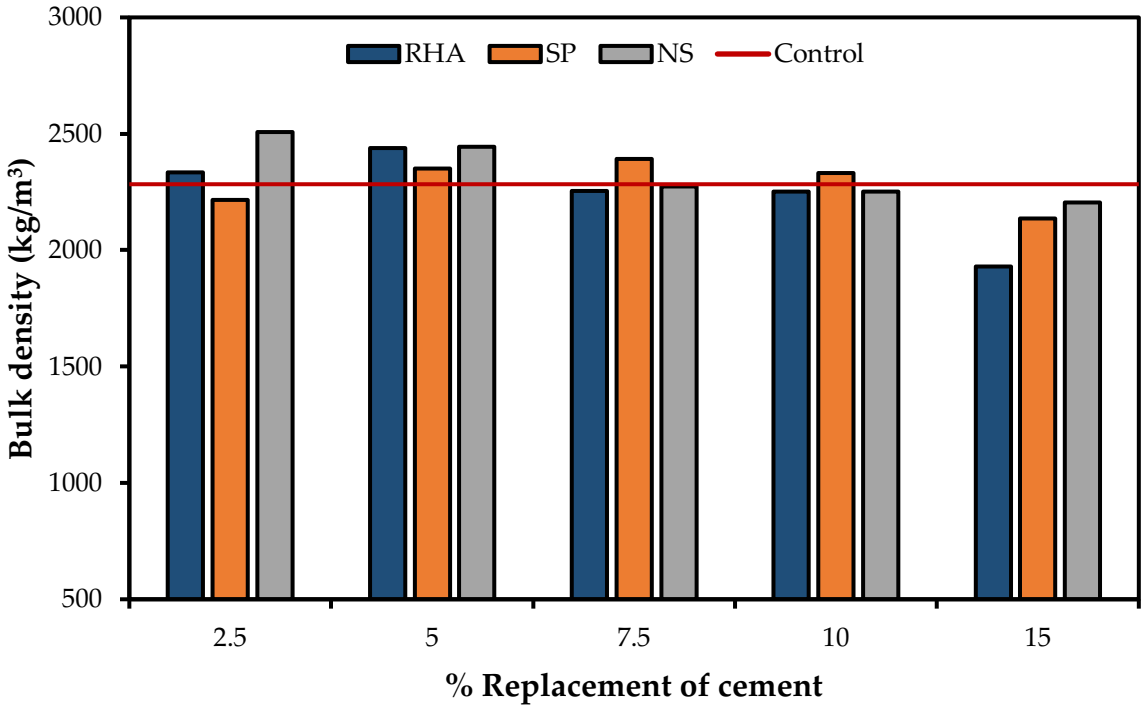

Figure 4.30: Bulk density of RHA, SP, and NS blended mortar at constant w/b ratio

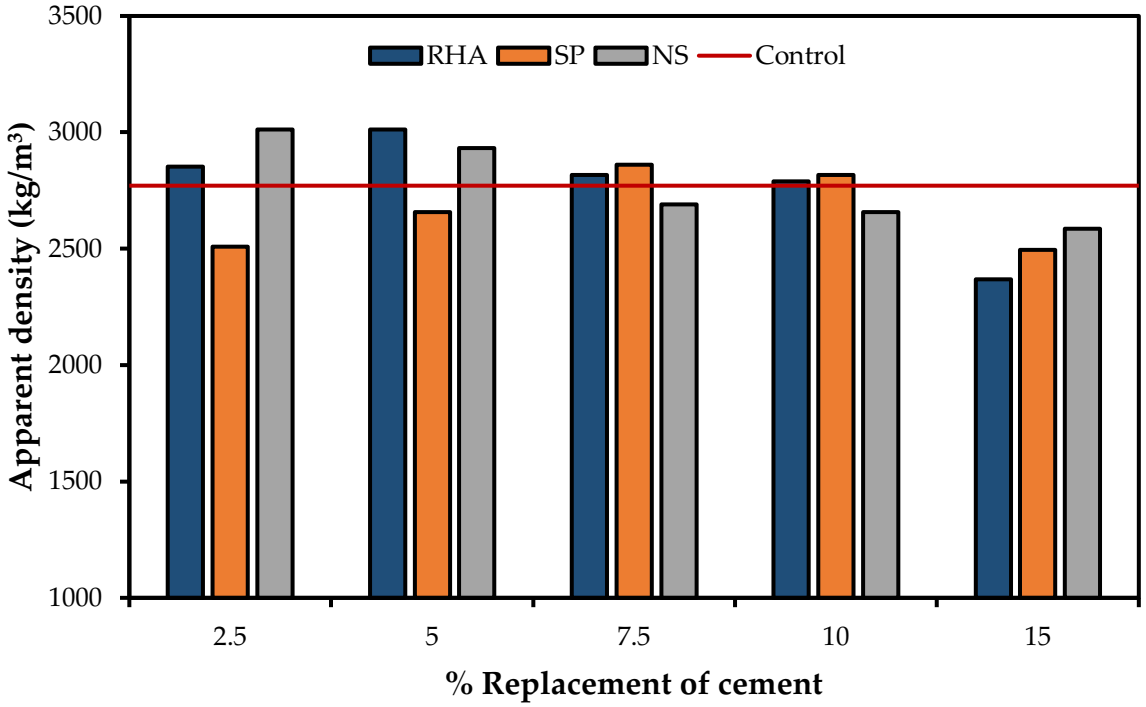

Figure 4.31: Apparent density of RHA, SP, and NS blended mortar at constant w/b ratio

b) Varying w/b ratios

Bulk density at various w/b ratios is shown in Figure 4.32. It shows that the bulk density was reduced by using RHA as a cement replacement at various w/b ratios. On the other side, the bulk density slightly increases when SP and NS replace cement at various w/b ratios. Maximum bulk density was achieved when 2.5% SP replaced cement, and it was 2360 kg/m^3. 2.5% NS also showed the maximum bulk density, and it was 2330 kg/m^3. Figure 4.33 shows the apparent density at various w/b ratios. Maximum apparent density is achieved with 2.5% RHA, SP, and NS. The apparent density values are 2820 kg/m^3, 2920 kg/m^3, and 2940 kg/m^3, respectively.

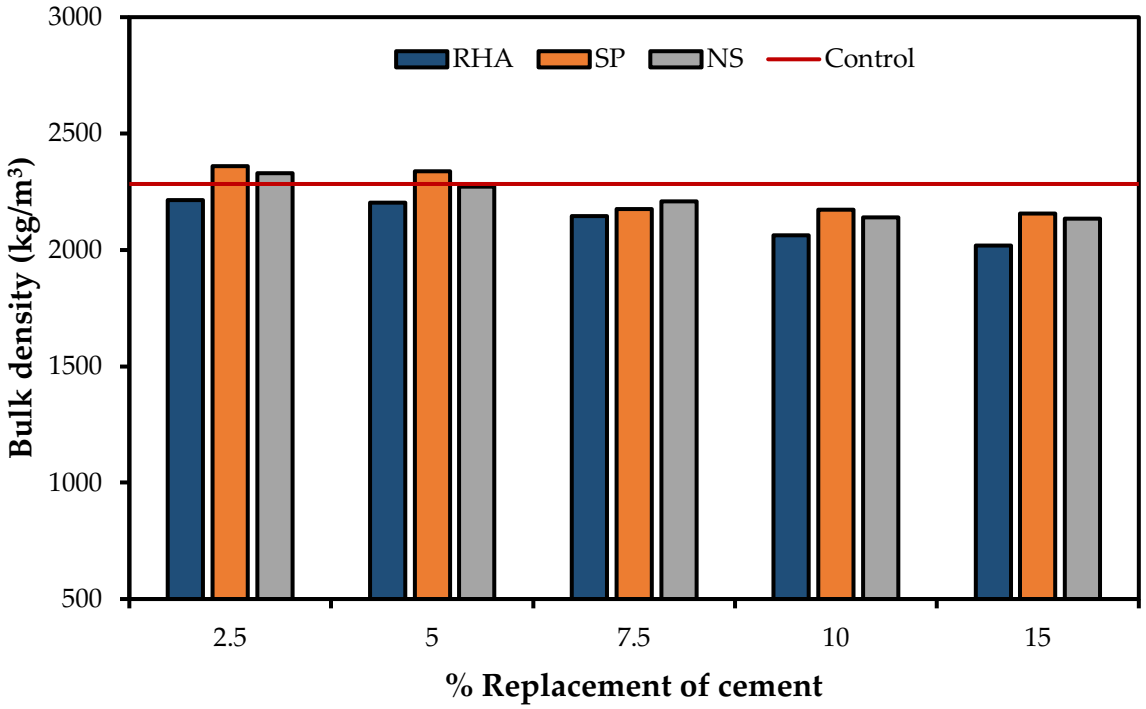

Figure 4.32: Bulk density of RHA, SP, and NS blended mortar at various w/b ratios

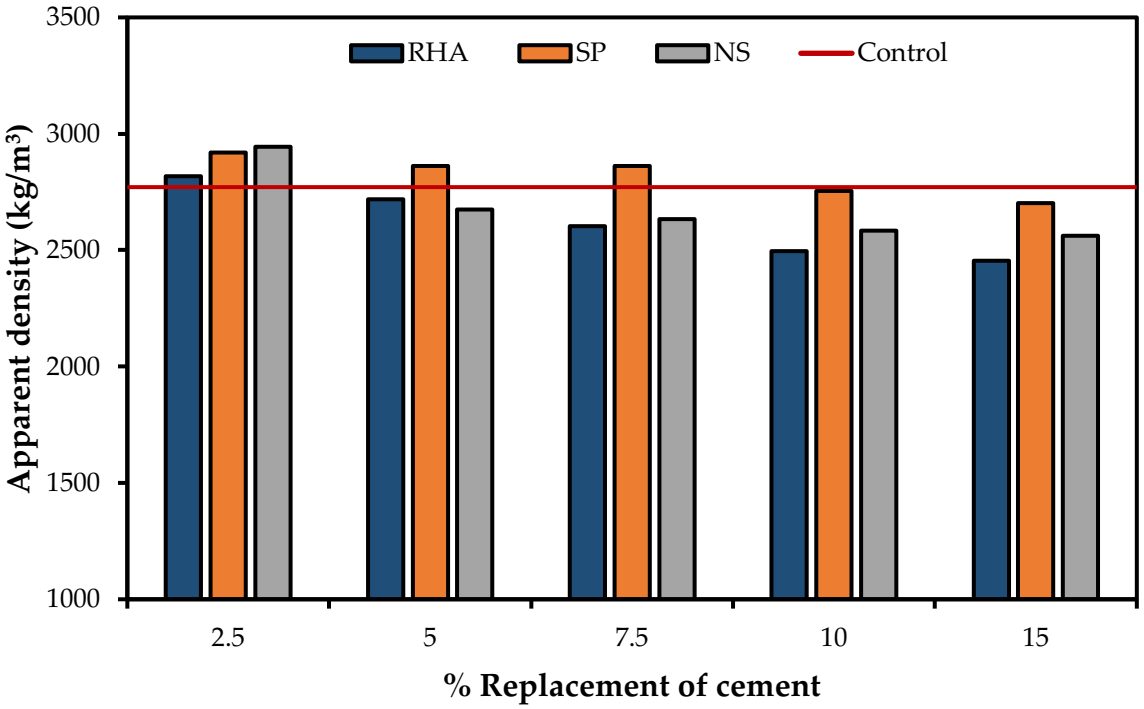

Figure 4.33: Apparent density of RHA, SP, and NS blended mortar at various w/b ratios

4.3.8 Volume of Permeable Pores

Volume of permeable pores of mortar samples with constant and varying w/b ratios was measured. The effect of water content on compaction and pozzolanic reaction should be compared with the porosity value.

a) Constant w/b ratio

Figure 4.34 shows the volume of permeable pores of the RHA, SP, and NS blended mortar at 90 days of curing. The control specimen volume of permeable pores was 17.6% at 90 days curing. With the addition of RHA as a replacement for cement, the volume of permeable pores increased, and as a result a water absorption increased (Figure 4.28). The 7.5% rice husk cement mortar exhibited the maximum volume of pores (20%), which was 13.5% times more than that of the control sample. Other

studies have found that adding rice husk increases the volume of permeable pores, which is consistent with our findings (Ahmad et al., 2015). The compressive strength is influenced by the degree of porosity. For a strength increased from around 54.6 to 59.2 MPa, the volume of permeable pores decreased from 20% to 18.2% with RHA. With 2.5% RHA, slightly increased water absorption and volume of permeable pores (3.3%) were observed. Because of this negligible increment, maximum compressive strength was found with 2.5% RHA. From Figure 4.34, it is evident that adding SP and NS reduced the volume of permeable pores. As the volume of permeable pores reduced, water absorption was also reduced with SP/NS incorporation in cement mortar.

Generally, compressive strength increases with the decrease of porosity; in the case of SP or NS blended mortar, a complex relation was noted. The porosity slightly increased from 14.4% to 17.3% with SP and from 14.8% to 16.6% with NS. However, strength increased from 55.5 to 60.8 MPa and from 49.3 to 56.2 MPa, respectively. SP or NS refines and rearranges pore structures. Hu (2024) found that the strongest link with compressive strength is seen in the fractal dimension of bubble distribution. Smaller, uniformly spaced pores hinder the easy propagation of fractures, preventing failure under compressive stress; hence, a refined, smaller-pore structure can nonetheless contribute to greater strength. Hu (2024) found that NS considerably increases the strength of mortar while simultaneously increasing its porosity, due to decreased fluidity.

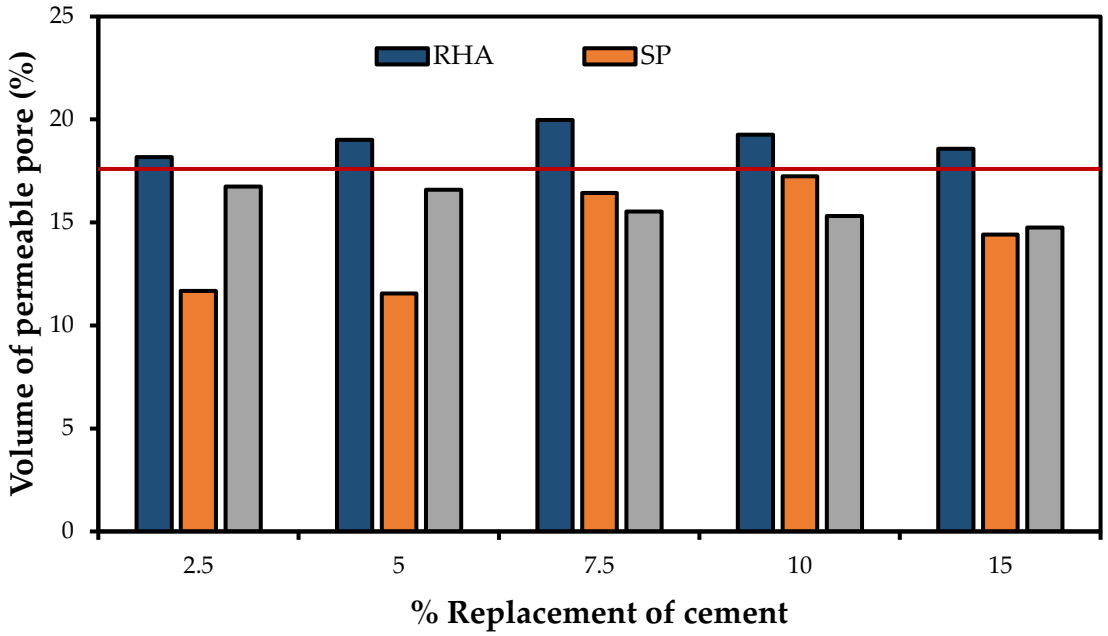

Figure 4.34: Volume of permeable pores of RHA, SP, and NS blended mortar at constant w/b ratio

b) Varying w/b ratios

Figure 4.35 displays the volume of permeable pores of the RHA, SP, and NS blended mortars with varying w/b ratios. The porosity increased as the w/b ratio increased in comparison to the constant w/b ratio. Excess water tends to cause voids in the hardened structure, increasing porosity when the w/b ratio is too high. 2.5% rice husk cement mortar gave the maximum porosity (21.4%), which is 21.8% more than that of the control sample. Whereas 7.5% SP showed the maximum porosity (24%), which is 36% more than the control sample. On the other side, NS reduced porosity in comparison to the control sample, although the w/b ratio increased. Only 2.5% replacement of cement with NS showed slightly higher porosity (20.8%), which was 18.3% more than the control sample. The findings showed that NS reduced the amount of permeable pore space in mortars with a constant w/b ratio, but it had no influence on the volume of permeable pores in mortars with high w/b ratios. This

might be because the large pores were split into smaller ones when NS was added, but the overall pore volume remained unchanged (Yogendran et al., 1987).

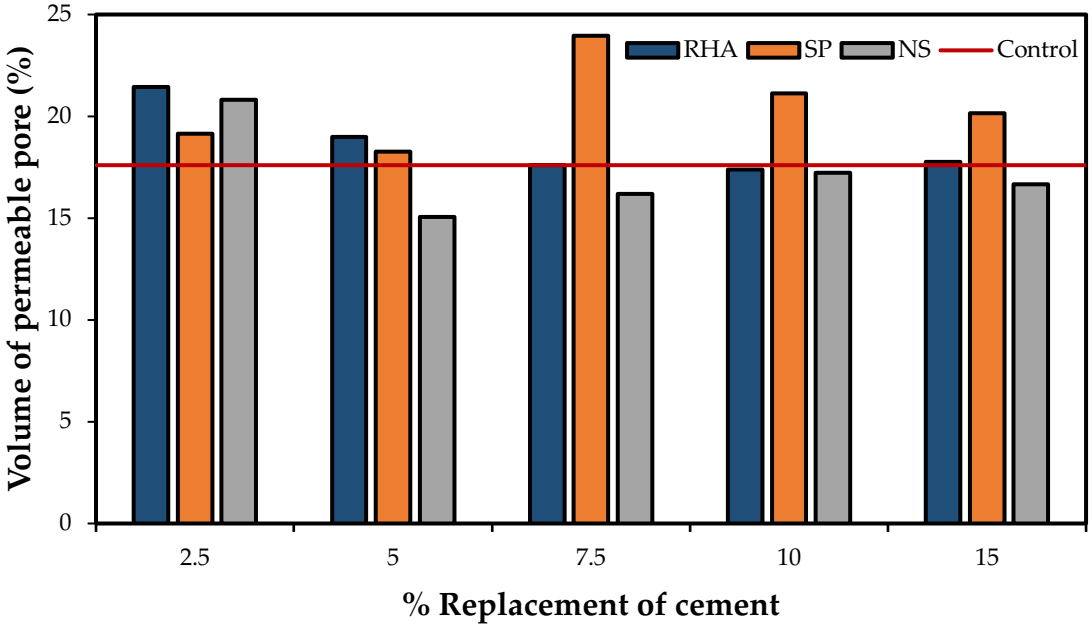

Figure 4.35: Volume of permeable pores of RHA, SP, and NS blended mortar at varying w/b ratios

The compressive strength decreased as the porosity increased with the replacement of cement by RHA. However, the relationship between compressive strength and porosity for SP or NS replaced mortar is not fully defined. Although the porosity increased from 20.2 to 23.9%, the compressive strength increased from 54.0 to 63.4 MPa with the replacement of cement by SP. Besides, when the compressive strength increased from 56.9 to 64.2 MPa, porosity increased from 16.7 to 20.8% with the replacement of cement by NS. However, the data is too scattered to define a relationship. Hu (2024) found that porosity does not primarily influence compressive strength. According to Kong (2019) observations, adding colloidal NS to mortar promotes strength by creating open pores that hold onto free water for the extended hydration of cement.

4.3.9 Drying Shrinkage Test

Figure 4.36 shows the shrinkage results of RHA, SP, and NS blended mortar at different ages. Cement was partially replaced in mortars with varying RHA, SP, and NS (0%, 2.5%, 5%, 7.5%, 10%, and 15%). A constant water-to-binder ratio (0.48) was used for all specimens. Figure 4.36(a) shows that replacement in volume percentage and mortar drying shrinkage are negatively impacted when amorphous silica is combined with coarse RHA particles. Numerous studies have demonstrated that concretes with pore refinement additives often exhibit higher creep and shrinkage values (Monteiro, 2006). The particle size and structure of RHA cause internal pore development in the cement paste. As the cement paste dries, the drying shrinkage increases due to the additional paths for moisture to evaporate created by these small interior holes. Beyond 5% replacement with RHA showed higher shrinkage than the control. It can be noted that a 15% ratio gave higher drying shrinkage than the control mortar by about 11.2%.

Figures 4.36(b) and (c) illustrate how SP and NS affect drying shrinkage. The drying shrinkage decreased from 5% to 15% replacement with SP and all replacement with NP with the curing ages (7 to 28 days). Compared to the control sample, at 28-day drying shrinkage decreased by 3.6%-13.1% when the amount of SP increased from 5% to 10%, as shown in Figure 4.36(b). From Figure 4.37(b), the optimum replacement of SP to produce the lowest shrinkage was 10%, which reduced shrinkage by 13.1% more than the control. Figure 4.37(c) shows that the optimum replacement of NS to produce the lowest shrinkage was 5%, which reduced shrinkage by 58.9% compared to the control. Because the C-S-H gel structure was improved and the microstructure was changed, the nano-mechanical qualities of paste with SP and NS replacement were enhanced (Shah et al., 2016).

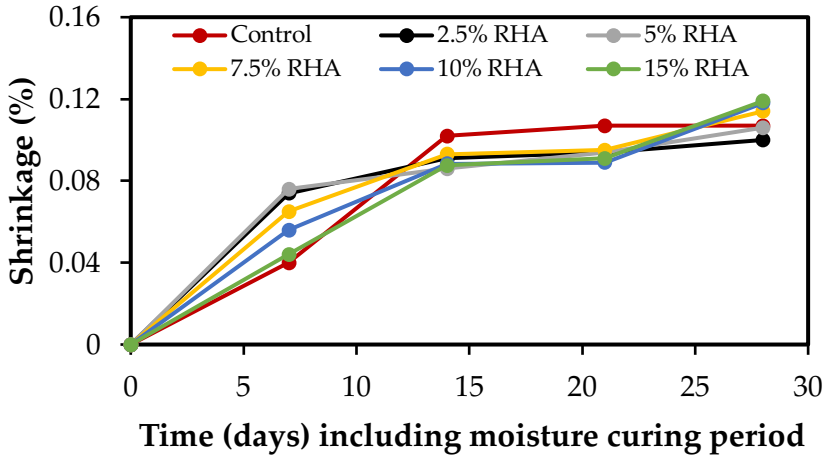

a) Effect of RHA on drying shrinkage

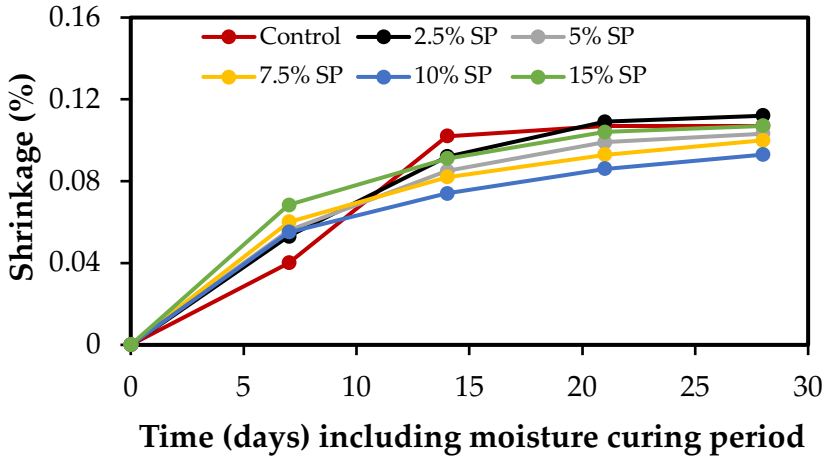

b) Effect of SP on drying shrinkage

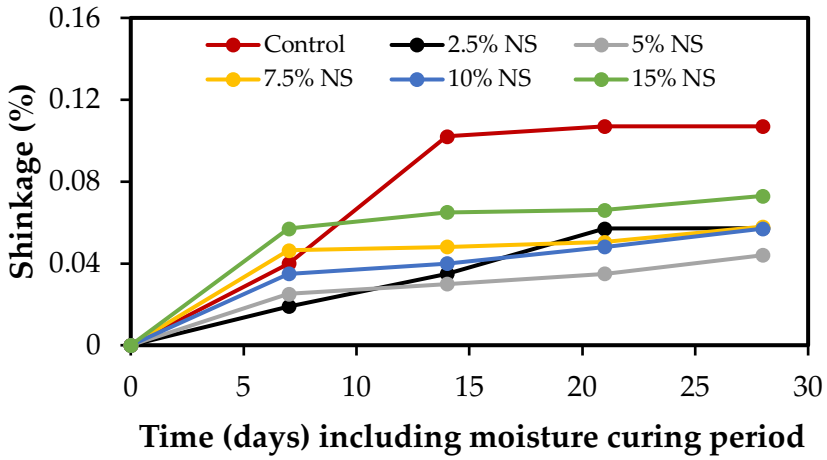

c) Effect of NS on drying shrinkage

Figure 4.36: Shrinkage of RHA, SP, and NS blended mortars

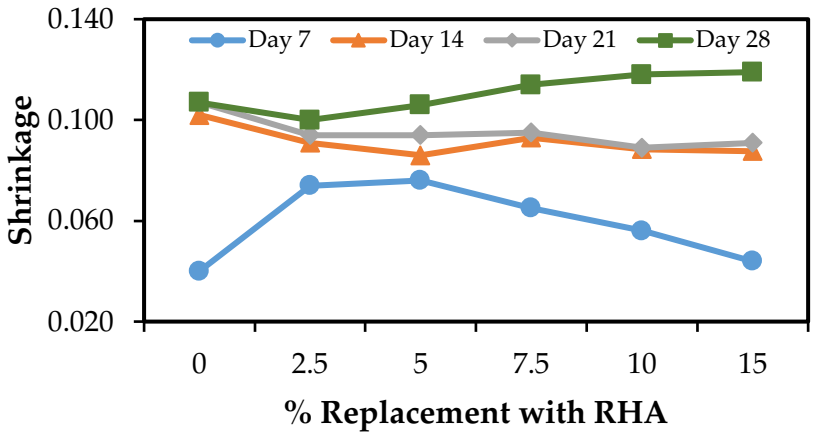

a) Shrinkage for different levels of RHA

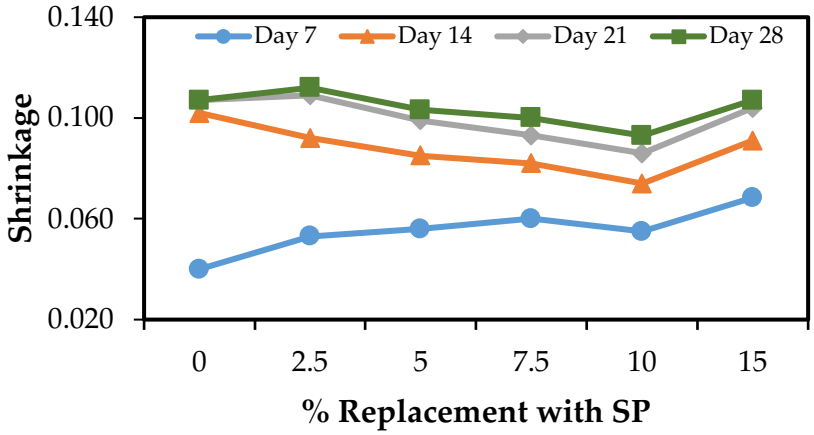

b) Shrinkage for different levels of SP

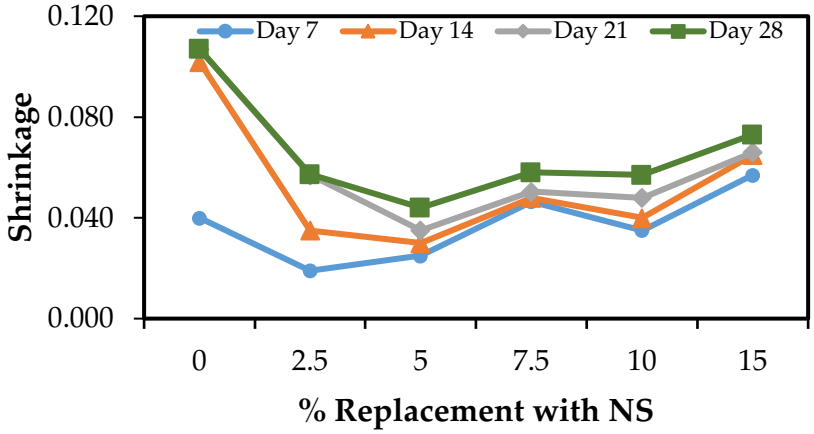

c) Shrinkage for different levels of NS

Figure 4.37: Effect of different RHA, SP, and NS levels at various curing ages.

Furthermore, the pore structure started to refine as the pore size decreased, and the proportion of pores in the paste decreased (Güneyisi et al., 2015; Ibrahim et al., 2020; M. K. Mohammed et al., 2014). The decreased shrinkage implied a more disjointed pore structure, where moisture is lost through convoluted paths more slowly. Du & Pang (2015) verifies the experimental findings from this study. Besides, compared to the control sample, at 28-day drying shrinkage decreased by 31.8%-58.9% when NS increased from 0% to 15%, as shown in Figure 4.36(c).

4.3.10 Sulfate Resistance Test

Figure 4.38 shows the expansion of mortar mixes with RHA/SP/NS in a sodium sulfate (Na_2SO_4) environment. The expansion started slowly and significantly increased after 4 weeks of immersion. With the increase of replacement by RHA, expansion slightly increased compared to the control (4 to 5%) due to the porosity. Only 10% RHA replacement showed lower expansion because it had lower porosity than the control mix.

Figure 4.38(b) shows that expansion slightly increased for all replacements by SP because it showed higher porosity than the control for increasing w/b ratios. Maximum expansion was observed for 15% replacement, which was 0.25% at 15 weeks of immersion. On the other side, 5% and 7.5% replacement by NS showed slightly lower expansion than the control (Figure 4.38(c)). This is because the increase in replacement as well as the w/b ratios by NS reduces the porosity. Low permeability is crucial because it prevents the diffusion of harmful chemicals into the concrete matrix (Neville, 2010).

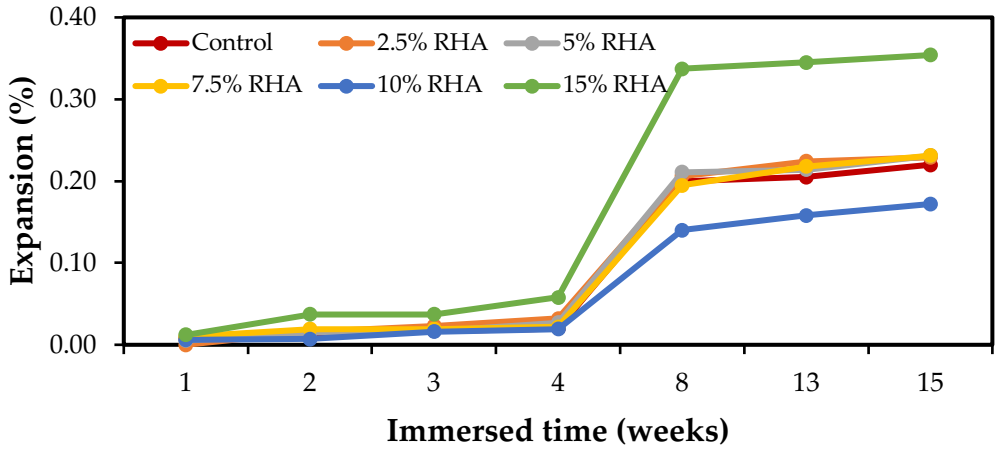

a) Expansion of RHA blended mortar

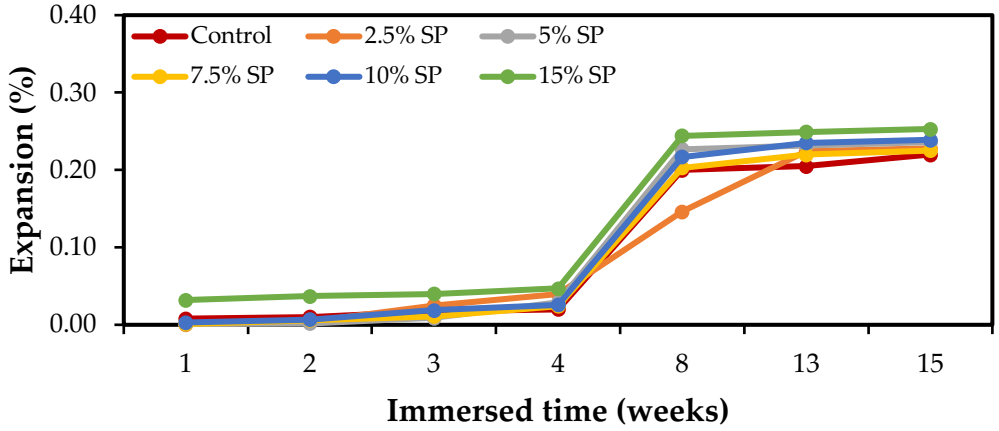

b) Expansion of SP blended mortar

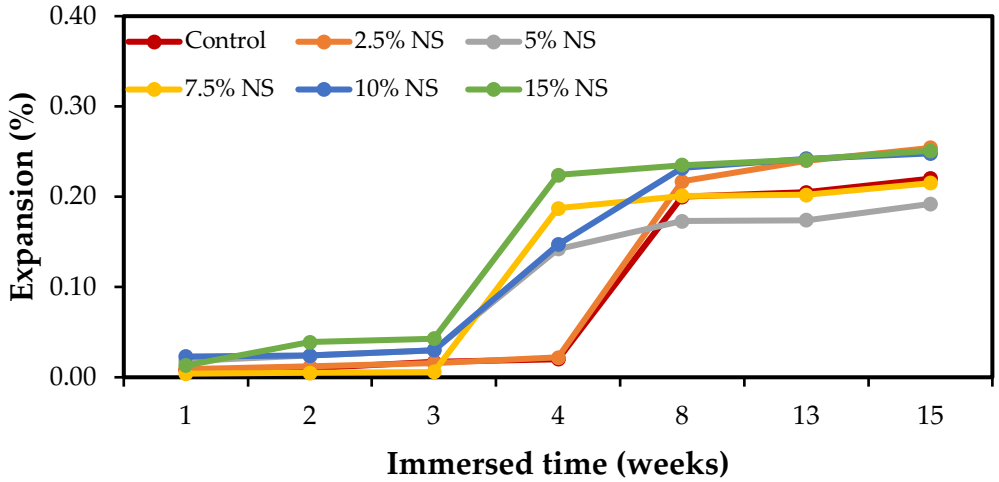

c) Expansion of NS blended mortar

Figure 4.38: Expansion of RHA, SP, and NS blended mortar

4.4 TEST RESULTS OF CONCRETE

In this section, the test results of concrete samples are discussed. Fresh density, workability, compressive strength, water absorption, hardened density, volume of permeable pore, UPV, RCPT, sorptivity, and surface electrical resistivity test results are included.

4.4.1 Fresh Density of Concrete

Figure 4.39 shows the fresh density of concrete. With the replacement of cement by RHA, SP, and NS, the fresh density reduced slightly. The fresh density of the control sample is 2375 kg/m^3. With 15% RHA, the density of the concrete decreased by 2.2% to 2320 kg/m^3. The high porosity and large specific surface area of RHA are responsible for the density decrease. As RHA has a lower density than cement, the density of concrete decreased when RHA was used in place of cement (Mayooran et al., 2017). It is important to note that the tendency of density decrease became more noticeable the more RHA was applied.

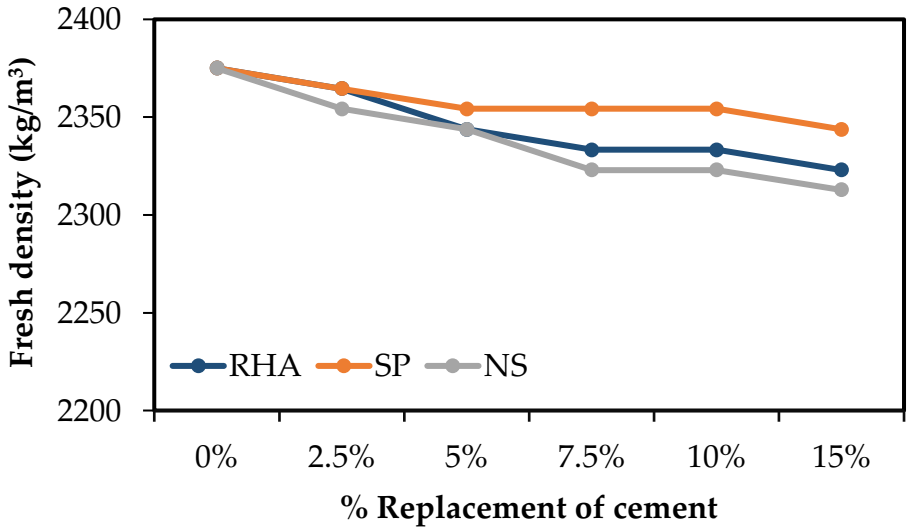

Figure 4.39: Fresh density of RHA, SP, and NS blended concrete

Besides, the fresh density of concrete mixes decreased as the level of SP or NS in the mixture increased. With 15% SP, the NS fresh density value was reduced by 1.3% and 2.6% respectively, compared to the control mix. SP or NS absorbs water quickly because of its higher surface area. The decreased workability validated this perception. As the amount of SP or NS in the concrete mix increases, it becomes less workable. Additionally, SP and NS have a specific gravity of 2.051 and 2.019, respectively, which is significantly lower than that of cement. The fresh density of concrete, therefore, decreases as SP or NS is used in place of cement.

4.4.2 Workability (Slump)

The workabilities, as determined by the slump test, decreased as RHA, SP, and NS increased, as shown in Figure 4.40. RHA has a relatively high specific surface area because it is a porous substance having macro and mesopores both within and outside the particles. As a result, there remains less free water, which reduces slump as the RHA absorbs some of the mixed water on its surface (Le et al., 2012; Rößler et al., 2013). The workability of mixes decreased with higher RHA content while maintaining a constant total amount of mixing water. At greater RHA dosages, such as beyond 10%, the workability drops to a minimum to qualify as workable concrete. It may be concluded that mixes containing RHA will need a greater water content than similar conventional mixes to achieve the necessary workability (Le et al., 2014).

In cases of SP or NS doses exceeding 7.5%, workability decreases drastically. This is because high dosages of NS have poor dispersion and a high packing density, which lowers the amount of free water (Seifan et al., 2020). The 15% SP and NS reduced workability by 91.4% and 95.7% respectively. In order to establish silanol (Si–OH) linkages, a portion of the water in the mixture migrates towards the surface of the SP or NS particles with unsaturated bonds, increasing the water demand for flowability (Mukharjee & Barai, 2020).

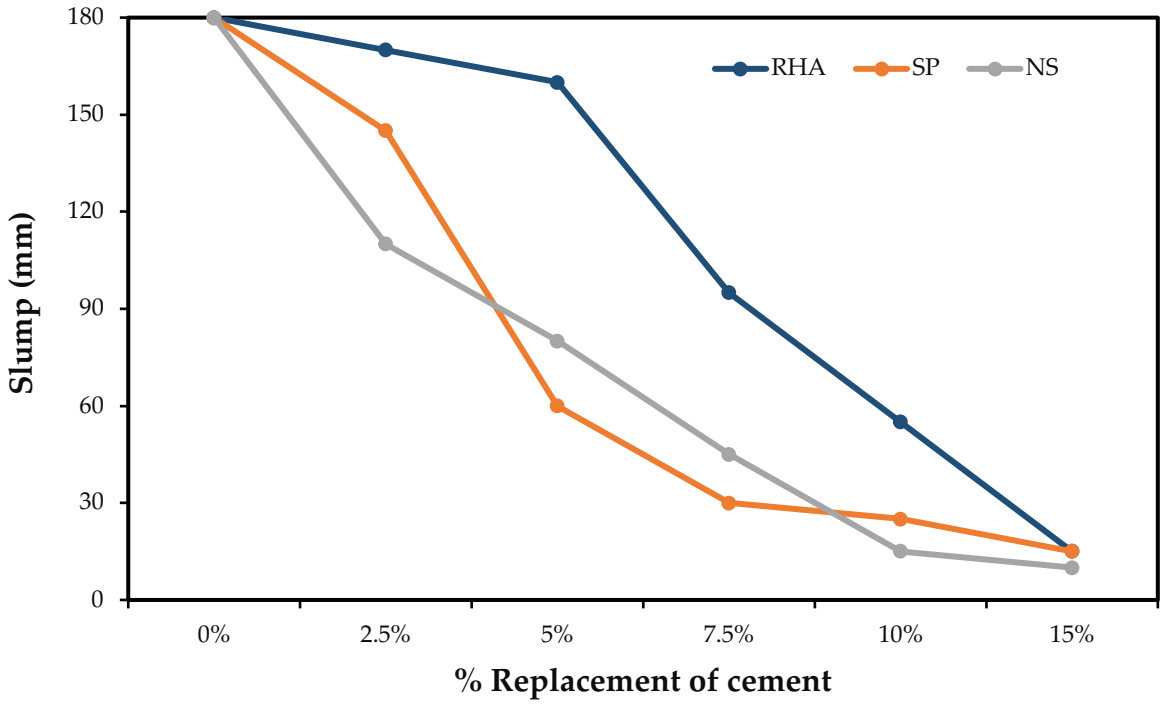

Figure 4.40: Workability of RHA, SP, and NS blended concrete

4.4.3 Compressive Strength

Figure 4.41 shows the compressive strength of concrete incorporating RHA, SP, and NS. The compressive strength of concrete is increased when RHA is used in place of the cement up to 10%, as shown in Figure 4.41(a). According to M.-H. Zhang (1996), 10% RHA replacement showed greater strength at all ages than control OPC. Concrete with 7.5% RHA had the greatest 56-day strength, 14.7% more than the control. The pozzolanic and filling effects are mostly responsible for the strength enhancement. The internal water curing action may be the reason why the insertion of the porous RHA raises the degree of cement hydration at 56 days. Additionally, the C-H consumption indicates that the pozzolanic reaction of RHA happens to a high extent at this age, causing a significant pore refinement.

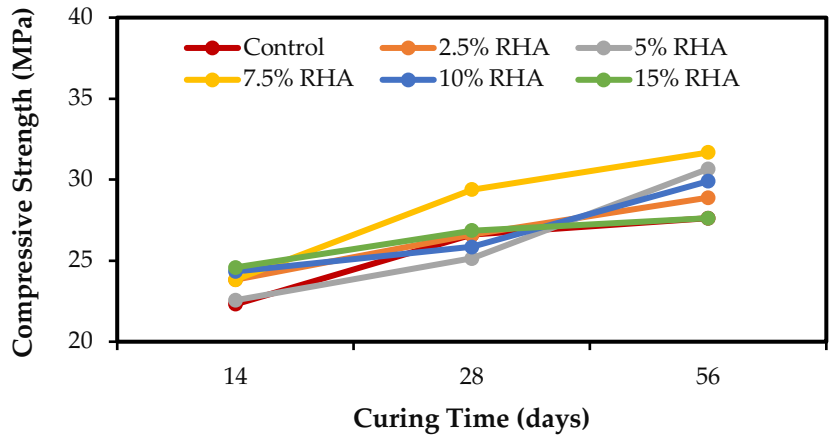

a) Cement replacement with RHA

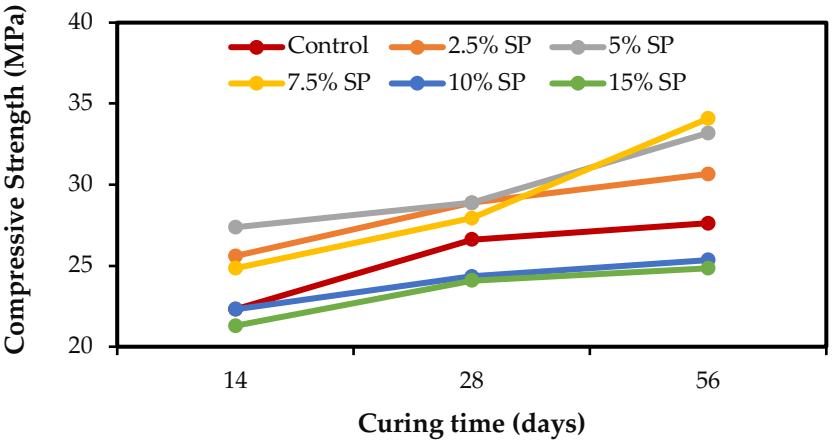

b) Cement replacement with SP

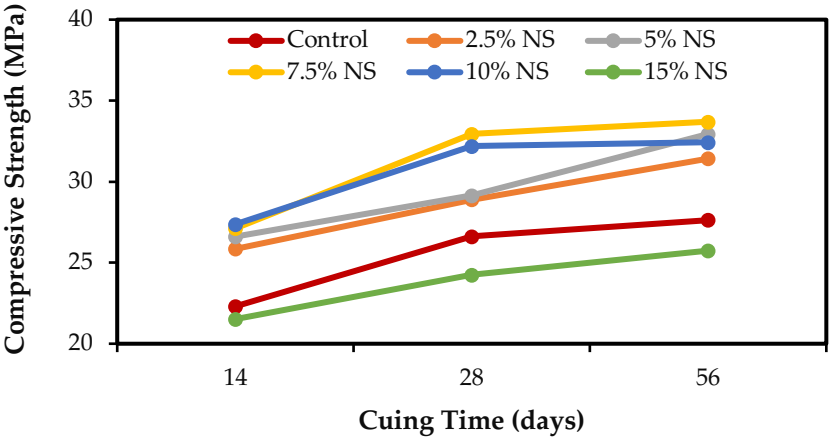

c) Cement replacement with NS

Figure 4.41: Compressive strength of RHA, SP, and NS blended concrete

Because the SP and NS have strong pozzolanic activity and reduced particle size, the compressive strength of concrete increased even at an early age, as shown in Figure 4.41(b) & (c). Concrete specimens with 7.5% SP were found to have a maximum 23.4% improvement in compressive strength when compared to control specimens. An excessive amount of SP results in agglomeration (confirmed by SEM analysis), which weakens the material due to open pores. The findings demonstrated that 7.5% cement may be substituted by SP, while the achieved workability could compact the sample properly. On the other hand, cement could be replaced by NS up to 10% to increase the compressive strength of concrete. Concrete with 7.5% NS had the greatest 56-day strength, 22% more than the control. Using excessive NS (>10%) reduces the workability, so to guarantee that specimens do not experience excessive self-desiccation and breaking, it is necessary to modify the water dosage in the mixture while utilizing a larger concentration of NS. As a result, with a constant w/b ratio, instead of strengthening composites, beyond 10% NS replacement reduced the strength due to agglomeration.

4.4.4 Water Absorption

Water absorption is one of the primary durability properties and increases the possibility of alkali aggregate reactions. Figure 4.42 shows the water absorption of RHA, SP, and NS blended concrete. Concrete with RHA reduces water absorption, a crucial factor for long-term durability. The addition of RHA to the composites was shown to have the potential to significantly refine the pores in the interface layer and matrix, which reduces water permeability. The radial expansion of Portland cement hydration products in pozzolanic particles would have a pore-modifying impact, consequently diminishing the interconnectivity among pores (Cook et al., 1989). Because of the decreased porosity at higher RHA concrete, the water absorption of concrete decreased as the RHA content increased. Water absorption in concretes with 2.5%–15% RHA dropped to 32.8%–46.8% compared to the control concrete.

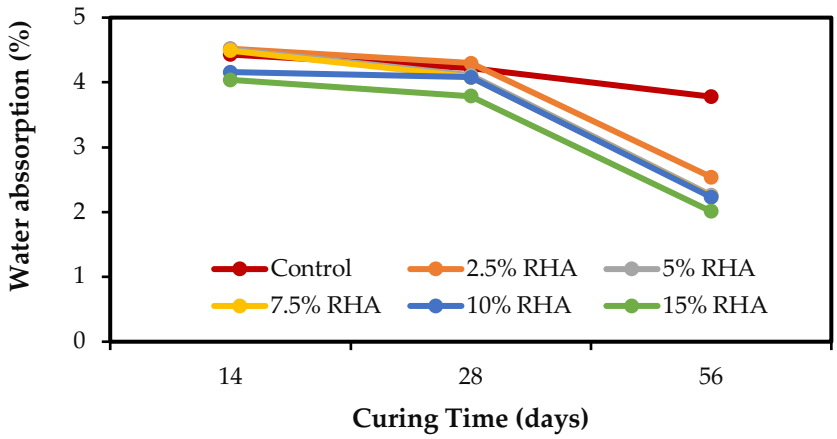

a) Cement replacement by RHA

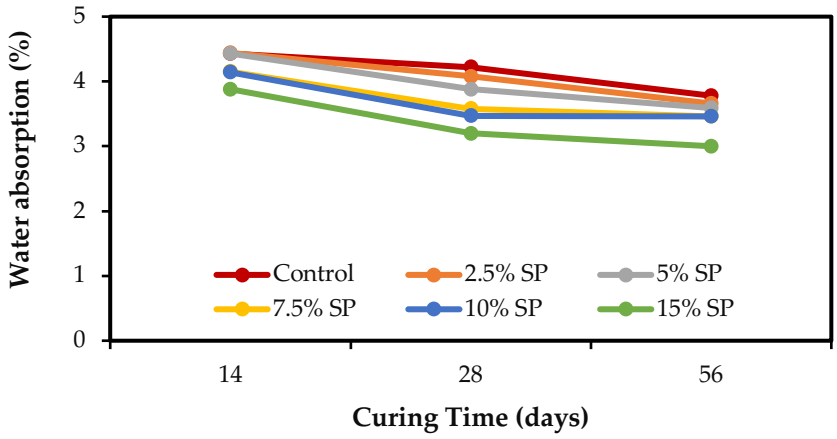

b) Cement replacement by SP

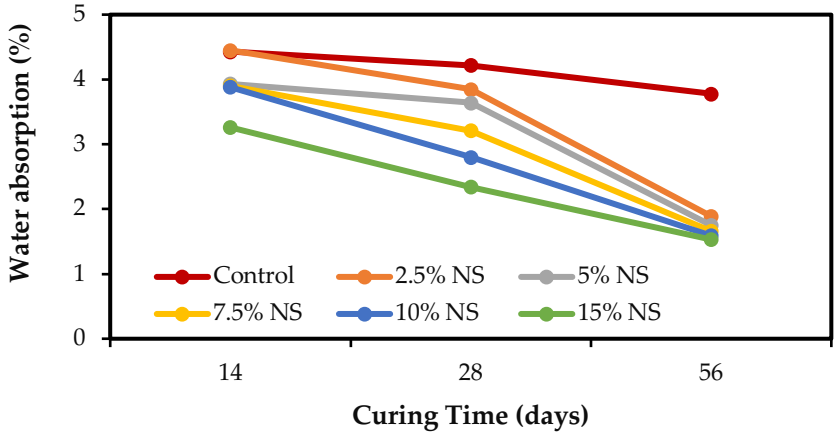

c) Cement replacement by NS

Figure 4.42: Water absorption of RHA, SP, and NS blended concrete

Figure 4.42(b) and (c) show that adding SP or NS in concrete decreased water absorption, which suggests fewer capillary holes and improved resistance to permeability. Water absorption in concretes with 2.5%–15% SP dropped to 3.2%–20.7% and with 2.5%-15% NS dropped to 50%-59.5%, as compared to the control concrete. By filling up the pores, NS could reduce the porosity and permeability of concrete (Mahdikhani et al., 2018). Additionally, the age of RHA, SP, and NS concrete affects how much water it absorbs. The findings also show that water absorption declined with age. Gel progressively fills up the initial water-filled gaps, which causes the water absorption to decrease with age.

4.4.5 Density

Concrete density plays a significant role in estimating lattice constants for the C-S-H phase in hydrated Portland cement, determining porosity, and evaluating strength and durability (Shatat, 2016). Figure 4.43 shows the bulk density of RHA, SP, and NS blended concrete. The density of concrete increased with RHA/SP/NS content in place of CEM I because of their strong pozzolanicity, filler effect, and pore refinement. The fineness, amorphous silica content, and replacement level of RHA/SP/NS affect the density of the concrete. Calcium hydroxide [$Ca(OH)_2$] and calcium silicate hydrates [C–S–H] were the key hydration and reaction products for the RHA/SP/NS paste. The reaction caused the paste containing pozzolana to have a lower $Ca(OH)_2$ content than the control Portland cement paste. The incorporation of RHA/SP/NS in concrete reduced its porosity.

In Figure 4.43(a), it has been shown that the density of RHA blended concrete increased. RHA decreases the porosity and width of the interfacial zone in a manner that increases density (Hadipramana et al., 2013). The pore structure of concrete became finer due to the increasing content and fineness of RHA, which decreased the volume of large pores and the overall porosity of concrete, as reported by van Nguyen (2011).

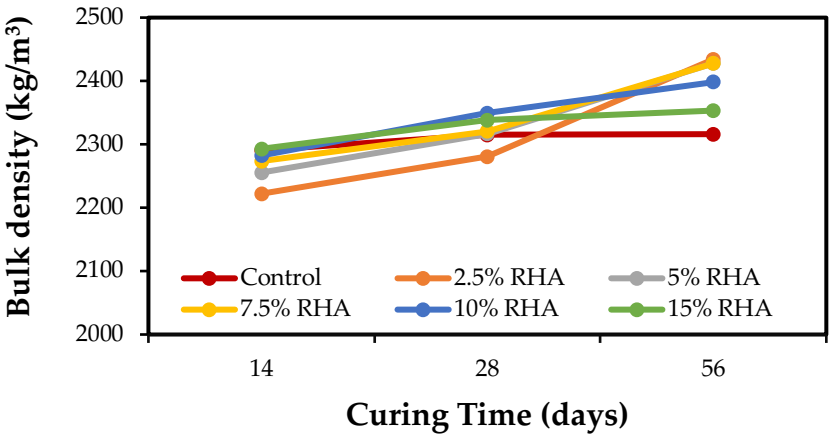

a) Cement replacement with RHA

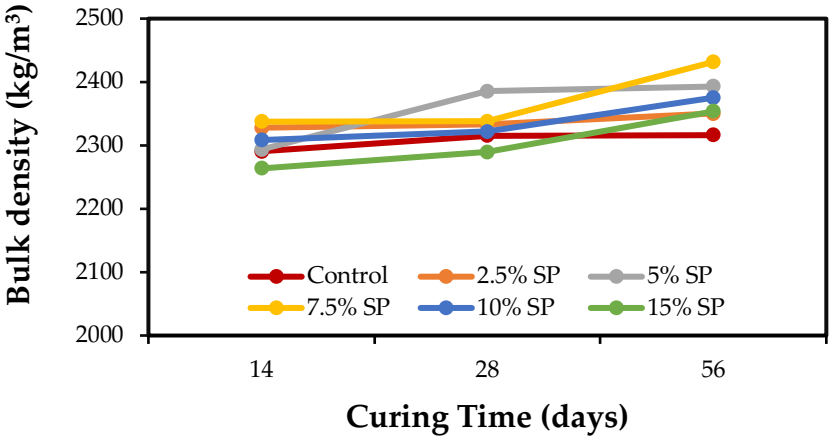

b) Cement replacement with SP

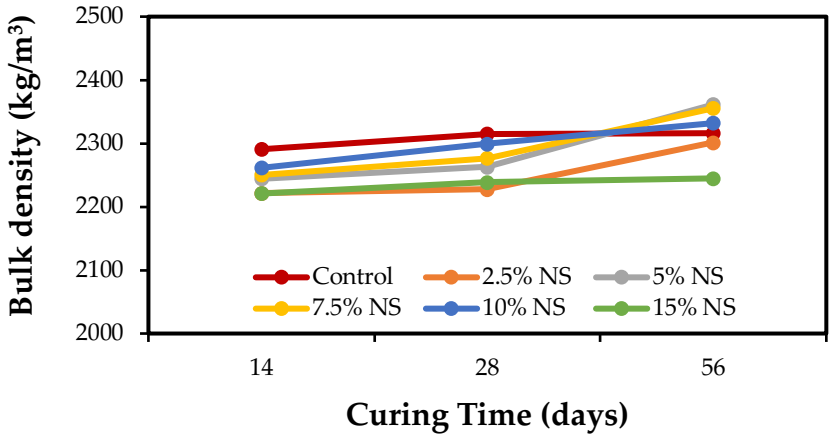

c) Cement replacement with NS

Figure 4.43: Bulk density of RHA, SP, and NS blended concrete

According to Adenuga (2010) and Yuzer (2013) reported, the density of RHA concrete was within the normal weight range, or between 2200 and 2550 kg/m^3, as recommended by the ACI Committee and Falade (2011). This study found the density of RHA blended concrete in the same range. The bulk densities of the concrete mixtures, including SP (for all replacement) or NS (5-10% replacement), were higher than those of the control mixture. The concrete combination with 7.5% SP and 5% NS has a remarkable maximum bulk density of 2430 and 2360 kg/m^{3,} respectively. Cavity filling, catalytic stimulation of hydration product formation, and faster pozzolanic processes are some of the connected mechanisms contributing to the observed increase in bulk density in concrete mixtures containing SP or NS.

Figure 4.43(c) shows that the bulk density value rises with the NS percentage until it reaches 10%, after that, it falls to 15%. Kondo (1968) gave the following interpretation of this- It is possible to calculate the distance between NS particles if they are evenly distributed throughout the cement paste and each one is encased in a cube pattern. The hydration products diffuse and cover the NS particles according to Legrand & Wirquin (1994) once the hydration process starts. By limiting the formation of $Ca(OH)_2$ crystals, the crystallization will be controlled to be in a proper state if the NS content and the distance between them are suitable. Additionally, the high activity of the NS found in cement paste, according to Legrand & Wirquin (1994) can further encourage cement hydration. This results in a more uniform and compact cement matrix and smaller $Ca(OH)_2$ crystals. This leads to an improvement in the pore structure. Additionally, using nano-silica as a catalyst in cementitious processes plays a critical role in driving the development of hydration products and enabling their production, ultimately leading to increased bulk density (Heikal et al., 2013).

Figure 4.44 shows the apparent density of RHA, SP, and NS blended concrete. The apparent density of RHA blended concrete slightly increased compared to the control mix. The 2.5% RHA replacement showed a higher apparent density of 2500 kg/m^3.

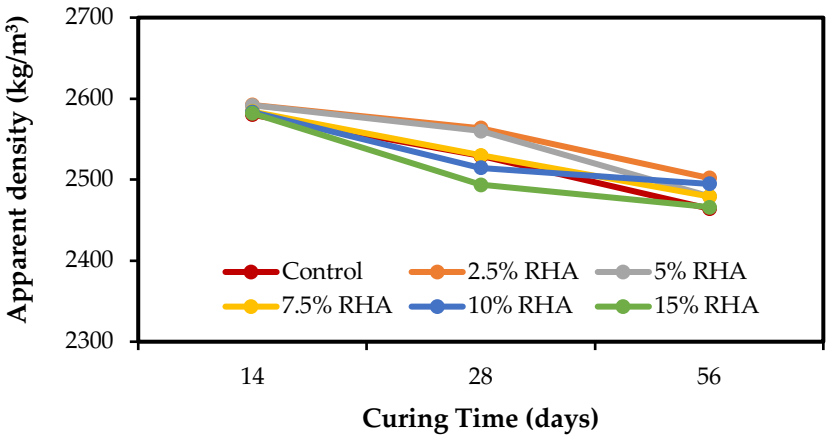

a) Cement replacement with RHA

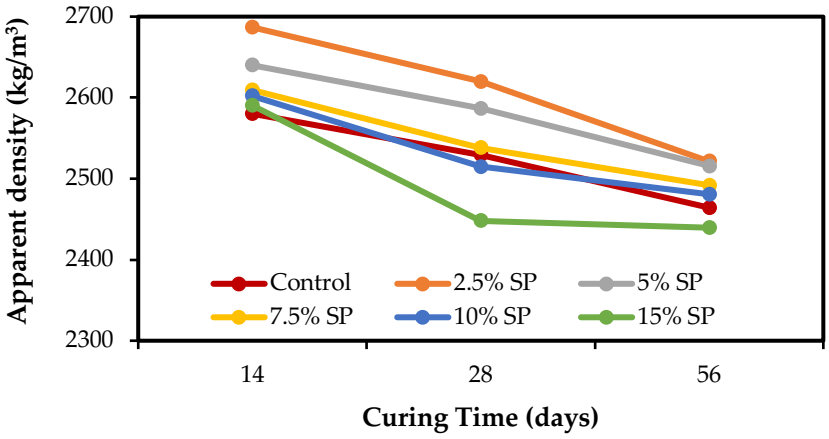

b) Cement replacement with SP

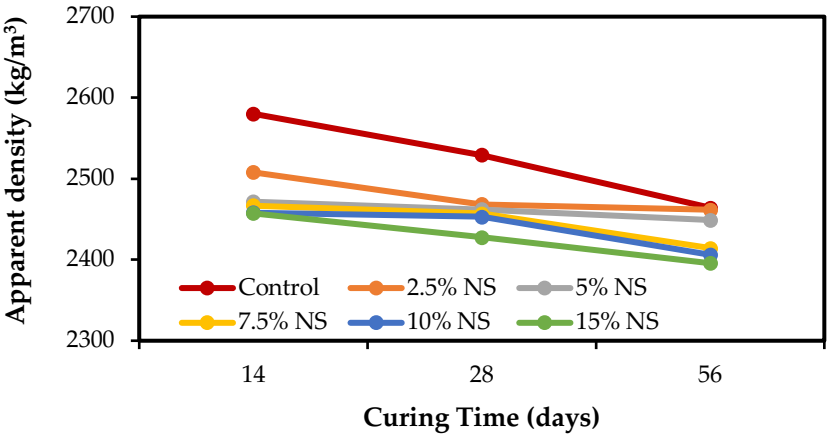

c) Cement replacement with NS

Figure 4.44: Apparent density of RHA, SP, and NS blended concrete

According to the literature, RHA serves as a filler in the early stages because it must wait for $Ca(OH)_2$ to be formed during the early stages of cement hydration before the pozzolanic reaction can start (Bapat, 2012). This is supported by the observation that densities decreased with curing age. Conversely, SP blended concrete showed higher apparent density than the control. Maximum apparent density was found by 2.5% SP replacement, which was 2520 kg/m^3.

However, with NS replacement, the apparent density decreased with the increased pozzolana percentage. Nano silica has a lower inherent density and much finer particles than cement. The total density of solid particles decreases when they replace cement. To produce the strength-giving calcium silicate hydrate (C-S-H), which is less dense than the cement components from which it is created, $Ca(OH)_2$ were consumed during secondary hydration (Bapat, 2012; Page & Page, 2007; Shetty & Jain, 2019). This is the reason for the gradual decrease in density. In addition, higher agglomeration with NS could be another reason for lower density.

4.4.6 Volume of Permeable Pores

Figure 4.45 shows the volume of permeable pores of RHA, SP, and NS blended concretes. Porosity was higher at the early age. With the increasing curing age, the porosity decreased compared to the control sample. Minimum porosity was observed for 7.5% for all types of replacements of pozzolans. RHA, SP, and NS showed 2.1%, 2.4%, and 2.4% volume of permeable pores, respectively.

At 15% replacement, the volume of permeable pores slightly increased for NS. This may have happened due to the decreased workability with increasing replacement of cement by NS. In general, the compressive strength was observed to decrease as porosity increased. After 56 days of curing, 7.5% RHA had a maximum strength of 30 MPa with a minimum porosity of 2.1%. Strength increased by 14.7% and porosity decreased by 65.3% when 7.5% RHA was substituted for cement.

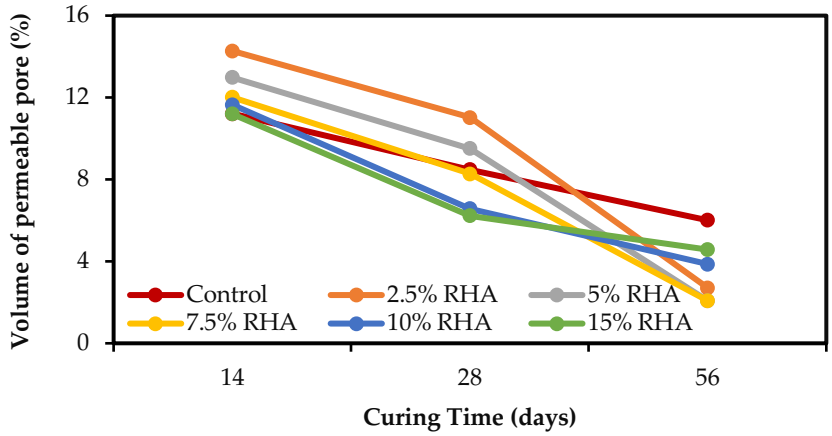

a) Cement replacement with RHA

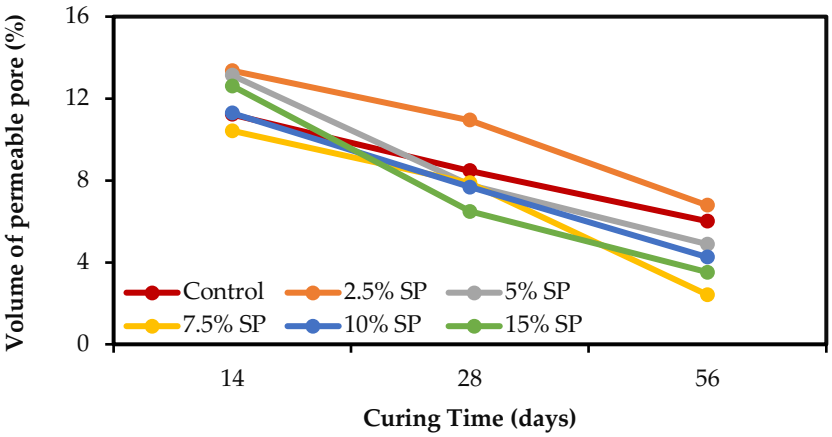

b) Cement replacement with SP

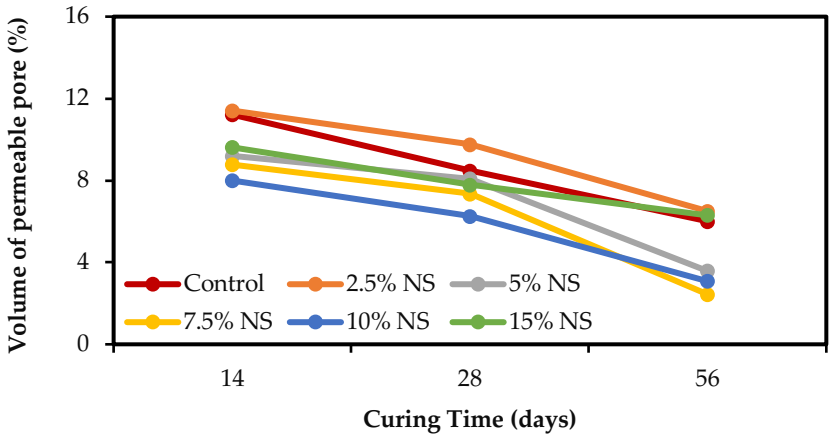

c) Cement replacement with NS

Figure 4.45: Volume of permeable pores of RHA, SP, and NS blended concrete

7.5% SP enhanced strength by 23.4% with 35 MPa and decreased porosity by 59.8% during the same curing days. Additionally, by reducing porosity by 59.4%, 7.5% NS enhanced strength by 22%. Because pozzolanic processes influence compressive strength and porosity in quite different ways, it is crucial to regulate them separately. Further extensive study with concrete may be necessary to conclude this relationship. Superplasticizer may require making SP or NS blended concrete workable.

4.4.7 Ultrasonic Pulse Velocity (UPV)

In general, high pulse velocity readings in concrete indicate high-quality concrete. According to Malhotra (1976), better durability is expected for concrete with a pulse velocity range between 3660 - 4575 m/s. Figure 4.46 shows that the RHA/SP/NS blended concrete has better quality than the control mix. The pulse travels through voids at a significantly slower pace than it does through solid matter, which extends its travel time and lowers the computed velocity. Greater pulse velocity propagation through the concrete will result from a smaller volume of capillary pores.

For RHA, up to 15% replacement showed better velocity than the control mix. Maximum pulse velocity of 4.5 km/s was observed for 7.5% RHA. That means that with 7.5% RHA, concrete gets denser than control, as a result, the volume of permeable pores was minimum (2.1%) in this replacement after 56 days of curing. Besides, for SP/NS up to 10% replacement showed better velocity than the control. Beyond that limit, the pulse velocity slightly dropped compared to the control mix. This is explained by the fact that for mixes containing SP/NS, the amount of water needed to achieve the same workability increased as the SP/NS level increased. As a result, as hydration progressed, more capillaries would remain in the SP/NS blended concrete. The most significant element influencing the velocity of ultrasonic pulse transmission in concrete has been identified as the existence of voids (Neville, 2011). In addition, the low workability for 15%SP and NS replacement may negatively influence the reduction of pore volume.

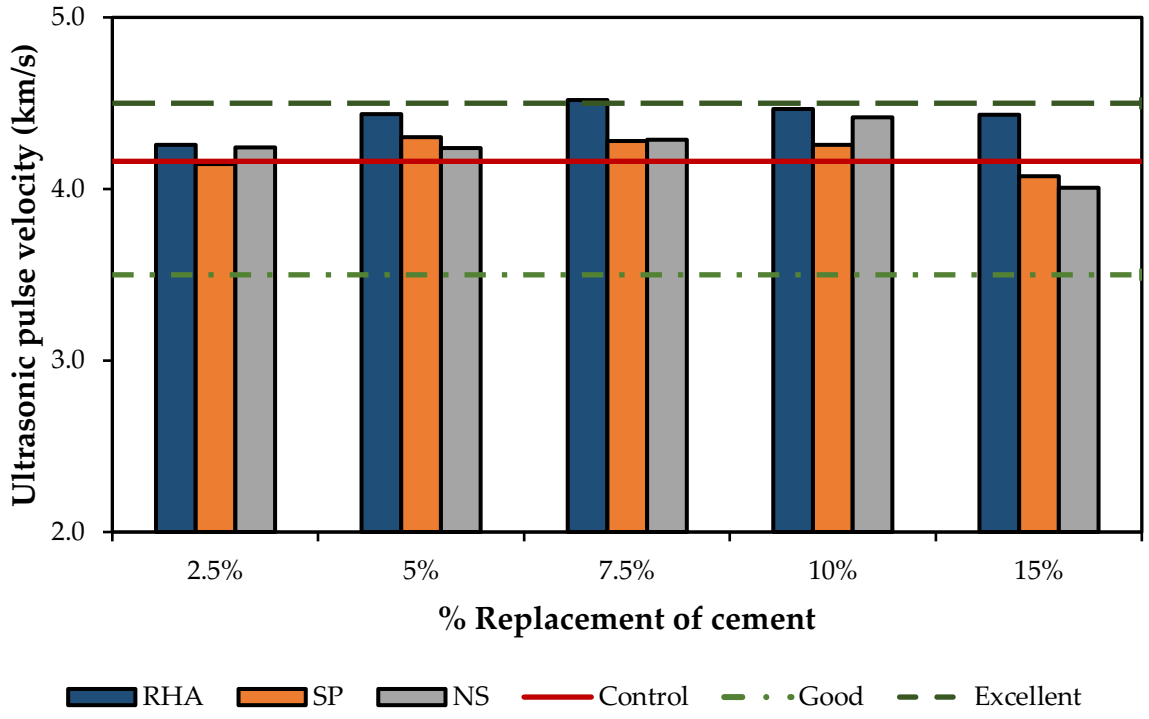

Figure 4.46: Ultrasonic pulse velocity of RHA, SP, and NS blended concrete

4.4.8 Rapid Chloride Penetration Test (RCPT)

Figure 4.47 shows that, in comparison to the control mixture, RHA/SP/NS-based concrete exhibits remarkable resistance to chloride penetration. Up to 15% replacement, the total coulomb charge flowing through RHA-blended concrete specimens steadily decreased. This is because the average pore size has reduced, and the interfacial zone has improved (Chindaprasirt et al., 2007). RHA and hydration products can limit the production of small, inconsistent pores, hence increasing the durability of concrete. According to Zahedi (2015), RHA concrete had the highest chloride resistance improvement at a 20% replacement ratio. All the pozzolans showed better resistance to chloride penetration. Because of the strong pozzolanic activity of SP/NS particles, the cement hydrates more quickly and produces more reaction products. Additionally, SiO_2 particles restore the particle packing density, which leads to the pore size refinement in cement paste.

The pozzolanic reaction and the nano-filler effect of nano-silica made the microstructure of the concrete mix more uniform and less porous. Alqamish & Al-Tamimi (2021) demonstrated that adding nano-silica increases durability against chloride penetration. Additionally, the SP/NS in the cement matrix can efficiently block capillaries in the concrete, creating tortuosity and more disjointed transport routes that increase the resistance of the concrete sample to chloride permeability (Du et al., 2014; Zhang et al., 2021).

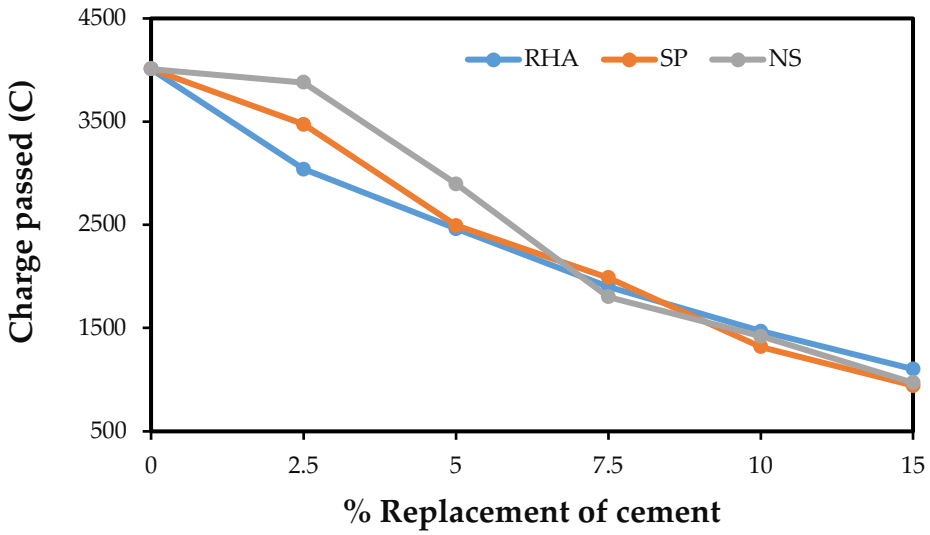

Figure 4.47: Chloride permeability of RHA, SP, and NS blended concrete

When added to the mixture at higher replacement ratios of SP/NS, the particles will adhere together and become unable to disperse uniformly in the cement matrix, as mentioned previously. As a result, the chloride ion permeability will be lower than that of the concrete with the ideal threshold SP/NS. The chloride resistance capability of concrete is therefore increased, and the quantity of free chloride ions in the pore system is decreased when cement is substituted with SP/NS. Removing unbound chloride ions would improve the durability of concrete since they encourage corrosion of steel reinforcement. The use of RHA/SP/NS in concrete implies that the steel embedded in the reinforced concrete is protected, which lowers the possibility of

concrete deterioration due to chloride intrusion, particularly in coastal areas or areas exposed to de-icing salts.

4.4.9 Sorptivity

Figure 4.48 shows the water absorption rate of RHA, SP, and NS blended concrete. The capillary absorption profiles can be classified as either initial (or primary) or secondary absorption depending on the varying rates of water uptake. In the first 24 hours, the micropores of the matrix and small capillary pores absorb water quickly, which is responsible for the primary rate of absorption. In contrast, larger capillary pores and voids in the matrix and interfacial zones (ITZ) cause slower secondary absorption, which starts after day 1 (Yang et al., 2006).

As shown in Figure 4.48(a), as the amount of RHA increased, absorption increased than the control mix. This might be explained by how the smaller voids are arranged when the larger RHA surface area is used (Siddique, 2007). The mix containing 7.5% RHA had a 21.2% increase in sorptivity compared to the estimated sorptivity of the control specimen, as shown in Figure 4.49. While the initial absorption of 7.5% RHA and control is equivalent, the secondary absorption of 7.5% RHA increases dramatically, as shown in Figure 4.48(a). This might be because unburned carbon in the rice husk weakens ITZ and introduces air gaps. The findings of this study comply with Singh & Shukla (2023) findings.

The average concrete water absorption values as a function of SP and NS concentration are shown in Figures 4.48 (b) and (c). With 7.5 and 10% SP, sorptivity was decreased, and only 7.5% NS showed lower sorptivity than the control. The enormous voids were partially filled with SP/NS, and the resulting C-S-H split the large pores into smaller ones. As a result, the concrete absorbed water at a slower pace due to the improved pore structure and decreased capillary pore connectivity. The microstructures in the ITZ were thinner and more uniform. As a result, the water

transport channel was either refined or partially stopped. Minimum absorption was observed with 10% SP and 7.5% NS. With the addition of 10% SP, sorptivity was reduced by 34.4%, and 7.5% NS reduced sorptivity by 36.9%, as shown in Figure 4.49.

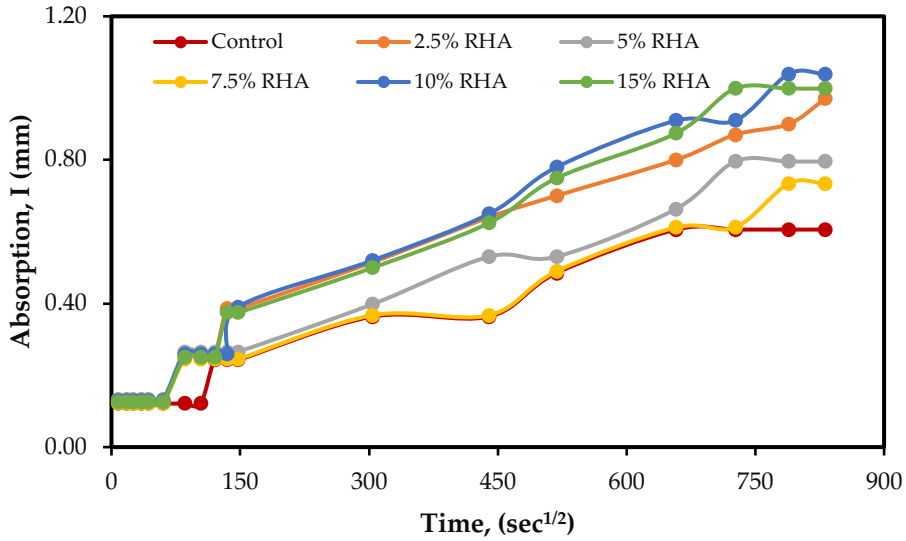

a) Cement replacement with RHA

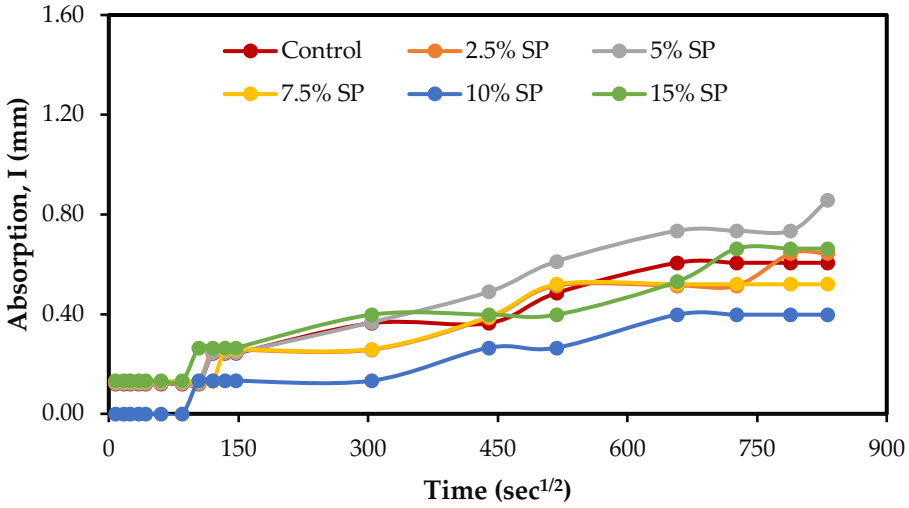

b) Cement replacement with SP

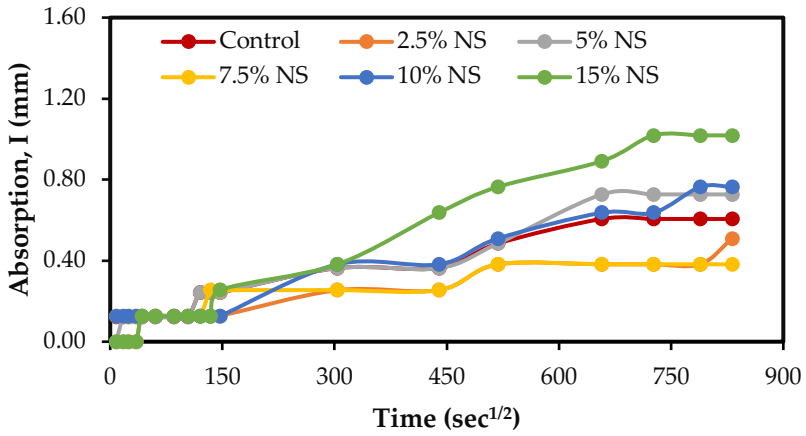

c) Cement replacement with NS

Figure 4.48: Water absorption rate of RHA, SP, and NS blended concrete

Replacement of cement with SP/NS also reduced the initial absorption. The observed decrease in absorption is consistent with Du (2014) and Najigivi (2012) research. Though the water absorption rate was slightly higher with RHA, the sorptivity of RHA blended concrete falls in an excellent durability class, as the values are < 6 mm/√h according to Table 3.12. As well as SP or NS blended concrete, it was also in an excellent durability class.

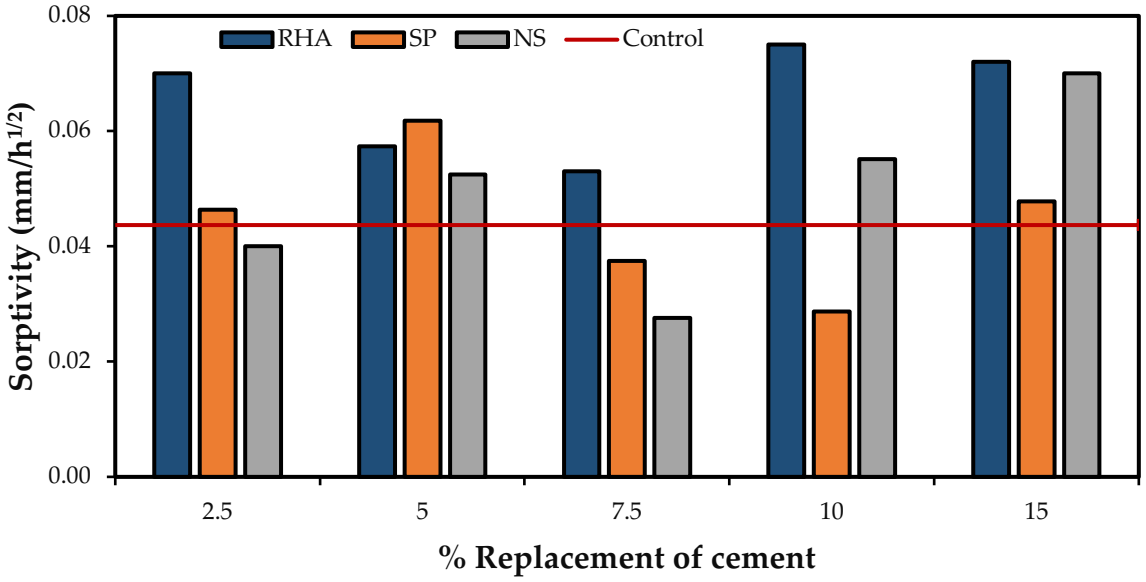

Figure 4.49: Sorptivity of RHA, SP, and NS blended concrete

4.4.10 Surface Electrical Resistivity

The electrical resistivity of all mixes appears to increase, according to data shown in Figure 4.50. The refined microstructure created by the silica-rich RHA interacting with the Portlandite produced by cement hydration may be the cause of the better electrical resistivity performance of RHA-based concrete mixes. The ideal level of electrical resistivity is achieved when 15% of cement is substituted with RHA. When 15% of mixes are aged for 56 days, their electrical resistivity increases by 22.6 kΩ-cm, which is an indication of low chloride ion permeability according to Table 3.12. On the other hand, SP and NS blended concrete showed more electrical resistance than RHA blended concrete. The 15% SP and NS blend showed surface electrical resistivity of 26.3 and 23.1 kΩ-cm, respectively. The surface electrical resistivity of concrete significantly increases because of efficient ion transport blocking, pore refinement, and permeability reduction by SP/NS.

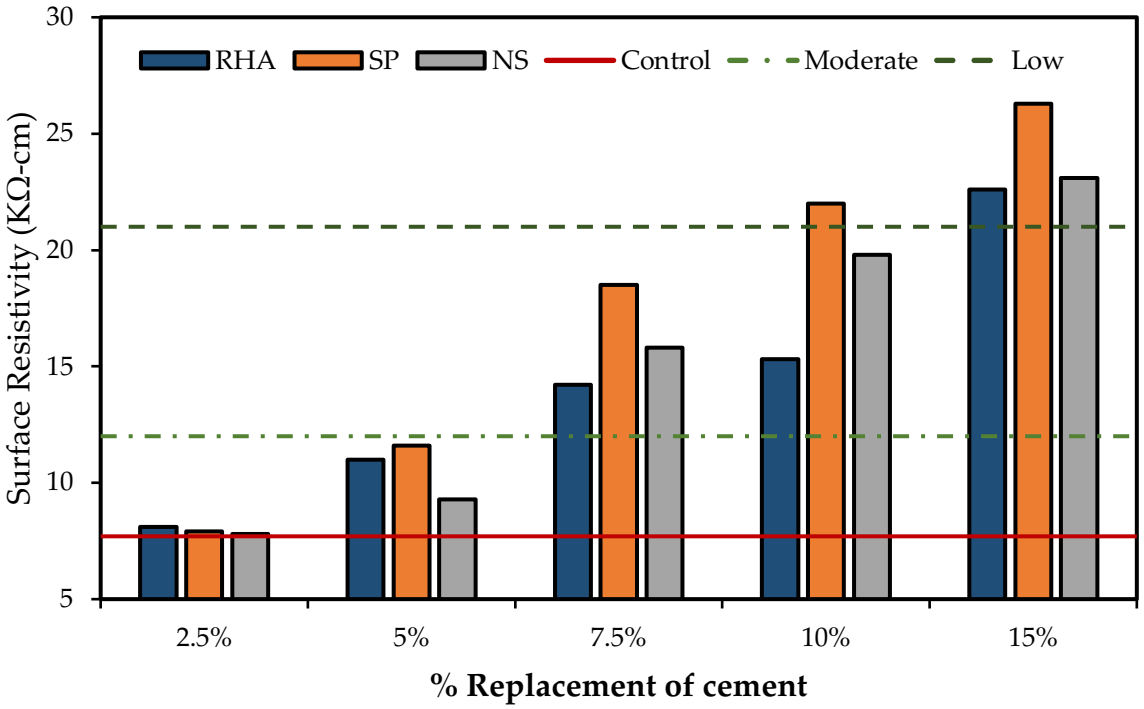

Figure 4.50: Surface electrical resistivity of RHA, SP, and NS blended concrete

4.5 CHAPTER SUMMARY

When RHA/SP/NS replaced cement due to the pozzolanic activity of these binders, secondary C-S-H gel was produced. Because of this secondary C-S-H, strength improvement was seen in RHA/SP/NS blended mortar or concrete. Cement could be replaced up to 5% with RHA/ 15% with SP/ 5% with NS in mortar samples with a constant w/b ratio. While 2.5% RHA increased compressive strength maximum (6.9%) after 90 days of curing, along with an increase in density increased 2.2%. Though RHA increased water absorption at a constant w/b ratio, the increment with 2.5% RHA was negligible (1.2%). As a result, porosity and expansion under sulfate attack were slightly increased, amounting to 3.3% and 4.1%, respectively. On the other hand, 2.5% RHA showed minimum shrinkage, which was 6.5% lower than the control.

In the case of SP/NS, early strength development was observed because of high pozzolanic activity. Strength development continued up to 90 days of curing, but with NS, later strength development was not significant due to higher agglomeration. With 10% SP, the strength increased by 41.4% after 7 days of curing, and by 9.7% after 90 days of curing. Besides, with 5% NS strength, the increment increased by 24.5% after 7 days of curing, but it dropped after 90 days of curing to only 1.4% increment over the control. When cement was replaced with SP/NS in mortar, better durability was observed than in RHA blended mortar. For concrete samples, a 7.5% replacement was possible to improve strength and durability at a constant w/b ratio, as HRWRA was used to maintain workability. Strength was improved 14.7%, 23.4%, and 22% with RHA, SP, and NS, respectively. In comparison to RHA, extracted SP and NS showed better strength and durability in mortar and concrete samples. Besides, due to early hydration behaviour, SP/NS could be used in that type of structure where early strength is necessary.

Chapter 5: CONCLUSIONS

This chapter summarizes the contents described in the introduction, methodology, results and discussions section without repetition. This contains the summary of the research work and key findings and conclusions.

5. 1 GENERAL

The primary goal of this research was to evaluate the viability of using RHA, SP, and NS as partial substitution of cement in mortar and concrete. The objective was to determine how RHA, SP, and NS enhanced mortar and concrete properties while lowering cement usage. Initially, the study focused on various materials characteristics of RHA, SP, and NS, including their physical, chemical, and morphological properties. PSD, XRF, and XRD were used to examine physical and chemical characteristics, and SEM analysis was done to investigate the morphology and hydration of RHA, SP, and NS blended paste. Normal consistency, setting time, and soundness test on paste samples revealed the effect of RHA, SP, and NS. In addition, the study used the flexural and compressive strength test, flow table test, water absorption test, drying shrinkage test, and sulfate resistance test to evaluate the microstructural characteristics of mortar. Workability, compressive strength, UPV, RCPT, water absorption, sorptivity, and surface electrical resistivity tests were done to assess fresh, hardened, and durability characteristics of concrete. With all these investigations, insights into the potential benefits of incorporating RHA, SP, and NS into mortar and concrete were made. By reducing the use of cement and utilizing industrial by-products, such as RHA, SP, and NS, the research contributes to environmental sustainability by minimizing pollution and promoting a more sustainable future for the construction industry.

5. 2 KEY FINDINGS

- **Material properties**

The physical and chemical characteristics of RHA, SP, and NS were carefully examined using XRF, XRD, and PSD. The results show that RHA, SP, and NS have a high silica concentration that was 79.4%, 79.3% and 92.6% respectively and a general amorphous structure, whereas SP has some crystalline components. In addition to its amorphous component, the specific surface area and particle fineness of RHA can be enhanced through controlled combustion and grinding. RHA comprised larger particles, whereas SP and NS had predominantly small particles with significant pozzolanic activity. RHA, SP, and NS pore size distribution is its primary physical characteristic that affects its pozzolanic reactivity, water requirement, and specific surface area (SSA). RHA particle microstructures are found to be irregularly shaped, with surface porosity. Agglomeration was seen for SP and NS in the SEM analysis. SP and NS have a high surface area and energy, which causes them to agglomerate and distribute unevenly in the cement matrix. SP/NS agglomeration and uneven dispersion may limit the number of sites available for the heterogeneous nucleation of hydration products.

- **Paste properties**

The study revealed that the addition of RHA, SP, and NS influenced the consistency and setting time of fresh cement paste. Increased water demand was noted for the proper workability of fresh cement paste with the addition of RHA, SP, and NS. Normal consistency increased 11.1 to 51.9% for RHA, 11.1% to 55.6% for SP, and 3.7% to 33.3% for NS. When cement was replaced by RHA beyond 2.5%, water demand exceeded the code limitation (115%), and with 15% RHA, water demand was 117.8%. With SP beyond 10% replacement water demand exceeded the code limitation, and with 15% SP, it was 116.7%. On the other hand, with NS replacement up to 15% the water demand was less than the limitation, and with 15% NS, it was 114.2%. Moreover, RHA and SP increased setting time, particularly with higher levels of RHA

and SP. Final setting time increased 12.2% to 73.3% for RHA and 13.3% to 27.2% for SP. However, NS reduced the setting time with higher replacement levels. Final setting time was decreased by 2.8% to 11.1% for NS by 2.5% to 15% replacement. SEM analysis showed more C-S-H with RHA, SP, and NS than the control. Due to secondary C-S-H production, the Ca/Si ratio decreased, as observed in EDX analysis.

- **Mortar properties**

The study shows that mortars containing RHA, SP, and NS gave better strength and durability than the control sample. Agglomeration was observed with a higher level of SP and NS. Flow was reduced with RHA, SP, and NS inclusion because of decreased particle size; flow decreased rapidly. Flow was reduced 5.5% to 23.1% for RHA, 7.5% to 28.0% for SP, and 22.5% to 29.8% for NS. Although SP and NS have a large surface area, due to agglomeration, they exhibit lower water demand compared to RHA.

It was found that mortar with RHA, SP, and NS improves flexural and compressive strength. The optimum RHA, SP, and NS replacement to improve flexural strength was 7.5%, and the strength improvement was 7.9%, 12.5%, and 7.7% respectively. This study suggests replacing cement with a maximum of 2.5% RHA, 10% SP, and 5% NS to improve compressive strength with a constant water-to-binder ratio. With 2.5% RHA, 10% SP, and 5% NS, the strength improved 5.9%, 9.7%, and 1.4% after 90 days of curing. With varying water-to-binder ratios, flexural strength slightly decreased with RHA, SP, and NS blended mortar, but compressive strength increased significantly. With 7.5% SP at varying w/b ratios, strength increased 14.4% and with 2.5% NS, the strength increased 15.8% after 90 days of curing. It was also observed that RHA and SP blended mortar achieved better strength at longer curing ages, while NS blended mortar achieved strength at an early age at a constant w/b ratio. A 5% NS strength improvement was observed after 7 days of curing, increasing to 24.5%. However, this improvement dropped to 1.4% after 90 days of curing. The rapid rise in early-day strength indicates the value of NS-modified concrete for building projects that require rapid strength development.

The RHA blended mortar absorbed more water than the control mortar at a constant w/b ratio. Water absorption increased 1.2% to 17.8% when cement was replaced with RHA from 2.5% to 15%. However, water absorption was reduced with SP and NS blended mortar in comparison to the control. With SP/ NS, water absorption decreased 17.6% to 7.9% and 13.7% to 9.0% respectively. It was found that mortars with RHA beyond 5% replacement had a higher drying shrinkage value than the control; however, with SP and NS, it was less than that of the control. 2.5% RHA showed 6.5% less shrinkage than the control. 13.1% less shrinkage value was observed with 10% SP. When cement was replaced with NS, up to 15% showed less value than the control, and lower shrinkage was found with 5% NS, which was 58.9% less than the control. NS showed better sulfate resistance than SP and RHA. With 5% NS expansion, the result was 12.7% less than the control. RHA/SP blended mortar shows slightly higher expansion than the control sample under sulfate attack. Expansion increased slightly under sulfate attack, 2.3% to 15% with SP in comparison to the control, whereas with RHA, expansion was 4.1% to 60.9%.

- **Concrete properties**

As with mortar, concrete workability decreased with increased amounts of RHA, SP, and NS. Workability decreased 91.7%, 91.7%, and 94.4% with RHA, SP, and NS, respectively, in comparison to the control. The 7.5% replacement showed optimum compressive strength for all pozzolanas in concrete. It was 14.7% strength improvement with RHA, 23.4% with SP, and 22.0% with NS. The durability of concrete, including water absorption, chloride penetration, and surface resistivity, decreased and increased upon incorporating RHA, SP, and NS into the concrete. Water absorption decreased 32.8% to 46.8% for RHA, 3.2% to 20.6% for SP, and 50% to 59.5% for NS. Chloride penetration decreased 24.2% to 72.5% for RHA, 13.3% to 76.4% for SP, and 3.2% to 75.8% for NS after 28 days of curing. Besides, surface resistivity increased 5.2% to 193.5% for RHA, 2.6% to 241.6% for SP, and 1.3% to 200%

for NS after 56 days of curing. RHA shows a higher rate of water absorption than SP/NS blended concrete, but the water absorption rate remains within the limit.

In case of mortar and concrete samples, the w/b ratio was kept constant at 0.5 and 0.45, respectively. But to maintain workability, high-range water reducing admixture (HRWRA) was used in concrete. When RHA replaced cement, the workability decreased with increasing replacement because of the high water demand of RHA. As a result, beyond 2.5% replacement with RHA strength, there was no improvement in mortar. On the other hand, by maintaining proper workability in concrete up to 7.5% replacement, higher strength was shown. On the other hand, in mortar, the w/b ratio was slightly higher than the concrete; as a result, up to 10% replacement was possible with SP in mortar. However, due to high water demand and agglomeration, despite using HRWRA, workability decreased with SP, and up to 7.5% replacement was possible.

In the case of NS, water demand was lower in comparison to RHA and SP because of higher agglomeration. For this instance, 5% replacement with NS showed high strength in mortar, but with proper dispersion and less agglomeration due to better workability, 7.5% replacement showed higher strength in concrete. The study concludes that the RHA, SP, and NS can be promising SCM options for cementitious media. It would enable a large amount of cement to be substituted, creating green concrete, which would ultimately help the building sector achieve a circular economy, ease climate change, and accomplish the Sustainable Development Goal (SDG13).

5. 3 LIMITATION OF THE STUDY

In SEM analysis, it was clear that with higher levels of replacement by SP/NS, agglomeration happened. Inadequate dispersion is one of the reasons for exacerbating SP/NS agglomeration. In this study, no dispersion method was applied to reduce agglomeration. Besides, workability was reduced by incorporating SP/NS in

cementitious media. No superplasticizer was used to maintain the workability in this study.

5. 4 RECOMMENDATION FOR FUTURE STUDY

In this study, it was found that with increasing w/b ratio and cement replacement with SP/NS, strength was also increased. The mechanisms behind it could be the future scope of the study. One significant issue that needs careful investigation is the dispersion of SP/NS into the cementitious media. The effect of chemical and physical means of dispersion could be the field of future study.

Bibliography

A. M. Neville, J. J. B. (2010). *Concrete Technology*.

A'yuni, D. Q., Subagio, A., Hadiyanto, H., Kumoro, A. C., & Djaeni, M. (2021). Microstructure silica leached by naoh from semi-burned rice husk ash for moisture adsorbent. *Archives of Materials Science and Engineering*, *108*(1), 5–15. https://doi.org/10.5604/01.3001.0015.0248

AASHTO T358. (2015). *Standard Method of Test for Surface Resistivity Indication of Concrete's Ability to Resist Chloride Ion Penetration*.

Abbas, S., Kazmi, S. M. S., & Munir, M. J. (2017). Potential of rice husk ash for mitigating the alkali-silica reaction in mortar bars incorporating reactive aggregates. *Construction and Building Materials*, *132*, 61–70.

Abhilash, P. P., Nayak, D. K., Sangoju, B., Kumar, R., & Kumar, V. (2021). Effect of nano-silica in concrete; a review. *Construction and Building Materials*, *278*, 122347.

ABrAMS, D. A. (1919). *Design of concrete mixtures* (Vol. 1). Structural Materials Research Laboratory, Lewis Institute.

Abu Bakar, B. H., Ramadhansyah, P. J., & Megat Azmi, M. J. (2011). Effect of rice husk ash fineness on the chemical and physical properties of concrete. *Magazine of Concrete Research*, *63*(5), 313–320.

ACI PRC-211.1. (2022). *Selecting Proportions for Normal-Density and High Density-Concrete - Guide*.

Adam, F., Ahmed, A. E., & Min, S. L. (2008). Silver modified porous silica from rice husk and its catalytic potential. *Journal of Porous Materials*, *15*, 433–444.

Adenuga, O. A., Soyingbe, A. A., & Ogunsanmi, O. E. (2010). *The use of rice husk ash as partial replacement for cement in concrete*.

Aggarwal, P., Singh, R. P., & Aggarwal, Y. (2015). Use of nano-silica in cement based materials—A review. *Cogent Engineering*, *2*(1). https://doi.org/10.1080/23311916.2015.1078018

Ahmad Alyosef, H., Schneider, D., Wassersleben, S., Roggendorf, H., Weiß, M., Eilert, A., Denecke, R., Hartmann, I., & Enke, D. (2015). Meso/macroporous silica from miscanthus, cereal remnant pellets, and wheat straw. *ACS Sustainable Chemistry & Engineering*, *3*(9), 2012–2021.

Ahmad, M. M., Ahmad, F., Azmi, M., & Mohd Zahid, M. Z. A. (2015). Properties of Cement Mortar Consisting Raw Rice Husk. *Applied Mechanics and Materials*, *802*(November), 267–271. https://doi.org/10.4028/www.scientific.net/amm.802.267

Ajeel, S. A., Sukkar, K. A., & Zedin, N. K. (2020). Extraction of high purity amorphous silica from rice husk by chemical process. *IOP Conference Series: Materials Science and Engineering*, *881*(1). https://doi.org/10.1088/1757-899X/881/1/012096

Al-Khalaf, M. N., & Yousif, H. A. (1984). Use of rice husk ash in concrete. *International Journal of Cement Composites and Lightweight Concrete*, *6*(4), 241–248.

Alexander, M. G., Mackechnie, J. R., & Ballim, Y. (1999). Guide to the use of durability indexes for achieving durability in concrete structures. *Research Monograph*, *2*, 102.

Alqamish, H. H., & Al-Tamimi, A. K. (2021). Development and evaluation of nano-silica sustainable concrete. *Applied Sciences (Switzerland)*, *11*(7). https://doi.org/10.3390/app11073041

Alvarez, J., Lopez, G., Amutio, M., Bilbao, J., & Olazar, M. (2014). Bio-oil production

from rice husk fast pyrolysis in a conical spouted bed reactor. *Fuel*, *128*, 162–169.

Amiri, A., Øye, G., & Sjöblom, J. (2009). Influence of pH, high salinity and particle concentration on stability and rheological properties of aqueous suspensions of fumed silica. *Colloids and Surfaces A: Physicochemical and Engineering Aspects*, *349*(1–3), 43–54.

Amrutha, N. G., Narasimhan, M. C., & Rajeeva, S. V. (2011). Chloride-ion impermeability of self-compacting high volume of fly ash concrete mixes. *International Journal of Civil & Environmental Engineering IJCEE-IJENS V*, *11*(4), 29–35.

Amutha, K., Ravibaskar, R., & Sivakumar, $ G. (2010). Extraction, Synthesis and Characterization of Nanosilica from Rice Husk Ash. *International Journal of Nanotechnology and Applications*, *4*(1), 61–66. http://www.ripublication.com/ijna.htm

An, D., Guo, Y., Zhu, Y., & Wang, Z. (2010). A green route to preparation of silica powders with rice husk ash and waste gas. *Chemical Engineering Journal*, *162*(2), 509–514.

Andreola, F., Barbieri, L., & Lancellotti, I. (2020). The Environmental Friendly Route to Obtain Sodium Silicate Solution from Rice Husk Ash: A Comparative Study with Commercial Silicates Deflocculating Agents. *Waste and Biomass Valorization*, *11*(11), 6295–6305. https://doi.org/10.1007/s12649-019-00849-w

Antiohos, S. K., Papadakis, V. G., & Tsimas, S. (2014). Rice husk ash (RHA) effectiveness in cement and concrete as a function of reactive silica and fineness. *Cement and Concrete Research*, *61*, 20–27.

Antiohos, S. K., Tapali, J. G., Zervaki, M., Sousa-Coutinho, J., Tsimas, S., & Papadakis, V. G. (2013). Low embodied energy cement containing untreated RHA: A

strength development and durability study. *Construction and Building Materials*, *49*, 455–463.

Aprianti, E., Shafigh, P., Bahri, S., & Farahani, J. N. (2015). Supplementary cementitious materials origin from agricultural wastes–A review. *Construction and Building Materials*, *74*, 176–187.

Asavapisit, S., & Ruengrit, N. (2005). The role of RHA-blended cement in stabilizing metal-containing wastes. *Cement and Concrete Composites*, *27*(7–8), 782–787.

ASTM C1012. (2022). *StandardTest Method for Length Change of Hydraulic-Cement Mortars Exposed to a Sulfate Solution*. 4–6. https://doi.org/10.1520/C1012

ASTM C1157. (2008). *Standard Performance Specification for Hydraulic Cement*.

ASTM C1202. (2012). Standard Test Method for Electrical Indication of Concrete's Ability to Resist Chloride Ion Penetration. *American Society for Testing and Materials.*, *C*, 1–8. https://doi.org/10.1520/C1202-12.2

ASTM C136. (2011). Standard Test Method for Sieve Analysis of Fine and Coarse Aggregates. *Annual Book of ASTM Standards*, *04*(571), 5–9.

ASTM C138. (2017). *Standard Test Method for Density (Unit Weight), Yield, and Air Content (Gravimetric) of Concrete*. *04*, 4–7. https://doi.org/10.1520/C0138

ASTM C143. (2008). Standard Test Method for Slump of Hydraulic-Cement Concrete. *Manual on Hydrocarbon Analysis, 6th Edition*, *i*, 545-545–3. https://doi.org/10.1520/mnl10913m

ASTM C151/C151M. (2018). *Standard Test Method for Autoclave Expansion of Hydraulic Cement*.

ASTM C1585. (2013). *Standard Test Method for Measurement of Rate of Absorption of Water*

by Hydraulic- Cement Concretes. *i*, 13–15. https://doi.org/10.1520/C1585-13.2

ASTM C187. (2016). *Standard Test Method for Amount of Water Required for Normal Consistency of Hydraulic Cement Paste*.

ASTM C188. (2023). *Standard Test Method for Density of Hydraulic Cement*.

ASTM C191. (2021). *Standard Test Methods for Time of Setting of Hydraulic Cement by Vicat Needle*.

ASTM C204. (2012). Standard Test Method for Fineness of Hydraulic Cement by the 150-μm Sieve. *ASTM International*, *100*, 5–7.

ASTM C33/C33M. (2023). *Standard Specification for Concrete Aggregates*.

ASTM C490. (2018). Use of Apparatus for the Determination of Length Change of Hardened Cement Paste, Mortar, and Concrete. *Designation: E 778 – 87 (Reapproved 2004)*, *i*(Reapproved), 3–5. https://doi.org/10.1520/C0490

ASTM C494/C494M. (2024). *Standard Specification for Chemical Admixtures for Concrete*.

ASTM C596. (2023). *Standard Test Method for Drying Shrinkage of Mortar Containing Hydraulic Cement*.

ASTM C597. (2003). Standard Test Method for Pulse Velocity Through Concrete. *United States: American Society for Testing and Material.*, *04*(02), 3–6.

ASTM C618-22. (2023). *Standard Specification for Coal Fly Ash and Raw or Calcined Natural Pozzolan for Use in Concrete*. https://www.astm.org/c0618-22.html

ASTM C642. (2022). *Standard Test Method for Density, Absorption, and Voids in Hardened Concrete*.

ASTM C778. (2021). *Standard Specification for Standard Sand*.

https://doi.org/10.1520/C0778-21

ASTM D2216. (2019). *Standard Test Methods for Laboratory Determination of Water (Moisture) Content of Soil and Rock by Mass*.

Azat, S., Korobeinyk, A. V, Moustakas, K., & Inglezakis, V. J. (2019). Sustainable production of pure silica from rice husk waste in Kazakhstan. *Journal of Cleaner Production*, *217*, 352–359.

Azizi, S. N., & Yousefpour, M. (2008). Spectroscopic Studies of Different Kind of Rice Husk Samples Grown in North of Iran and the Extracted Silica by Using XRD, XRF, IR, AA and NMR Techniques. *Eurasian Journal of Analytical Chemistry*, *3*(3).

Babu, G. R., Ramana, N. V, Kumar, T. N., & Kumar, K. V. (2019). Effect of nanosilica on properties and durability in cement. *Materials Today: Proceedings*, *19*, 599–605.

Bajpai, S., Shreyash, N., Sonker, M., Tiwary, S. K., & Biswas, S. (2021). Investigation of SiO2 nanoparticle retention in flow channels, its remediation using surfactants and relevance of artificial intelligence in the future. *Chemistry*, *3*(4), 1371–1380.

Bakar, R. A., Yahya, R., & Gan, S. N. (2016). Production of high purity amorphous silica from rice husk. *Procedia Chemistry*, *19*, 189–195.

Bakdash, R. S., Aljundi, I. H., Basheer, C., & Abdulazeez, I. (2020). Rice husk derived Aminated Silica for the efficient adsorption of different gases. *Scientific Reports*, *10*(1), 19526.

Balakrishnan, V., Ab Wab, H. A., Abdul Razak, K., & Shamsuddin, S. (2013). In vitro evaluation of cytotoxicity of colloidal amorphous silica nanoparticles designed for drug delivery on human cell lines. *Journal of Nanomaterials*, *2013*(1), 729306.

Bapat, J. D. (2012). *Mineral admixtures in cement and concrete*. CRC press.

Barkakati, P., Bordoloi, D., & Borthakur, P. C. (1994). Paddy husk as raw material and fuel for making Portland cement. *Cement and Concrete Research*, *24*(4), 613–620.

Barman, D., & Dash, S. K. (2022). Stabilization of expansive soils using chemical additives: A review. *Journal of Rock Mechanics and Geotechnical Engineering*, *14*(4), 1319–1342.

Basso, A. M., Nicola, B. P., Bernardo-Gusmao, K., & Pergher, S. B. C. (2020). Tunable effect of the calcination of the silanol groups of KIT-6 and SBA-15 mesoporous materials. *Applied Sciences*, *10*(3), 970.

Bažant, Z. P. (1996). Size effect aspects of measurement of fracture characteristics of quasibrittle material. *Advanced Cement Based Materials*, *4*(3–4), 128–137.

Beidaghy Dizaji, H., Zeng, T., Hartmann, I., Enke, D., Schliermann, T., Lenz, V., & Bidabadi, M. (2019). Generation of high quality biogenic silica by combustion of rice husk and rice straw combined with pre-and post-treatment strategies—A review. *Applied Sciences*, *9*(6), 1083.

Bekem Kara, İ., & Durmuş, Ö. F. (2019). Effect of nano silica on cement mortars containing micro silica. *Challenge Journal of Concrete Research Letters*, *10*(2), 42. https://doi.org/10.20528/cjcrl.2019.02.003

Björnström, J., Martinelli, A., Matic, A., Börjesson, L., & Panas, I. (2004). Accelerating effects of colloidal nano-silica for beneficial calcium–silicate–hydrate formation in cement. *Chemical Physics Letters*, *392*(1–3), 242–248.

Black, L. (2016). Low clinker cement as a sustainable construction material. *Sustainability of Construction Materials*, 415–457.

Bolhassani, M., & Samani, M. (2015). Effect of type, size, and dosage of nanosilica and microsilica on properties of cement paste and mortar. *ACI Materials Journal*,

112(2), 259–266. https://doi.org/10.14359/51686995

Borges, A. L., Soares, S. M., Freitas, T. O. G., Oliveira Júnior, A. de, Ferreira, E. B., & Ferreira, F. G. da S. (2021). Evaluation of the pozzolanic activity of glass powder in three maximum grain sizes. *Materials Research*, *24*, e20200496.

Bryleva, E. Y., Vodolazkaya, N. A., Mchedlov-Petrossyan, N. O., Samokhina, L. V, Matveevskaya, N. A., & Tolmachev, A. V. (2007). Interfacial properties of cetyltrimethylammonium-coated SiO2 nanoparticles in aqueous media as studied by using different indicator dyes. *Journal of Colloid and Interface Science*, *316*(2), 712–722.

BS 1881. (2021). *Testing Concrete - Methods for analysis of hardened concrete*.

BS 3892-1. (1997). *Pulverized-fuel ash - Specification for pulverized-fuel ash for use with Portland cement*.

BS 8615-1. (2019). Specification for pozzolanic materials for use with portland cement Part-1 Natural pozzolana and natural calcined pozzolana. *BSI Standards Publication*, 1–16. https://www.en-standard.eu/bs-8615-1-2019-specification-for-pozzolanic-materials-for-use-with-portland-cement-natural-pozzolana-and-natural-calcined-pozzolana/

BS EN 196-1. (2016). *Methods of testing cement - Determination of strength*.

Bui, D. D. (2001). *Rice husk ash a mineral admixture for high performance concrete*.

Bui, D. D., & Stroeven, P. (1999). Rice husk ash-based binders and their use in high strength concrete in Vietnam. *Infrastructure Regeneration and Rehabilitation Improving the Quality of Life through Better Construction: A Vision for the next Millennium (Sheffield, 28 June-2 July 1999)*, 263–274.

Calica Jr, M. G. (2008). Influence of rice husk ash as supplementary material in cement paste and concrete. *NLR Journal*, *2*, 80–92.

Carmona, V. B., Oliveira, R. M., Silva, W. T. L., Mattoso, L. H. C., & Marconcini, J. M. (2013). Nanosilica from rice husk: extraction and characterization. *Industrial Crops and Products*, *43*, 291–296.

Carpinteri, A. (1994). Scaling laws and renormalization groups for strength and toughness of disordered materials. *International Journal of Solids and Structures*, *31*(3), 291–302.

Chandra, S. (1996). *Waste materials used in concrete manufacturing*. Noyes Publications.

Chandrasekhar, S., Pramada, P. N., & Majeed, J. (2006). Effect of calcination temperature and heating rate on the optical properties and reactivity of rice husk ash. *Journal of Materials Science*, *41*, 7926–7933.

Chandrasekhar, S., Satyanarayana, K. G., Pramada, P. N., Raghavan, P., & Gupta, T. N. (2003). Review processing, properties and applications of reactive silica from rice husk—an overview. *Journal of Materials Science*, *38*, 3159–3168.

Chen, H., Wang, W., Martin, J. C., Oliphant, A. J., Doerr, P. A., Xu, J. F., DeBorn, K. M., Chen, C., & Sun, L. (2013). Extraction of lignocellulose and synthesis of porous silica nanoparticles from rice husks: a comprehensive utilization of rice husk biomass. *ACS Sustainable Chemistry & Engineering*, *1*(2), 254–259.

Chen, P., Bie, H., & Bie, R. (2018). Leaching characteristics and kinetics of the metal impurities present in rice husk during pretreatment for the production of nanosilica particles. *Korean Journal of Chemical Engineering*, *35*, 1911–1918.

Chindaprasirt, P., Chotithanorm, C., Cao, H. T., & Sirivivatnanon, V. (2007). Influence of fly ash fineness on the chloride penetration of concrete. *Construction and*

Building Materials, *21*(2), 356–361.

Chindaprasirt, P., Kanchanda, P., Sathonsaowaphak, A., & Cao, H. T. (2007). Sulfate resistance of blended cements containing fly ash and rice husk ash. *Construction and Building Materials*, *21*(6), 1356–1361.

Chindaprasirt, P., Rukzon, S., & Sirivivatnanon, V. (2008). Resistance to chloride penetration of blended Portland cement mortar containing palm oil fuel ash, rice husk ash and fly ash. *Construction and Building Materials*, *22*(5), 932–938.

Chopra, S. K. (1981). Technology and manufacture of rice-husk ash masonry (RHAM) cement. *Proceedings of ESCAP/RCTT, Workshop on Rice-Husk Ash Cement, 1981*.

Chun, J., Gu, Y. M., Hwang, J., Oh, K. K., & Lee, J. H. (2020). Synthesis of ordered mesoporous silica with various pore structures using high-purity silica extracted from rice husk. *Journal of Industrial and Engineering Chemistry*, *81*, 135–143.

Chun, J., & Lee, J. H. (2020). Recent progress on the development of engineered silica particles derived from rice husk. *Sustainability*, *12*(24), 10683.

Cisse, I. K., Jauberthie, R., Temimi, M., & Camps, J. P. (1999). Rice husk ash: a filler for sand concrete. In *Exploiting Wastes in Concrete* (pp. 309–317). Thomas Telford Publishing.

Colston, S. L., O'connor, D., Barnes, P., Mayes, E. L., Mann, S., Freimuth, H., & Ehrfeld, W. (2000). Functional micro-concrete: The incorporation of zeolites and inorganic nano-particles into cement micro-structures. *Journal of Materials Science Letters*, *19*, 1085–1088.

Committee, A. C. I. (1989). Fly Ash, Slag, Silica Fume, and Natural Pozzolans in Concrete. *Proceedings of the Third International Conference, USA*, 54–72.

Cook, D. J. (1986). Cement replacement material-Rice husk ash. *Concrete Technology and Design*, *3*, 171–195.

Cook, D. J., Hinczak, I., Jedy, M., & Cao, H. T. (1989). Behaviour of Slag Cement Concretes in Marine Environment-Chloride Ion Penetration. *Special Publication*, *114*, 1467–1484.

Cordeiro, G. C., Toledo Filho, R. D., & de Moraes Rego Fairbairn, E. (2009). Use of ultrafine rice husk ash with high-carbon content as pozzolan in high performance concrete. *Materials and Structures*, *42*, 983–992.

Cordon, W. A., & Gillespie, H. A. (1963). Variables in concrete aggregates and Portland cement paste which influence the strength of concrete. *Journal Proceedings*, *60*(8), 1029–1052.

Costa, J. A. S., & Paranhos, C. M. (2018). Systematic evaluation of amorphous silica production from rice husk ashes. *Journal of Cleaner Production*, *192*, 688–697.

Daulay, A., Andriayani, Marpongahtun, & Gea, S. (2021). Extraction silica from rice husk with naoh leaching agent with temperature variation burning rice husk. *Rasayan Journal of Chemistry*, *14*(3), 2125–2128. https://doi.org/10.31788/RJC.2021.1436351

Della, V. P., Kühn, I., & Hotza, D. (2002). Rice husk ash as an alternate source for active silica production. *Materials Letters*, *57*(4), 818–821.

Deshmukh, P., Bhatt, J., Peshwe, D., & Pathak, S. (2012). Determination of silica activity index and XRD, SEM and EDS studies of amorphous SiO 2 extracted from rice Husk Ash. *Transactions of the Indian Institute of Metals*, *65*, 63–70.

Diamond, S., Sahu, S., & Thaulow, N. (2004). Reaction products of densified silica fume agglomerates in concrete. *Cement and Concrete Research*, *34*(9), 1625–1632.

Doran, P. M. (1995). *Bioprocess engineering principles*. Academic Press INC.

Du, H., Du, S., & Liu, X. (2014). Durability performances of concrete with nano-silica. *Construction and Building Materials*, *73*, 705–712.

Du, H. J., & Pang, S. D. (2015). Effect of colloidal nano-silica on the mechanical and durability performances of mortar. *Key Engineering Materials*, *629*, 443–448.

Dwivedi, V. N., Singh, N. P., Das, S. S., & Singh, N. B. (2006). A new pozzolanic material for cement industry: Bamboo leaf ash. *International Journal of Physical Sciences*, *1*(3), 106–111.

El-Dakroury, A., & Gasser, M. S. (2008). Rice husk ash (RHA) as cement admixture for immobilization of liquid radioactive waste at different temperatures. *Journal of Nuclear Materials*, *381*(3), 271–277.

EN 1015-3. (2004). *Determination of consistence of fresh mortar (by flow table)*.

EN 196-2. (2005). *Methods of testing cement - Chemical analysis of cement*.

Esumi, K. (2001). Interactions between surfactants and particles: dispersion, surface modification, and adsolubilization. *Journal of Colloid and Interface Science*, *241*(1), 1–17.

Falade, F., Ikponmwosa, E. E., & Arogundade, A. (2011). *Investigation Of Some Structural Properties Of Foamed Aerated Concrete.*

Farooque, K. N., Zaman, M., Halim, E., Islam, S., Hossain, M., Mollah, Y. A., & Mahmood, A. J. (2009). Characterization and utilization of rice husk ash (RHA) from rice mill of Bangladesh. *Bangladesh Journal of Scientific and Industrial Research*, *44*(2), 157–162.

Feng, Q., Yamamichi, H., Shoya, M., & Sugita, S. (2004). Study on the pozzolanic

properties of rice husk ash by hydrochloric acid pretreatment. *Cement and Concrete Research*, *34*(3), 521–526.

Feret, R. (1896). Essais de divers sables et mortiers hydrauliques. *Ann. Ponts Chauss. Mémoires et Documents*, *7*, 174–197.

Fernandes, I. J., Calheiro, D., Kieling, A. G., Moraes, C. A. M., Rocha, T. L. A. C., Brehm, F. A., & Modolo, R. C. E. (2016). Characterization of rice husk ash produced using different biomass combustion techniques for energy. *Fuel*, *165*, 351–359.

Ganesan, K., Rajagopal, K., & Thangavel, K. (2008). Rice husk ash blended cement: Assessment of optimal level of replacement for strength and permeability properties of concrete. *Construction and Building Materials*, *22*(8), 1675–1683.

Ghorbani, F., Sanati, A. M., & Maleki, M. (2015). Production of silica nanoparticles from rice husk as agricultural waste by environmental friendly technique. *Environmental Studies of Persian Gulf*, *2*(1), 56–65.

Giaccio, G., de Sensale, G. R., & Zerbino, R. (2007). Failure mechanism of normal and high-strength concrete with rice-husk ash. *Cement and Concrete Composites*, *29*(7), 566–574.

Givi, A. N., Rashid, S. A., Aziz, F. N. A., & Salleh, M. A. M. (2010a). Contribution of rice husk ash to the properties of mortar and concrete: a review. *Journal of American Science*, *6*(3), 157–165.

Givi, A. N., Rashid, S. A., Aziz, F. N. A., & Salleh, M. A. M. (2010b). Experimental investigation of the size effects of SiO2 nano-particles on the mechanical properties of binary blended concrete. *Composites Part B: Engineering*, *41*(8), 673–677.

Gomes, G. M. F., Philipssen, C., Bard, E. K., Dalla Zen, L., & de Souza, G. (2016). Rice husk bubbling fluidized bed combustion for amorphous silica synthesis. *Journal of Environmental Chemical Engineering*, *4*(2), 2278–2290.

Gonç alves, M. C., & Fernanda, M. (2015). Materials for construction and civil engineering: Science, processing, and design. In *Materials for Construction and Civil Engineering: Science, Processing, and Design*. https://doi.org/10.1007/978-3-319-08236-3

Gosalvitr, P., Srinophakun, P., Kanchanapiya, P., & Danwittayakul, S. (2015). The Effects of particle size and content of rice husk ash from textile wastewater treatment on the properties of Portland cement-base solidification. *International Conference on Biological, Environment and Food Engineering (BEFE-2015)*, 15–16.

Gu, S., Zhou, J., Luo, Z., Wang, Q., & Shi, Z. (2015). Kinetic study on the preparation of silica from rice husk under various pretreatments. *Journal of Thermal Analysis and Calorimetry*, *119*, 2159–2169.

Güneyisi, E., Gesoglu, M., Al-Goody, A., & İpek, S. (2015). Fresh and rheological behavior of nano-silica and fly ash blended self-compacting concrete. *Construction and Building Materials*, *95*, 29–44.

H.F.W. Taylor. (1997). *Cement Chemistry*. Thomas Telford Publishing.

Haach, V. G., Vasconcelos, G., & Lourenço, P. B. (2011). Influence of aggregates grading and water/cement ratio in workability and hardened properties of mortars. *Construction and Building Materials*, *25*(6), 2980–2987.

Habeeb, G. A., & Mahmud, H. Bin. (2010). Study on properties of rice husk ash and its use as cement replacement material. *Materials Research*, *13*, 185–190.

Hadipramana, J., Samad, A. A. A., Ahmad Mujahid, A. Z., Mohammad, N., & Riza, F.

V. (2013). Effect of uncontrolled burning rice husk ash in foamed concrete. *Advanced Materials Research*, *626*, 769–775.

Hamidu, I., Afotey, B., Kwakye-Awuah, B., & Anang, D. A. (2025). Synthesis of silica and silicon from rice husk feedstock: A review. *Heliyon*, *11*(4). https://doi.org/10.1016/j.heliyon.2025.e42491

Hasparyk, N. P., Monteiro, P. J. M., & Carasek, H. (2000). Effect of silica fume and rice husk ash on alkali-silica reaction. *Materials Journal*, *97*(4), 486–492.

He, Q., Zhang, Z., Gao, Y., Shi, J., & Li, Y. (2009). Intracellular localization and cytotoxicity of spherical mesoporous silica nano-and microparticles. *Small*, *5*(23), 2722–2729.

Heikal, M., Abd El Aleem, S., & Morsi, W. M. (2013). Characteristics of blended cements containing nano-silica. *HBRC Journal*, *9*(3), 243–255.

Hossain, M. T., Zaman, M., Sakib, S., & Mahmud, S. M. I. (2024). Hazard Assessment of Rice Husk Ash Generated from Rice Mills in Bangladesh and Way Forward to Overcome or Adopt the Hazards. *IOP Conference Series: Materials Science and Engineering*, *1305*(1), 012016. https://doi.org/10.1088/1757-899x/1305/1/012016

Hossain, S. K. S., Mathur, L., & Roy, P. K. (2018). Rice husk/rice husk ash as an alternative source of silica in ceramics: A review. *Journal of Asian Ceramic Societies*, *6*(4), 299–313.

Hou, P., Kawashima, S., Kong, D., Corr, D. J., Qian, J., & Shah, S. P. (2013). Modification effects of colloidal nanoSiO2 on cement hydration and its gel property. *Composites Part B: Engineering*, *45*(1), 440–448.

Hu, S., Liao, Y., Xu, Y., & Wang, J. (2024). Quantitative Relationship Between Strength and Porosity of Nano-Silica-Modified Mortar Based on Fractal Theory. *Fractal and*

Fractional, *8*(12). https://doi.org/10.3390/fractalfract8120694

Hudson, S. P., Padera, R. F., Langer, R., & Kohane, D. S. (2008). The biocompatibility of mesoporous silicates. *Biomaterials*, *29*(30), 4045–4055.

Hwang, C. L., & Chandra, S. (1996). The use of rice husk ash in concrete. In *Waste materials used in concrete manufacturing* (pp. 184–234). Noyes Publications.

Ibrahim, M., Johari, M. A. M., Hussaini, S. R., Rahman, M. K., & Maslehuddin, M. (2020). Influence of pore structure on the properties of green concrete derived from natural pozzolan and nanosilica. *Journal of Sustainable Cement-Based Materials*, *9*(4), 233–257.

Iler, R. K. (1979). The chemistry of silica, Solubility, Polymerization. *Colloid and Surface Properties, and Biochemistry*, *866*.

IS 456. (2000). *Plain and Reinforced Concrete - Code of Practice*.

Isaia, G. C., GASTALDInI, A. L. G., & Moraes, R. (2003). Physical and pozzolanic action of mineral additions on the mechanical strength of high-performance concrete. *Cement and Concrete Composites*, *25*(1), 69–76.

Islam, G. M. S., & Akter, A. (2012). Rice husk ash as a sustainable construction material for Bangladesh. *1st International Conference on Advances in Civil Engineering (ICACE 2012)*.

James, J., & Rao, M. S. (1986). Reactivity of rice husk ash. *Cement and Concrete Research*, *16*(3), 296–302.

Jamil, M., Khan, M. N. N., Karim, M. R., Kaish, A., & Zain, M. F. M. (2016). Physical and chemical contributions of Rice Husk Ash on the properties of mortar. *Construction and Building Materials*, *128*, 185–198.

Jang, H., Lim, Y.-T., Kang, J.-H., So, S., & So, H. (2018). Influence of calcination and cooling conditions on pozzolanic reactivity of paper mill sludge. *Construction and Building Materials*, *166*, 257–270.

Jang, I.-S., Park, J. Y., Park, H., Gu, Y. M., Lee, J. H., & Chun, J. (2022). Simplified synthesis of spherical silica microparticles from rice husk. *Chemical Engineering & Technology*, *45*(2), 381–384.

Jo, B.-W., Kim, C.-H., Tae, G., & Park, J.-B. (2007). Characteristics of cement mortar with nano-SiO2 particles. *Construction and Building Materials*, *21*(6), 1351–1355.

Jo, B. W., Kim, C. H., & Lim, J. H. (2007). Investigations on the development of powder concrete with nano-SiO 2 particles. *KSCE Journal of Civil Engineering*, *11*, 37–42.

John, V. T., Simmons, B., McPherson, G. L., & Bose, A. (2002). Recent developments in materials synthesis in surfactant systems. *Current Opinion in Colloid & Interface Science*, *7*(5–6), 288–295.

Jones, A. E. K. (1997). *Development of an holistic approach to ensure the durability of new concrete construction*. British Cement Association.

Jung, C. Y., Kim, J. S., Chang, T. S., Kim, S. T., Lim, H. J., & Koo, S. M. (2010). One-step synthesis of structurally controlled silicate particles from sodium silicates using a simple precipitation process. *Langmuir*, *26*(8), 5456–5461.

Junpen, A., Pansuk, J., Kamnoet, O., Cheewaphongphan, P., & Garivait, S. (2018). Emission of air pollutants from rice residue open burning in Thailand, 2018. *Atmosphere*, *9*(11), 449.

Kalapathy, U., Proctor, A., & Shultz, J. (2000). Silica xerogels from rice hull ash: Structure, density and mechanical strength as affected by gelation pH and silica concentration. *Journal of Chemical Technology and Biotechnology*, *75*(6), 464–468.

https://doi.org/10.1002/1097-4660(200006)75:6<464::AID-JCTB235>3.0.CO;2-C

Kalapathy, U., Proctor, A., & Shultz, J. (2002). An improved method for production of silica from rice hull ash. *Bioresource Technology*, *85*(3), 285–289.

Kamath, S. R., & Proctor, A. (1998). Silica gel from rice hull ash: preparation and characterization. *Cereal Chemistry*, *75*(4), 484–487.

Kang, S.-H., Hong, S.-G., & Moon, J. (2019). The use of rice husk ash as reactive filler in ultra-high performance concrete. *Cement and Concrete Research*, *115*, 389–400.

Karihaloo, B. L., Abdalla, H. M., & Xiao, Q. Z. (2003). Size effect in concrete beams. *Engineering Fracture Mechanics*, *70*(7–8), 979–993.

Karim, M. R., Hossain, M. M., Khan, M. N. N., Zain, M. F. M., Jamil, M., & Lai, F. C. (2014). On the utilization of pozzolanic wastes as an alternative resource of cement. *Materials*, *7*(12), 7809–7827.

Karunarathne, V. K., Paul, S. C., & Šavija, B. (2019). Development of nano-SiO2 and bentonite-based mortars for corrosion protection of reinforcing steel. *Materials*, *12*(16), 2622.

Kasaniya, M., Thomas, M. D. A., & Moffatt, E. G. (2021). Pozzolanic reactivity of natural pozzolans, ground glasses and coal bottom ashes and implication of their incorporation on the chloride permeability of concrete. *Cement and Concrete Research*, *139*, 106259.

Keykhosravi, A., & Simjoo, M. (2019). Insights into stability of silica nanofluids in brine solution coupled with rock wettability alteration: An enhanced oil recovery study in oil-wet carbonates. *Colloids and Surfaces A: Physicochemical and Engineering Aspects*, *583*, 124008.

Khan, K., Ullah, M. F., Shahzada, K., Amin, M. N., Bibi, T., Wahab, N., & Aljaafari, A. (2020). Effective use of micro-silica extracted from rice husk ash for the production of high-performance and sustainable cement mortar. *Construction and Building Materials*, *258*, 119589.

Khan, M. H., Mohan, K., & Taylor, H. F. W. (1985). Pastes of tricalcium silicate with rice husk ash. *Cement and Concrete Research*, *15*(1), 89–92.

Khan, M. N. N., Jamil, M., Karim, M. R., Zain, M. F. M., & Kaish, A. B. M. A. (2015). Utilization of rice husk ash for sustainable construction: A review. *Research Journal of Applied Sciences, Engineering and Technology*, *9*(12), 1119–1127.

Khan, R., Jabbar, A., Ahmad, I., Khan, W., Khan, A. N., & Mirza, J. (2012). Reduction in environmental problems using rice-husk ash in concrete. *Construction and Building Materials*, *30*, 360–365.

Kim, J. J., Foley, E. M., & Taha, M. M. R. (2013). Nano-mechanical characterization of synthetic calcium–silicate–hydrate (C–S–H) with varying CaO/SiO2 mixture ratios. *Cement and Concrete Composites*, *36*, 65–70.

Kim, S., Park, J. Y., Gu, Y. M., Jang, I.-S., Park, H., Oh, K. K., Lee, J. H., & Chun, J. (2021). Eco-friendly and facile synthesis of size-controlled spherical silica particles from rice husk. *Nanoscale Advances*, *3*(24), 6965–6973.

Kim, T. H., Ryu, H. J., & Oh, K. K. (2019). Improvement of organosolv fractionation performance for rice husk through a low acid-catalyzation. *Energies*, *12*(9), 1800.

Kirby, G. H., & Lewis, J. A. (2004). Comb polymer architecture effects on the rheological property evolution of concentrated cement suspensions. *Journal of the American Ceramic Society*, *87*(9), 1643–1652.

Kondo, R. (1968). Kinetics and Mechanism of the Hydration of Cements. *Proc. of 5th*

Int. Symp. on the Chem. of Cem., Tokyo, II-4, 1968.

Kong, D., Corr, D. J., Hou, P., Yang, Y., & Shah, S. P. (2015). Influence of colloidal silica sol on fresh properties of cement paste as compared to nano-silica powder with agglomerates in micron-scale. *Cement and Concrete Composites*, *63*, 30–41.

Kong, D., Pan, H., Wang, L., Corr, D. J., Yang, Y., Shah, S. P., & Sheng, J. (2019). Effect and mechanism of colloidal silica sol on properties and microstructure of the hardened cement-based materials as compared to nano-silica powder with agglomerates in micron-scale. *Cement and Concrete Composites*, *98*, 137–149.

Kong, D., Su, Y., Du, X., Yang, Y., Wei, S., & Shah, S. P. (2013). Influence of nano-silica agglomeration on fresh properties of cement pastes. *Construction and Building Materials*, *43*, 557–562.

Kontoleontos, F., Tsakiridis, P. E., Marinos, A., Kaloidas, V., & Katsioti, M. (2012). Influence of colloidal nanosilica on ultrafine cement hydration: Physicochemical and microstructural characterization. *Construction and Building Materials*, *35*, 347–360.

Krishnarao, R. V, & Godkhindi, M. M. (1992). Distribution of silica in rice husks and its effect on the formation of silicon carbide. *Ceramics International*, *18*(4), 243–249.

Kuli, I., Abu-Lebdeh, T. M., Fini, E. H., & Hamoush, S. A. (2016). The use of nano-silica for improving mechanical properties of hardened cement paste. *Am. J. Eng. Applied Sci*, *9*, 146–154.

Kumar Das, S., Adediran, A., Rodrigue Kaze, C., Mohammed Mustakim, S., & Leklou, N. (2022). Production, characteristics, and utilization of rice husk ash in alkali activated materials: An overview of fresh and hardened state properties. *Construction and Building Materials*, *345*(February). https://doi.org/10.1016/j.conbuildmat.2022.128341

Kumar, S., Ali, N., Begum, S., & Rahman, Z. (2021). Characterization, properties and microstructure studies of cement mortar incorporating nano-SiO2. *Materials Today: Proceedings*, *37*, 425–430.

Land, G., & Stephan, D. (2012). The influence of nano-silica on the hydration of ordinary Portland cement. *Journal of Materials Science*, *47*, 1011–1017.

Lasko, K., & Vadrevu, K. (2018). Improved rice residue burning emissions estimates: Accounting for practice-specific emission factors in air pollution assessments of Vietnam. *Environmental Pollution*, *236*, 795–806.

Le, H. T., Nguyen, S. T., & Ludwig, H.-M. (2014). A study on high performance fine-grained concrete containing rice husk ash. *International Journal of Concrete Structures and Materials*, *8*, 301–307.

Le, H. T., Siewert, K., & Ludwig, H. M. (2012). Synergistic effects of rice husk ash and fly ash on properties of self-compacting high performance concrete. *Proceedings of Symposium on Ultra High Performance Concrete and Nanotechnology for High Performance Construction Materials, Kassel, Germany*, 187–195.

Le, V. H., Thuc, C. N. H., & Thuc, H. H. (2013). Synthesis of silica nanoparticles from Vietnamese rice husk by sol–gel method. *Nanoscale Research Letters*, *8*, 1–10.

Lee, J. H., Kwon, J. H., Lee, J.-W., Lee, H., Chang, J. H., & Sang, B.-I. (2017). Preparation of high purity silica originated from rice husks by chemically removing metallic impurities. *Journal of Industrial and Engineering Chemistry*, *50*, 79–85.

Legrand, C., & Wirquin, E. (1994). Study of the strength of very young concrete as a function of the amount of hydrates formed—influence of superplasticizer. *Materials and Structures*, *27*, 106–109.

Liou, T.-H. (2004). Preparation and characterization of nano-structured silica from rice

husk. *Materials Science and Engineering: A*, *364*(1–2), 313–323.

Liou, T.-H., & Yang, C.-C. (2011). Synthesis and surface characteristics of nanosilica produced from alkali-extracted rice husk ash. *Materials Science and Engineering: B*, *176*(7), 521–529.

Ltifi, M., Guefrech, A., Mounanga, P., & Khelidj, A. (2011). Experimental study of the effect of addition of nano-silica on the behaviour of cement mortars. *Procedia Engineering*, *10*(0), 900–905.

Lun, Y., Zhou, M., Cai, X., & Xu, F. (2008). Methods for improving volume stability of steel slag as fine aggregate. *Journal of Wuhan University of Technology-Mater. Sci. Ed.*, *23*, 737–742.

Ma, X., Zhou, B., Gao, W., Qu, Y., Wang, L., Wang, Z., & Zhu, Y. (2012). A recyclable method for production of pure silica from rice hull ash. *Powder Technology*, *217*, 497–501.

Mahdikhani, M., Bamshad, O., & Shirvani, M. F. (2018). Mechanical properties and durability of concrete specimens containing nano silica in sulfuric acid rain condition. *Construction and Building Materials*, *167*, 929–935.

Mahoney, L., & Koodali, R. T. (2014). Versatility of evaporation-induced self-assembly (EISA) method for preparation of mesoporous TiO2 for energy and environmental applications. *Materials*, *7*(4), 2697–2746.

Malhotra, V. M. (1976). *Testing hardened concrete: nondestructive methods*.

Mamlouk, M. S., & Zaniewski, J. P. (2014). *Materials for civil and construction engineers*. Pearson London, UK:

Marthong, C. (2012). Effect of rice husk ash (RHA) as partial replacement of cement

on concrete properties. *International Journal of Engineering Research & Technology*, *1*(6), 1–9.

Massazza, F. (1998). Pozzolana and pozzolanic cements. *Lea's Chemistry of Cement and Concrete*, *4*, 471–631.

Mayooran, S., Ragavan, S., & Sathiparan, N. (2017). Comparative study on open air burnt low-and high-carbon rice husk ash as partial cement replacement in cement block production. *Journal of Building Engineering*, *13*, 137–145.

Mboya, H. A., King'ondu, C. K., Njau, K. N., & Mrema, A. L. (2017). Measurement of pozzolanic activity index of scoria, pumice, and rice husk ash as potential supplementary cementitious materials for Portland cement. *Advances in Civil Engineering*, *2017*(1), 6952645.

McCarthy, M. J., Sadiqul Islam, G. M., Csetenyi, L. J., & Jones, M. R. (2013). Investigating techniques for rapidly assessing fly ash reactivity for use in concrete. *World of Coal Ash, Lexington, KY, USA. See Http://Www. Flyash. Info (Accessed 07/05/2018)*.

Mehta, P. K. (1978). *Siliceous ashes and hydraulic cements prepared therefrom*. Google Patents.

Mehta, P. K. (1979). The chemistry and technology of cements rice husk ash made from rice husk ash. *Proc. Unido-Escap/RCTT Workshop on Rice Husk Ash Cement, 1979*, 113–122.

Mehta, P. K. (1994). Rice husk ash--A unique supplementary cementing material. *Advances in Concrete Technology*, 419–443.

Mehta, P. K., & Aïtcin, P.-C. (1990). Principles underlying production of high-performance concrete. *Cement, Concrete, and Aggregates*, *12*(2), 70–78.

Mehta, P. K., & Monteiro, P. J. M. (2001). *Concrete: Microstructure, Properties, and Materials*.

Mehta, P. K., & Pirtz, D. (1978). Use of rice hull ash to reduce temperature in high-strength mass concrete. *Journal Proceedings*, *75*(2), 60–63.

Mehta, P. K., & Pitt, N. (1976). Energy and industrial materials from crop residues. *Resource Recovery and Conservation*, *2*(1), 23–38.

Mendes, T. M., & Repette, W. L. (2021). Effect of nano-silica on Portland cement matrices containing supplementary cementitious materials. *Revista IBRACON de Estruturas e Materiais*, *14*(4), 1–12. https://doi.org/10.1590/S1983-41952021000400001

Meyer, C. (2009). The greening of the concrete industry. *Cement and Concrete Composites*, *31*(8), 601–605.

Mohammed, B. S., Liew, M. S., Alaloul, W. S., Khed, V. C., Hoong, C. Y., & Adamu, M. (2018). Properties of nano-silica modified pervious concrete. *Case Studies in Construction Materials*, *8*, 409–422.

Mohammed, M. K., Dawson, A. R., & Thom, N. H. (2014). Macro/micro-pore structure characteristics and the chloride penetration of self-compacting concrete incorporating different types of filler and mineral admixture. *Construction and Building Materials*, *72*, 83–93.

Monteiro, P. (2006). *Concrete: microstructure, properties, and materials*. McGraw-Hill Publishing.

Moranville-Regourd, M. (2002). New cementitious systems and composite materials. *Key Engineering Materials*, *206*.

Msinjili, N. S., Schmidt, W., Mota, B., Leinitz, S., Kühne, H.-C., & Rogge, A. (2017). The effect of superplasticizers on rheology and early hydration kinetics of rice husk ash-blended cementitious systems. *Construction and Building Materials*, *150*, 511–519.

Mukharjee, B. B., & Barai, S. V. (2014). Assessment of the influence of Nano-Silica on the behavior of mortar using factorial design of experiments. *Construction and Building Materials*, *68*, 416–425.

Mukharjee, B. B., & Barai, S. V. (2020). Influence of incorporation of colloidal nano-silica on behaviour of concrete. *Iranian Journal of Science and Technology, Transactions of Civil Engineering*, *44*, 657–668.

Mukherjee, I., Mylonakis, A., Guo, Y., Samuel, S. P., Li, S., Wei, R. Y., Kojtari, A., & Wei, Y. (2009). Effect of nonsurfactant template content on the particle size and surface area of monodisperse mesoporous silica nanospheres. *Microporous and Mesoporous Materials*, *122*(1–3), 168–174.

Mussa, M. H., Abdulhadi, A. M., Abbood, I. S., Mutalib, A. A., & Yaseen, Z. M. (2020). Late age dynamic strength of high-volume fly ash concrete with nano-silica and polypropylene fibres. *Crystals*, *10*(4), 243.

Nair, D. G., Fraaij, A., Klaassen, A. A. K., & Kentgens, A. P. M. (2008). A structural investigation relating to the pozzolanic activity of rice husk ashes. *Cement and Concrete Research*, *38*(6), 861–869.

Najigivi, A., Abdul Rashid, S., Nora A. Aziz, F., & Mohd Salleh, M. A. (2012). Water absorption control of ternary blended concrete with nano-SiO 2 in presence of rice husk ash. *Materials and Structures*, *45*, 1007–1017.

NAKATA, Y., SUZUKI, M., OKUTANI, T., KIKUCHI, M., & AKIYAMA, T. (1989). Preparation and properties of SiO2 from rice hulls. *Journal of the Ceramic Society of*

Japan, *97*(1128), 842–849.

Nassar, R., Abbas, S., & Saeed, D. (2021). Effect of Initial Cracking and Bitumen Coating on Performance of Concrete in Sulfate Environment. *Civil Engineering and Architecture*, *9*(6), 1846–1853.

Nayak, P. P., & Datta, A. K. (2021). Synthesis of SiO2-nanoparticles from rice husk ash and its comparison with commercial amorphous silica through material characterization. *Silicon*, *13*(4), 1209–1214.

Nazari, A., & Riahi, S. (2011). RETRACTED: The effects of SiO2 nanoparticles on physical and mechanical properties of high strength compacting concrete. *Composites Part B: Engineering*, *42*(3), 570–578.

Ndahirwa, D., Zmamou, H., Lenormand, H., & Leblanc, N. (2022). The role of supplementary cementitious materials in hydration, durability and shrinkage of cement-based materials, their environmental and economic benefits: A review. *Cleaner Materials*, *5*, 100123.

Nduka, D. O., Olawuyi, B. J., Fagbenle, E. O., & Fonteboa, B. G. (2022). Mechanical and microstructural properties of high-performance concrete made with rice husk ash internally cured with superabsorbent polymers. *Heliyon*, *8*(9).

Neville, A. M. (2011). Properties of Concrete, 4th. *London Pearson Education Limited*, *443*(846), 444.

Ngun, B. K., Mohamad, H., Sakai, E., & Ahmad, Z. A. (2010). Effect of rice husk ash and silica fume in ternary system on the properties of blended cement paste and concrete. *Journal of Ceramic Processing Research*, *11*(3), 311–315.

Nila, N. I., Piyes, M. T. I., Islam, G. M. S., & Islam, M. M. (2024). *Cementitious Properties Of Rice Husk Ash (Rha) And Extracted Silica Powder From RHA, ICACE 2024, CUET*.

NPCS (NIIR Project Consultancy Service). (2013). *Rice Husk, Rice Hull, Rice Husk Ash (Agricultural waste) based Projects*. www.niir.org/

Nzereogu, P. U., Omah, A. D., Ezema, F. I., Iwuoha, E. I., & Nwanya, A. C. (2023). Silica extraction from rice husk: Comprehensive review and applications. *Hybrid Advances*, *4*(August), 100111. https://doi.org/10.1016/j.hybadv.2023.100111

O'Sullivan, E. C., Ward, A. J. I., & Budd, T. (1994). Obvious and nonobvious influences of surfactants on the formation of nanosized particles. *Langmuir*, *10*(9), 2985–2992.

Oh, D.-Y., Noguchi, T., Kitagaki, R., & Park, W.-J. (2014). CO2 emission reduction by reuse of building material waste in the Japanese cement industry. *Renewable and Sustainable Energy Reviews*, *38*, 796–810.

Olawale, O., & Oyawale, F. A. (2012). Characterization of rice husk via atomic absorption spectrophotometer for optimal silica production. *International Journal of Science and Technology*, *2*(4), 210–213.

P. G . Fookes, Aughan P. R. V. (1985). *A Handbook of Engineering Geomorphology.pdf*. Surrey University Press.

Page, C. L., & Page, M. M. (2007). *Durability of concrete and cement composites*. Woodhead Publishing Limited.

Palmqvist, A. E. C. (2003). Synthesis of ordered mesoporous materials using surfactant liquid crystals or micellar solutions. *Current Opinion in Colloid & Interface Science*, *8*(2), 145–155.

Papatzani, S., Paine, K., & Calabria-Holley, J. (2015). A comprehensive review of the models on the nanostructure of calcium silicate hydrates. *Construction and Building Materials*, *74*, 219–234.

Patel, K. G., Shettigar, R. R., & Misra, N. M. (2017). Recent advance in silica production technologies from agricultural waste stream. *Journal of Advanced Agricultural Technologies*, *4*(3).

Pathak, U., Kumari, S., Kumar, A., & Mandal, T. (2020). Process parametric optimization toward augmentation of silica yield using Taguchi technique and artificial neural network approach. *Energy, Ecology and Environment*, *5*, 294–312.

Pedersen, M., Viksø-Nielsen, A., & Meyer, A. S. (2010). Monosaccharide yields and lignin removal from wheat straw in response to catalyst type and pH during mild thermal pretreatment. *Process Biochemistry*, *45*(7), 1181–1186.

Pelisser, F., Gleize, P. J. P., & Mikowski, A. (2012). Effect of the Ca/Si molar ratio on the micro/nanomechanical properties of synthetic CSH measured by nanoindentation. *The Journal of Physical Chemistry C*, *116*(32), 17219–17227.

Pitt, N. (1976). *Process for the preparation of siliceous ashes*. U.S. Patent 3,959,007.

Pode, R. (2016). Potential applications of rice husk ash waste from rice husk biomass power plant. *Renewable and Sustainable Energy Reviews*, *53*, 1468–1485.

Porro, A., Dolado, J. S., Campillo, I., Erkizia, E. d, De Miguel, Y., de Ibarra, Y. S., & Ayuela, A. (2005). Effects of nanosilica additions on cement pastes. *Applications of Nanotechnology in Concrete Design: Proceedings of the International Conference Held at the University of Dundee, Scotland, UK on 7 July 2005*, 87–96.

Portet, F., Desbene, P. L., & Treiner, C. (1998). Polydispersity of a non-ionic surfactant as related to its adsorption characteristics on porous silica particles in water. *Journal of Colloid and Interface Science*, *208*(2), 415–421.

Potty, N. S., Vallyutham, K., Yusoff, M. F., Anwar, A., Haron, M. F., & Alias, M. N. (2014). Properties of rice husk Ash (RHA and MIRHA) mortars. *Research Journal*

of Applied Sciences, Engineering and Technology, *7*(18), 3872–3882. https://doi.org/10.19026/rjaset.7.745

Purwaningsih, H., Ervianto, Y., Pratiwi, V. M., Susanti, D., & Purniawan, A. (2019). Effect of cetyl trimethyl ammonium bromide as template of mesoporous silica mcm-41 from rice husk by sol-gel method. *IOP Conference Series: Materials Science and Engineering*, *515*(1), 12051.

Qing, Y., Zenan, Z., Deyu, K., & Rongshen, C. (2007). Influence of nano-SiO2 addition on properties of hardened cement paste as compared with silica fume. *Construction and Building Materials*, *21*(3), 539–545.

Rafiee, E., Shahebrahimi, S., Feyzi, M., & Shaterzadeh, M. (2012). Optimization of synthesis and characterization of nanosilica produced from rice husk (a common waste material). *International Nano Letters*, *2*, 1–8.

Rahman, I. A., & Padavettan, V. (2012). Synthesis of silica nanoparticles by sol-gel: size-dependent properties, surface modification, and applications in silica-polymer nanocomposites—a review. *Journal of Nanomaterials*, *2012*(1), 132424.

Rai, S., & Tiwari, S. (2018). Nano silica in cement hydration. *Materials Today: Proceedings*, *5*(3), 9196–9202.

Raman, S. N., Ngo, T., Mendis, P., & Mahmud, H. B. (2011). High-strength rice husk ash concrete incorporating quarry dust as a partial substitute for sand. *Construction and Building Materials*, *25*(7), 3123–3130.

Ramezanianpour, A. A., Mahdikhani, M., & Ahmadibeni, G. H. (2009). *The effect of rice husk ash on mechanical properties and durability of sustainable concretes*.

Rao, G. A. (2001). Generalization of Abrams' law for cement mortars. *Cement and Concrete Research*, *31*(3), 495–502.

Rao, G. A. (2003). Investigations on the performance of silica fume-incorporated cement pastes and mortars. *Cement and Concrete Research*, *33*(11), 1765–1770.

Reches, Y., Thomson, K., Helbing, M., Kosson, D. S., & Sanchez, F. (2018). Agglomeration and reactivity of nanoparticles of SiO2, TiO2, Al2O3, Fe2O3, and clays in cement pastes and effects on compressive strength at ambient and elevated temperatures. *Construction and Building Materials*, *167*, 860–873.

Richardson, I. G. (1999). The nature of CSH in hardened cements. *Cement and Concrete Research*, *29*(8), 1131–1147.

Richardson, I. G. (2008). The calcium silicate hydrates. *Cement and Concrete Research*, *38*(2), 137–158.

Rößler, C., Bui, D.-D., & Ludwig, H.-M. (2013). Mesoporous structure and pozzolanic reactivity of rice husk ash in cementitious system. *Construction and Building Materials*, *43*, 208–216.

Rößler, C., Bui, D.-D., & Ludwig, H.-M. (2014). Pozzolanic reactivity of mesoporous amorphous rice husk ash in portlandite solution. *Construction and Building Materials*, *59*, 111–119.

Rubio, J., & Kitchener, J. A. (1976). The mechanism of adsorption of poly (ethylene oxide) flocculant on silica. *Journal of Colloid and Interface Science*, *57*(1), 132–142.

Rukzon, S., & Chindaprasirt, P. (2006). Strength of ternary blended cement mortar containing portland cement rice husk ash fly ash. *Engineering Journal of Research and Development*, *17*(2), 33–38.

Rukzon, S., Chindaprasirt, P., & Mahachai, R. (2009). Effect of grinding on chemical and physical properties of rice husk ash. *International Journal of Minerals, Metallurgy and Materials*, *16*(2), 242–247.

Said, A. M., Zeidan, M. S., Bassuoni, M. T., & Tian, Y. (2012). Properties of concrete incorporating nano-silica. *Construction and Building Materials*, *36*, 838–844.

Sakr, K. (2006). Effects of silica fume and rice husk ash on the properties of heavy weight concrete. *Journal of Materials in Civil Engineering*, *18*(3), 367–376.

Santasnachok, C., Kurniawan, W., & Hinode, H. (2015). Characterization of Thailand rice husk ash from biomass power plant and synthesized zeolite. *J. Life Sci*, *9*, 127–130.

Santhanam, M., Cohen, M. D., & Olek, J. (2002). Mechanism of sulfate attack: A fresh look: Part 1: Summary of experimental results. *Cement and Concrete Research*, *32*(6), 915–921.

Santhanam, M., Cohen, M. D., & Olek, J. (2003). Mechanism of sulfate attack: a fresh look: Part 2. Proposed mechanisms. *Cement and Concrete Research*, *33*(3), 341–346.

Sata, V., Jaturapitakkul, C., & Kiattikomol, K. (2007). Influence of pozzolan from various by-product materials on mechanical properties of high-strength concrete. *Construction and Building Materials*, *21*(7), 1589–1598.

Seifan, M., Mendoza, S., & Berenjian, A. (2020). Mechanical properties and durability performance of fly ash based mortar containing nano-and micro-silica additives. *Construction and Building Materials*, *252*, 119121.

Senff, L., Hotza, D., Repette, W. L., Ferreira, V. M., & Labrincha, J. A. (2010). Mortars with nano-SiO2 and micro-SiO2 investigated by experimental design. *Construction and Building Materials*, *24*(8), 1432–1437.

Senff, L., Labrincha, J. A., Ferreira, V. M., Hotza, D., & Repette, W. L. (2009). Effect of nano-silica on rheology and fresh properties of cement pastes and mortars. *Construction and Building Materials*, *23*(7), 2487–2491.

Setyawan, N., Hoerudin, & Yuliani, S. (2021). Synthesis of silica from rice husk by sol-gel method. *IOP Conference Series: Earth and Environmental Science*, *733*(1). https://doi.org/10.1088/1755-1315/733/1/012149

Shafigh, P., Mahmud, H. Bin, Jumaat, M. Z., & Zargar, M. (2014). Agricultural wastes as aggregate in concrete mixtures–A review. *Construction and Building Materials*, *53*, 110–117.

Shah, S. P., Hou, P., & Konsta-Gdoutos, M. S. (2016). Nano-modification of cementitious material: Toward a stronger and durable concrete. *Journal of Sustainable Cement-Based Materials*, *5*(1–2), 1–22.

Sharma, N. K., Williams, W. S., & Zangvil, A. (1984). Formation and structure of silicon carbide whiskers from rice hulls. *Journal of the American Ceramic Society*, *67*(11), 715–720.

Shatat, M. R. (2016). Hydration behavior and mechanical properties of blended cement containing various amounts of rice husk ash in presence of metakaolin. *Arabian Journal of Chemistry*, *9*, S1869–S1874.

Shetty, M. S., & Jain, A. K. (2019). *Concrete Technology (Theory and Practice), 8e*. S. Chand Publishing.

Shukla, A., Singh, C. K., & Sharma, A. K. (2011). *Study of the properties of concrete by partial replacement of ordinary Portland cement by rice husk ash*.

Shwe, E., Oo, S., Aung, M., & Chan, Y. (2020). EFFECT OF pH LEVEL ON THE FORMATION OF SILICA AEROGEL SYNTHESIZED FROM RICE HUSK ASH. *J. Myanmar Acad. Arts Sci*, *2*(2), 3–10. http://www.maas.edu.mm/Research/Admin/pdf/49. Daw Ei Shwe Sin Oo(453-460).pdf

Siddique, R. (2004). Performance characteristics of high-volume Class F fly ash concrete. *Cement and Concrete Research*, *34*(3), 487–493.

Siddique, R. (2007). *Waste materials and by-products in concrete*. Springer Science & Business Media.

Singh, J., & Singh, H. (2015). A review on utilization of rice husk ash in concrete. *International Journal of Innovations in Engineering Research and Technology*, *2*(11), 1–7.

Singh, L. P., Bhattacharyya, S. K., & Ahalawat, S. (2012). Preparation of size controlled silica nano particles and its functional role in cementitious system. *Journal of Advanced Concrete Technology*, *10*(11), 345–352.

Singh, S., & Shukla, D. A. (2023). Effect of Rice Husk Ash on the Properties of Concrete. *International Journal for Research in Applied Science and Engineering Technology*, *11*(10), 1056–1062. https://doi.org/10.22214/ijraset.2023.56100

Skrifvars, B.-J., Yrjas, P., Laurén, T., Kinni, J., Tran, H., & Hupa, M. (2005). The fouling behavior of rice husk ash in fluidized-bed combustion. 2. Pilot-scale and full-scale measurements. *Energy & Fuels*, *19*(4), 1512–1519.

Smith, R. G., & Kamwanja, G. A. (1986). The use of rice husk for making a cementitious material. *Proc. Joint Symposium on the Use of Vegetable Plants and Their Fibers as Building Material, Baghdad*.

Soltani, N., Bahrami, A., Pech-Canul, M. I., & González, L. A. (2015). Review on the physicochemical treatments of rice husk for production of advanced materials. *Chemical Engineering Journal*, *264*, 899–935.

Sriwuryandari, L., Priantoro, E. A., Janetasari, S. A., Butar Butar, E. S., & Sembiring, T. (2020). Utilization of rice husk (Oryza sativa) for amorphous biosilica (SiO2)

production as a bacterial attachment. *IOP Conference Series: Earth and Environmental Science*, *483*(1). https://doi.org/10.1088/1755-1315/483/1/012023

Stanley, C. C. (1982). *Highlights in the History of Concrete* (Issues 97-408 Monograph).

Suka, I. G., Simanjuntak, W., Sembiring, S., & Trisnawati, E. (2009). Karakteristik Silika Sekam Padi dari Provinsi Lampung yang Diperoleh dengan Metoda Ekstraksi. *MIPA Dan Pembelajarannya*, *37*(1), 220397.

Sukontasukkul, P., Nimityongskul, P., & Mindess, S. (2004). Effect of loading rate on damage of concrete. *Cement and Concrete Research*, *34*(11), 2127–2134.

Szekeres, M., Dékány, I., & De Keizer, A. (1998). Adsorption of dodecyl pyridinium chloride on monodisperse porous silica. *Colloids and Surfaces A: Physicochemical and Engineering Aspects*, *141*(3), 327–336.

Tanesi, J., & Ardani, A. (2012). *Surface resistivity test evaluation as an indicator of the chloride permeability of concrete.* United States. Federal Highway Administration.

Tazawa, E., Miyazawa, S., & Kasai, T. (1995). Chemical shrinkage and autogenous shrinkage of hydrating cement paste. *Cement and Concrete Research*, *25*(2), 288–292.

Tharani, D., & Ananthasubramanian, M. (2024). Influence of pre-treatment processes on the purity and characteristics of silica extracted from rice husk. *Biomass Conversion and Biorefinery*, *14*(11), 12517–12529.

Thomas, J. J., Jennings, H. M., & Chen, J. J. (2009). Influence of nucleation seeding on the hydration mechanisms of tricalcium silicate and cement. *The Journal of Physical Chemistry C*, *113*(11), 4327–4334.

Thuadaij, N., & Nuntiya, A. (2008). Preparation of nanosilica powder from rice husk ash by precipitation method. *Chiang Mai Journal of Science*, *35*(1), 206–211.

Uchikawa, H. (1986). Effect of blending components on hydration and structure formation. *Invited Paper, 8th International Congress on the Chemistry of Cement, Rio de Janeiro*, 249–280.

Ugheoke, I. B., & Mamat, O. (2012). A critical assessment and new research directions of rice husk silica processing methods and properties. *Maejo International Journal of Science and Technology*, *6*(3), 430.

van Nguyen, T. (2011). Rice husk ash as a mineral admixture for ultra high performance concrete. *Delft University of Technology*.

Van Tuan, N., Ye, G., Van Breugel, K., Fraaij, A. L. A., & Dai Bui, D. (2011). The study of using rice husk ash to produce ultra high performance concrete. *Construction and Building Materials*, *25*(4), 2030–2035.

Vayghan, A. G., Khaloo, A. R., & Rajabipour, F. (2013). The effects of a hydrochloric acid pre-treatment on the physicochemical properties and pozzolanic performance of rice husk ash. *Cement and Concrete Composites*, *39*, 131–140.

Venkatanarayanan, H. K., & Rangaraju, P. R. (2015). Effect of grinding of low-carbon rice husk ash on the microstructure and performance properties of blended cement concrete. *Cement and Concrete Composites*, *55*, 348–363.

Villar-Cociña, E., Valencia-Morales, E., Gonzalez-Rodrıguez, R., & Hernandez-Ruız, J. (2003). Kinetics of the pozzolanic reaction between lime and sugar cane straw ash by electrical conductivity measurement: A kinetic–diffusive model. *Cement and Concrete Research*, *33*(4), 517–524.

Vu, D. D., Bui, D. D., & Stroeven, P. (1997). Experimental study of the use of calcinated clay, rice husk ash and gap-graded aggregate in PC-based mortars and concretes. *Proceedings of Non-Conventional Construction Materials, Nat. Resources Develop. Found., Bhubaneswar, India*, 96–110.

Wang, J., Xie, J., Wang, Y., Liu, Y., & Ding, Y. (2020). Rheological properties, compressive strength, hydration products and microstructure of seawater-mixed cement pastes. *Cement and Concrete Composites*, *114*, 103770.

Wang, L., Zheng, D., Zhang, S., Cui, H., & Li, D. (2016). Effect of nano-SiO2 on the hydration and microstructure of Portland cement. *Nanomaterials*, *6*(12), 241.

Wang, W., Gu, B., & Liang, L. (2005). Effect of surfactants on the formation, morphology, and surface property of synthesized SiO2 nanoparticles. *Journal of Dispersion Science and Technology*, *25*(5), 593–601.

Wang, W., Gu, B., Liang, L., & Hamilton, W. A. (2004). Adsorption and structural arrangement of cetyltrimethylammonium cations at the silica nanoparticle− water interface. *The Journal of Physical Chemistry B*, *108*(45), 17477–17483.

Weaver, W. S., Isabelle, H. L., & Williamson, F. (1974). A study of cement and concrete correlation. *Journal of Testing and Evaluation*, *2*(4), 260–303.

Witchakorn, C., & Bundhit, E. (2004). Sizing and location of electrical power generation from rice husk in Thailand. *19th World Energy Congress*, *5*.

Xu, W., Lo, T. Y., Wang, W., Ouyang, D., Wang, P., & Xing, F. (2016). Pozzolanic reactivity of silica fume and ground rice husk ash as reactive silica in a cementitious system: A comparative study. *Materials*, *9*(3), 146.

Yang, Z., Weiss, W. J., & Olek, J. (2006). Water transport in concrete damaged by tensile loading and freeze–thaw cycling. *Journal of Materials in Civil Engineering*, *18*(3), 424–434.

Yeoh, A. K., Bidin, R., Chong, C. N., & Tay, C. Y. (1979). The relationship between temperature and duration of burning of rice-husk in the development of amorphous rice-husk ash silica. *Proceedings of UNIDO/ESCAP/RCTT, Follow-up*

Meeting on Rice-Husk Ash Cement, Alor Setar, Malaysia.

Yildirim, A., Turkaydin, M., Garipcan, B., & Bayindir, M. (2016). Cytotoxicity of multifunctional surfactant containing capped mesoporous silica nanoparticles. *RSC Advances*, *6*(38), 32060–32069.

Yogendran, V., Langan, B. W., Haque, M. N., & Ward, M. A. (1987). Silica fume in high-strength concrete. *Materials Journal*, *84*(2), 124–129.

Younesi, H., & Ghasemi, Z. (2011). Preparation and characterization of nanozeolite NaA from rice husk at room temperature without organic additives. *Journal of Nanomaterials*, *2011*. https://doi.org/10.1155/2011/858961

Yu, Q., Sawayama, K., Sugita, S., Shoya, M., & Isojima, Y. (1999). The reaction between rice husk ash and Ca (OH) 2 solution and the nature of its product. *Cement and Concrete Research*, *29*(1), 37–43.

Yuvakkumar, R., Elango, V., Rajendran, V., & Kannan, N. (2014). High-purity nano silica powder from rice husk using a simple chemical method. *Journal of Experimental Nanoscience*, *9*(3), 272–281. https://doi.org/10.1080/17458080.2012.656709

Yuzer, N., Cinar, Z., Akoz, F., Biricik, H., Gurkan, Y. Y., Kabay, N., & Kizilkanat, A. B. (2013). Influence of raw rice husk addition on structure and properties of concrete. *Construction and Building Materials*, *44*, 54–62.

Zahedi, M., Ramezanianpour, A. A., & Ramezanianpour, A. M. (2015). Evaluation of the mechanical properties and durability of cement mortars containing nanosilica and rice husk ash under chloride ion penetration. *Construction and Building Materials*, *78*, 354–361.

Zain, M. F. M., Islam, M. N., Mahmud, F., & Jamil, M. (2011). Production of rice husk

ash for use in concrete as a supplementary cementitious material. *Construction and Building Materials*, *25*(2), 798–805.

Zerbino, R., Giaccio, G., & Isaia, G. C. (2011). Concrete incorporating rice-husk ash without processing. *Construction and Building Materials*, *25*(1), 371–378.

Zhang, H. (2011). *Building materials in civil engineering*. Woodhead Publishing Limited.

Zhang, H., Ding, X., Chen, X., Ma, Y., Wang, Z., & Zhao, X. (2015). A new method of utilizing rice husk: Consecutively preparing d-xylose, organosolv lignin, ethanol and amorphous superfine silica. *Journal of Hazardous Materials*, *291*, 65–73.

Zhang, M.-H., Islam, J., & Peethamparan, S. (2012). Use of nano-silica to increase early strength and reduce setting time of concretes with high volumes of slag. *Cement and Concrete Composites*, *34*(5), 650–662.

Zhang, M.-H., Lastra, R., & Malhotra, V. M. (1996). Rice-husk ash paste and concrete: some aspects of hydration and the microstructure of the interfacial zone between the aggregate and paste. *Cement and Concrete Research*, *26*(6), 963–977.

Zhang, M.-H., & Malhotra, V. M. (1996). High-performance concrete incorporating rice husk ash as a supplementary cementing material. *ACI Materials Journal*, *93*, 629–636.

Zhang, M., & Li, H. (2011). Pore structure and chloride permeability of concrete containing nano-particles for pavement. *Construction and Building Materials*, *25*(2), 608–616.

Zhang, P., Sha, D., Li, Q., Zhao, S., & Ling, Y. (2021). Effect of nano silica particles on impact resistance and durability of concrete containing coal fly ash. *Nanomaterials*, *11*(5), 1296.

Zhang, X., Ruiz, G., Rena, C. Y., Poveda, E., & Porras, R. (2012). Rate effect on the mechanical properties of eight types of high-strength concrete and comparison with FIB MC2010. *Construction and Building Materials*, *30*, 301–308.

Zulfiqar, U., Subhani, T., & Husain, S. W. (2015). Towards tunable size of silica particles from rice husk. *Journal of Non-Crystalline Solids*, *429*, 61–69.

Zulkifli, N. S. C., Ab Rahman, I., Mohamad, D., & Husein, A. (2013). A green sol–gel route for the synthesis of structurally controlled silica particles from rice husk for dental composite filler. *Ceramics International*, *39*(4), 4559–4567.

Zulu, S. N. F. (2017). *Optimizing the usage of fly ash in concrete mixes*.

Zuwanna, I., Riza, M., & Aprilia, S. (2021). The impact of solvent concentration on the characteristic of silica from rice husk ash using sol gel method. *IOP Conference Series: Materials Science and Engineering*, *1087*(1), 12060.

Appendices

Table A.1: Normal consistency of Control, RHA, SP, and NS blended pastes

% RHA	Normal Consistency (%)	% SP	Normal Consistency (%)	% NS	Normal Consistency (%)
0	27	0	27	0	27
2.5	30	2.5	30	2.5	28
5	32	5	32	5	29.5
7.5	35	7.5	35	7.5	30.5
10	36.5	10	37	10	32.5
15	41	15	42	15	36

Table A.2: Setting times of cement paste using different replacement of RHA

% RHA	Initial setting time (min)	Final setting time (min)
0	85	180
2.5	111	202
5	118	210
7.5	145	230
10	160	246
15	176	312

Table A.3: Setting times of cement paste using different replacement levels of SP

% SP	Initial setting time (min)	Final setting time (min)
0	85	180
2.5	106	204
5	115	215
7.5	116	228
10	113	225
15	124	229

Table A.4: Setting times of cement paste using different replacement of NS

% NS	Initial setting time (min)	Final setting time (min)
0	85	180
2.5	117	175
5	115	171
7.5	99	165
10	97	162
15	94	160

Table A.5: Soundness of RHA, SP, and NS blended cement pastes

% RHA	Expansion (mm)	% SP	Expansion (mm)	% NS	Expansion (mm)
0	2	0	2	0	2
2.5	2	2.5	2	2.5	1
5	1	5	4	5	5
7.5	2	7.5	3	7.5	3
10	3	10	4	10	1
15	1	15	1	15	1

Table A.6: Autoclave expansion of RHA, SP, and NS blended cement pastes

% RHA	Expansion (%)	% SP	Expansion (%)	% NS	Expansion (%)
0	0.02	0	0.02	0	0.02
2.5	0.06	2.5	0.04	2.5	0.04
5	0.07	5	0.03	5	0.03
7.5	0.05	7.5	0.07	7.5	0.09
10	0.10	10	0.06	10	0.04
15	0.07	15	0.10	15	0.04

Appendix B: Test results of RHA, SP, and NS blended mortar samples

Table B.1: Flow test of RHA, SP, and NS blended mortars

% RHA	Flow (mm)	% SP	Flow (mm)	% NS	Flow (mm)
0	163	0	163	0	163
2.5	154	2.5	150	2.5	126
5	143	5	129	5	123
7.5	135	7.5	126	7.5	119
10	131	10	121	10	117
15	125	15	117	15	114

Table B.2: Flexural strength of RHA blended mortars with constant w/b ratio

% RHA	Flexural strength (MPa)			
	3 days	7 days	28 days	90 days
0	4.99	5.10	5.63	6.33
2.5	4.84	5.22	5.45	6.49
5	4.34	4.88	6.16	6.35
7.5	4.20	4.80	6.45	6.83
10	4.02	4.60	5.81	6.49
15	3.82	5.00	5.82	6.42

Table B.3: Flexural strength of SP blended mortars with constant w/b ratio

% SP	Flexural strength (MPa)			
	3 days	7 days	28 days	90 days
0	4.99	5.10	5.63	6.33
2.5	4.07	4.27	6.40	6.59
5	4.06	4.70	6.32	6.73
7.5	4.00	4.75	6.51	7.12
10	4.24	5.27	6.49	7.03
15	4.04	4.19	5.73	6.45

Table B.4: Flexural strength of NS blended mortars with constant w/b ratio

% NS	Flexural strength (MPa)			
	3 days	7 days	28 days	90 days
0	4.99	5.10	5.63	6.33
2.5	4.58	5.60	6.08	6.31
5	4.51	5.82	5.98	6.33
7.5	4.52	5.91	6.21	6.82
10	4.34	5.88	6.08	6.44
15	4.27	5.88	5.95	6.33

Table B.5: Flexural strength of RHA blended mortars with varying w/b ratios

% RHA	Flexural strength (MPa)			
	3 days	7 days	28 days	90 days
0	4.99	5.10	5.63	6.33
2.5	4.36	4.54	5.44	5.49
5	4.64	4.90	5.43	5.61
7.5	4.51	4.55	5.65	5.67
10	4.85	4.98	5.34	5.74
15	4.08	4.35	5.17	6.09

Table B.6: Flexural strength of SP blended mortars with varying w/b ratios

% SP	Flexural strength (MPa)			
	3 days	7 days	28 days	90 days
0	4.99	5.10	5.63	6.33
2.5	4.45	5.05	5.16	6.72
5	4.06	4.87	5.30	6.51
7.5	4.37	4.58	5.09	6.34
10	4.00	4.61	4.98	6.04
15	3.96	4.14	4.87	5.61

Table B.7: Flexural strength of NS blended mortars with varying w/b ratios

% NS	Flexural strength (MPa)			
	3 days	7 days	28 days	90 days
0	4.99	5.10	5.63	6.33
2.5	4.51	4.54	4.60	5.60
5	4.37	4.45	5.16	5.74
7.5	4.13	4.53	5.17	5.83
10	3.87	5.05	5.39	5.93
15	3.70	4.93	4.98	5.19

Table B.8: Compressive strength of RHA blended mortars with constant w/b ratio

% RHA	Compressive strength (MPa)			
	3 days	7 days	28 days	90 days
0	32.3	35.2	50.2	55.4
2.5	31.0	37.8	58.2	59.2
5	26.7	38.8	53.9	56.1
7.5	29.7	31.8	51.4	54.6
10	25.4	32.3	48.4	49.0
15	28.5	29.6	47.4	47.9

Table B.9: Compressive strength of SP blended mortars with constant w/b ratio

% SP	Compressive strength (MPa)			
	3 days	7 days	28 days	90 days
0	32.3	35.2	50.2	55.4
2.5	36.0	46.5	53.5	57.6
5	34.5	46.7	57.6	58.5
7.5	34.1	47.2	58.0	58.6
10	35.1	49.7	59.8	60.8
15	32.4	39.7	51.9	55.6

Table B.10: Compressive strength of NS blended mortars with constant w/b ratio

%NS	Compressive strength (MPa)			
	3 days	7 days	28 days	90 days
0	32.3	35.2	50.2	55.4
2.5	34.5	42.2	52.8	52.9
5	35.1	43.8	50.4	56.2
7.5	32.7	44.4	51.1	51.5
10	32.3	42.2	49.6	50.5
15	29.5	39.5	47.8	49.3

Table B.11: Compressive strength of RHA blended mortars with varying w/b ratios

% RHA	Compressive strength (MPa)			
	3 days	7 days	28 days	90 days
0	32.3	35.2	50.2	55.4
2.5	33.3	37.6	51.4	55.3
5	31.4	34.0	51.5	56.5
7.5	29.3	31.4	50.4	56.5
10	29.2	35.8	45.5	56.3
15	26.1	32.8	39.9	53.1

Table B.12: Compressive strength of SP blended mortars with varying w/b ratios

% SP	Compressive strength (MPa)			
	3 days	7 days	28 days	90 days
0	32.3	35.2	50.2	55.4
2.5	38.2	44.3	52.2	61.4
5	35.8	48.6	52.4	61.6
7.5	33.3	47.2	53.3	63.4
10	32.4	47.2	50.6	59.9
15	25.7	36.5	42.9	54.0

Table B.13: Compressive strength of NS blended mortars with varying w/b ratios

%NS	Compressive strength (MPa)			
	3 days	7 days	28 days	90 days
0	32.3	35.2	50.2	55.4
2.5	39.8	48.0	49.1	64.2
5	36.9	47.0	49.4	61.2
7.5	35.4	48.7	50.2	60.3
10	34.2	47.9	48.7	59.1
15	30.7	41.1	45.3	57.0

Table B.14: Water absorption of RHA, SP, and NS blended mortar after 90 days curing with constant w/b ratio

% RHA	Water absorption (%)	% SP	Water absorption (%)	% NS	Water absorption (%)
0	7.5	0	7.5	0	7.5
2.5	7.6	2.5	6.2	2.5	6.5
5	7.6	5	6.2	5	6.6
7.5	8.1	7.5	6.6	7.5	6.7
10	8.4	10	6.9	10	6.8
15	8.9	15	6.9	15	6.8

Table B.15: Water absorption of RHA, SP, and NS blended mortar after 90 days curing with varying w/b ratios

% RHA	Water absorption (%)	% SP	Water absorption (%)	% NS	Water absorption (%)
0	7.5	0	7.5	0	7.5
2.5	6.5	2.5	7.1	2.5	5.5
5	6.9	5	7.1	5	6.4
7.5	7.1	7.5	7.2	7.5	7.2
10	7.4	10	7.6	10	7.5
15	7.5	15	7.7	15	9.1

Table B.16: Bulk density of RHA, SP, and NS blended mortars after 90 days curing with constant w/b ratio

% RHA	Bulk density (kg/m^3)	% SP	Bulk density (kg/m^3)	% NS	Bulk density (kg/m^3)
0	2285	0	2285	0	2285
2.5	2335	2.5	2215	2.5	2505
5	2440	5	2350	5	2445
7.5	2255	7.5	2390	7.5	2275
10	2250	10	2330	10	2250
15	1930	15	2135	15	2205

Table B.17: Apparent density of RHA, SP, and NS blended mortars after 90 days curing with constant w/b ratio

% RHA	Apparent density (kg/m^3)	% SP	Apparent density (kg/m^3)	% NS	Apparent density (kg/m^3)
0	2770	0	2770	0	2770
2.5	2850	2.5	2510	2.5	3010
5	3010	5	2660	5	2930
7.5	2820	7.5	2860	7.5	2690
10	2790	10	2820	10	2660
15	2370	15	2495	15	2585

Table B.18: Bulk density of RHA, SP, and NS blended mortars after 90 days curing with varying w/b ratios

% RHA	Bulk density (kg/m^3)	% SP	Bulk density (kg/m^3)	% NS	Bulk density (kg/m^3)
0	2285	0	2285	0	2285
2.5	2215	2.5	2360	2.5	2330
5	2200	5	2340	5	2270
7.5	2145	7.5	2175	7.5	2210
10	2060	10	2175	10	2140
15	2020	15	2155	15	2135

Table B.19: Apparent density of RHA, SP, and NS blended mortars after 90 days curing with varying w/b ratios

% RHA	Apparent density (kg/m^3)	% SP	Apparent density (kg/m^3)	% NS	Apparent density (kg/m^3)
0	2770	0	2770	0	2770
2.5	2820	2.5	2920	2.5	2940
5	2720	5	2860	5	2675
7.5	2600	7.5	2860	7.5	2635
10	2495	10	2755	10	2585
15	2455	15	2700	15	2560

Table B.20: Volume of permeable pores in RHA, SP, and NS blended mortars after 90 days curing with constant w/b ratio

% RHA	Porosity (%)	% SP	Porosity (%)	% NS	Porosity (%)
0	17.6	0	17.6	0	17.6
2.5	18.2	2.5	11.7	2.5	16.7
5	19.0	5	11.6	5	16.6
7.5	19.9	7.5	16.4	7.5	15.6
10	19.3	10	17.3	10	15.3
15	18.6	15	14.4	15	14.8

Table B.21: Volume of permeable pores in RHA, SP, and NS blended mortars after 90 days curing with varying w/b ratios

% RHA	Porosity (%)	% SP	Porosity (%)	% NS	Porosity (%)
0	17.6	0	17.6	0	17.6
2.5	21.4	2.5	19.2	2.5	20.8
5	18.9	5	18.3	5	15.1
7.5	17.6	7.5	23.9	7.5	16.2
10	17.4	10	21.1	10	17.2
15	17.8	15	20.2	15	16.7

Table B.22: Shrinkage value of RHA blended mortars

Time	Shrinkage of RHA blended mortars at different replacement level (%)					
(days)	0	2.5	5	7.5	10	15
7	0.040	0.074	0.076	0.065	0.056	0.044
14	0.102	0.091	0.086	0.093	0.088	0.088
21	0.107	0.094	0.094	0.095	0.089	0.091
28	0.107	0.100	0.106	0.114	0.118	0.119

Table B.23: Shrinkage value of SP blended mortars

Time	Shrinkage of SP blended mortars at different replacement level (%)					
(days)	0	2.5	5	7.5	10	15
7	0.040	0.053	0.056	0.060	0.055	0.068
14	0.102	0.092	0.085	0.082	0.074	0.091
21	0.107	0.109	0.099	0.093	0.086	0.104
28	0.107	0.121	0.103	0.100	0.093	0.107

Table B.24: Shrinkage value of NS blended mortars

Time (days)	Shrinkage of NS blended mortars at different replacement level (%)					
	0	2.5	5	7.5	10	15
7	0.040	0.019	0.025	0.046	0.035	0.057
14	0.102	0.035	0.030	0.048	0.040	0.065
21	0.107	0.057	0.035	0.050	0.048	0.066
28	0.107	0.057	0.044	0.058	0.057	0.073

Table B.25: Expansion of RHA blended mortar under sulfate attack

Replacement level (%)	RHA blended mortar expansion (%) at different curing time (weeks)						
	1	2	3	4	8	13	15
0	0.008	0.010	0.017	0.020	0.200	0.205	0.220
2.5	0.000	0.016	0.023	0.032	0.206	0.224	0.229
5	0.005	0.015	0.017	0.027	0.211	0.214	0.231
7.5	0.010	0.019	0.019	0.022	0.195	0.218	0.231
10	0.006	0.007	0.016	0.019	0.140	0.158	0.172
15	0.012	0.037	0.037	0.058	0.337	0.345	0.354

Table B.26: Expansion of SP blended mortar under sulfate attack

Replacement level (%)	SP blended mortar expansion (%) at different curing time (weeks)						
	1	2	3	4	8	13	15
0	0.008	0.010	0.017	0.020	0.200	0.205	0.220
2.5	0.000	0.004	0.025	0.040	0.146	0.224	0.228
5	0.001	0.002	0.009	0.029	0.227	0.232	0.236
7.5	0.001	0.006	0.011	0.024	0.203	0.220	0.225
10	0.003	0.007	0.019	0.026	0.217	0.235	0.239
15	0.032	0.037	0.040	0.047	0.244	0.249	0.253

Table B.27: Expansion of NS blended mortar under sulfate attack

Replacement level (%)	NS blended mortar expansion (%) at different curing time (weeks)						
	1	2	3	4	8	13	15
0	0.008	0.010	0.017	0.020	0.200	0.205	0.220
2.5	0.009	0.012	0.016	0.022	0.217	0.240	0.254
5	0.018	0.024	0.030	0.142	0.173	0.174	0.192
7.5	0.004	0.005	0.006	0.187	0.201	0.202	0.215
10	0.023	0.024	0.030	0.147	0.232	0.242	0.248
15	0.013	0.039	0.043	0.224	0.235	0.241	0.251

Appendix C: Test results of RHA, SP, and NS blended concrete samples

Table C.1: Fresh density of RHA, SP, and NS blended concretes

% RHA	Fresh density (kg/m^3)	% SP	Fresh density (kg/m^3)	% NS	Fresh density (kg/m^3)
0	2375	0	2375	0	2375
2.5	2365	2.5	2365	2.5	2355
5	2345	5	2355	5	2345
7.5	2335	7.5	2355	7.5	2320
10	2335	10	2355	10	2320
15	2320	15	2345	15	2290

Table C.2: Workability of RHA, SP, and NS blended concretes

% RHA	Slump (mm)	% SP	Slump (mm)	% NS	Slump (mm)
0	180	0	180	0	180
2.5	170	2.5	145	2.5	110
5	160	5	60	5	80
7.5	95	7.5	30	7.5	45
10	55	10	25	10	15
15	15	15	15	15	10

Table C.3: Compressive strength of RHA blended concretes

% Replacement level	Compressive strength of RHA blended concrete (MPa) at different curing days		
	14 days	28 days	56 days
0	22.3	26.6	27.6
2.5	23.8	26.6	28.9
5	22.6	25.1	30.7
7.5	23.8	29.4	31.7
10	24.3	25.9	29.9
15	24.6	26.9	27.6

Table C.4: Compressive strength of SP blended concretes

% Replacement level	Compressive strength of SP blended concrete (psi) at different curing days		
	14 days	28 days	56 days
0	22.3	26.6	27.6
2.5	25.	28.9	30.7
5	27.4	28.9	33.2
7.5	24.8	27.9	34.2
10	22.3	24.3	25.3
15	21.4	24.1	24.9

Table C.5: Compressive strength of NS blended concretes

% Replacement level	Compressive strength of NS blended concrete (psi) at different curing days		
	14 days	28 days	56 days
0	22.3	26.6	27.6
2.5	25.9	28.9	31.4
5	26.6	29.1	32.9
7.5	27.1	32.9	33.7
10	27.4	32.2	32.4
15	21.5	24.2	25.7

Table C.6: Water absorption of RHA blended concretes

% Replacement level	Water absorption of RHA blended concrete (%) at different curing ages		
	14 days	28 days	56 days
0	4.4	4.2	3.8
2.5	4.5	4.3	2.5
5	4.5	4.1	2.3
7.5	4.5	4.1	2.2
10	4.2	4.1	2.2
15	4.0	3.8	2.0

Table C.7: Water absorption of SP blended concretes

% Replacement level	Water absorption of SP blended concrete (%) at different curing ages		
	14 days	28 days	56 days
0	4.4	4.2	3.8
2.5	4.4	4.1	3.7
5	4.4	3.9	3.6
7.5	4.2	3.6	3.5
10	4.1	3.5	3.5
15	3.9	3.2	3.0

Table C.8: Water absorption of NS blended concretes

% Replacement level	Water absorption of NS blended concrete (%) at different curing ages		
	14 days	28 days	56 days
0	4.4	4.2	3.8
2.5	4.5	3.9	1.9
5	3.9	3.6	1.8
7.5	3.9	3.2	1.7
10	3.9	2.8	1.6
15	3.3	2.3	1.5

Table C.9: Bulk density of RHA blended concretes

% Replacement level	Bulk density (kg/m^3) of RHA blended concrete at different curing ages		
	14 days	28 days	56 days
0	2290	2315	2315
2.5	2220	2280	2435
5	2255	2315	2430
7.5	2275	2320	2430
10	2280	2350	2400
15	2295	2340	2355

Table C.10: Bulk density of SP blended concretes

% Replacement level	Bulk density (kg/m^3) of SP blended concrete at different curing ages		
	14 days	28 days	56 days
0	2290	2315	2315
2.5	2330	2335	2350
5	2295	2385	2390
7.5	2340	2340	2430
10	2310	2320	2375
15	2265	2290	2355

Table C.11: Bulk density of NS blended concretes

% Replacement level	Bulk density (kg/m^3) of NS blended concrete at different curing ages		
	14 days	28 days	56 days
0	2290	2315	2315
2.5	2220	2230	2300
5	2245	2260	2360
7.5	2250	2275	2355
10	2260	2300	2330
15	2220	2240	2245

Table C.12: Apparent density of RHA blended concretes

% Replacement level	Apparent density (kg/m^3) of RHA blended concrete at different curing ages		
	14 days	28 days	56 days
0	2580	2530	2465
2.5	2590	2565	2500
5	2590	2560	2480
7.5	2585	2530	2480
10	2585	2515	2495
15	2580	2495	2465

Table C.13: Apparent density of SP blended concretes

% Replacement level	Apparent density (kg/m^3) of SP blended concrete at different curing ages		
	14 days	28 days	56 days
0	2580	2530	2465
2.5	2685	2620	2520
5	2640	2585	2515
7.5	2610	2540	2490
10	2600	2515	2480
15	2590	2450	2440

Table C.14: Apparent density of NS blended concretes

% Replacement level	Apparent density (kg/m^3) of NS blended concrete at different curing ages		
	14 days	28 days	56 days
0	2580	2530	2465
2.5	2510	2470	2460
5	2470	2460	2450
7.5	2465	2460	2415
10	2460	2450	2405
15	2460	2430	2395

Table C.15: Volume of permeable pores of RHA blended concretes

% Replacement level	Porosity (%) of RHA blended concrete at different curing ages		
	14 days	28 days	56 days
0	11.2	8.5	6.0
2.5	14.3	11.0	2.7
5	12.9	9.5	2.1
7.5	12.0	8.3	2.1
10	11.7	6.6	3.9
15	11.2	6.2	4.6

Table C.16: Volume of permeable pore space of SP blended concretes

% Replacement level	Porosity (%) of SP blended concrete at different curing ages		
	14 days	28 days	56 days
0	11.2	8.5	6.0
2.5	13.4	10.9	6.8
5	13.1	7.8	4.9
7.5	10.4	7.9	2.4
10	11.3	7.7	4.3
15	12.6	6.5	3.5

Table C.17: Volume of permeable pore space of NS blended concretes

% Replacement level	Porosity (%) of NS blended concrete at different curing ages		
	14 days	28 days	56 days
0	11.2	8.5	6.0
2.5	11.4	9.8	6.5
5	9.2	8.1	3.6
7.5	8.8	7.4	2.4
10	8.0	6.3	3.1
15	9.6	7.8	6.3

Table C.18: Ultrasonic Pulse Velocity of RHA, SP, and NS blended concretes after 56 days of curing

% RHA	Velocity (km/s)	% SP	Velocity (km/s)	% NS	Velocity (km/s)
0	4.16	0	4.16	0	4.16
2.5	4.26	2.5	4.15	2.5	4.24
5	4.44	5	4.30	5	4.24
7.5	4.52	7.5	4.28	7.5	4.29
10	4.47	10	4.26	10	4.42
15	4.43	15	4.08	15	4.01

Table C.19: Rapid Chloride Penetration test result of RHA, SP, and NS blended concretes after 28 days curing

% RHA	Charge passed (C)	% SP	Charge passed (C)	% NS	Charge passed (C)
0	4008.8	0	4008.8	0	4008.8
2.5	3039.8	2.5	3474.3	2.5	3880.3
5	2463.1	5	2494.5	5	2895.9
7.5	1900.4	7.5	1986.9	7.5	1801.4
10	1469.2	10	1319.8	10	1421.9
15	1103.5	15	944.4	15	97.6

Table C.20: Sorptivity test results of RHA, SP, and NS blended concretes after 28 days curing

% RHA	Sorptivity ($mm/s^{1/2}$)	% SP	Sorptivity ($mm/s^{1/2}$)	% NS	Sorptivity ($mm/s^{1/2}$)
0	0.04	0	0.04	0	0.04
2.5	0.07	2.5	0.05	2.5	0.04
5	0.06	5	0.06	5	0.05
7.5	0.05	7.5	0.04	7.5	0.03
10	0.08	10	0.03	10	0.06
15	0.07	15	0.05	15	0.07

Table C.21: Surface electrical resistivity result of RHA, SP, and NS blended concretes

% RHA	Resistivity (kΩ-cm)	% SP	Resistivity (kΩ-cm)	% NS	Resistivity (kΩ-cm)
0	7.7	0	7.7	0	7.7
2.5	8.1	2.5	7.9	2.5	7.8
5	11.0	5	11.6	5	9.3
7.5	14.2	7.5	18.5	7.5	15.8
10	15.3	10	22.0	10	19.8
15	22.6	15	26.3	15	23.1